GEORGIA INSTITUTE OF TECHNOLOGY — OFFICE OF CONTRACT ADMINISTRATION

PROJECT ADMINISTRATION DATA SHEET

[x] ORIGINAL [ ] REVISION NO. ____

Project No. E-20-661 J.P. Gould — GTRI/~~GIT~~ XXX — DATE 5 / 10 / 84

Project Director: ~~Dr. Byung R. Kim~~ — School/~~Lab~~ XXX Civil Engineering

Sponsor: Department of Interior; Bureau of Reclamation

Type Agreement: 14-08-0001-G-1010 Grant No. ~~4-FG-93-00120~~

Award Period: From 4/15/84 To ~~4/14/86~~ 1-15-87 (Performance) 8/14/86 (Reports)

Sponsor Amount:	This Change	Total to Date
Estimated:	$ 96,712	$ 96,712
Funded:	$ 96,712	$ 96,712

Cost Sharing Amount: $ 3,690 Cost Sharing No: E-20-345

Title: Adsorption of Organic Dyes on Synthetic Resins from Textile Wastewaters

ADMINISTRATIVE DATA OCA Contact Brian J. Lindberg x-4820

1) Sponsor Technical Contact:

Director, Office of Water Research
Code 1700
~~Bureau of Reclamation~~ Geological Survey
U. S. Department of the Interior
18th and C Sts., N. W.
Washington, D. C. 20240

2) Sponsor Admin/Contractual Matters:

Same as 1)

Defense Priority Rating: N/A Military Security Classification: N/A

(or) Company/Industrial Proprietary: N/A

RESTRICTIONS

See Attached N/A Supplemental Information Sheet for Additional Requirements.

Travel: Foreign travel must have prior approval – Contact OCA in each case. Domestic travel requires sponsor approval where total will exceed greater of $500 or 125% of approved proposal budget category.

Equipment: Title vests with Sponsor. Prior approval required from Grants Officer for purchase or acquisitions of equipment over $1,000.

COMMENTS:

Sponsor I.D. No. 02.111.000.84.R01

COPIES TO:

Project Director
Research Administrative Network
Research Property Management
Accounting
Procurement/EES Supply Services
Research Security Services
Reports Coordinator (OCA)
~~Research Communications~~ (2)
GTRI
Library
Project File
Other I. Newton

FORM OCA 4:383

GEORGIA INSTITUTE OF TECHNOLOGY OFFICE OF CONTRACT ADMINISTRATION

SPONSORED PROJECT TERMINATION/CLOSEOUT SHEET

Date 2/24/88

Project No. E-20-661 School/~~Unit~~ CE

Includes Subproject No.(s) n/a

Project Director(s) J. P. Gould GTRC/~~GIT~~

Sponsor DOI/Geological Survey

Title ~~Absorption~~ Adsorption of Organic Dyes on Synthetic Resins from Textile Wastewaters

Effective Completion Date: 1/15/87 (Performance) 1/15/87 (Reports)

Grant/Contract Closeout Actions Remaining:

- [ ] None
- [x] Final Invoice or Copy of Last Invoice Serving as Final
- [ ] Release and Assignment
- [x] Final Report of Inventions and/or Subcontract:
  Patent and Subcontract Questionnaire sent to Project Director [x]
- [x] Govt. Property Inventory & Related Certificate
- [ ] Classified Material Certificate
- [ ] Other _____

Continues Project No. _____ Continued by Project No. _____

COPIES TO:

Project Director
Research Administrative Network
Research Property Management
Accounting
Procurement/GTRI Supply Services
Research Security Services
Reports Coordinator (OCA)
Program Administration Division
Contract Support Division
Facilities Management - ERB
Library
GTRC
Project File
Other _____

E-20-661

Quarterly Progress Report

(Project Number E-20-661)

By

Byung R. Kim
School of Civil Engineering
Georgia Institute of Technology

For
Bureau of Reclamation
U. S. Department of Interior

The project, "Adsorption of Organic Dyes on Synthetic Resins from Textile Wastewaters," was initiated on April 15, 1984. Two research assistants were hired for this project: Ms. Kimberly A. Groff, a Ph.D. student, and Mr. Siamak Yari, a M.S. student. At this stage, we are setting up a laboratory space and ordering materials, such as glasswares, chemicals, synthetic resin, etc. So far, we have not been able to perform any laboratory experiments. We hope we will be able to produce some results for the next progress report.

E-20-661

Progress Report to October 1985
(Project Number E-20-661)
(Grant Number 14-08-0001-G-1070)
(Sponsor: U.S. Geological Survey)

INTRODUCTION

The progress report for the period ending September 30, 1985 follows. During this period the following phases of the research have been carried out.

a) Batch equilibrium studies for all compounds on all resins have been completed.

b) Examination of existing adsorption models has continued in the context of the growing body of data.

c) The methodology for clean-up of large quantities of resin needed for column studies has been developed.

d) An experimental column system has been designed, tested and, in consequence, redesigned to permit greater ease of operation and improved structural system integrity.

e) Initial resin regeneration studies have been carried out.

Adsorption Isotherm Studies

The compounds selected for study thus far, include 4-aminoazobenzene, 4-hydroxyazobenzene, phenylazobenzoic acid, methyl red, methyl orange, FD&C red 40 and FD&C yellow 6. In addition, p-nitrophenol has been selected for comparison purposes. A summary of the compound structures and characteristics is shown in Table 1. As previously noted the resins chosen include A-7, S-761, XAD-7 and XAD-16. Further study of XAD-8 has not been pursued due to the fact that the adsorptive behavior of this resin was not found to be much different than XAD-7. A summary of the resin characteristics is shown in Table 2.

During this quarter the collection of isotherm data has continued using the compounds and resins mentioned above. In addition, isotherm data collected previously have been critically evaluated and supplemental data have been generated to provide consistent and complete isotherms on all compounds and resins. Isotherm data were collected on all compounds, with the exception of phenylazobenzoic acid, at a pH near 6. This pH was chosen to insure that each compound in solution was predominantly in either an ionized or neutral form. For phenylazobenzoic acid a pH of 8.5 was chosen due to the fact that the pKa of this compound is near 6.

The isotherm data collected to date for all compounds and resins studied are shown in Figures 1 through 12. Resin A-7 appeared to be the best resin for the removal of p-nitrophenol, methyl orange, methyl red, red 40 and yellow 6. For compounds which exist in the ionized form, such as methyl red, methyl

Table 1 Summary of Compound Characteristics

Name	Molecular Weight	Purity	Solubility	pKa
p-nitrophenol	139.11	99%	1.69g 100g	7.16
4-aminoazobenzene	194.24	98%	Slightly Soluble	11.12
4-hydroxyazobenzene	198.23	98%	Slightly Soluble	9.38
phenylazobenzoic acid	226.24	-	Slightly Soluble	6-7
methyl red	291.32	95%	Soluble	2.50 9.95
methyl orange	327.25	95%	Soluble	3.63 >11.20
yellow 6	452.37	92%	Very Soluble	< 1.03 > 8.98
red 40	496.44	91%	Very Soluble	< 1.04 >10.09

Table 2 Summary of Resin Characteristics

Resin	A-7	S-761	XAD-7	XAD-16
Matrix	Phenolic	Phenolic	Acrylic Ester	Polystyrene
Class	Weak Base Anion Exchange	Adsorbent	Adsorbent	Adsorbent
Mesh Range	16-50	16-50	20-60	20-60
Total Capacity (meq/ml)	2.2	--	--	--
pH Range	0-6	0-8	--	--
Wet Density g/cc	1.12	1.11	1.05	1.02
Moisture Content (%)	52-60	55-60	65-70	60-70
Functional Group	Poly-Functional Amine	Hydroxyl	--	--
Surface Area (m^2/g)	--	100-300	450	800
Pore Size (A)	--	--	90	100

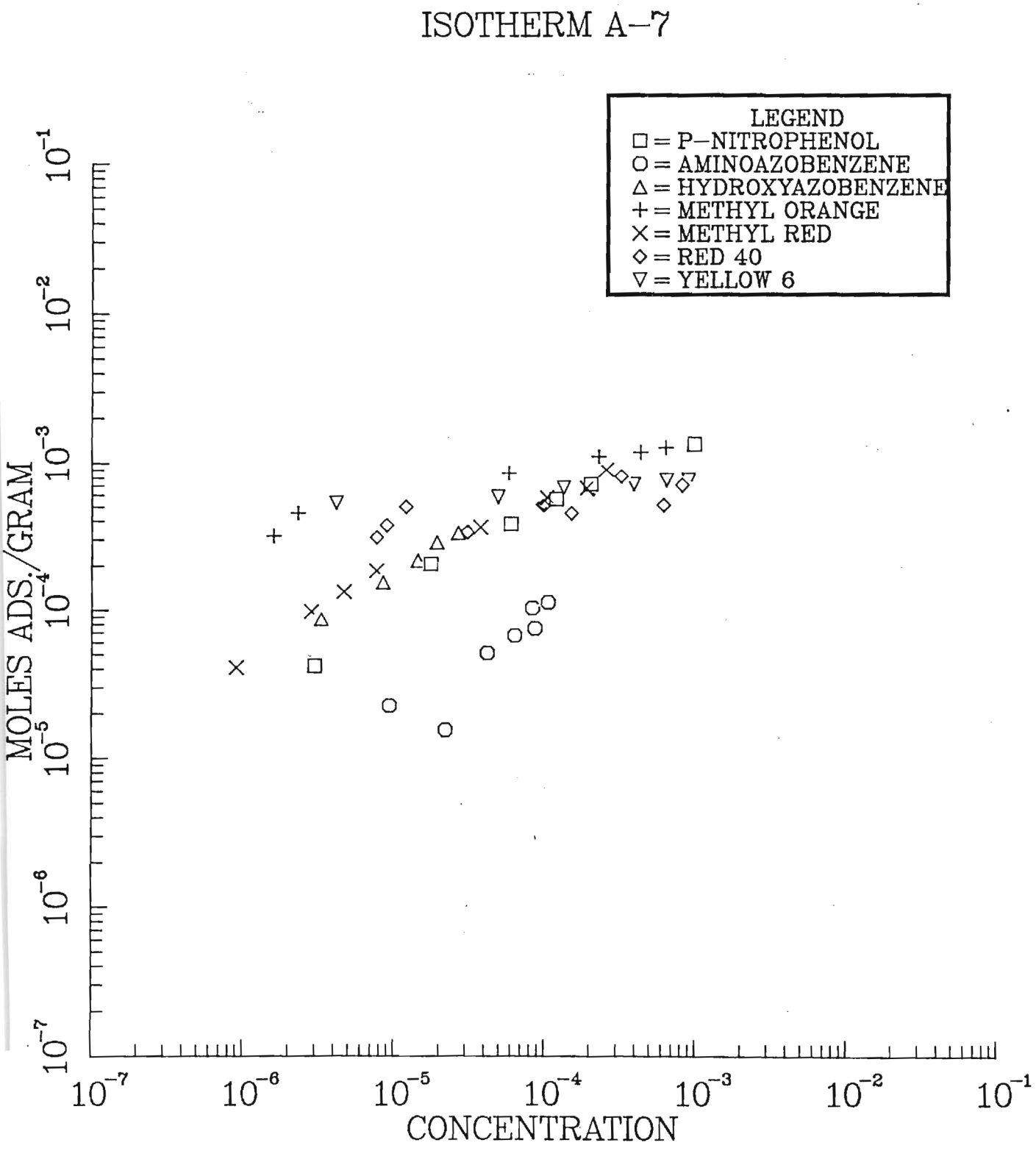

Figure 1. Sorption Isotherms on Resin A-7.

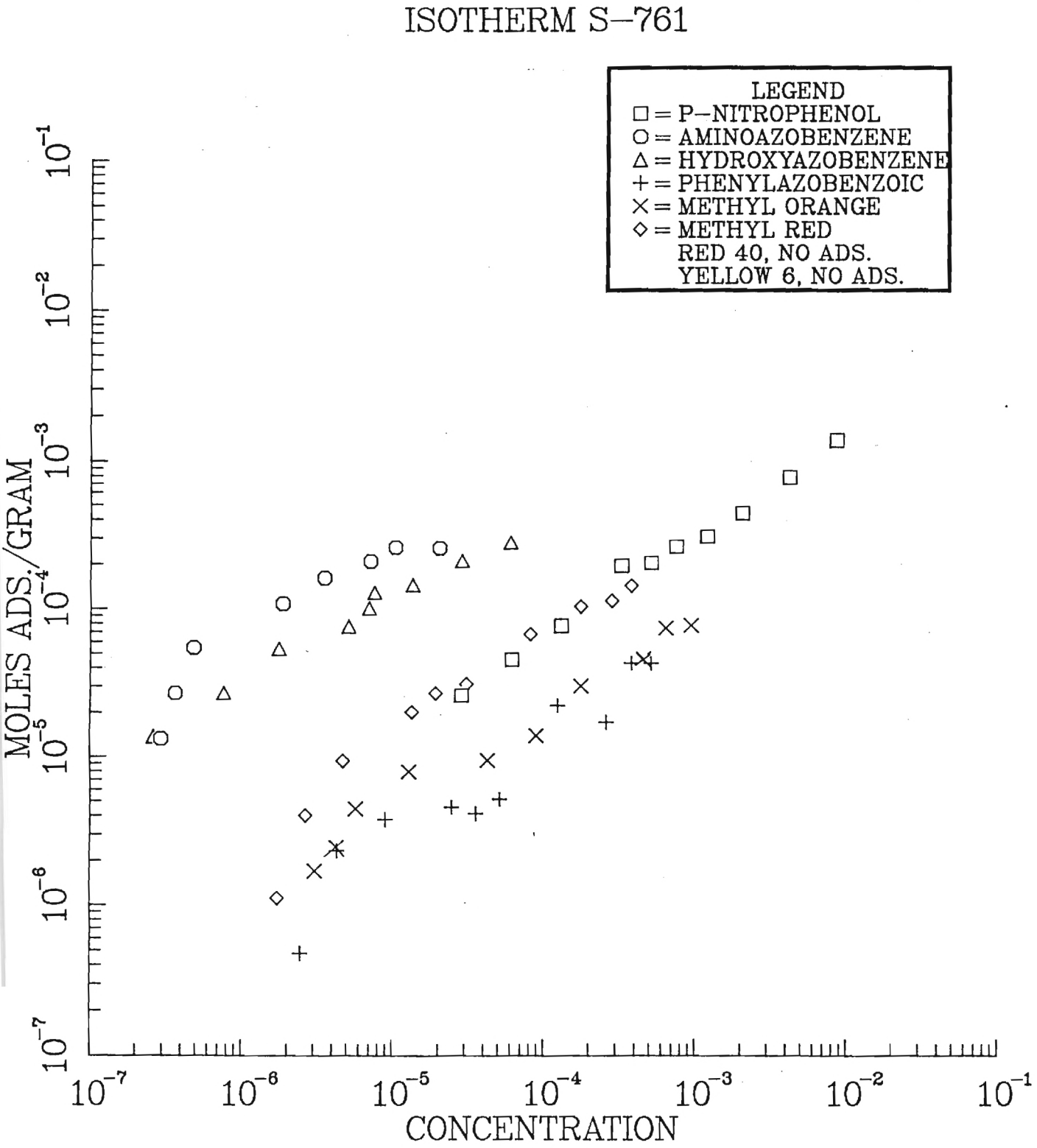

Figure 2. Sorption Isotherms on Resin S-761.

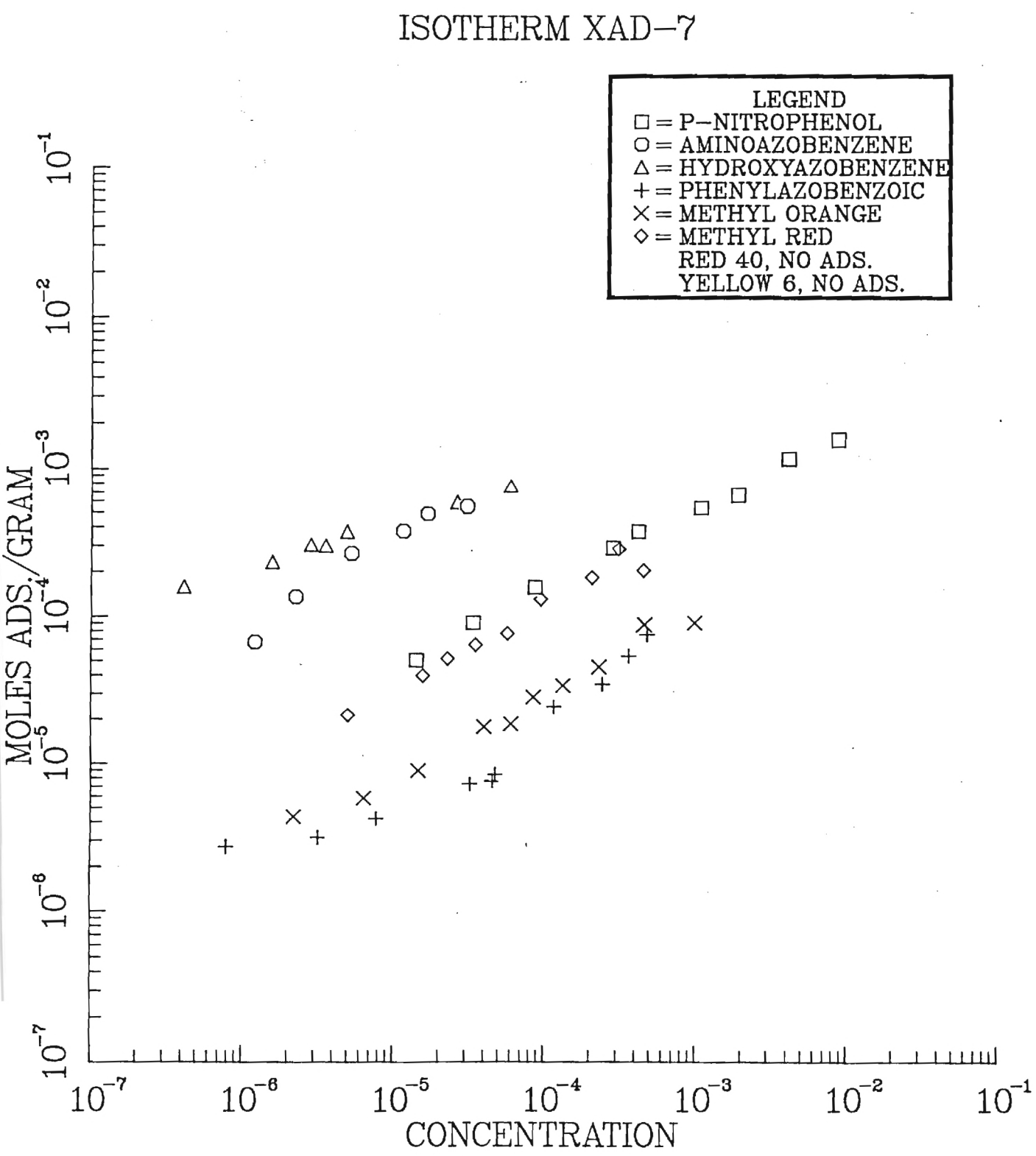

Figure 3. Sorption Isotherms on Resin XAD-7.

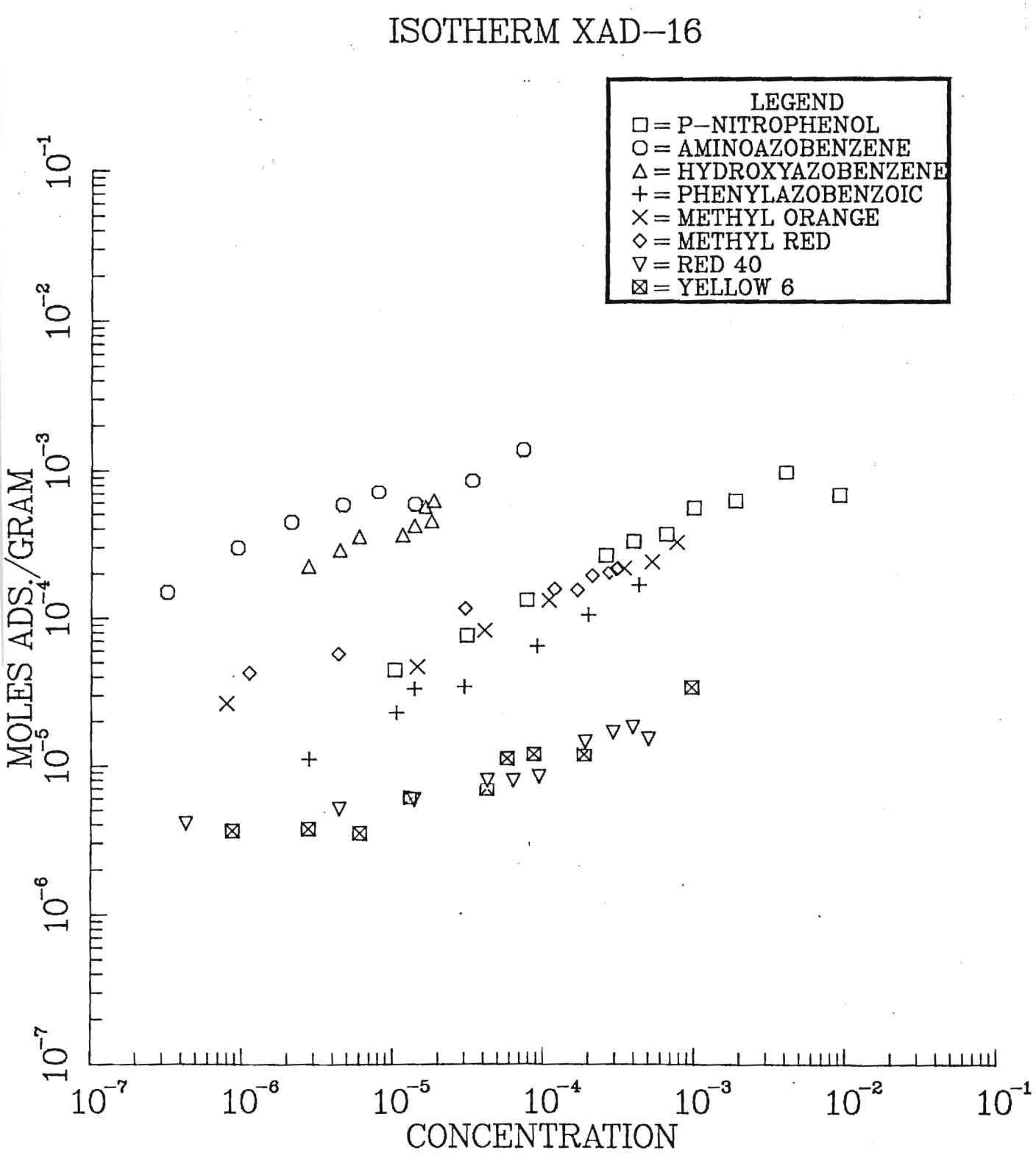

Figure 4. Sorption Isotherms on Resin XAD-16.

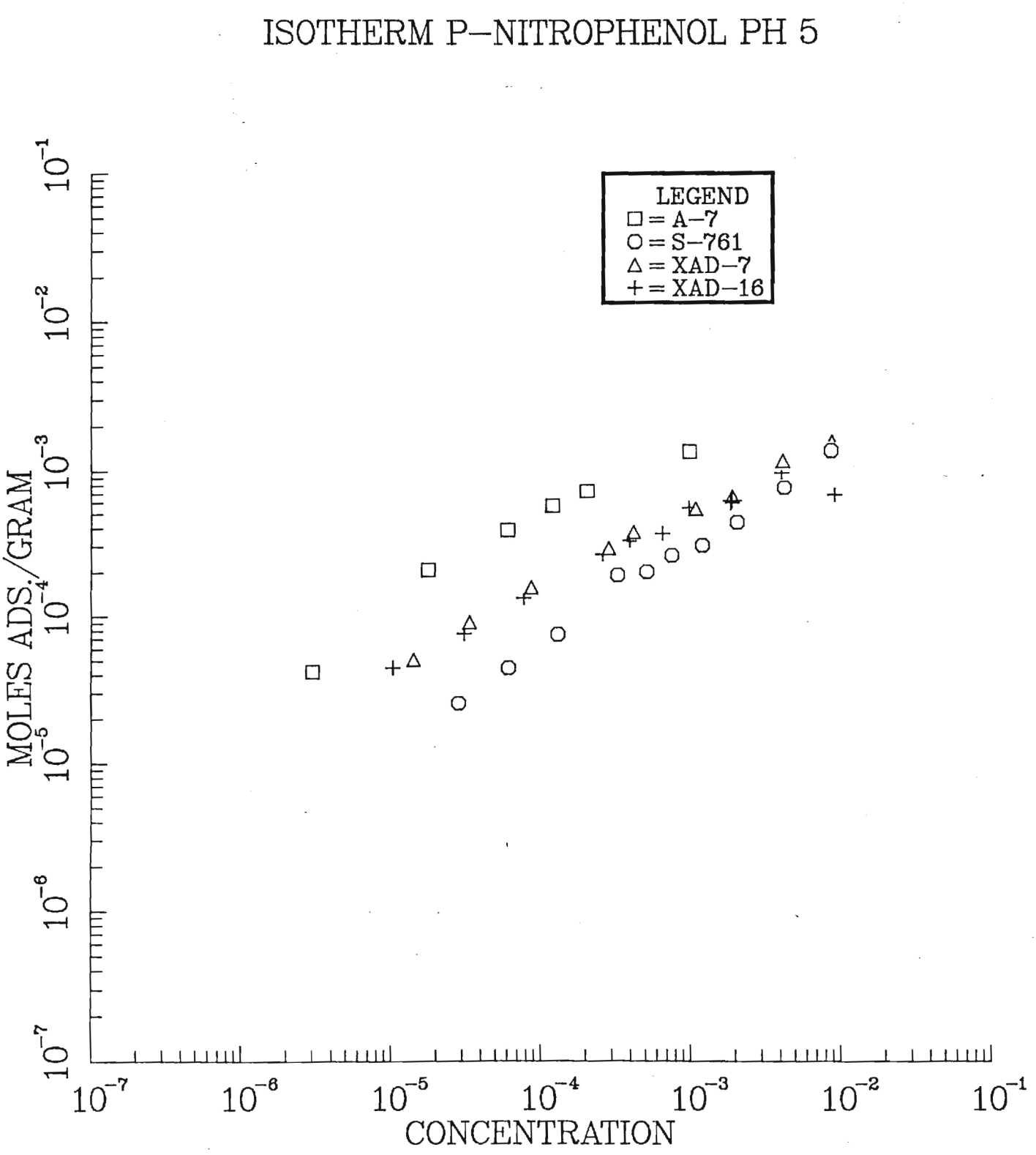

Figure 5. Adsorption Isotherms for p-Nitrophenol.

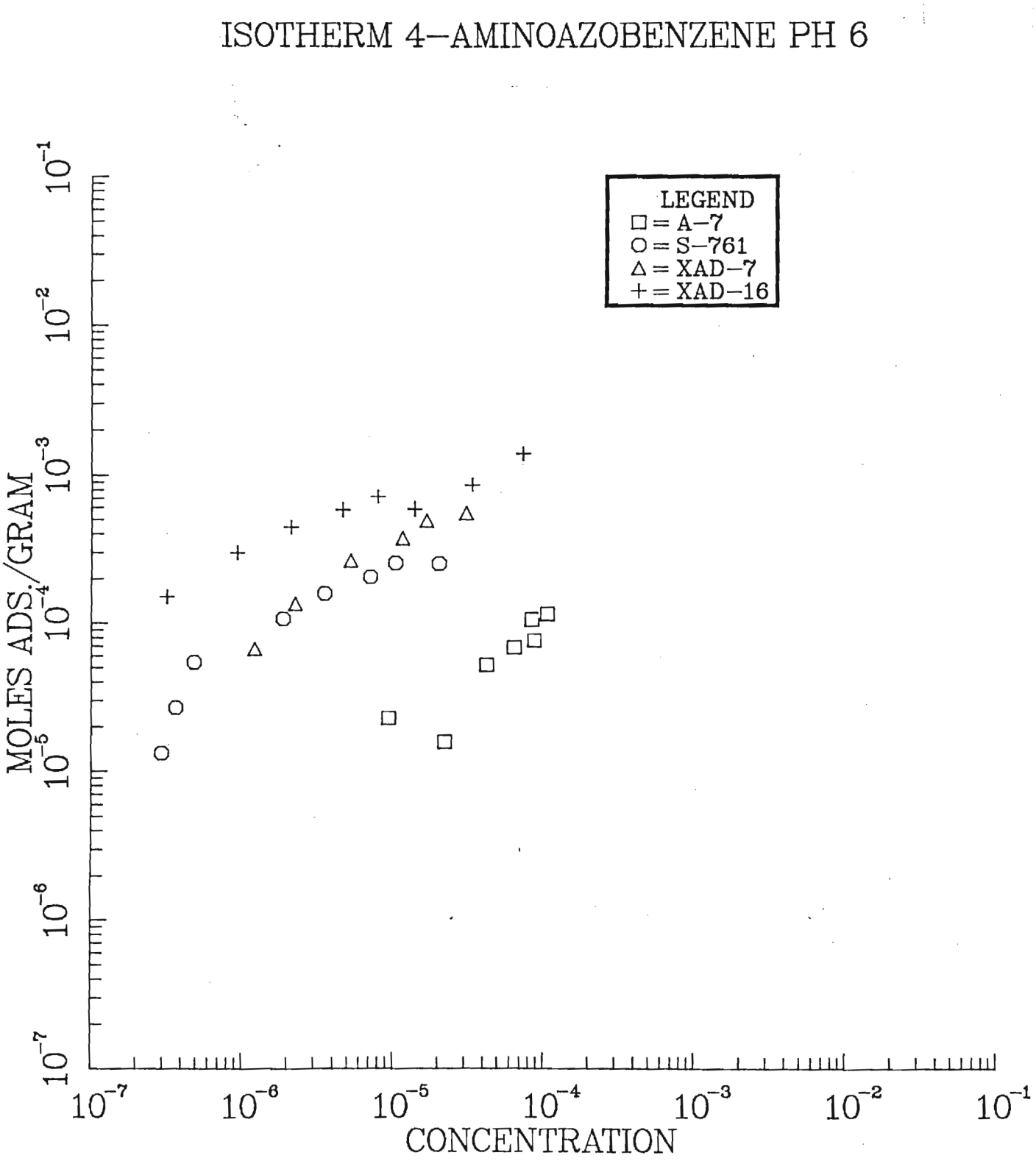

Figure 6. Adsorption Isotherms for 4-Aminoazobenzene.

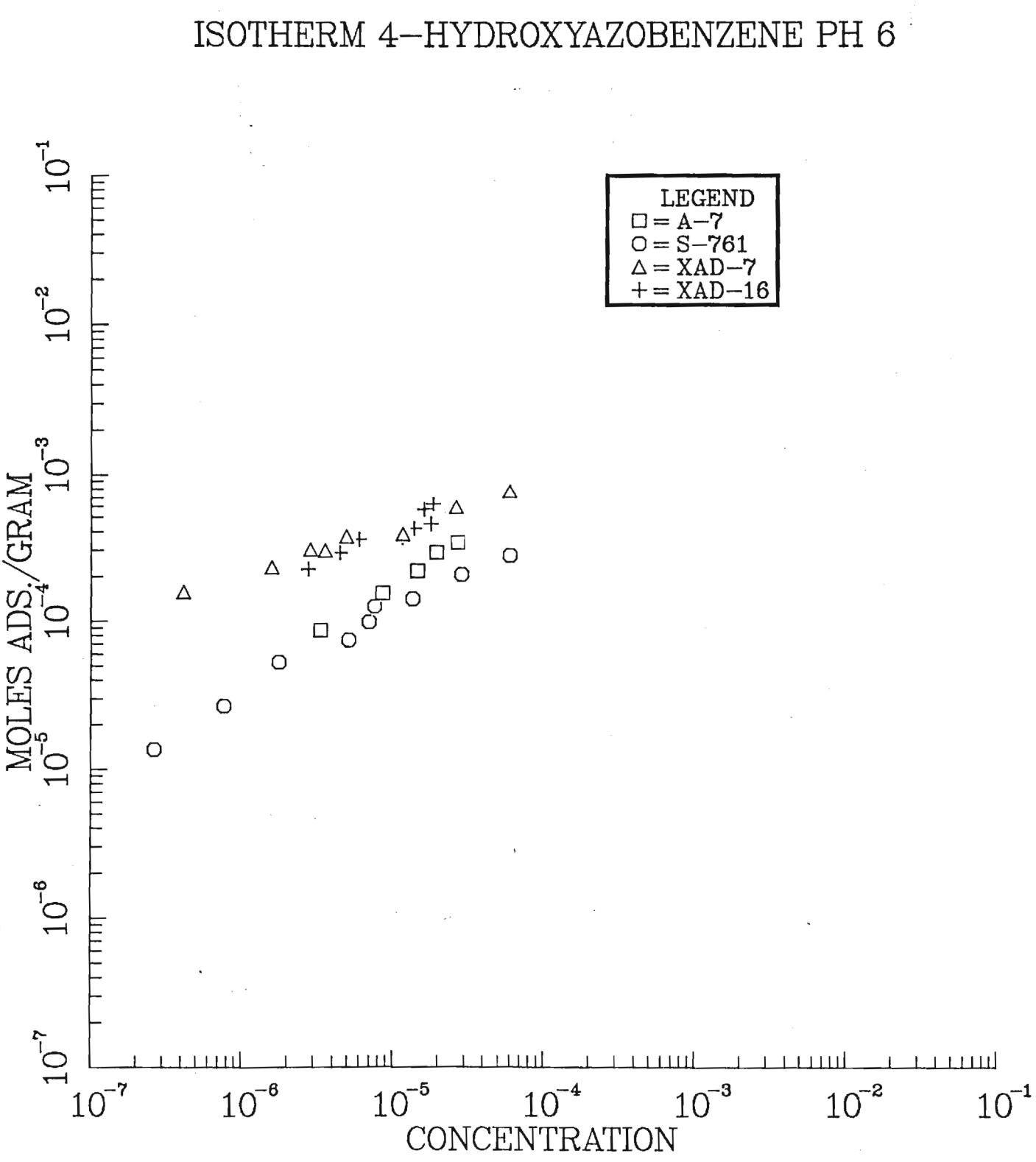

Figure 7. Adsorption Isotherms for 4-Hydroxyazobenzene.

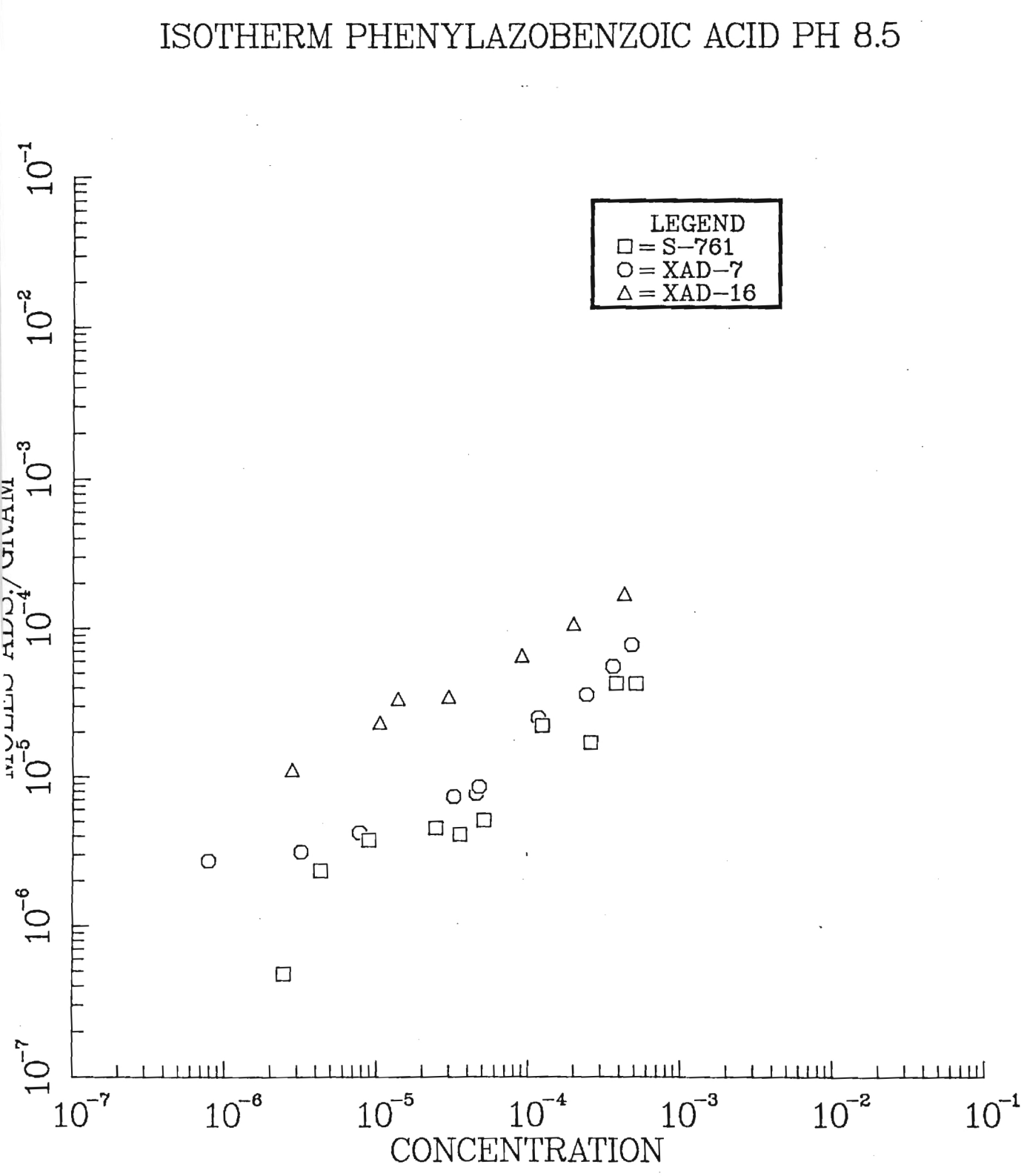

Figure 8. Adsorption Isotherms for Phenylazobenzoic Acid.

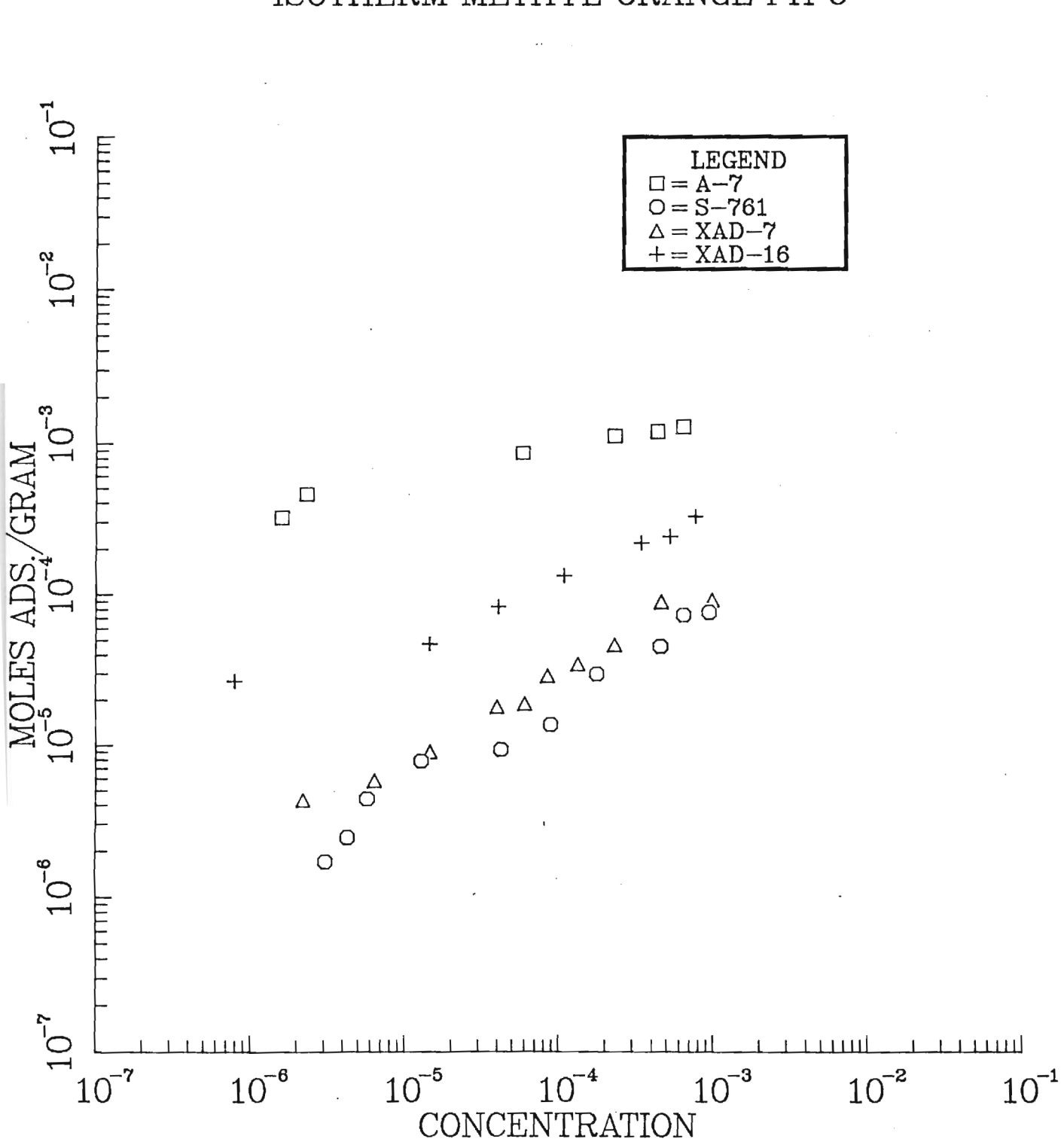

Figure 9. Adsorption Isotherms for Methyl Orange.

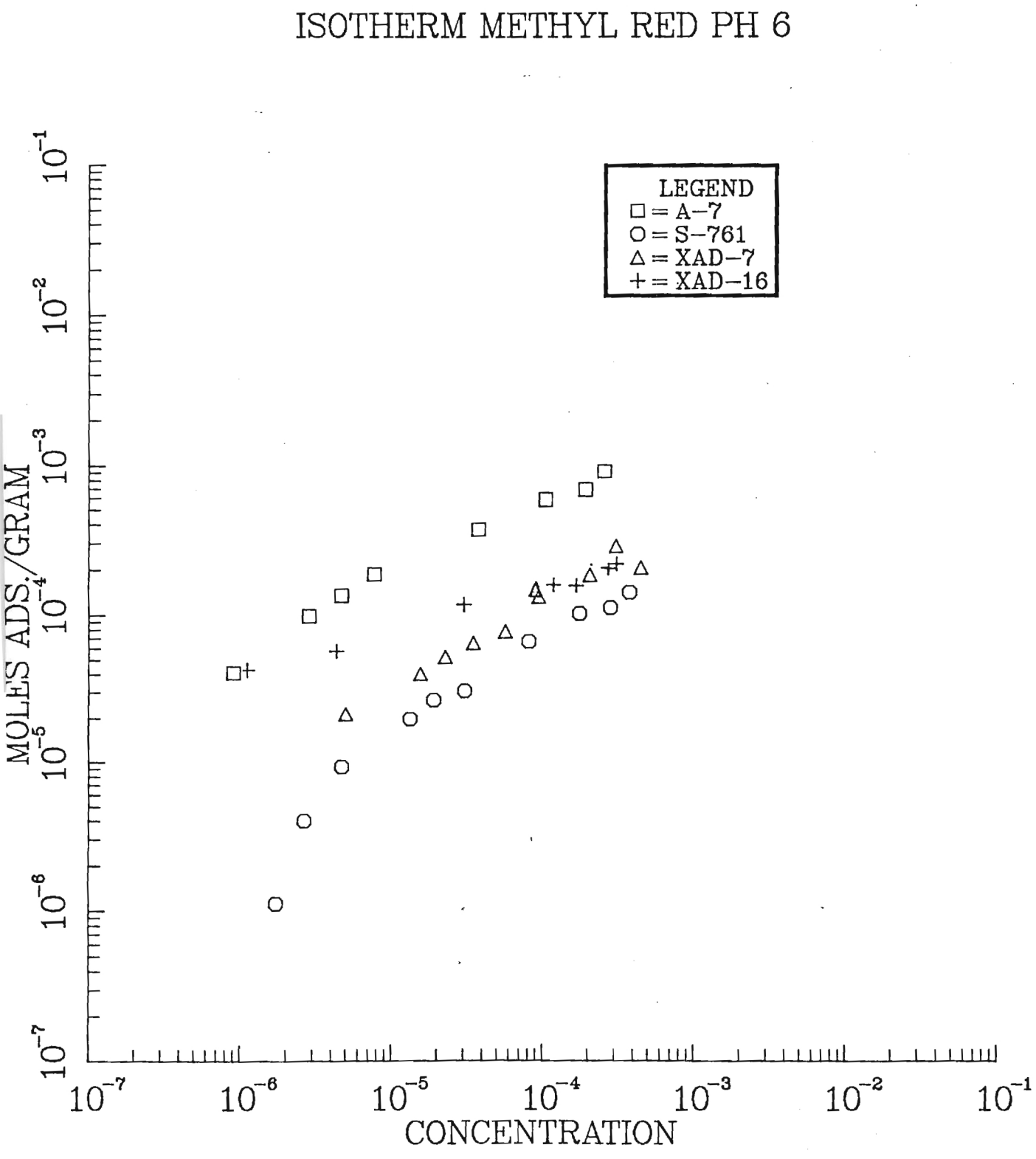

Figure 10. Adsorption Isotherms for Methyl Red.

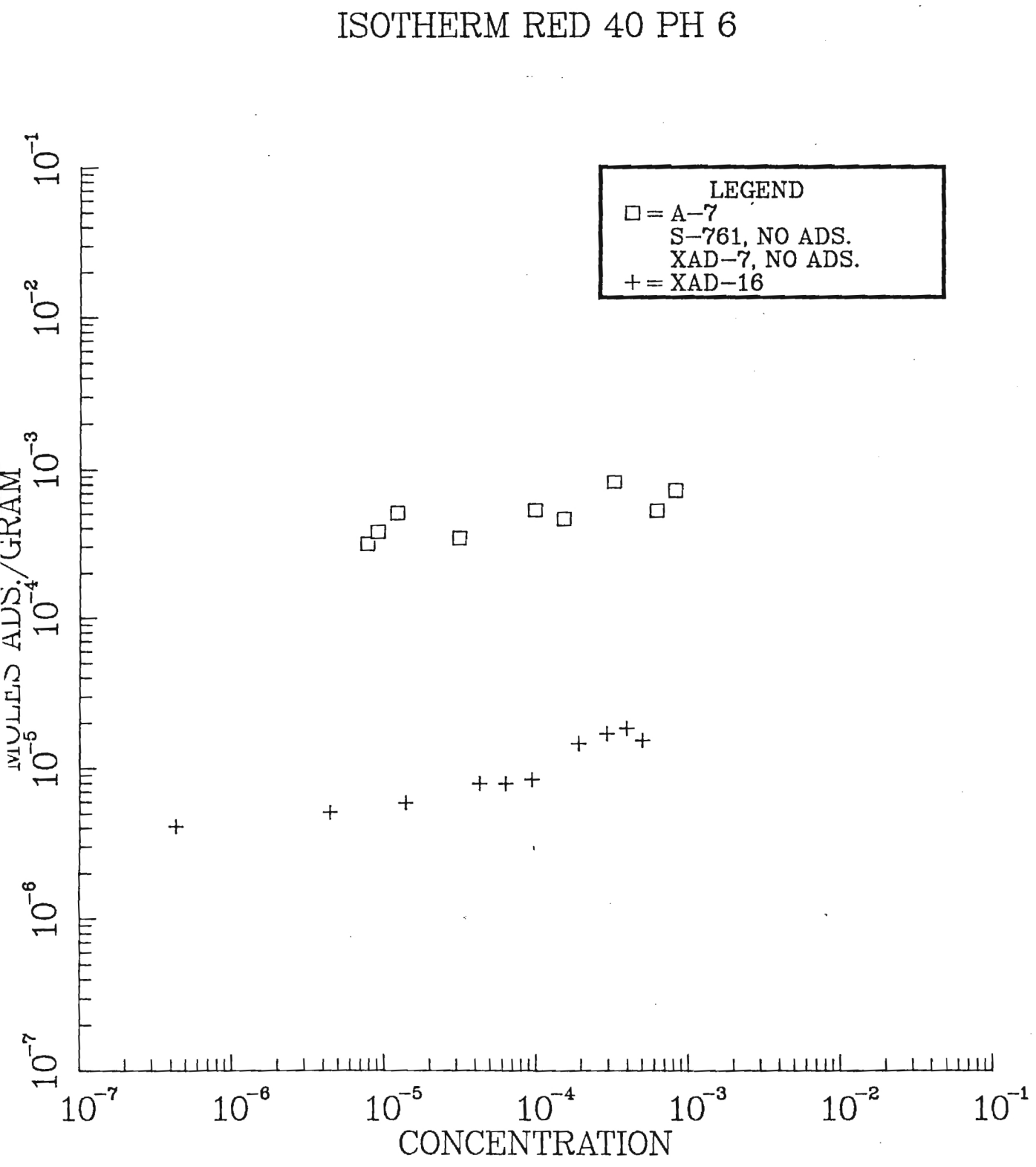

Figure 11. Adsorption Isotherms for FD&C Red 40.

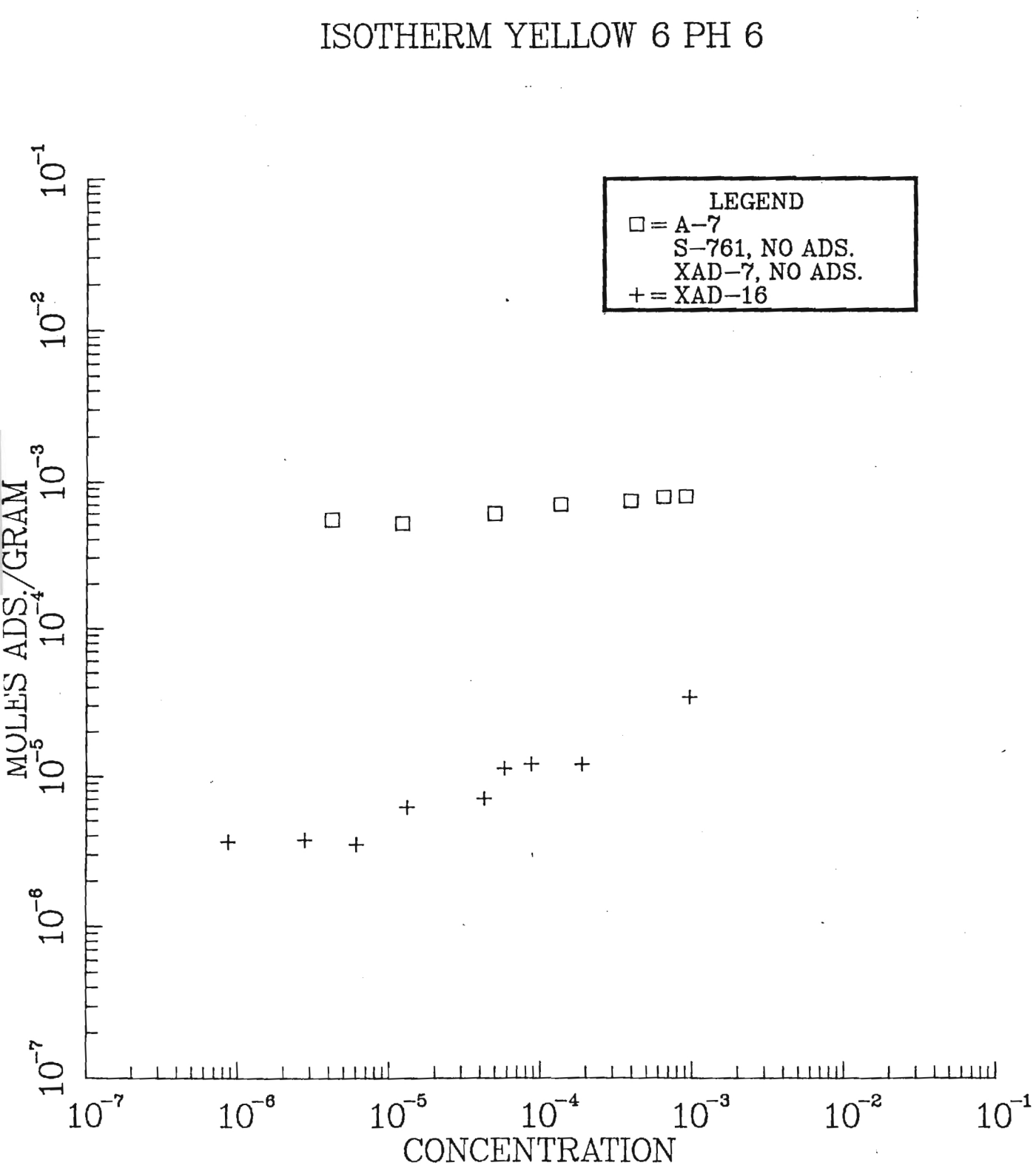

Figure 12. Adsorption Isotherms for FD&C Yellow 6.

orange, red 40 and yellow 6, it was likely that an ion exchange mechanism prevailed in the removal process. However, for a neutral compound, such as p-nitrophenol, the dominate mechanism was most likely physical adsorption. XAD-16 adsorbed 4-aminoazobenzene and phenylazobenzoic more strongly than the other resins. XAD-7 and XAD-16 exhibited the highest adsorption capacity for 4-hydroxyazobenzene. Red 40 and yellow 6 were the least adsorbable compounds on all resins except A-7. This could possibly be attributed to the higher solubility of the red 40 and yellow 6 in comparison to the other dyes. The effectiveness of A-7 may have been due to ion exchange with the sulfonic acid functional groups present in red 40 and yellow 6.

The same order of adsorption affinity was observed in both S-761 and XAD-7. 4-Aminoazobenzene and 4-hydroxyazobenzene were adsorbed most strongly followed by p-nitrophenol, methyl red, methyl orange, and phenlyazobenzoic acid. Neither red 40 nor yellow 6 adsorbed on S-761 or XAD-7. XAD-16 followed a similar pattern with 4-aminoazobenzene and 4-hydroxyazobenzene being adsorbed in the largest quantity and methyl orange, methyl red, phenylazobenzoic acid, and p-nitrophenol, adsorbing in the same region. The most poorly adsorbed compounds on XAD-16 were red 40 and yellow 6. All the compounds adsorbed similarly on A-7 with the exception of 4-aminoazobenzene. 4-Aminoazobenzene did not adsorb well due to the positive charge on the compound at the pH studied.

Future efforts in the batch equilibrium phase of this project will be directed toward generating supplemental data as well as evaluating how well isotherm models, such as those of Freundlich and Langmuir fit the experimental data. The fitted isotherm expression will be incorporated into the overall model being refined, to account for adsorption equilibria in the prediction of breakthrough curves. Finally, efforts will be directed toward the linking of structural differences in the compounds and resins with variations in the adsorption behavior.

RESIN CONDITIONING

In the early part of the summer much time and effort was expended on cleaning the adsorbent resin, XAD-16. This was the first of the resins to be cleaned and emphasis was placed on bulk processing, to save time and to assure consistency in the quality of the resin. The resin cleaning procedure consisted of:

1. distilled water rinse to remove fines (upflow column);

2. a 24-hour Soxhlet extraction with methanol; and,

3. rinsing, as necessary, to remove methanol from the resin (upflow column).

In an effort to accelerate the process, a large extraction unit was borrowed from Geophysical Sciences, but it proved unusable. The design of the unit did not permit a periodic draining of the solvent as in a Soxhlet extraction apparatus. Instead, the resin and the solvent remained in contact throughout the procedure, resulting in low efficiency. Therefore, small Soxhlet extraction units (as used before) were employed. Four of these units were available. By operating all four of these units simultaneously, a large volume of resin could be washed in a single time period.

The distilled water rinse was found to be the most time-consuming step in the bulk resin clean-up process. Initially, two glass columns (1" I.D. x 36" length) were operated in the upflow mode. Since it has become clear that this is an inordinately slow method of rinsing the resin, a larger glass column (3" I.D. x 36" length) will be used for all remaining upflow rinses. When available, a schedule to clean all remaining resins will be instituted. This will permit the washing of larger quantities of resin to insure quality control and save time. The savings in time will be especially evident when cleaning the A-7 resin, which requires successive treating with several solvents.

COLUMN STUDIES

The early months of the summer were devoted to the design and construction of the column systems to be used in these studies. An initial pair of column studies was conducted in mid-July on the basis of which several substantial structural changes in the design and set-up of the system were carried out. The purpose of these changes was to facilitate access to the apparatus and to make easier the response to and correction of leaks in the system. In addition, several weeks were spent conditioning the entire stock of XAD-16 resin. This procedure has since been changed and is described in a subsequent section. The results of each of the column experiments is described separately below.

An initial set of two column studies was conducted on July 19, 1985. The adsorbate was methyl orange, while the adsorbent was XAD-16. The concentration of methyl orange in the feed solution was 2×10^{-4} M and each of the columns was charged with 11.6 g (dry weight basis) of the resin. The solution flow rate was 36 ml/min, equivalent to 65 bed volumes per hour. The runs were conducted for a period of three hours. The resulting breakthrough curves are shown in Figure 13. As can be seen, the two breakthrough curves were essentially similar to each other indicating an excellent degree of reproducibility in these systems. While substantial initial breakthrough was quite rapid with 50% breakthrough attained at 30-60 minutes, the ultimate attainment of full capacity was very gradual. Indeed, only 70-75% of full capacity had been attained after one hour and there was virtually no change thereafter up to termination of the studies at three hours.

During these studies several unattractive features of the experimental apparatus became apparent. The entire system was cumbersome to use. It was difficult to pack the resins in the temperature regulation bath. Similarly, leaks were hard to detect and the columns, once in place, were almost impossible to observe. Changing influent reservoirs, without adding air to the system, was not possible. The arrangement of long lengths of copper tubing between reservoirs and pumps, and pumps and columns, is unnecessary and undesirable.

The researchers, therefore, rebuilt the entire system according to the following objectives: 1) Elimination of the temperature regulation bath thereby providing greater control over the system and more ease in manipulating it. Temperature will be maintained by control of the laboratory temperature and monitored continuously to insure that it remains essentially constant. 2) A general restructuring of the system was carried out which made it more user friendly, less space intensive, and provided greater access to the various components. 3) Installation of valves and quick connectors to now permit facile changing of reservoirs without entraining air.

After the system was rebuilt, a second set of column adsorption studies with methyl orange and XAD-16 was conducted. Two columns were run as replicates. The experimental set-up was identical to the July 19 study except that less concentrated solutions (9.85×10^{-5} and 9.43×10^{-5} M) and less resin (8.24 and 8.34 g dry weight) were used. A reduced flow rate (12 ml/min = 720 ml/hr), equivalent to 30 bed volumes per hour, provided greater contact between solute and resin than in the previous runs. This also resulted in

less short circuiting and provided smooth breakthrough curves (Figure 14). Although samples were collected for 25 hours, complete breakthrough was not achieved. A decision must be made for future studies. If complete breakthrough is needed, it may be necessary to change some of the design parameters or to tolerate very long adsorption runs, or both.

Regeneration with 0.05 N and 0.1 N NaOH was attempted, unsuccessfully. The methyl oragne solution trapped within the sand bed dissolved in the base and was removed from the system. However, no detectable migration of the solute from the adsorbed phase to the solution phase was recorded.

The new column system functioned well. The problems with entrapped air, observed in the first experiment and described below, did not recur, and influent reservoirs could be changed with more precision and control. The new design is less cumbersom to use and provides the necessary control over system hydraulics.

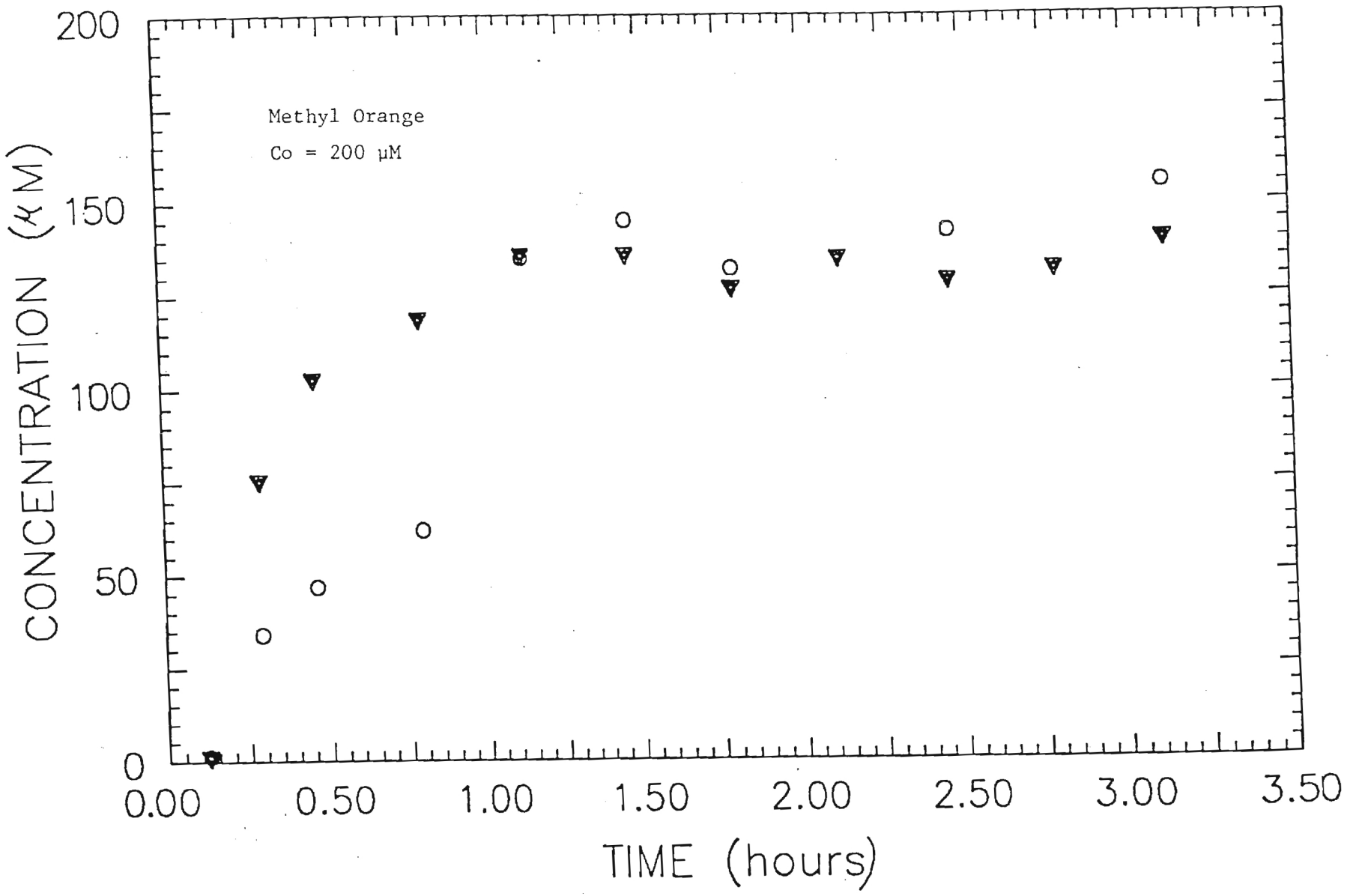

Figure 13. Column Adsorption Studies of July 19, 1985

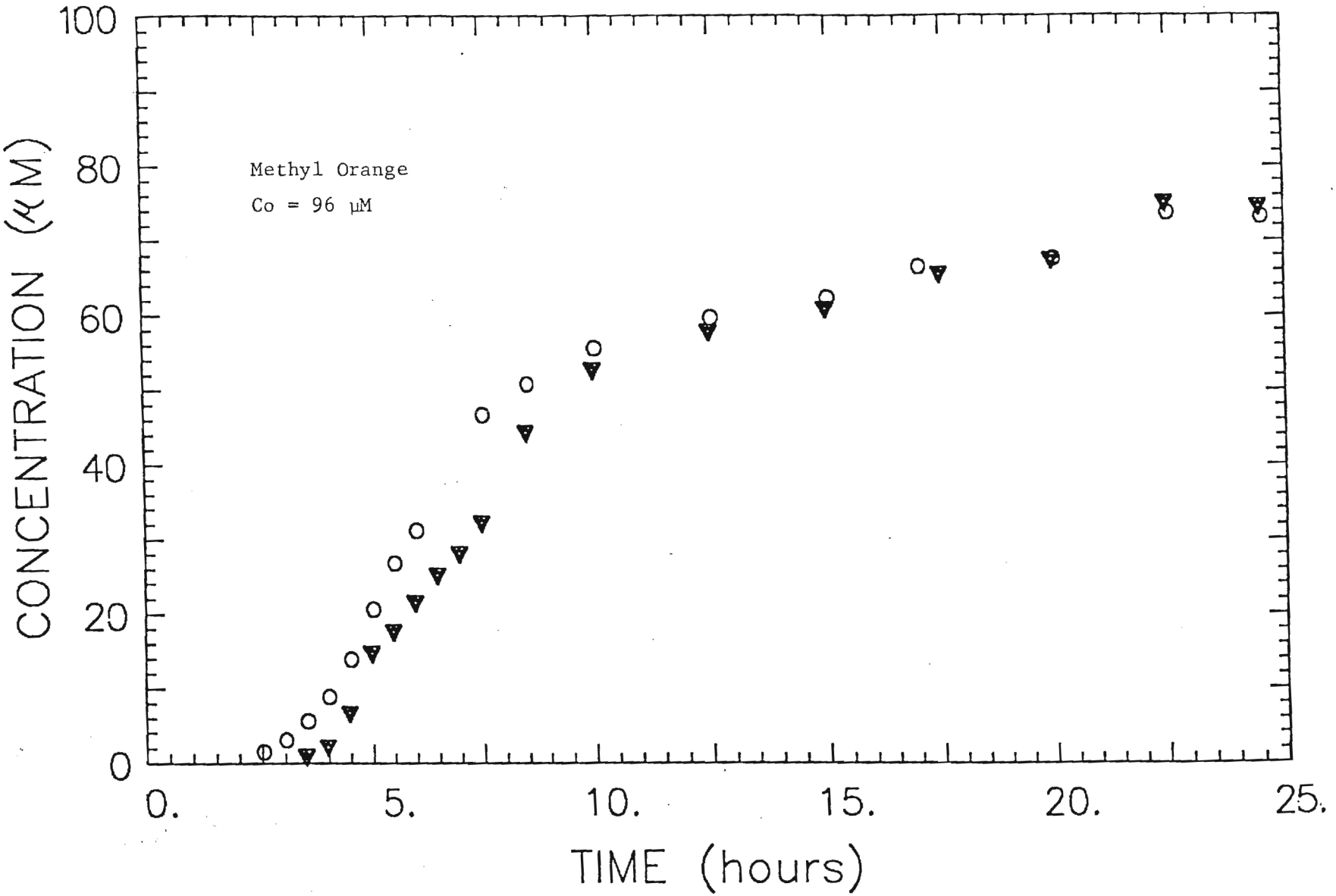

Figure 14. Column Adsorption Studies of September 10, 1985

REGENERATION

Following termination of the first pair of column adsorption studies, regeneration was carried out by passing methanol through the columns at the same volumetric flow rate as was used for the adsorption studies. After approximately 40 liters of methanol had been passed through each column no further methyl orange was being eluted and regeneration was assumed to be essentially complete. At this point, the columns still retained substantial methyl orange as evidenced by their intense orange color. The volume of regenerant was more than six times the original volume of adsorbate solution. This is obviously not an ideal regeneration technique.

Further problems were encountered when it was attempted to wash the columns with water in preparation for a second set of adsorption studies. The passage of water into the methanol saturated columns resulted in the immediate formation of large air bubbles in the resin beds. This phenomenon which has been observed in many mixed solvent sorption systems may be due to factors such as differences in oxygen solubility and temperature changes consequent to the thermodynamics of dissolution of one solvent in another. While the exact cause of this phenomenon is unclear, the effect is to produce essentially irremediable air binding sufficient to render the adsorbent column unusable for subsequent sorption studies. This is obviously an area which will need substantial further study.

Because of problems encountered in the regeneration of methyl orange from XAD-16, it was decided on completion of the second set of column studies, to collect some preliminary, qualitative data on possible regenerants. Resin, impregnated with methyl orange, from the second column adsorption study was divided into eight, approximately equal, amounts, which were placed in 125 ml glass bottles. To these, the following solutions (100 ml) were added: deionized water, concentrated HCl, saturated triethyl amine, methanol, methanol with 5% HCl, NaOH (1 N and 0.5 N) and ammonium hydroxide. The bottles were placed on a laboratory shaker and allowed to mix for 2 days.

Methanol, acidified methanol and saturated triethyl amine were the best regenerants. Some removal occurred with ammonium hydroxide and deionized water, but both acids and bases were ineffective.

In summary, problems encountered this summer with the column adsorption system and the cleaning of resins appear to have been solved. Column studies will be continued this fall at a minimum rate of one set per week. Immediate plans are to examine sorbates other than methyl orange and to retain the same resin, XAD-16. Additionally, batch kinetic studies will be completed. When enough complementary batch and column data have been collected, work with the computer simulation models will begin.

E-20-661

Progress Report through January 1986
(Project Number E20-661)
(Grant Number 14-08-0001-G-1070)
(Sponsor: U.S. Geological Survey)

This most recent period of research was characterized by operational difficulties which have seriously delayed progress. Specifically, while column adsorption studies on methyl orange, Red-40 and Yellow-6 using XAD-16 resin proceeded smoothly, methanol regeneration gave rise to a phenomenon which rendered the regeneration process essentially inoperable. This phenomenon was the development of massive numbers of gas bubbles in each column shortly after the initiation of methanol flow. This led to head loss of sufficient magnitude as to prevent flow totally at times.

Three possible explanations for this phenomenon were advanced based on consultations within the research group and with personnel in Chemical Engineering and at Rohm and Haas.

1. Biological activity within the columns might have been producing CO_2 and other gases. The coincidence of the gas formation with the introduction of essentially pure methanol rendered this unlikely.

2. Catalytic conversion of methanol to methane by dye sulfonic acid groups sorbed on the resin was occurring. The column head space gases were analyzed by means of a gas partitioner to investigate this possibility. The gases in the head space were found to correspond with air in composition. No methane was detected.

3. Outgassing of air adsorbed from the aqueous solutions was occurring. This explanation was favored by the Technical Support Manager of the Fluid Process Chemicals Group at Rohm and Haas who also informed us that he had observed the same phenomenon.

Assuming this was the correct explanation, it was decided at the end of January to operate the columns under pressure. (Previously the system was open to the atmosphere). A pressure regulator was installed on the Yellow-6 column which had been standing for over one month. The bed of this column had lost its integrity, being riddled with gas bubbles. Water was pumped through the column under approximately 1 atm excess pressure. Within one hour all visible air spaces were removed. Subsequently, when methanol was pumped through the column no additional air spaces were generated.

At present, pressure regulators have been placed on order. When they are received, the column system will be replumbed, and all further experiments will be conducted under pressure. The kinetics of adsorption/desorption are not expected to be noticeably affected.

Taking into account the implications of inconsistent regenerant flows, some data can be presented on both dye adsorption and desorption in column systems on XAD-16 resin (Figures 1-6). During desorption studies, methanol

water mixtures were occasionally substituted for methanol alone in an effort to minimize the gas bubble formation. The periods when these mixtures were used are depicted on the plots by solid circles. Most striking is the highly irratic flow rate resulting from bubble fouling and consequent head loss problems. Otherwise, it is clear that attainment of effluent levels in excess of 90% of influent levels of dye concentration during the adsorption phase was rapid in all cases. Data on regeneration are much more difficult to evaluate. However, an estimate of percent of adsorbed dye desorbed by methanol in these studies is presented in Table 1.

Table 1. Dye Adsorption and Recovery

Dye	Grams Adsorbed	Grams Desorbed	% Desorbed
Methyl Orange (MO)	0.478	0.079	16.5
Yellow-6 (Y6)	0.148	0.056	37.9
Red-40 (R40)	0.176	0.016	9.0

Again it must be emphasized that the desorption data presented above were obtained from rather unsatisfactory experimental studies and any effort at interpretation of these results must await acquisition of more reliable data.

Batch Kinetic Studies

Batch kinetic studies are well underway. Initial plots for the kinetics of adsorption of 4-aminoazobenzene (4-AAB), 4-hydroxyazobenzene (4-HAB) and methyl red are shown in Figures 7-10.

Program for the Upcoming Report Period

The next quarter of this project will see completion of most of the batch adsorption kinetic studies and substantial progress in the completion of several column adsorption and desorption studies using the pressurized system to prevent outgassing and consequent resin bed fouling. Upon acquisition of reliable data, the mathematical model for this system will be tested and the process of model verification and refinement initiated.

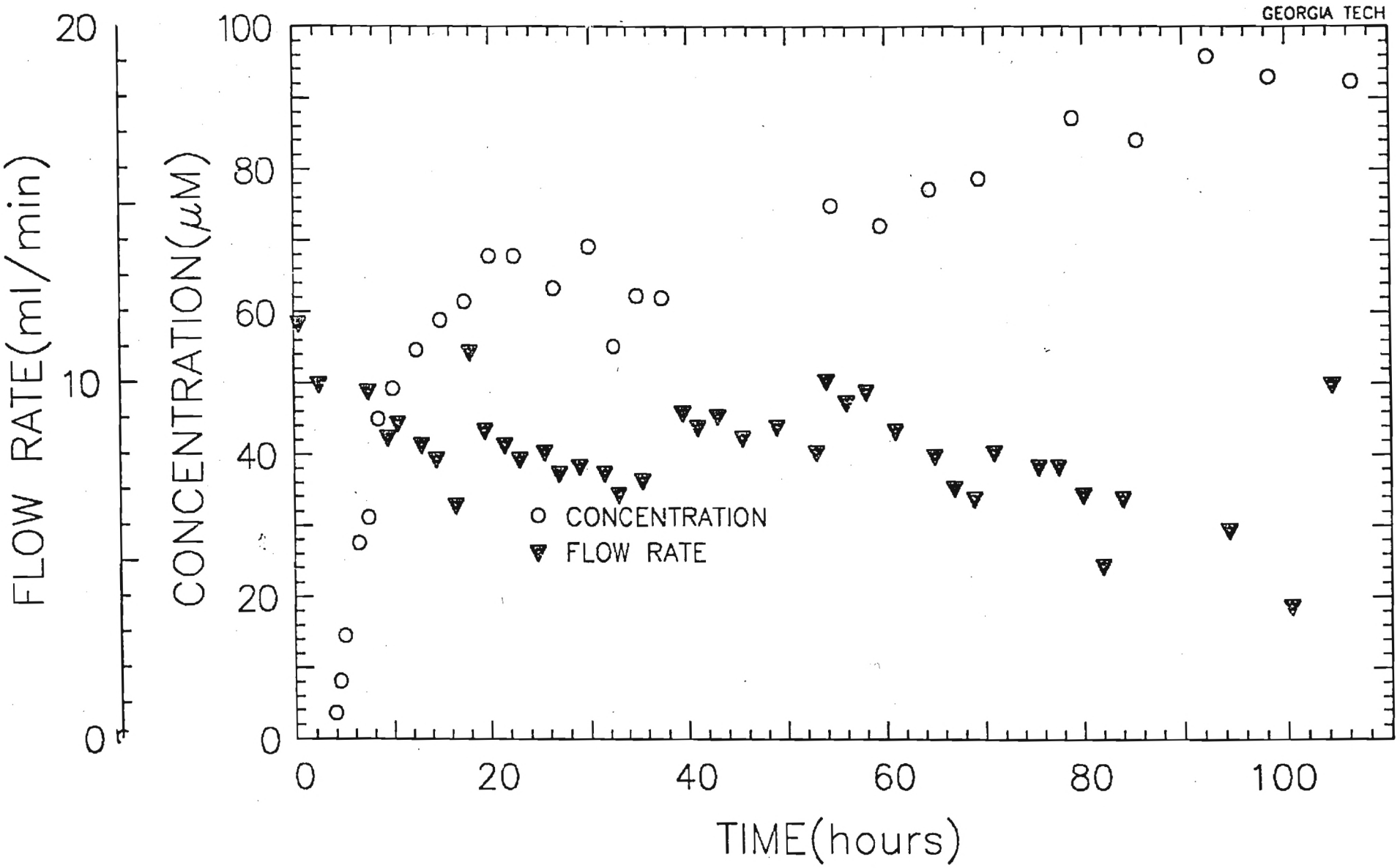

Figure 1. COLUMN ADSORPTION OF M.O. ON XAD-16

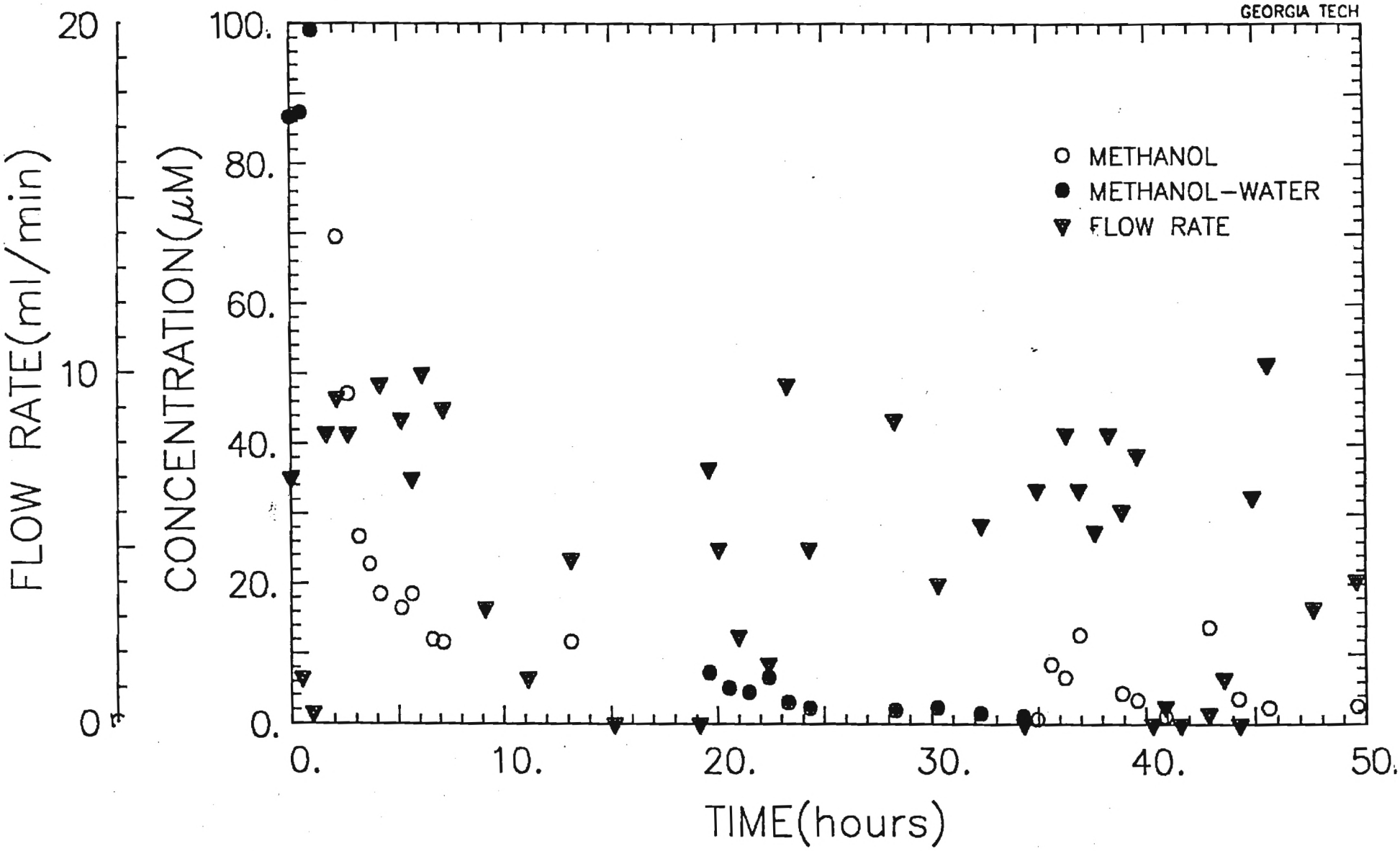

Figure 2. COLUMN DESORPTION OF M.O. FROM XAD–16

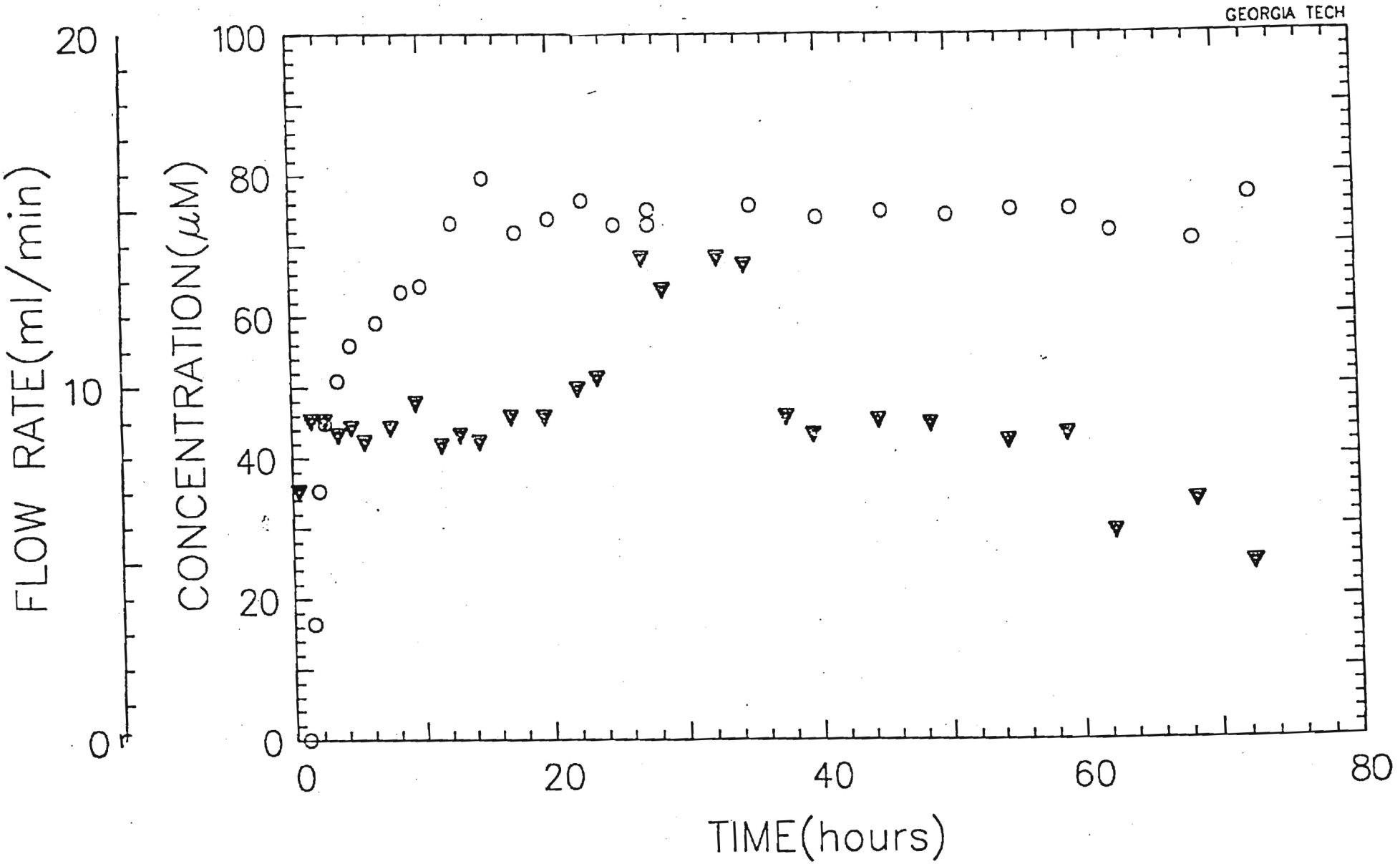

Figure 3. COLUMN ADSORPTION OF R40 ON XAD-16

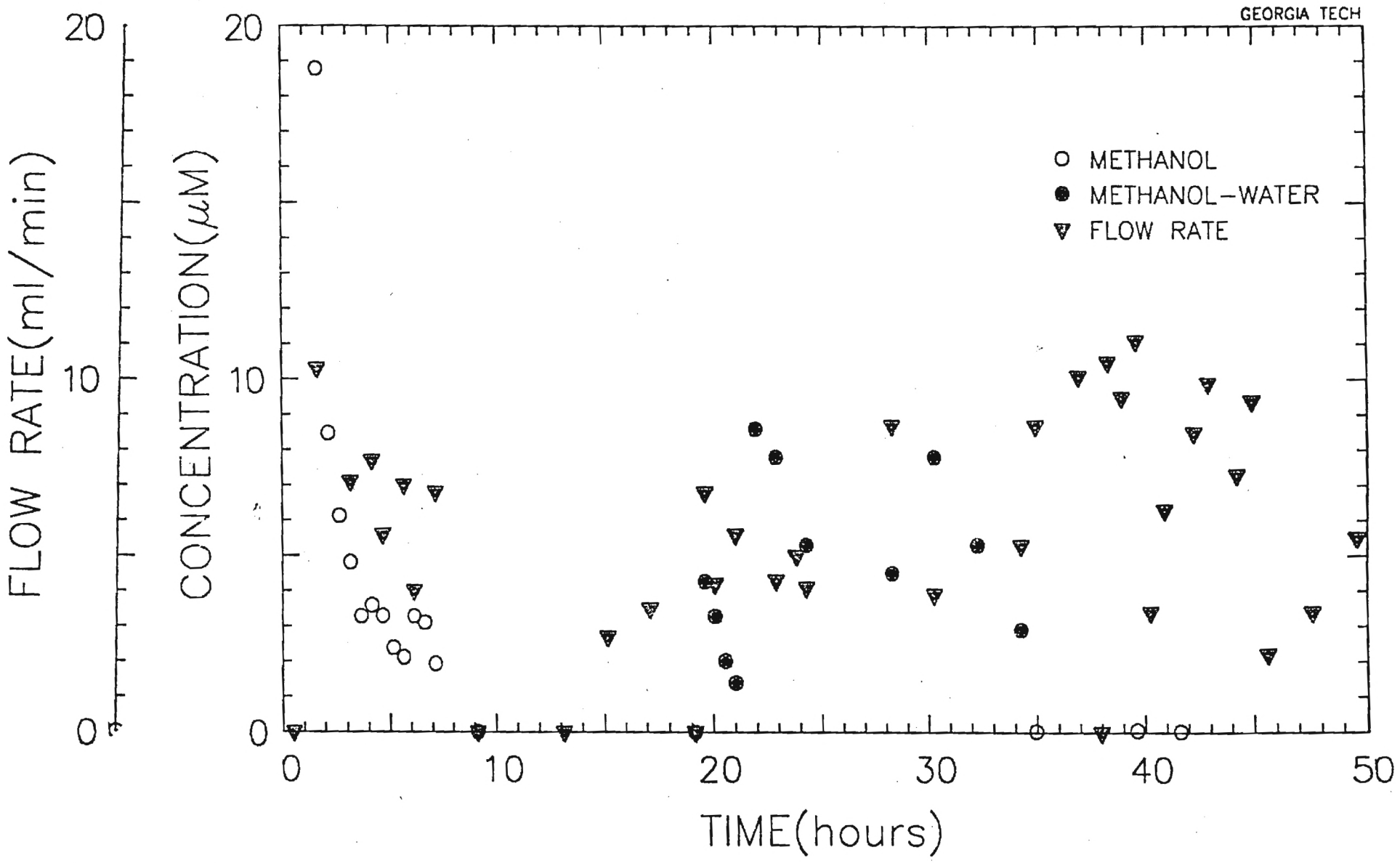

Figure 4. COLUMN DESORPTION OF R40 FROM XAD–16

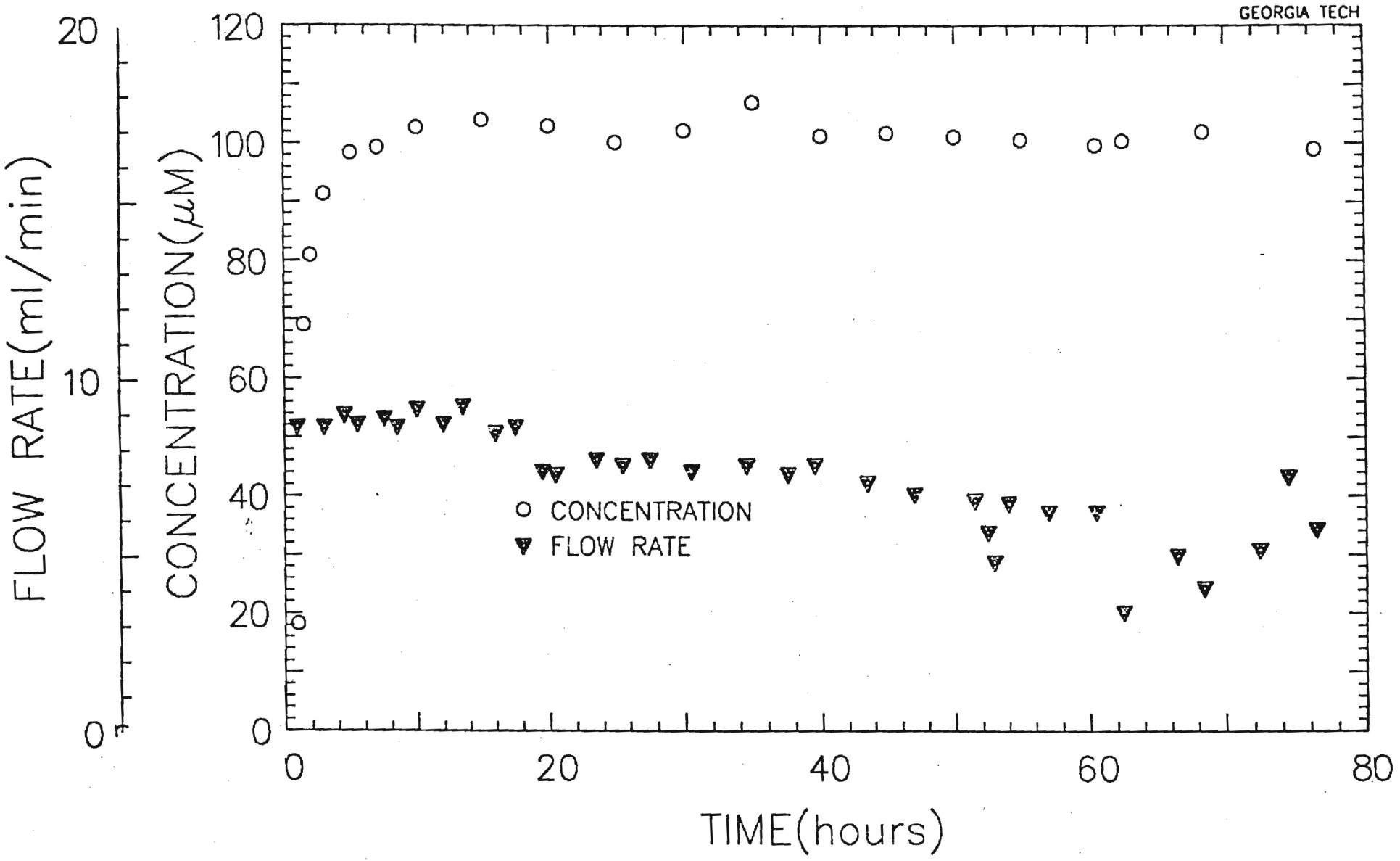

Figure 5. COLUMN ADSORPTION OF Y6 ON XAD-16

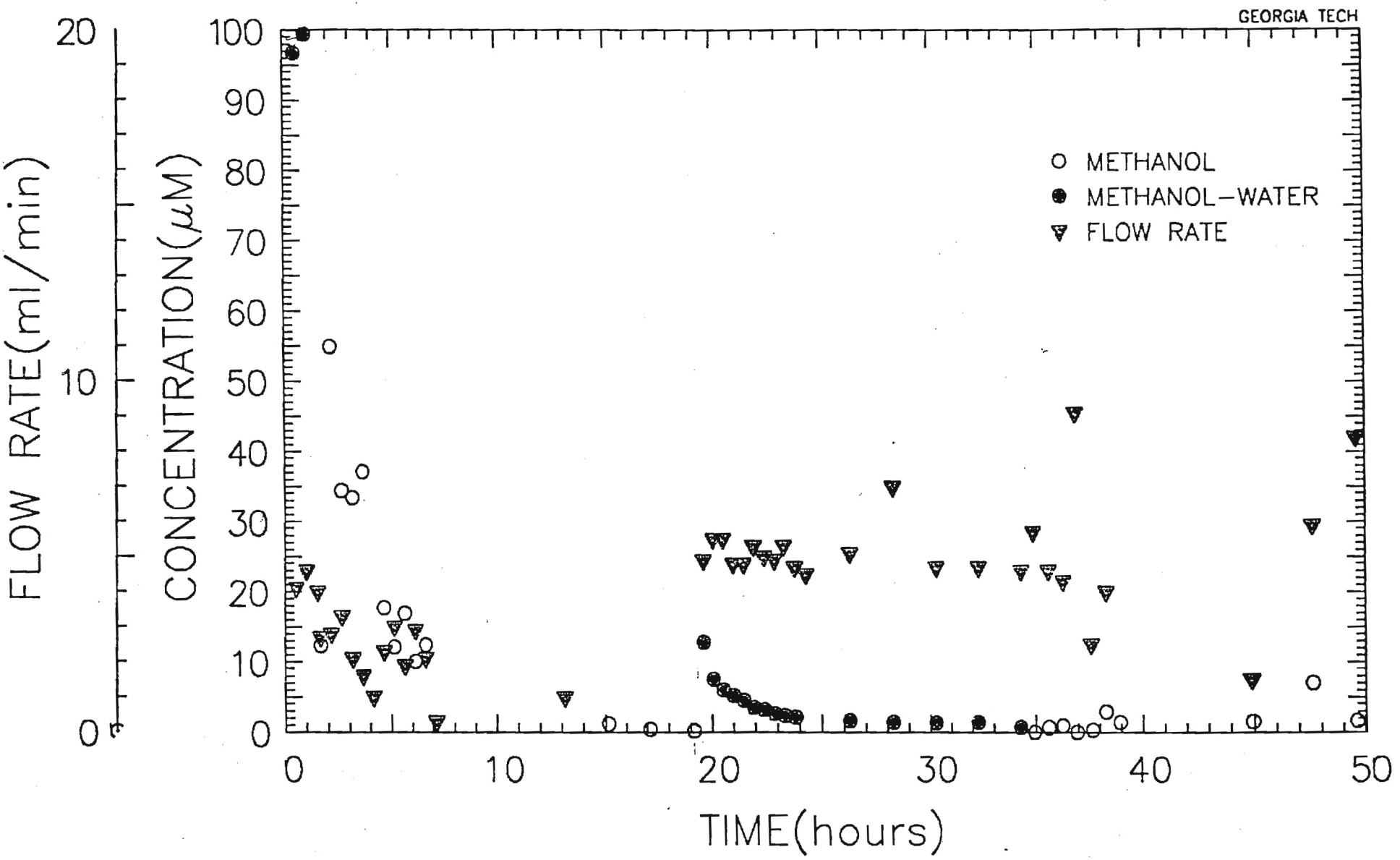

Figure 6. COLUMN DESORPTION OF Y6 FROM XAD–16

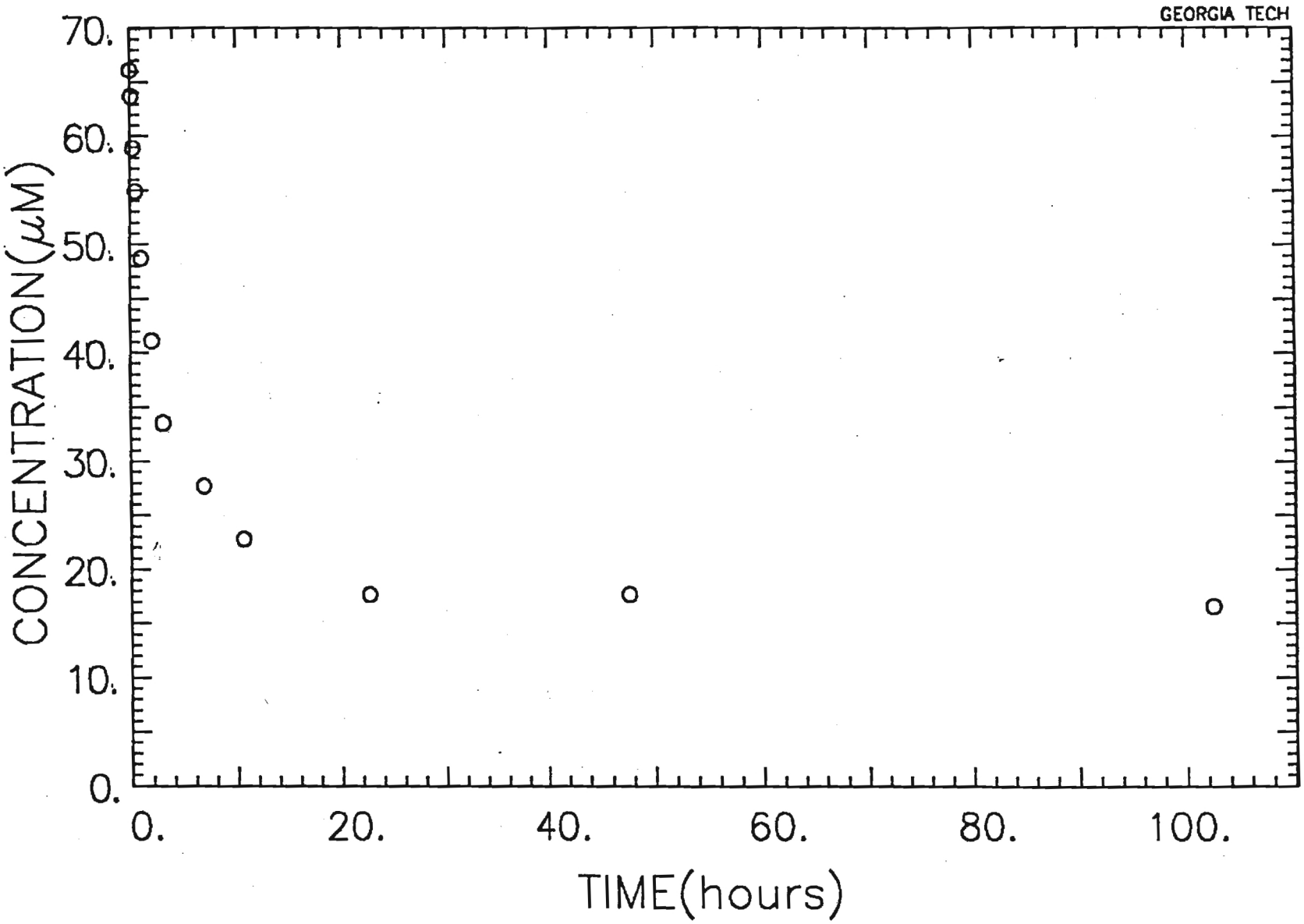

Figure 7. BATCH KINETICS OF 4-AAB ON XAD-7

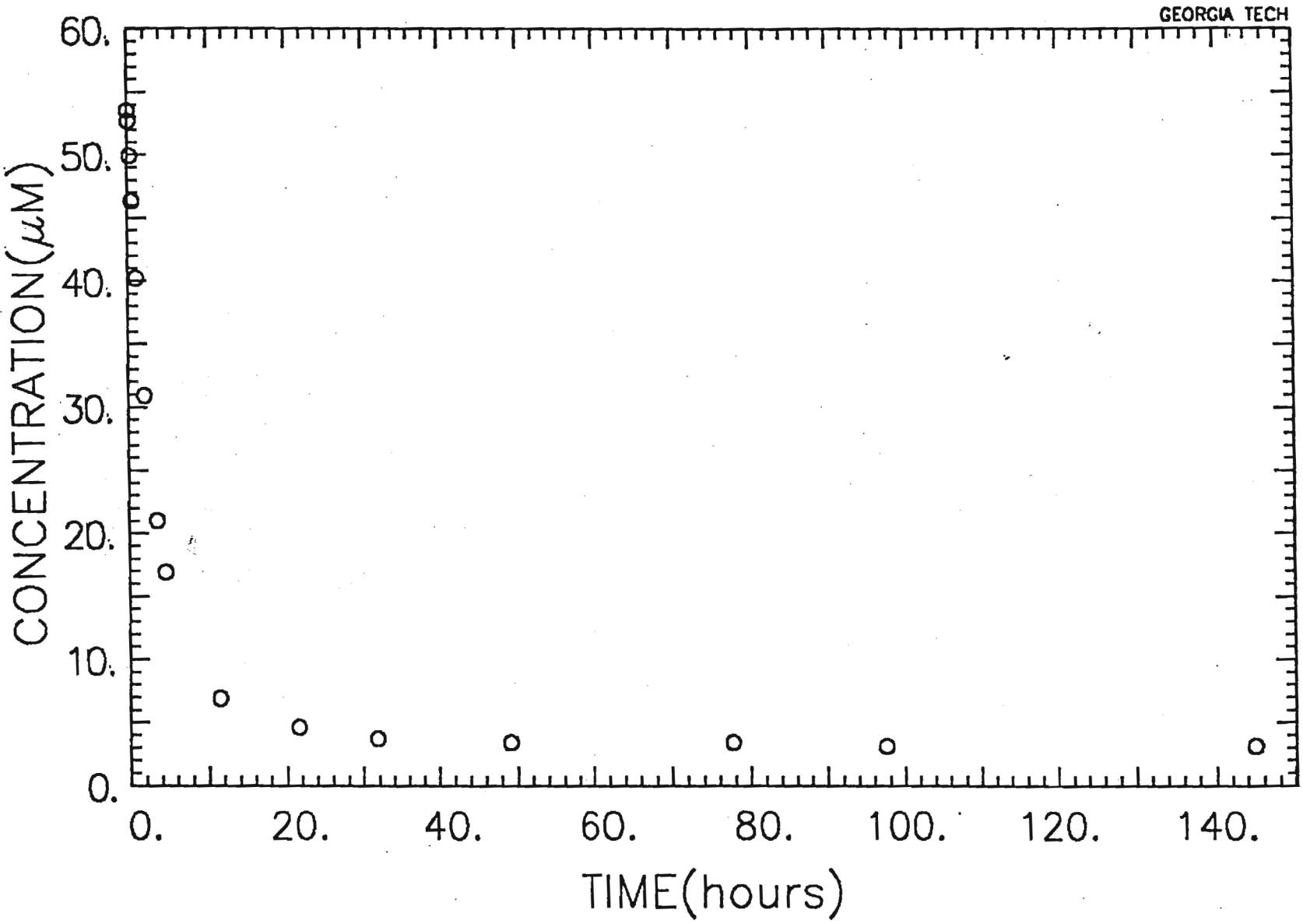

Figure 8. BATCH KINETICS OF 4-AAB ON XAD-16

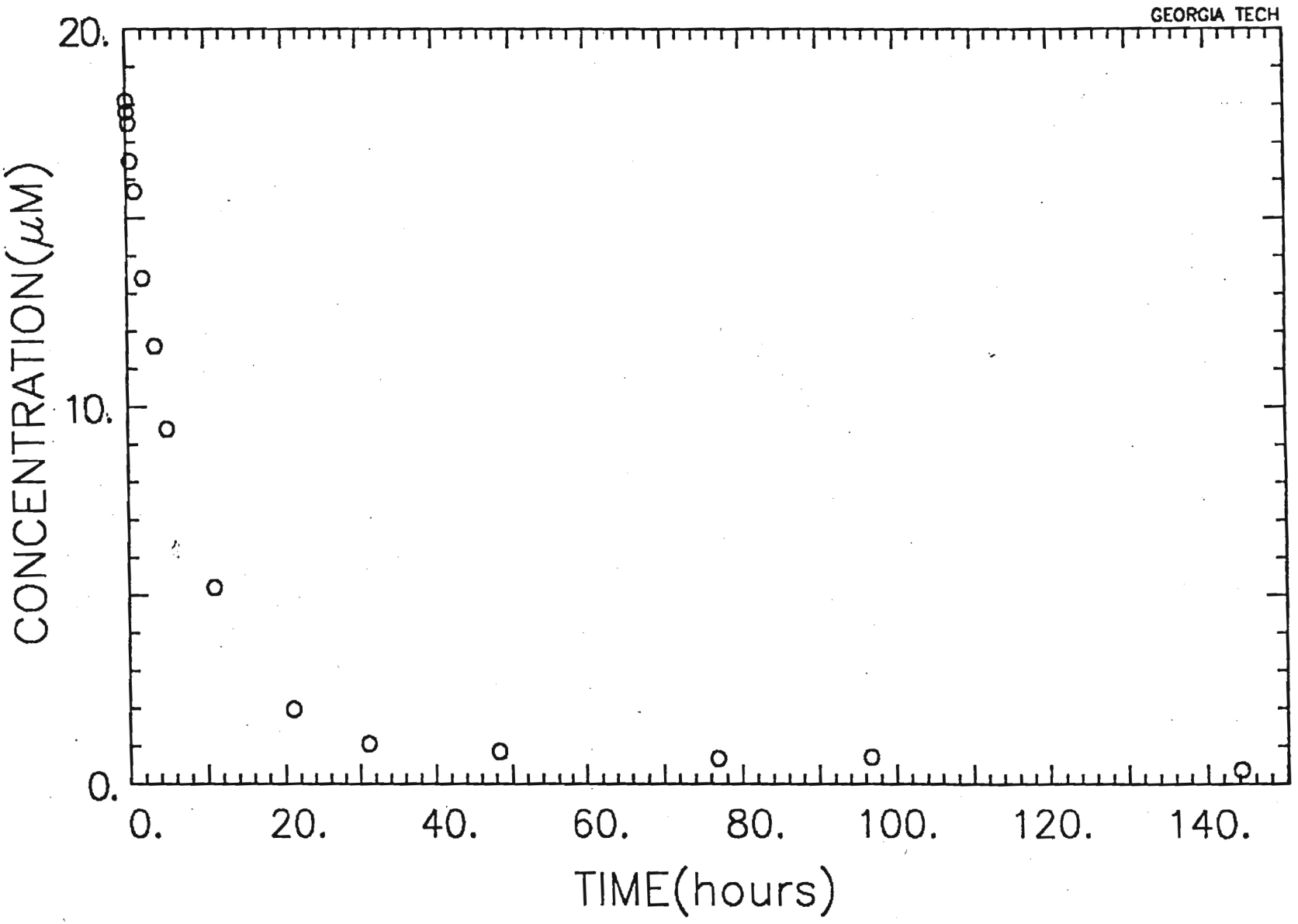

Figure 9. BATCH KINETICS OF 4-HAB ON XAD-16

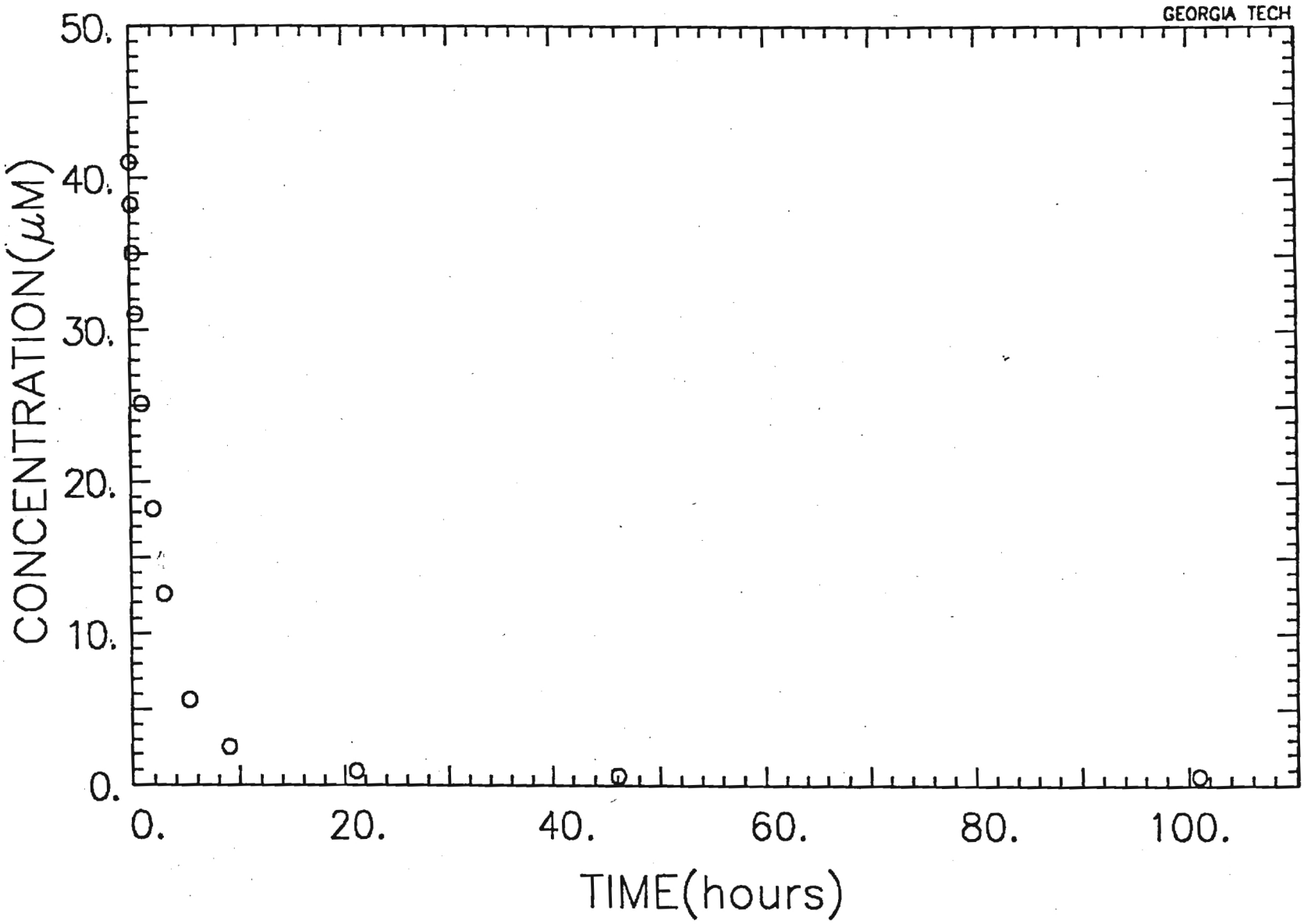

Figure 10. BATCH KINETICS OF MR ON XAD-16

PROJECT PROGRESS REPORT TO OCTOBER 1, 1986

Project Title: Adsorption of Organic Dyes on Synthetic Resins from Textile Wastewaters

Project Number: E-20-661

Grant Number: 14-08-0001-G-1070

Sponsor: U.S. Geological Survey

Investigators: Dr. Joseph P. Gould
Jack Mizner
Kim Groff

Project Location: School of Civil Engineering
Georgia Institute of Technology
Atlanta, GA 30332

During this reporting period the final stages of data collection were completed. Included were sequential batch adsorption and desorption kinetic studies and column adsorption and desorption studies. The latter studies had been significantly delayed by the production of gas bubbles in the columns during the regeneration phase. This had the consequence of producing significant head loss in the systems with total loss of regenerant flows. It was concluded that this phenomenon was a result of desorption of air from the resin upon contacting with the solvent.

The solution of the problem necessitated redesign the column systems in such a way as to permit imposition of pressure in excess of ambient throughout the column systems. It was found that a pressure of ~0.07-0.10 atmospheres above ambient was sufficient to suppress totally the generation of these bubbles and permit resumption of column studies. The delay engendered by diagnosis and solution of this problem was approximately three months.

RESULTS

Batch Studies

The adsorption/desorption data obtained for paranitrophenol (PNP) on three commercial resins are shown in Figures 1 through 8. Capacities of the resins for this substrate were uniformly high and strikingly, the recoveries by methanol extraction were very rapid and, in most cases, very near 100% of the originally adsorbed PNP. In systems in which several adsorption desorption cycles were run, the recovery of capacity was also excellent indicating that, for this sorbate, methanol regeneration was an efficient process for recovery of reusable capacity.

Batch adsorption and desorption of methyl orange (MO) is shown in Figures 9 through 17. This dye was found to behave in a manner rather similar to that observed in the case of PNP, although adsorption capacities were somewhat lower in the case of this dye. Recovery of MO and of corresponding adsorption capacities by methanol desorption was very successful and attainment of desorptive equilibrium essentially complete within the first few minutes of the process.

The adsorption and desorption kinetics of the commercial dye Red-40 (R40) are shown in Figures 18 through 21. This dye was characterized by both limited uptake by the resin and limited recovery of capacity on methanol regeneration. It is possible that, while the combination of high water solubility and relatively high molecular size had the effect of hindering adsorption of the R40, by the resins, the dye molecules once adsorbed were quite difficult to desorb by methanol extraction. Interestingly, in both adsorption-desorption cycles on XAD-16 (Figs. 14 and 15) the same quantity of R40 (d19 moles) was recovered by the methanol desorption suggesting that a fixed portion of the resin capacity equivalent in this case to approximately 3 moles per gram was subject to regeneration by methanol extraction while the balance of the capacity was impervious to methanol regeneration. This behavior might be consistent with the presence of two types of sorption sites, one type methanol reversible the other irreversible.

Batch adsorption-desorption kinetics for 4-aminoazobenzene (4-AAB) are shown in Figures 22 through 26. The behavior of this compound was consistent with its low water solubility and substantially hydrophobic nature. Capacities were very high with uptakes of 400-1100 moles per gram of resin obtained. These are adsorption levels which range from ~10 to 20%

of the adsorbent on a weight per weight basis. In addition, only about 20% of this capacity was found to be accessible to methanol regeneration in these systems. Clearly, the very sparingly soluble and hydrophobic 4-AAB adsorbs very strongly on the resins used and once adsorbed is not amenable to desorption to any great extent by methanol extraction. This suggests that solvent extraction efficiency might be substantially reduced when the adsorbed molecule is highly hydrophobic and the regenerant solvent a substantially hydrophilic one such as methanol.

Column Studies

The results of column adsorption and desorption studies for PNP are shown in Figures 27 through 30. In these as in all column studies flow rates were 10-15 mL per min for the adsorption phase and 5-10 mL per min for the desorption. Preliminary examination of these figures indicates that, as was the case in the batch studies, a substantial fraction of adsorption capacity was regenerated during the desorption phase.

Methyl organge (Figs. 31 through 35) adsorption-desorption results on resin XAD-16 were similar to those obtained for the PNP and again in good agreement with the results of the batch studies.

Red 40 results shown in Figures 36 and 37 indicate limited levels of adsorption and recovery of the dye using XAD-16. This resin was the only one which, in batch tests, gave a reasonable level of R40 uptake and was hence the only one studied in these column systems. It seems unlikely that this resin would be useful for removal of R40 from wastewaters in spite of its relatively favorable behavior in batch systems.

Column studies for 4-AAB (Figs. 38 through 41) were consistent in behavior with results obtained in batch reactors being characterized by a

high level of adsorption and sharp eventual approach to complete breakthrough and limited recovery of capacity by methanol extraction.

TASKS TO BE COMPLETED IN REMAINDER OF PROJECT

The following project related activities are underway at this time.

a) Batch equilibrium and kinetic data are being systematized for analysis and incorporation into the final report.

b) Column data are being analyzed with the intention of establishing mass balances of adsorbed and desorbed organic compounds as an index of the process efficiencies.

c) Process modelling is underway under the auspices of Dr. B. R. Kim; now with General Motors, Inc. in Detroit.

d) Final report preparation is ongoing.

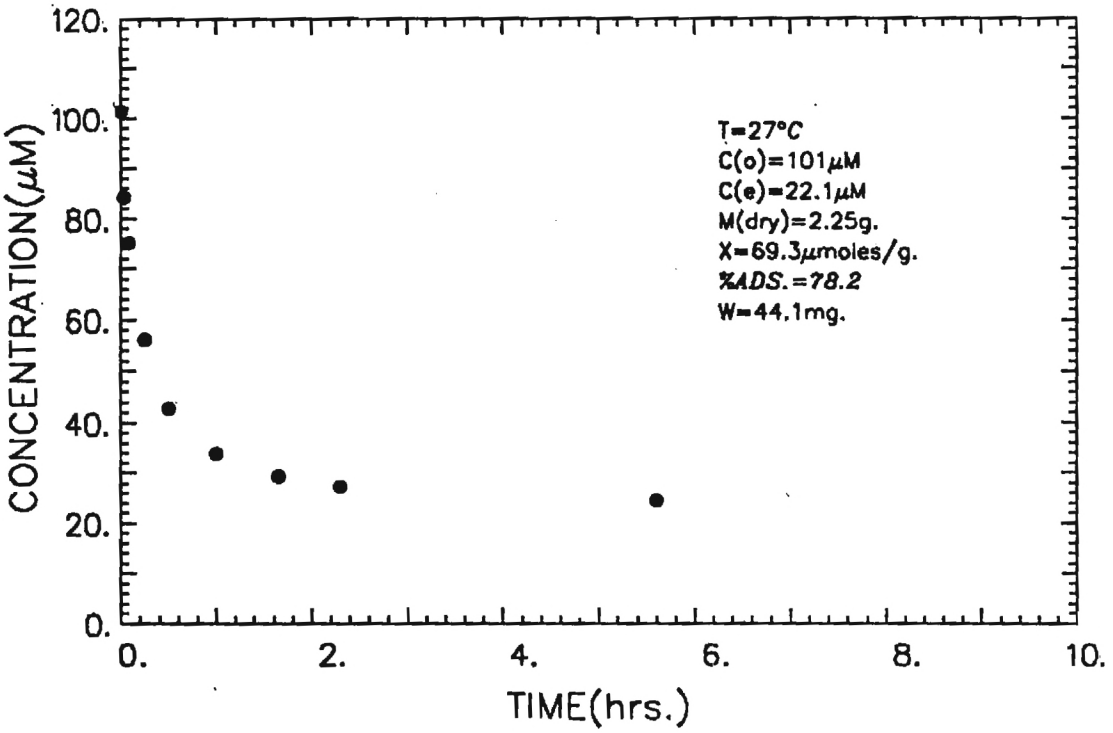

BATCH ADSORPTION OF PNP ON XAD-7

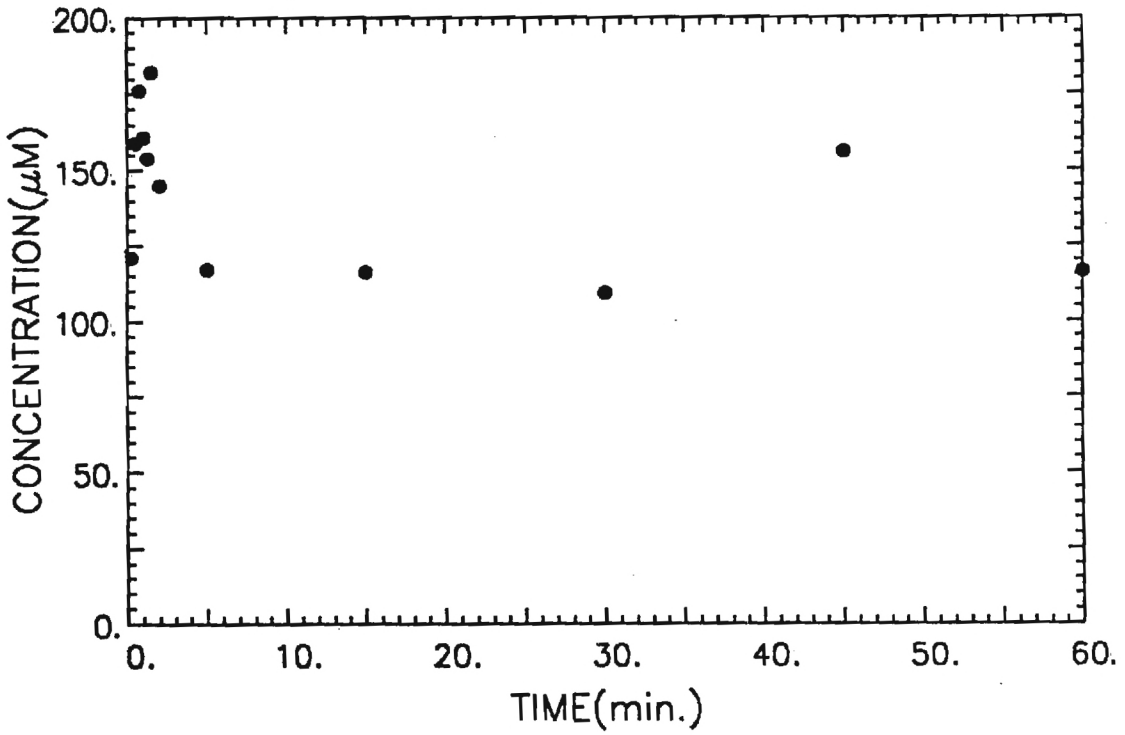

BATCH DESORPTION OF PNP FROM XAD-7

Figure 1

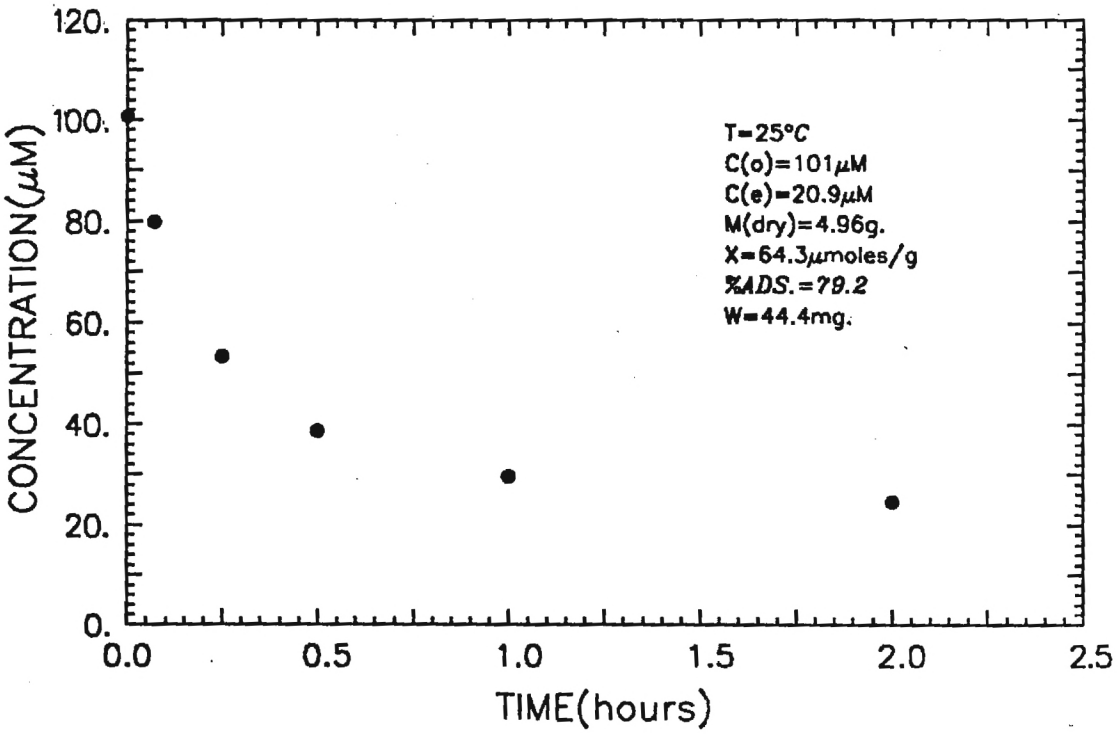

BATCH ADSORPTION OF PNP ON XAD-16(1)

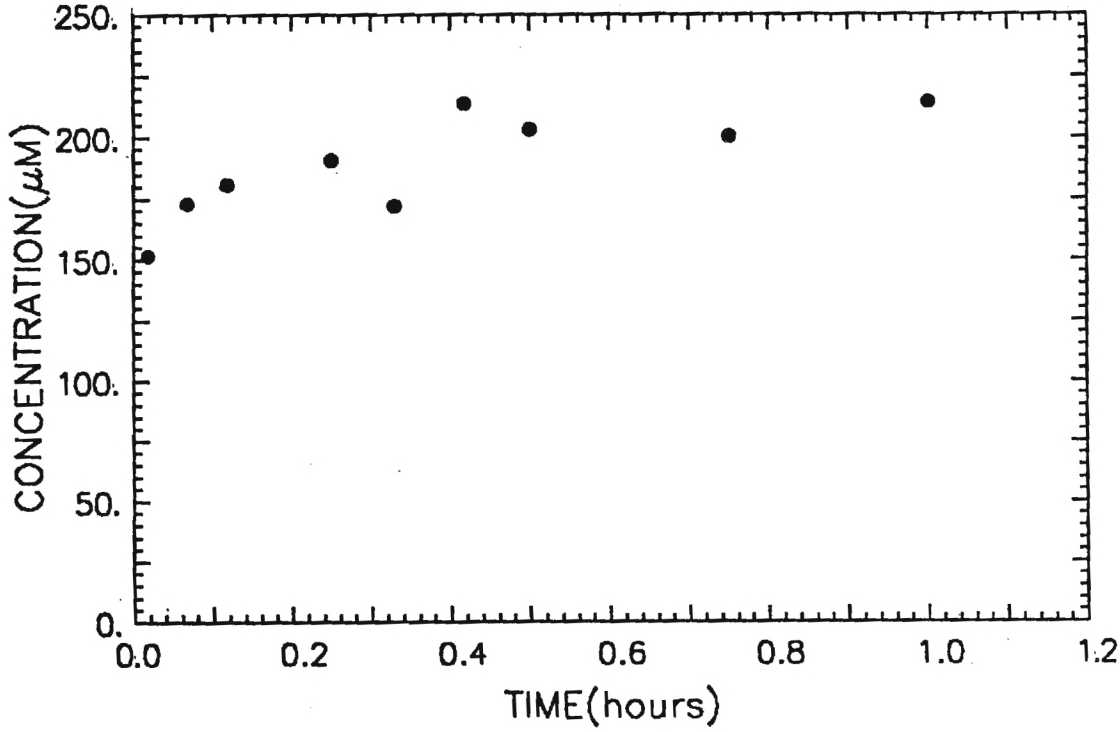

BATCH DESORPTION OF PNP FROM XAD-16(1)

Figure 2

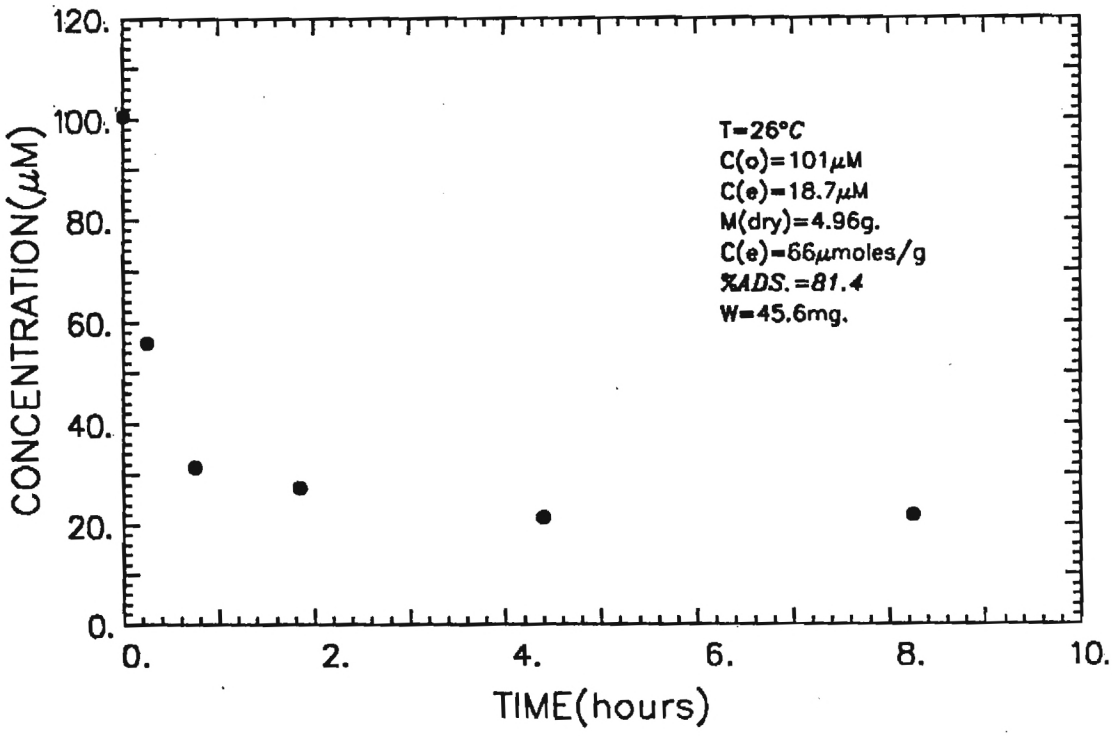

BATCH ADSORPTION OF PNP ON XAD-16(2)

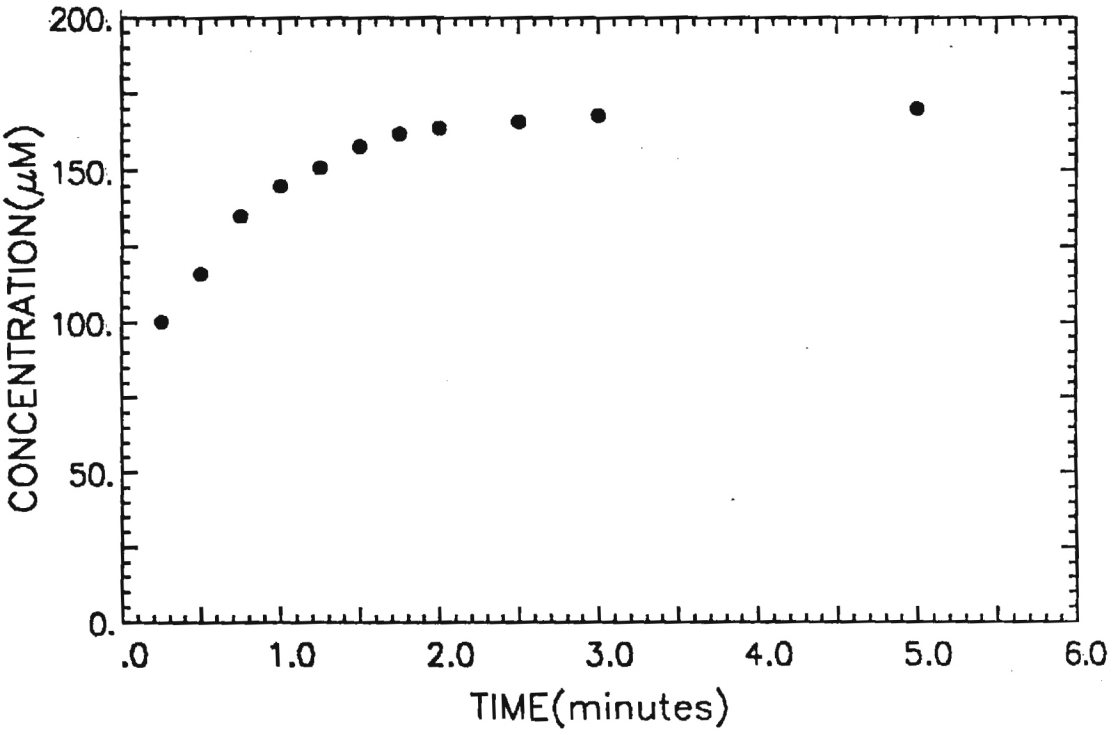

BATCH DESORPTION OF PNP FROM XAD-16(2)

Figure 3

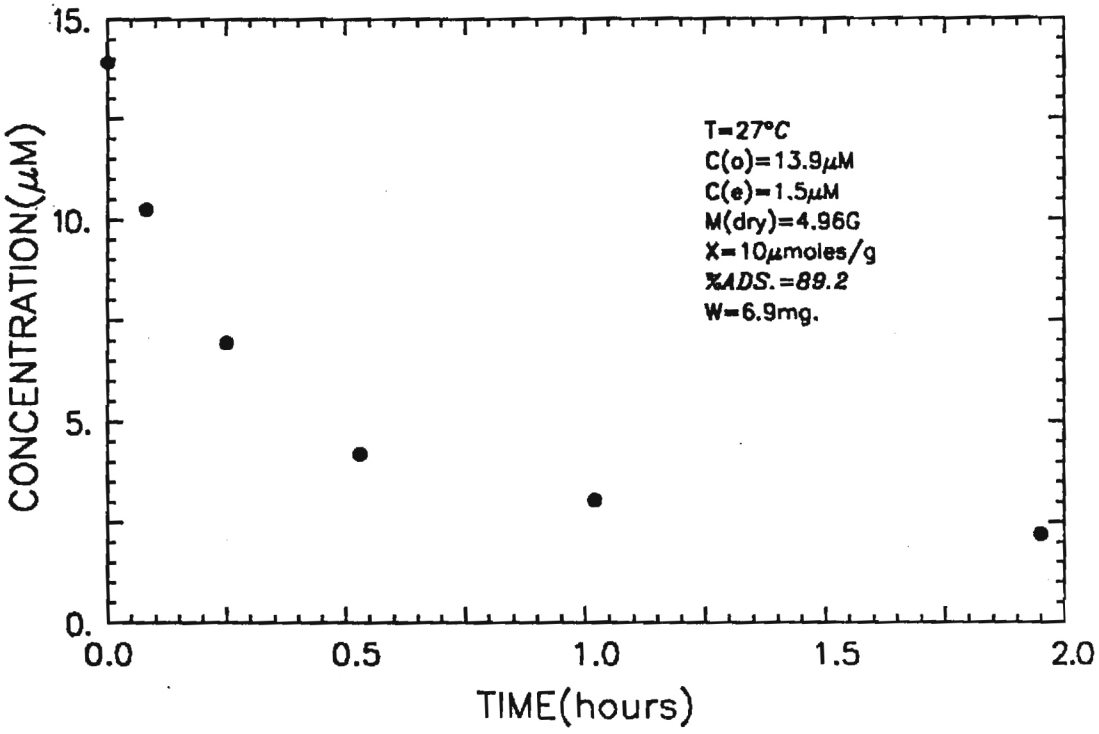

BATCH ADSORPTION OF PNP ON XAD-16(3)

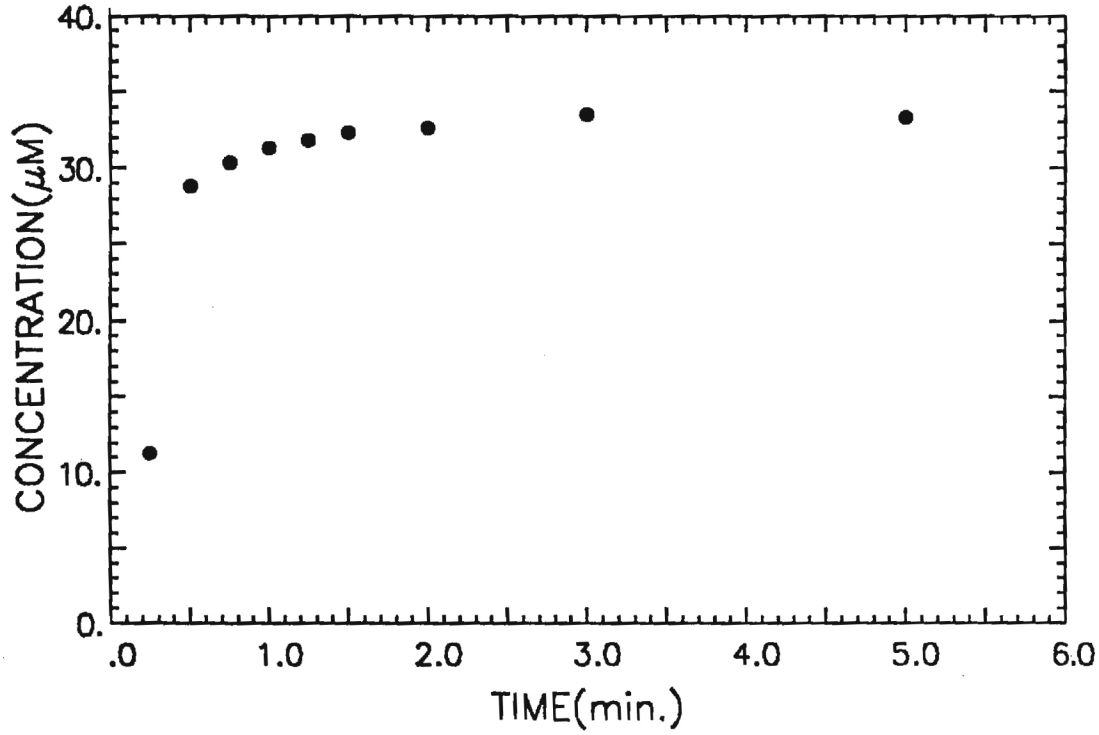

BATCH DESORPTION OF PNP FROM XAD-16(3)

Figure 4

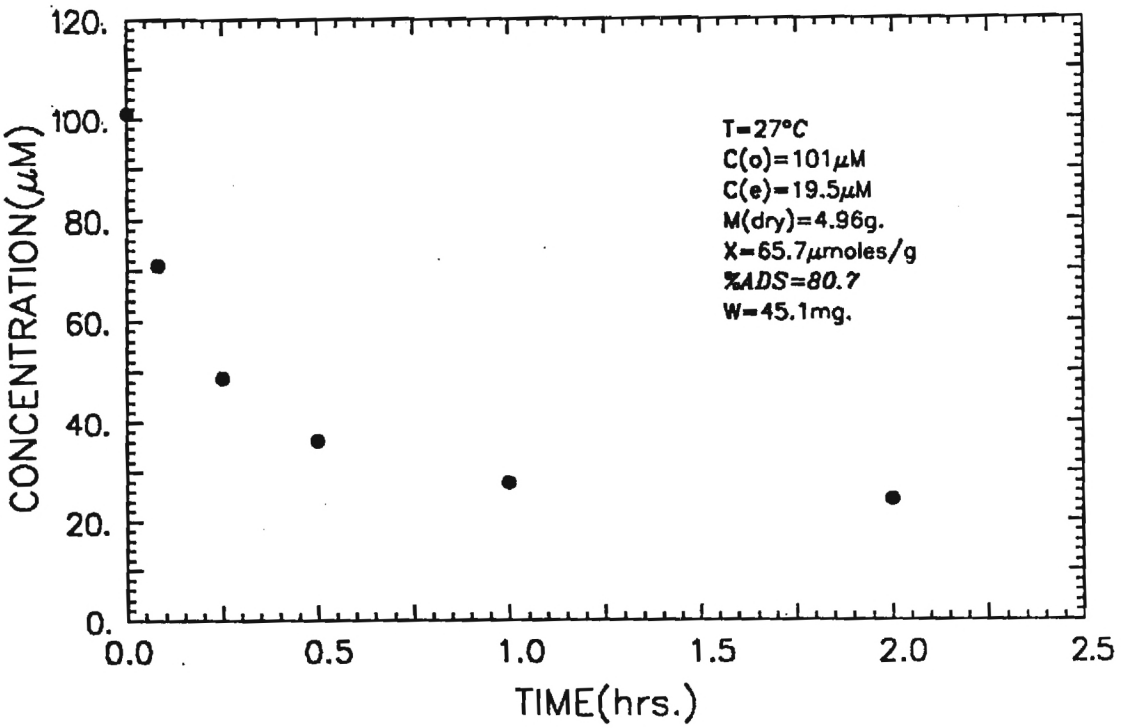

BATCH ADSORPTION OF PNP ON XAD-16(4)

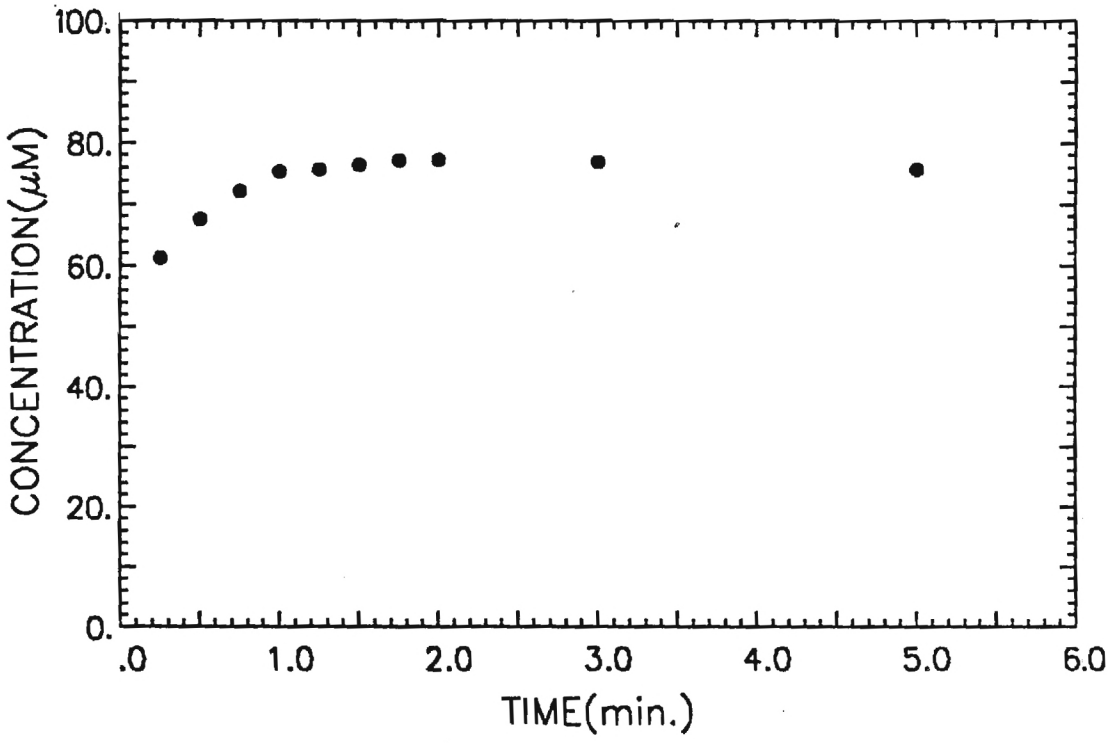

BATCH DESORPTION OF PNP FROM XAD-16(4)

Figure 5

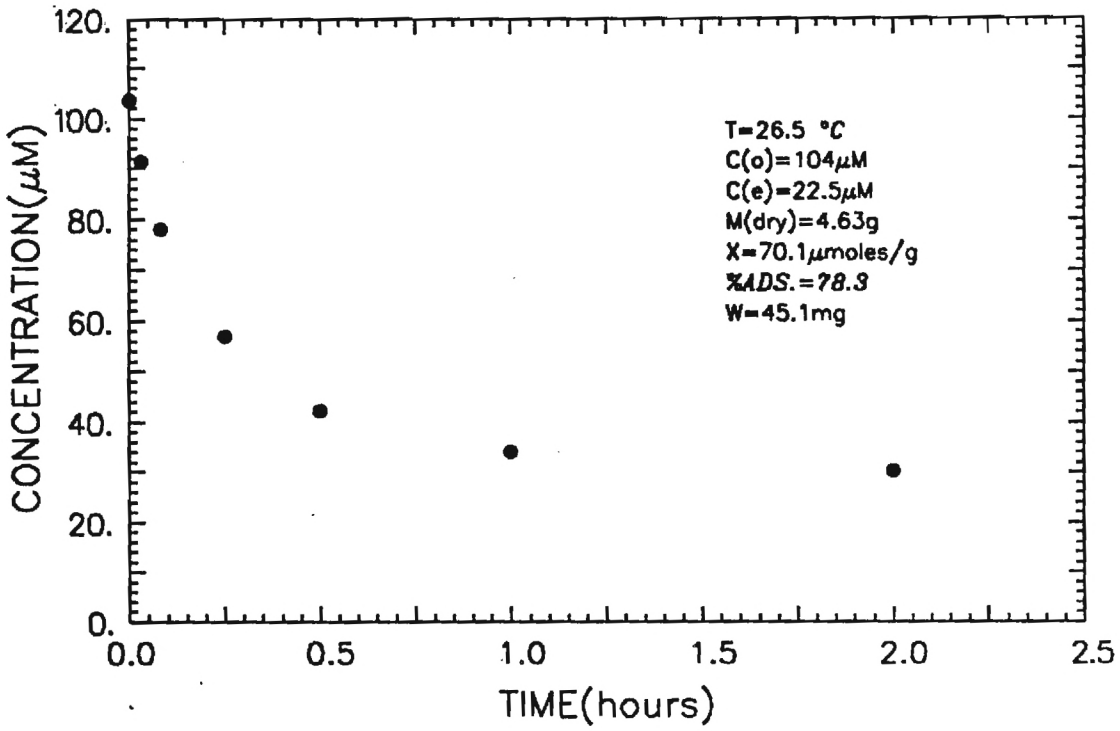

BATCH ADSORPTION OF PNP ON XAD-16(5)

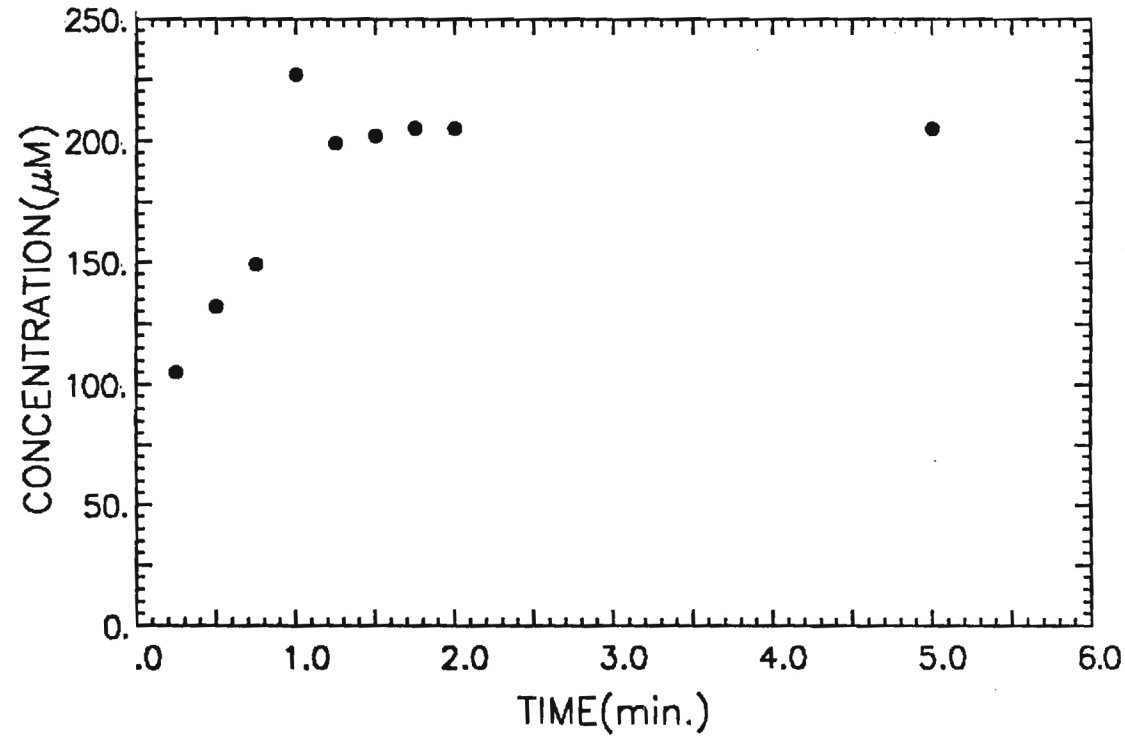

BATCH DESORPTION OF PNP FROM XAD-16(5)

Figure 6

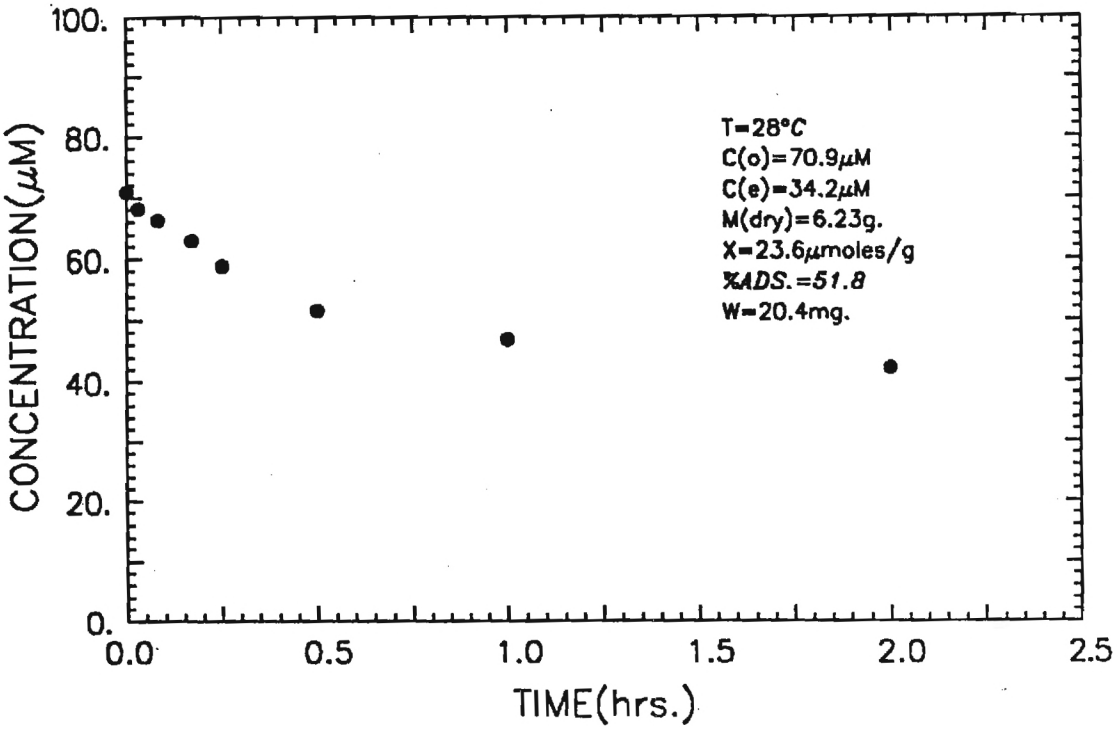

BATCH ADSORPTION OF PNP ON S-761(1)

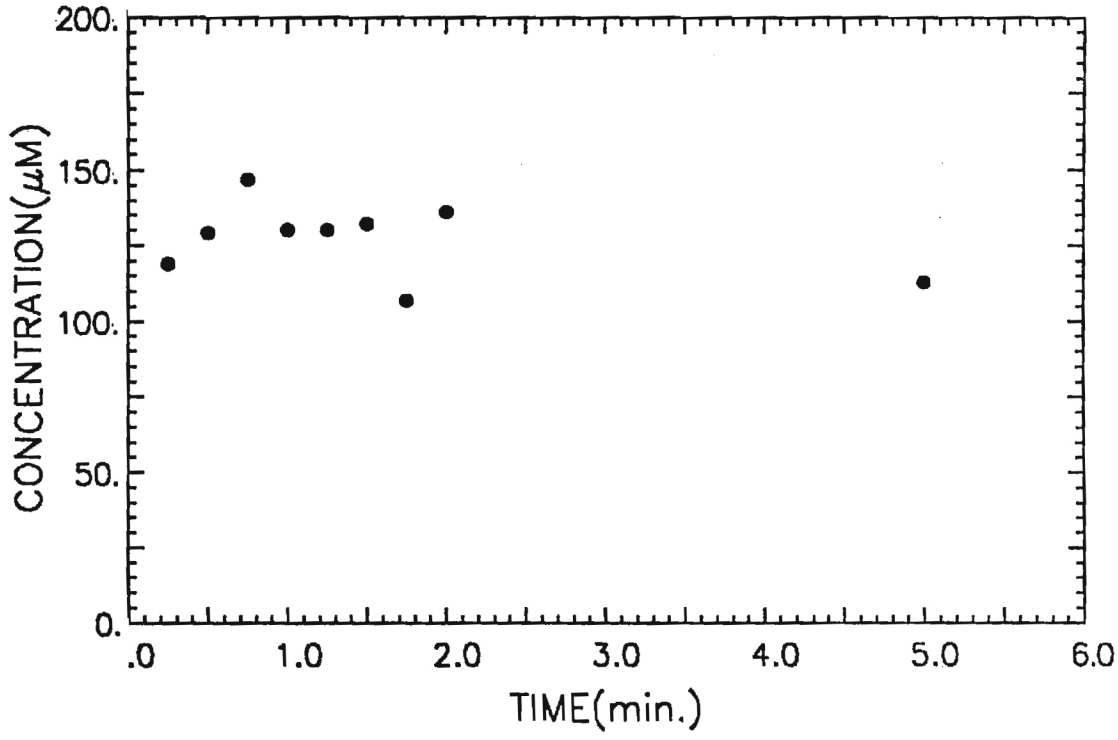

BATCH DESORPTION OF PNP FROM S-761(1)

Figure 7

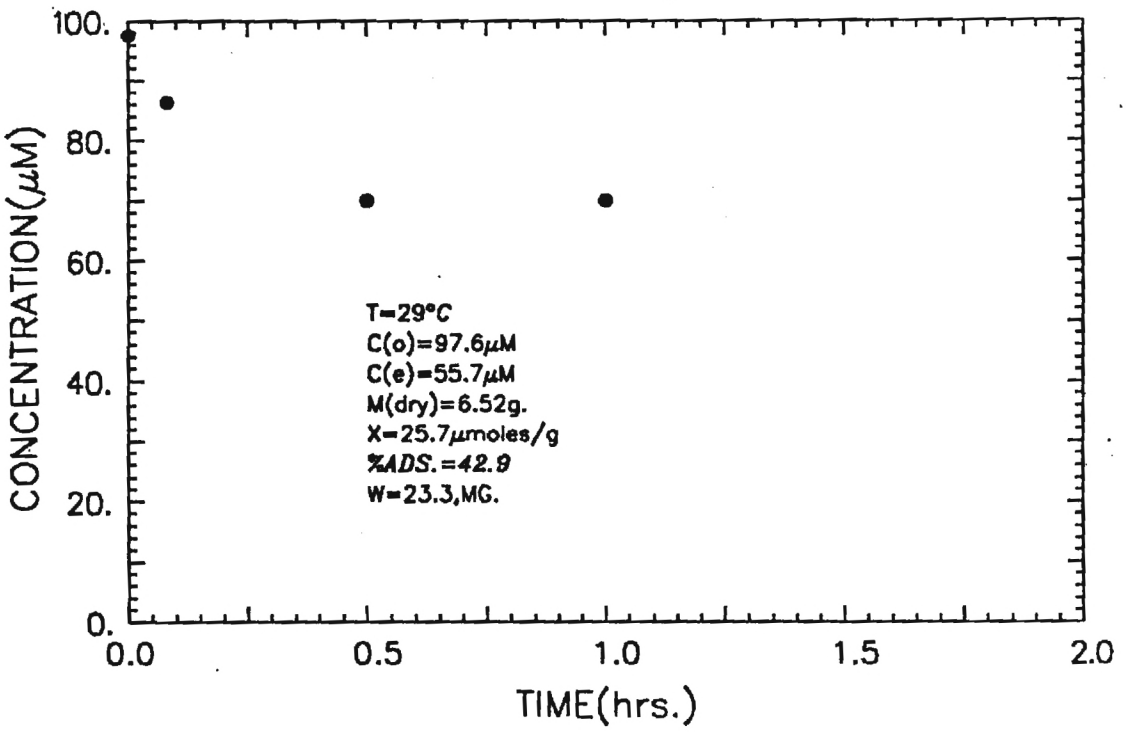

BATCH ADSORPTION OF PNP ON S-761(2)

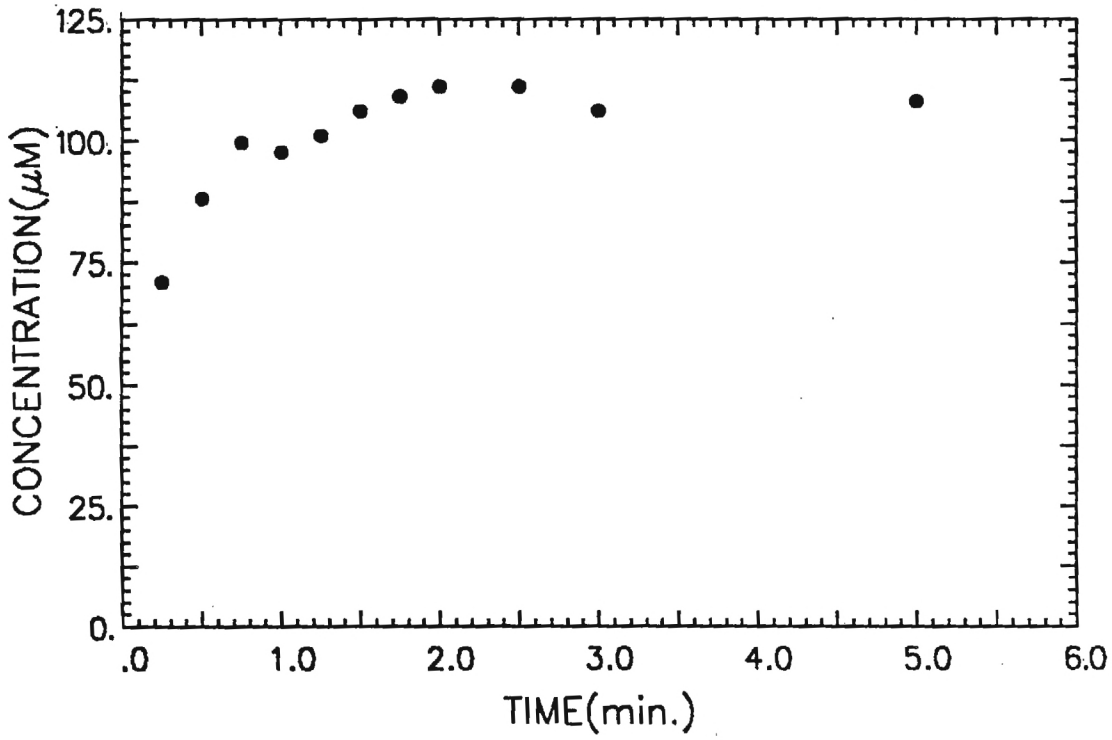

BATCH DESORPTION OF PNP FROM S-761(2)

Figure 8

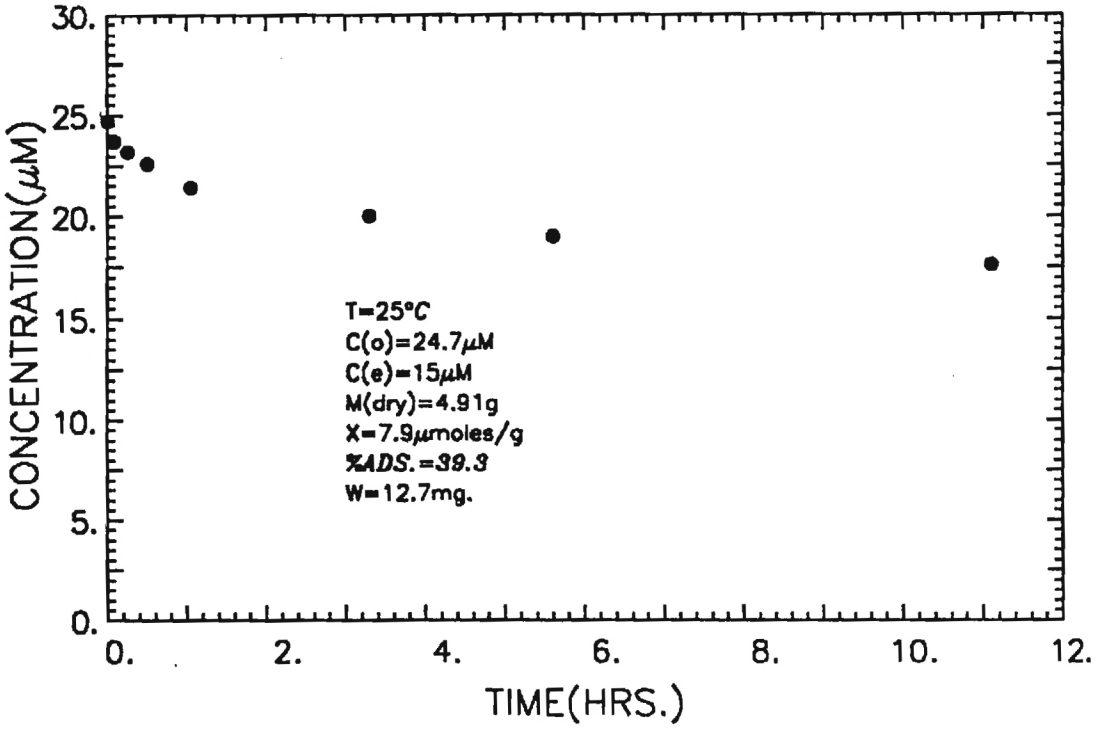

BATCH ADSORPTION OF M.O. ON XAD-7(1)

Figure 9

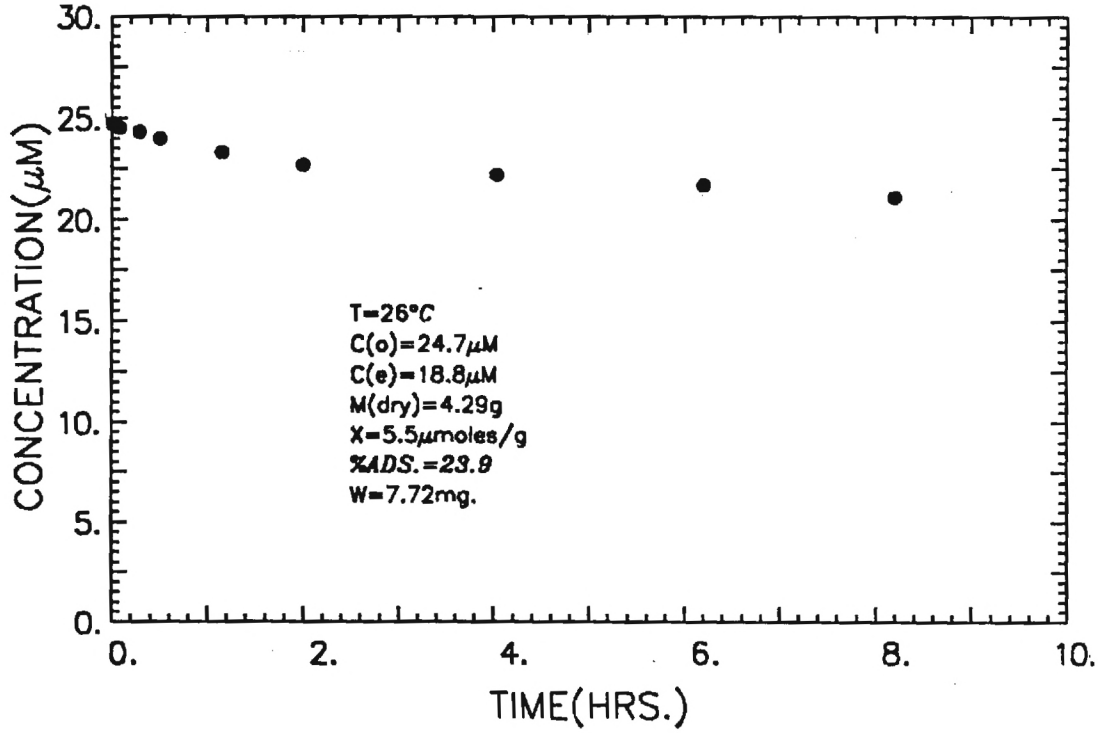

BATCH ADSORPTION OF M.O. ON XAD-7(2)

Figure 10

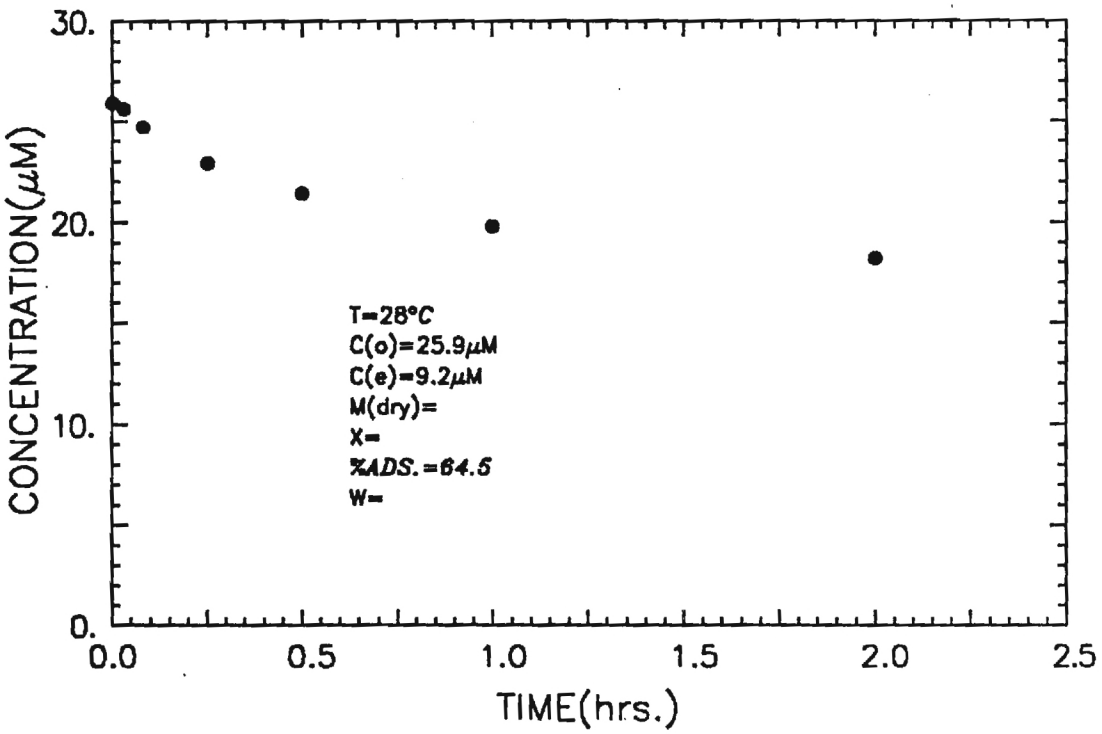

BATCH ADSORPTION OF M.O. ON XAD-7(4)

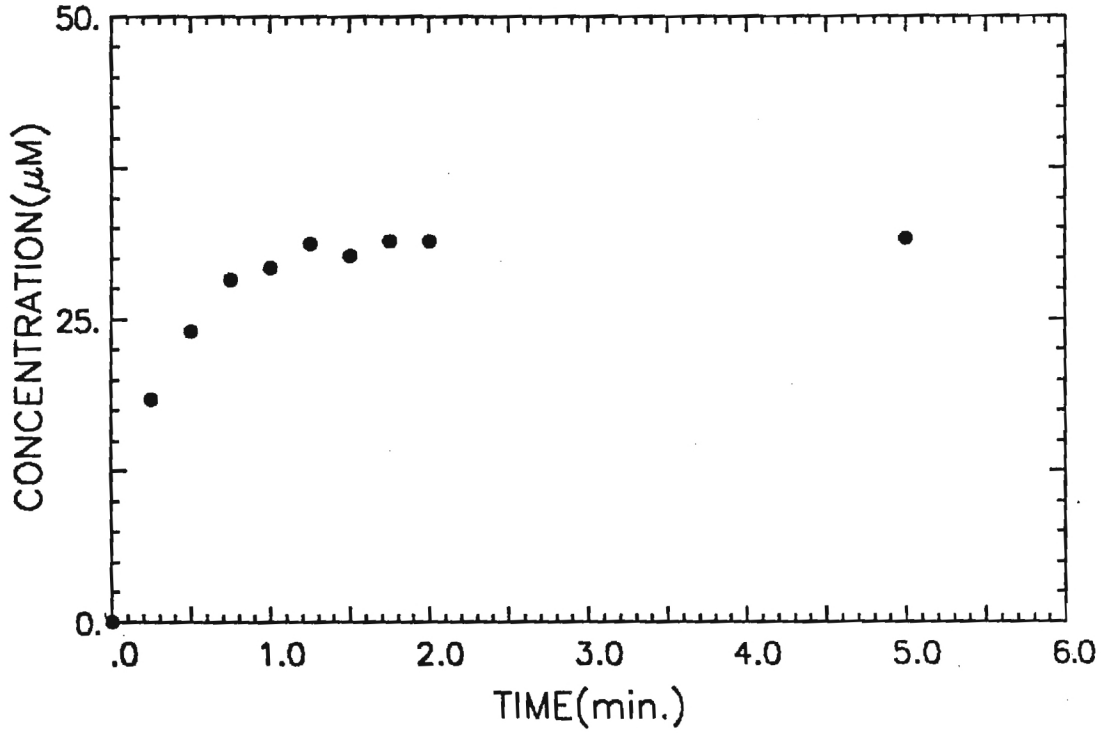

BATCH DESORPTION OF M.O. FROM XAD-7(4)

Figure 11

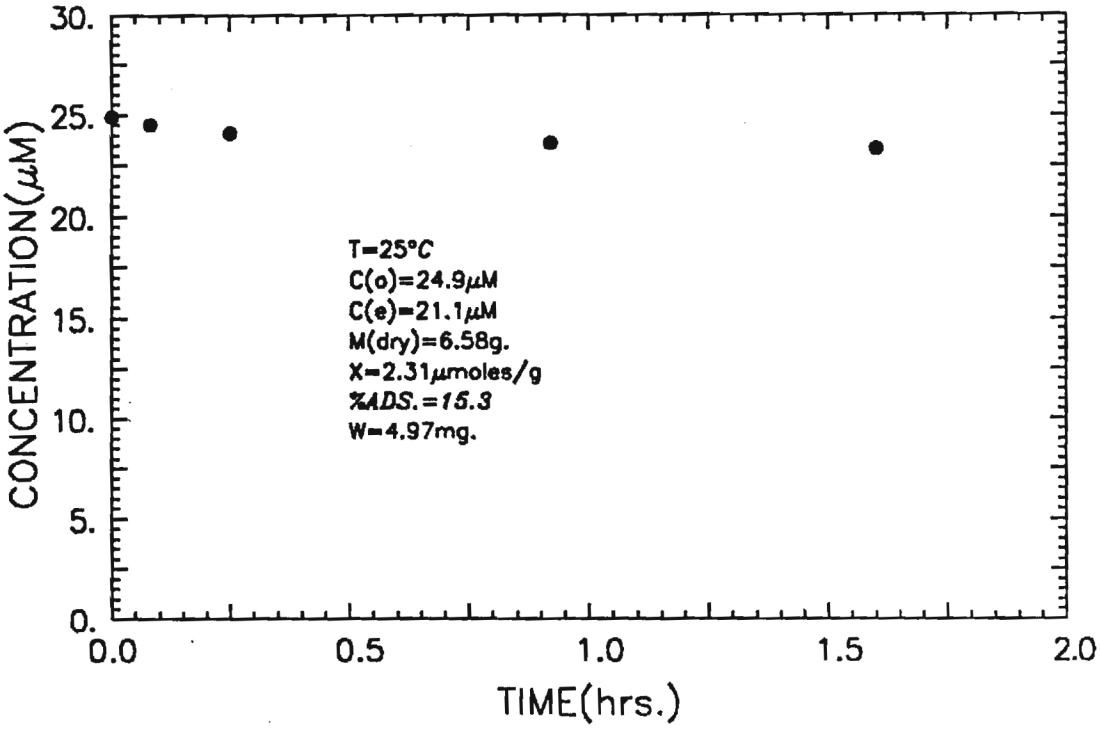

BATCH ADSORPTION OF M.O. ON XAD-8

Figure 12

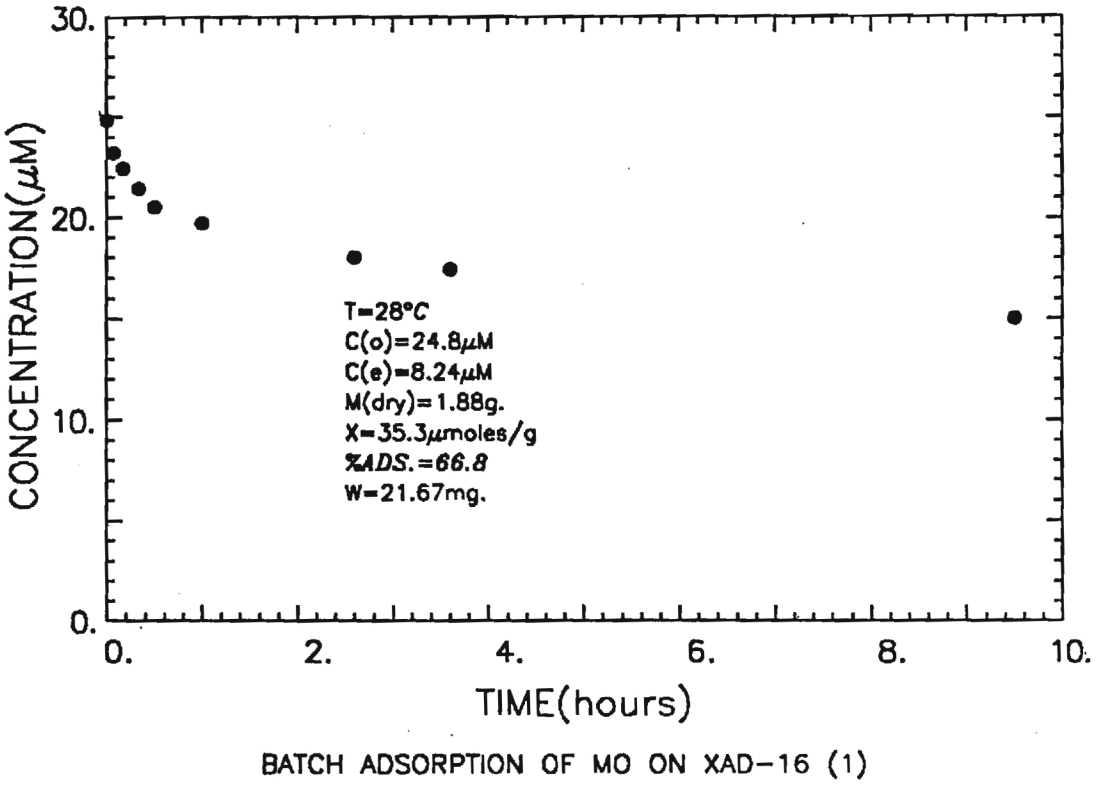
30.
20.
10.
0.
CONCENTRATION(μM)
T=28°C
C(o)=24.8μM
C(e)=8.24μM
M(dry)=1.88g.
X=35.3μmoles/g
%ADS.=66.8
W=21.67mg.
0.
2.
4.
6.
8.
10.
TIME(hours)
BATCH ADSORPTION OF MO ON XAD-16 (1)

Figure 13

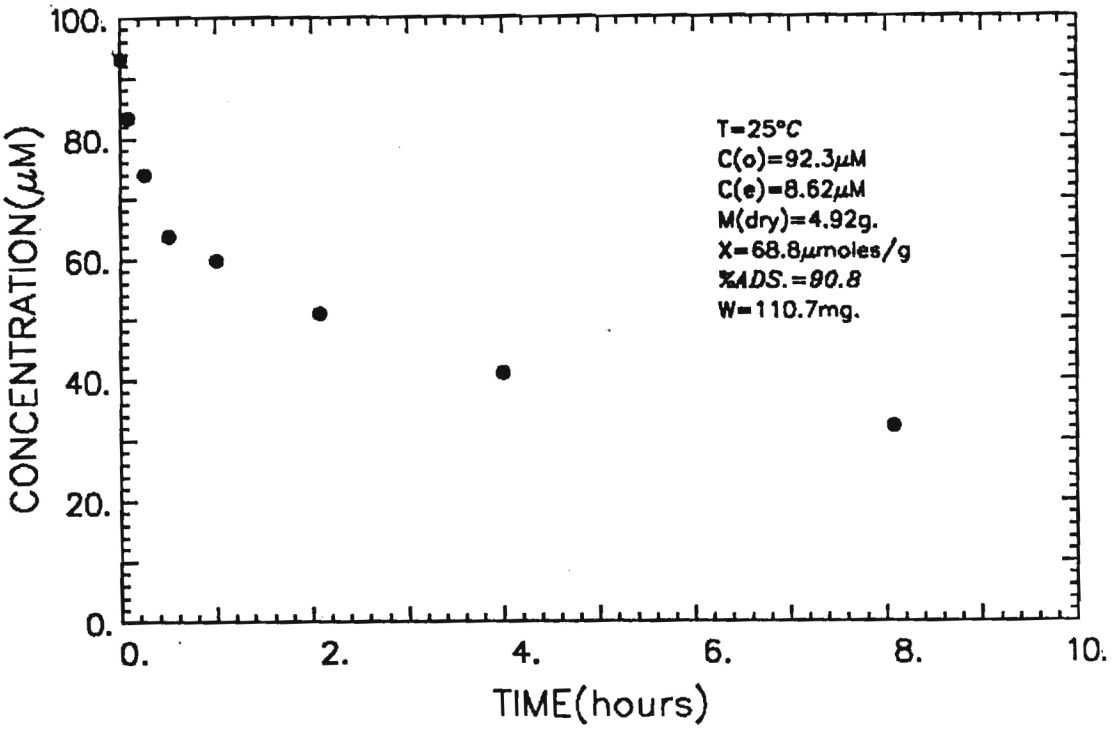

BATCH ADSORPTION OF MO ON XAD-16 (2)

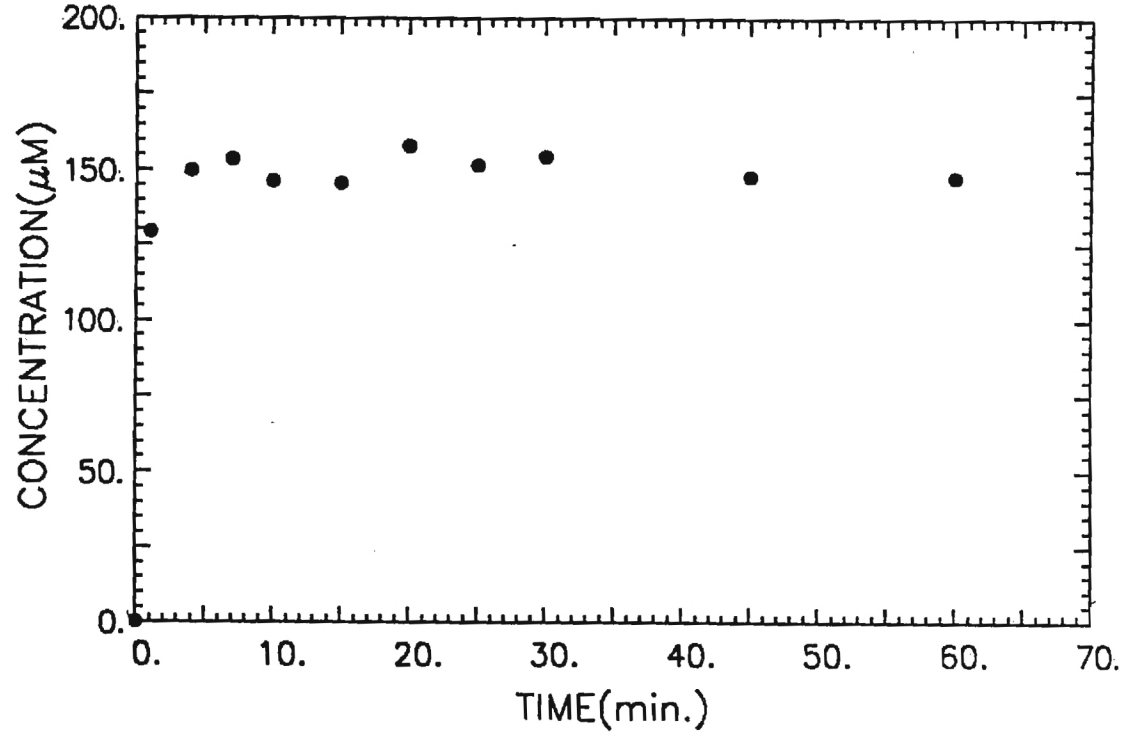

BATCH DESORPTION OF M.O. FROM XAD-16(2)

Figure 14

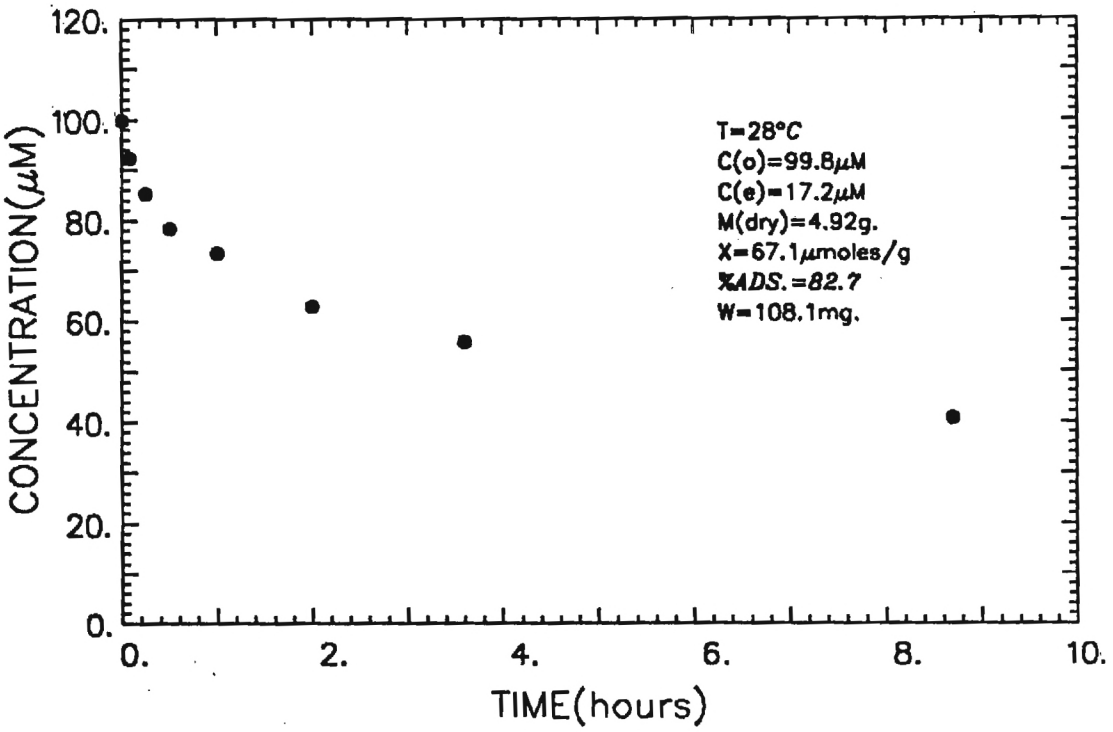

BATCH ADSORPTION OF MO ON XAD-16 (3)

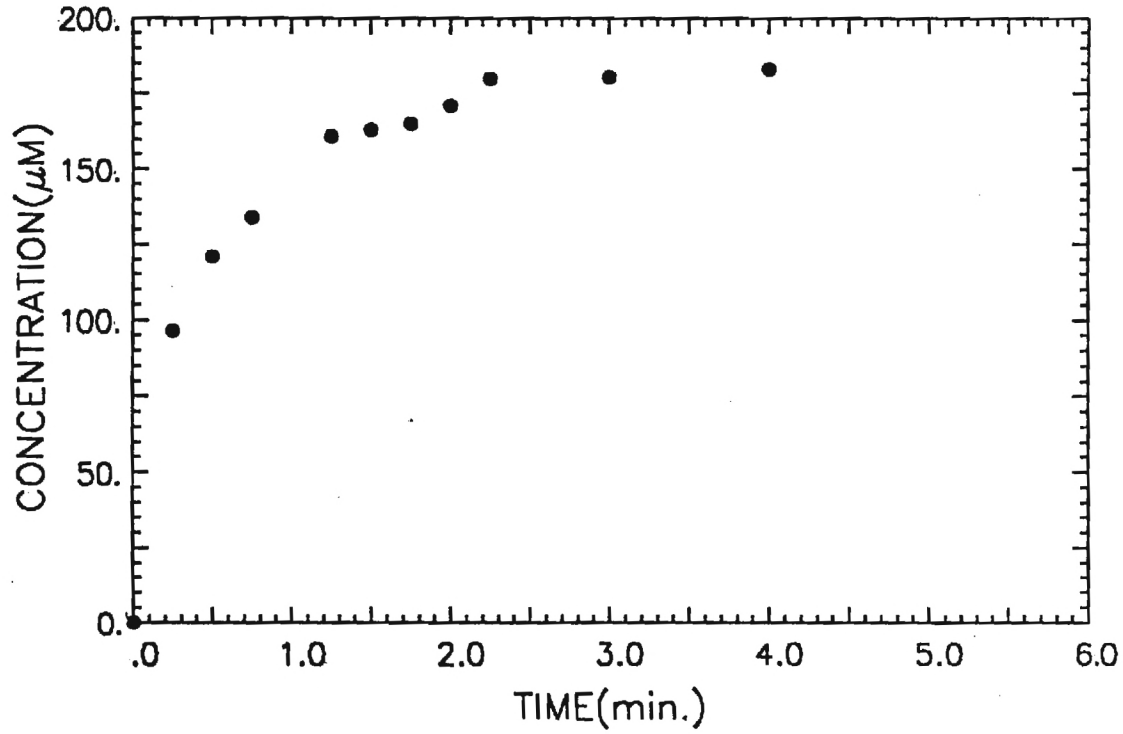

BATCH DESORPTION OF M.O. FROM XAD-16(3)

Figure 15

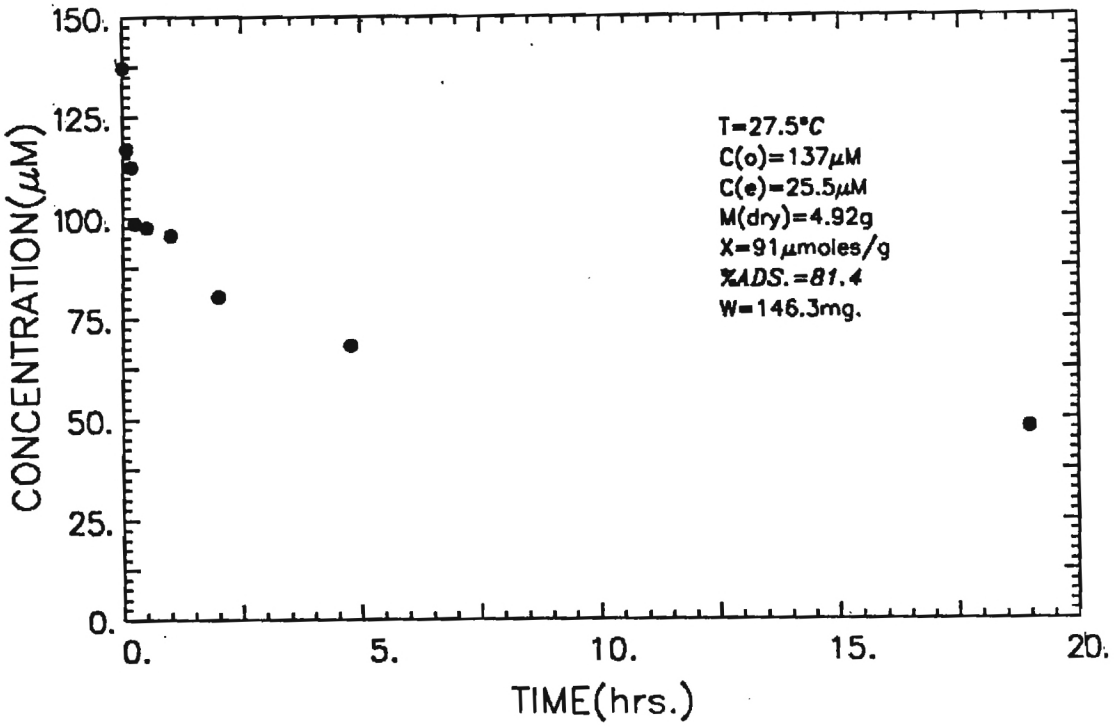

BATCH ADSORPTION OF M.O. ON XAD-16(4)

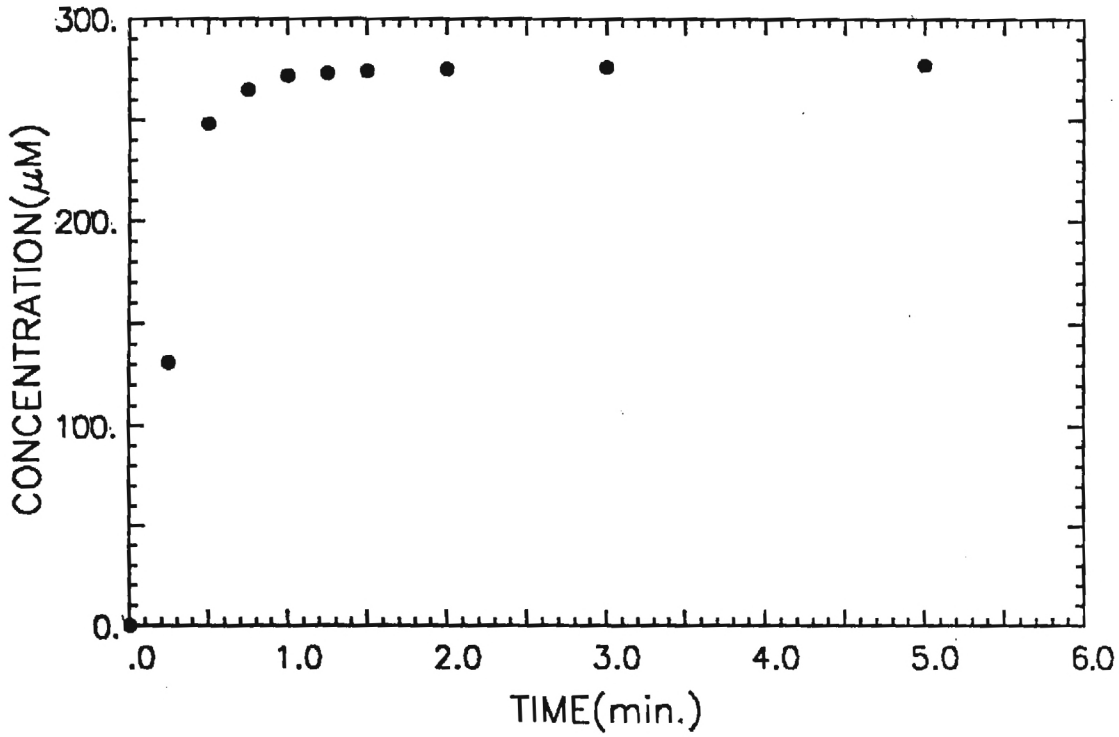

BATCH DESORPTION OF M.O. FROM XAD-16(4)

Figure 16

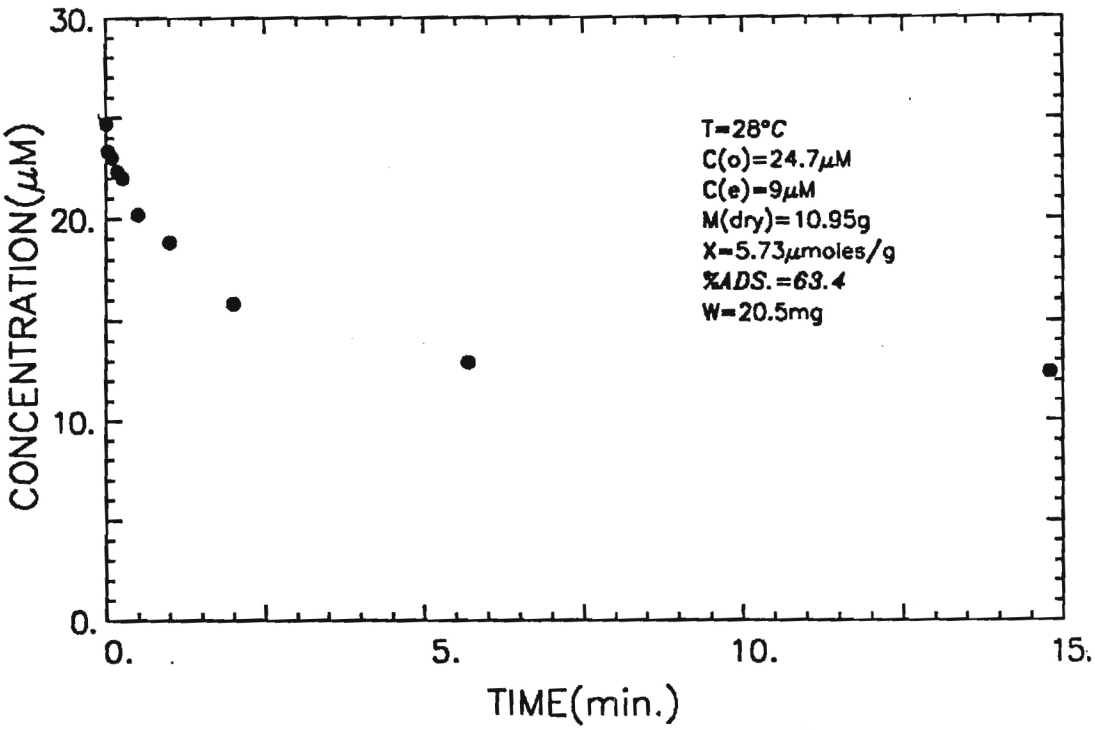

BATCH ADSORPTION OF M.O. ON S-761

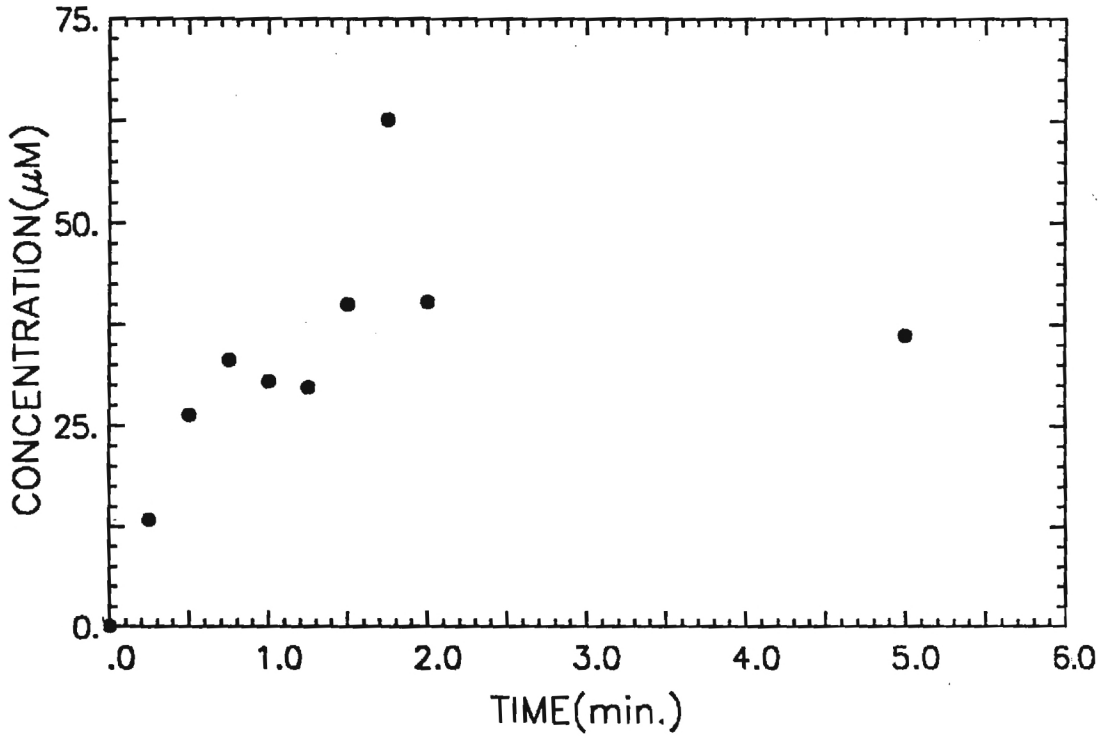

BATCH DESORPTION OF M.O. FROM S-761

Figure 17

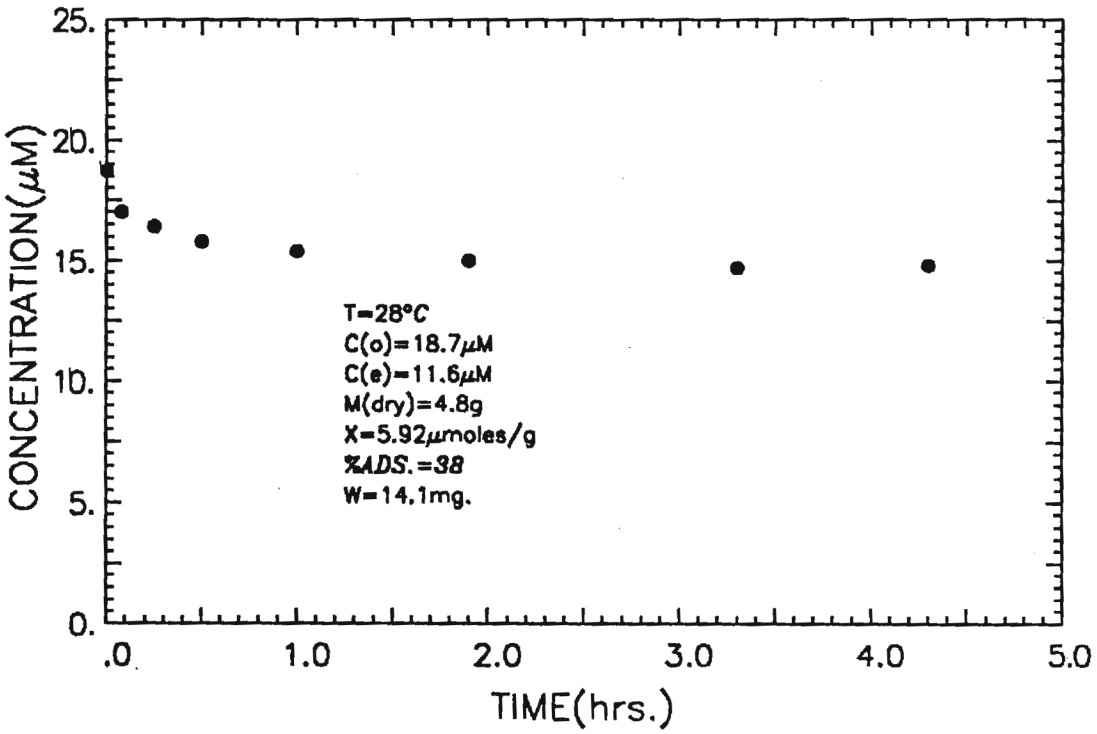

BATCH ADSORPTION OF R40 ON XAD-16(1)

Figure 18

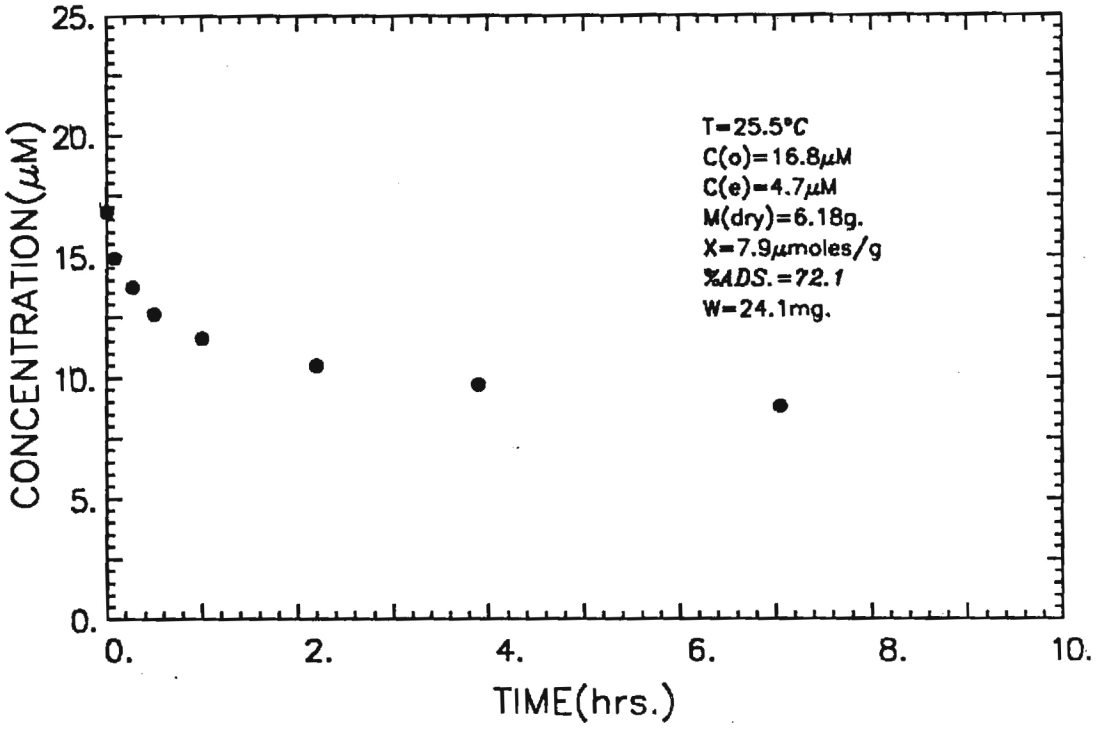

BATCH ADSORPTION OF R40 ON XAD-16(2)

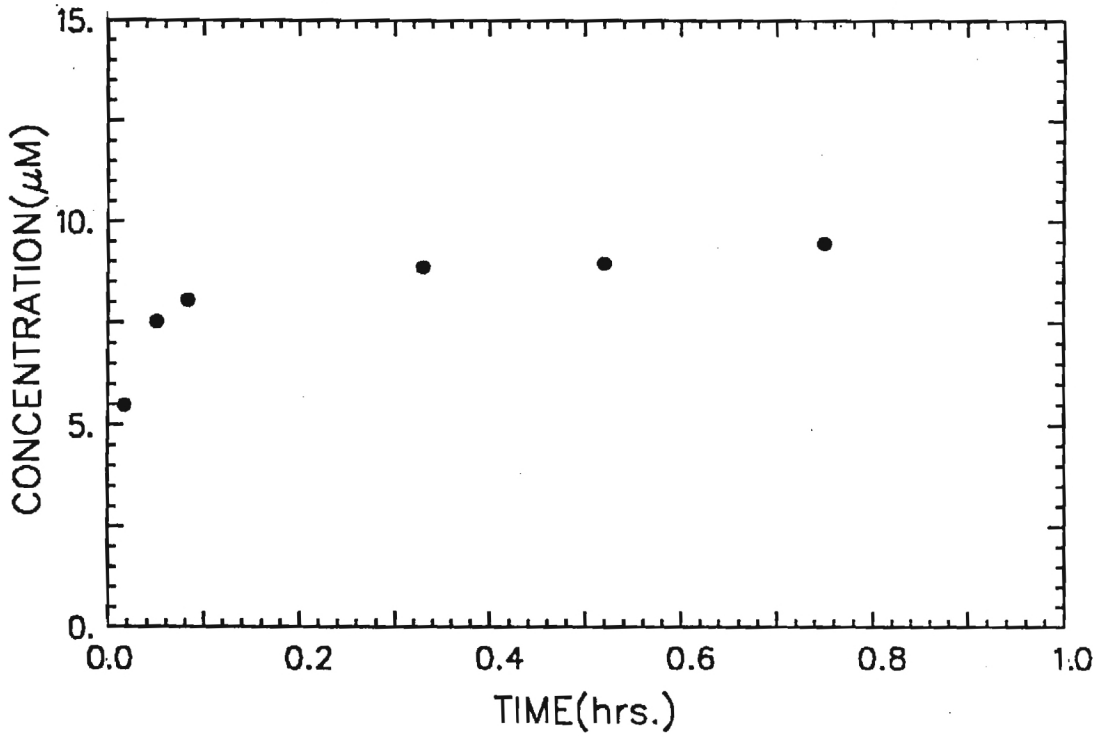

BATCH DESORPTION OF R40 FROM XAD-16(2)

Figure 19

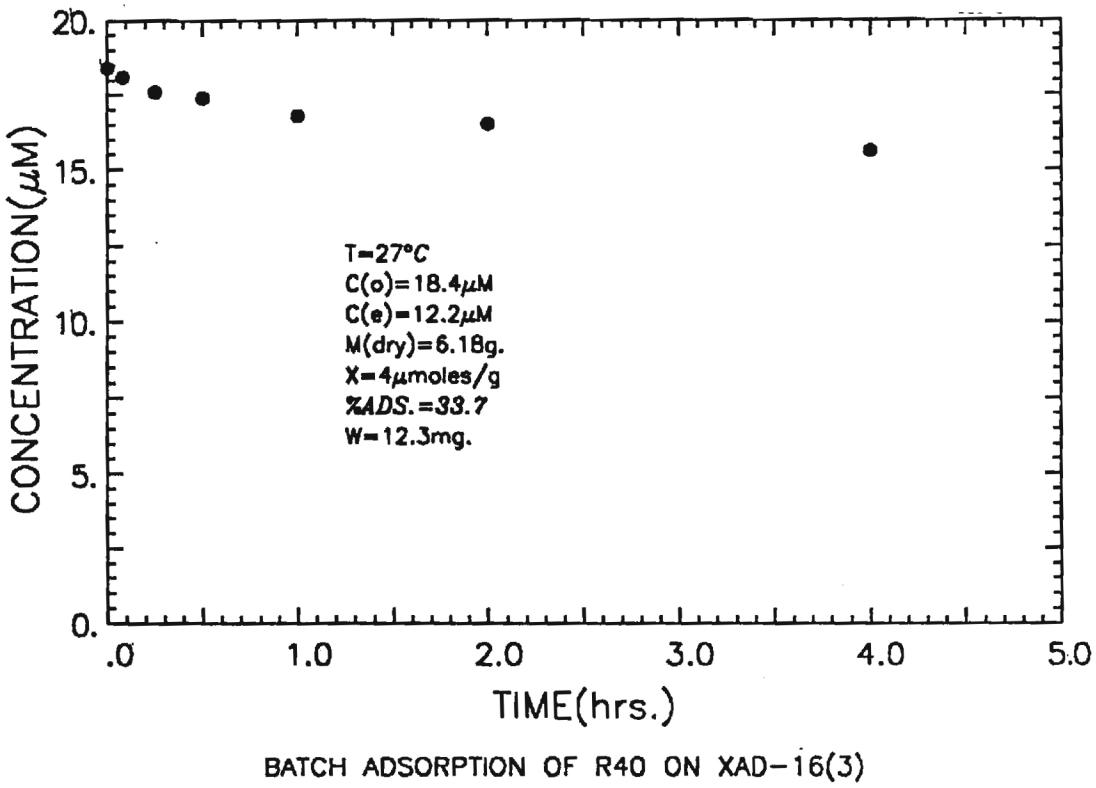
20.
15.
10.
5.
0.
CONCENTRATION(μM)
T=27°C
C(o)=18.4μM
C(e)=12.2μM
M(dry)=6.18g.
X=4μmoles/g
%ADS.=33.7
W=12.3mg.
.0
1.0
2.0
3.0
4.0
5.0
TIME(hrs.)
BATCH ADSORPTION OF R40 ON XAD-16(3)

Figure 20

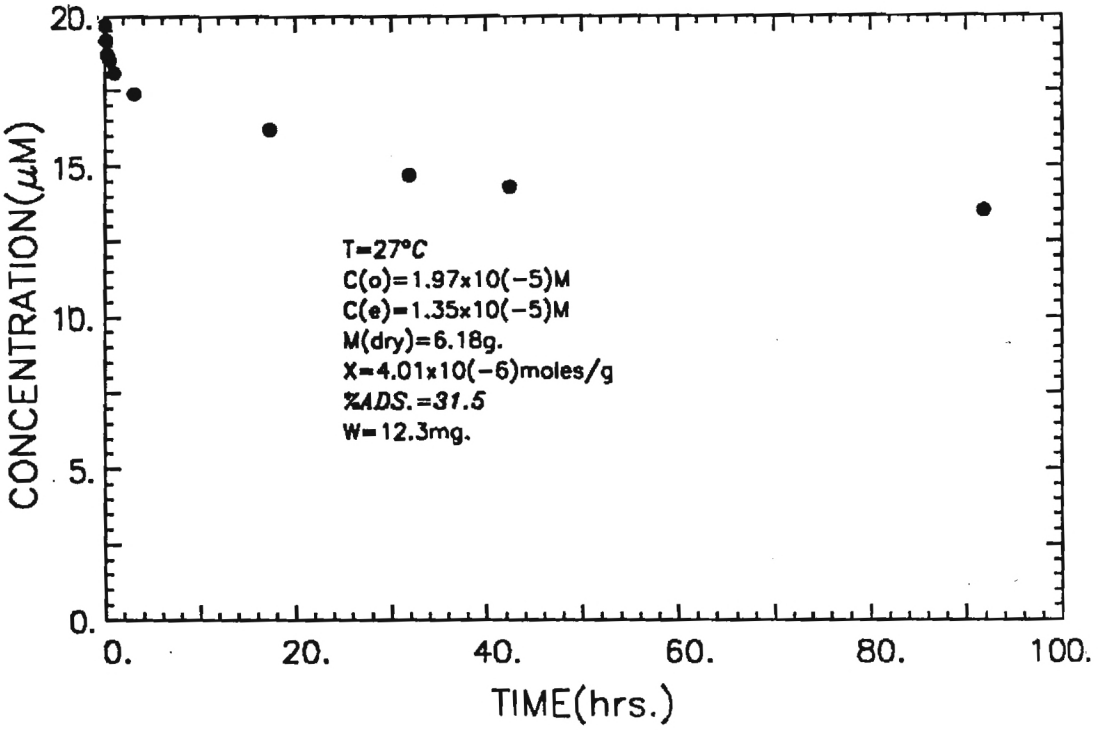

BATCH ADSORPTION OF R40 ON XAD-16(4)

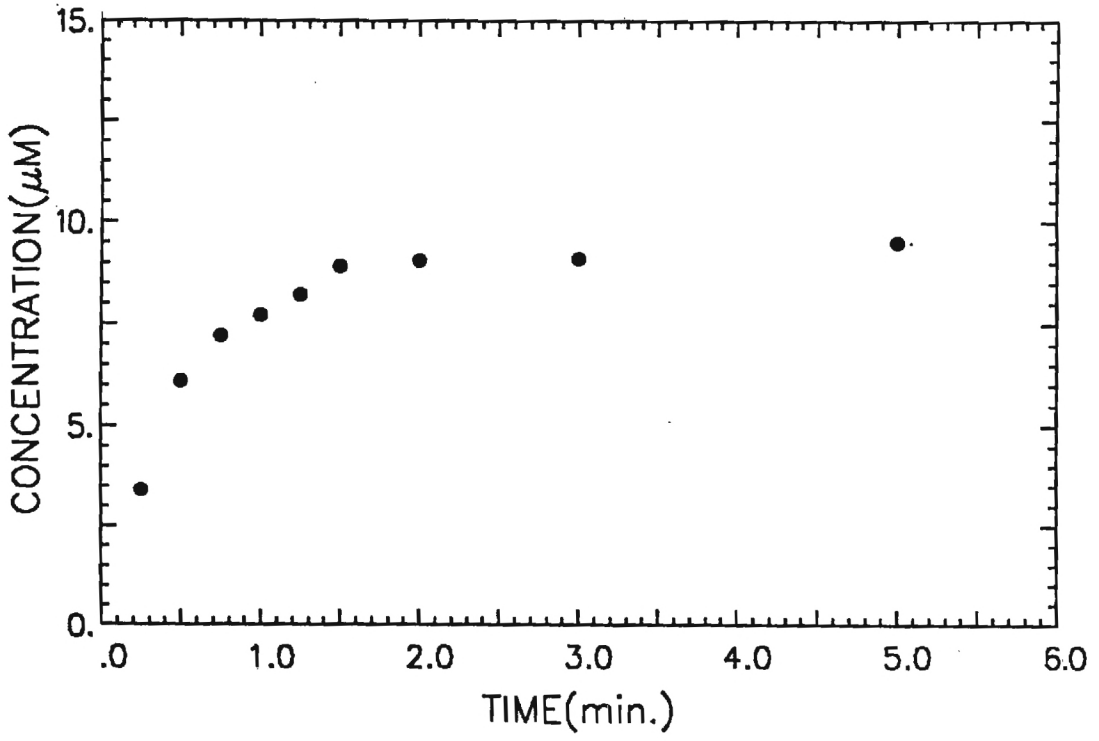

BATCH DESORPTION OF R40 FROM XAD-16(4)

Figure 21

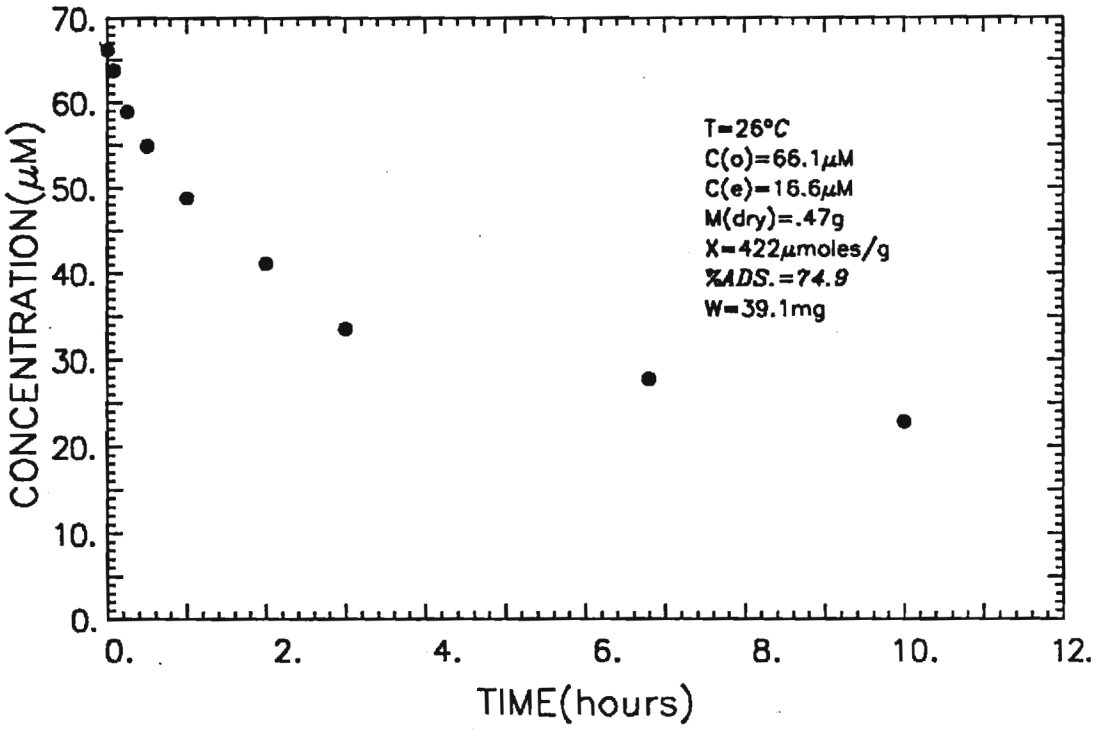

BATCH ADSORPTION OF 4-AAB ON XAD-7(1)

Figure 22

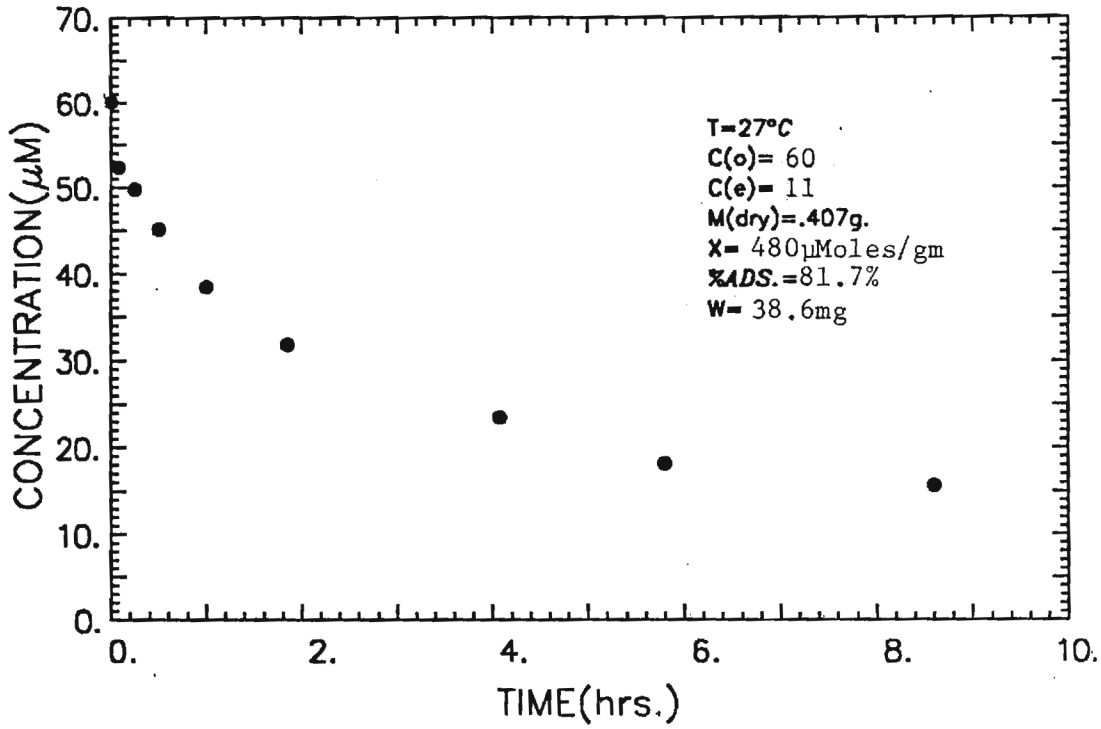

BATCH ADSORPTION OF 4AAB ON XAD-7(2)

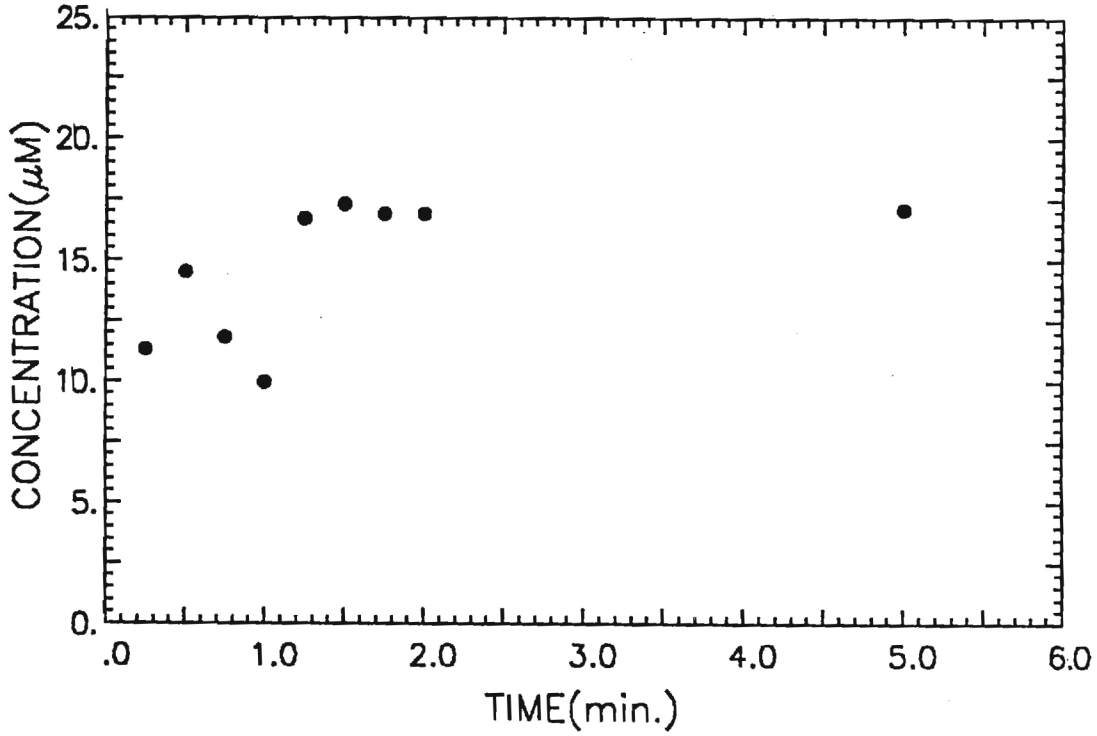

BATCH DESORPTION OF 4AAB FROM XAD-7(2)

Figure 23

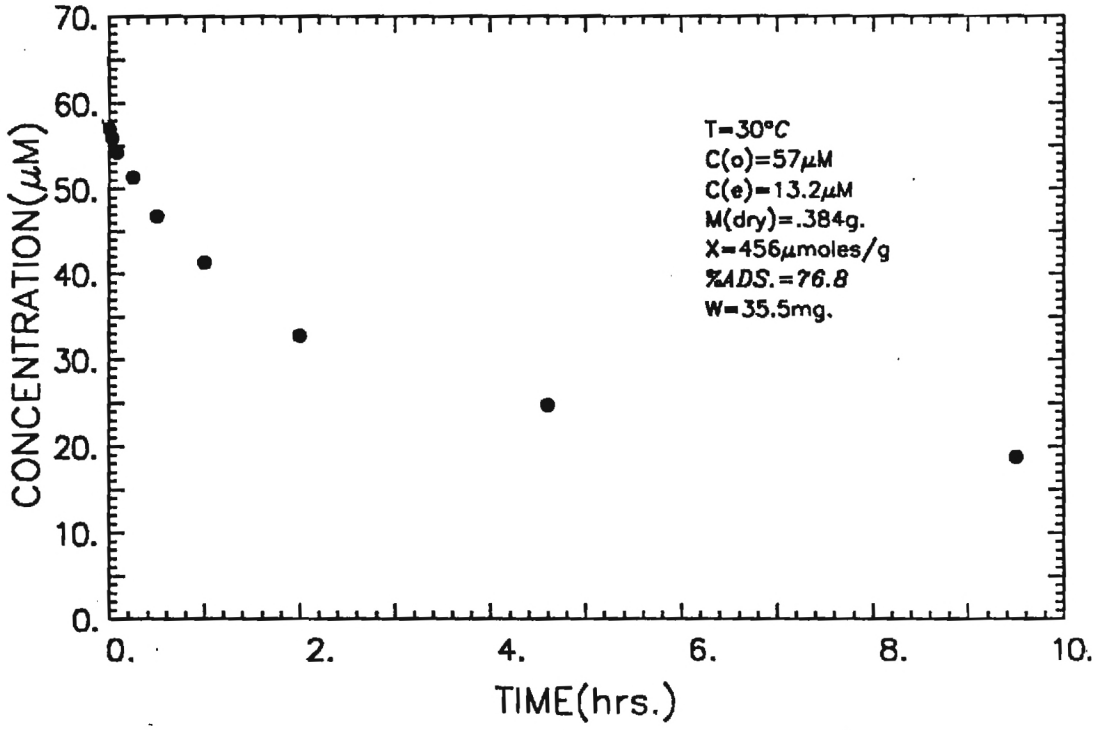

BATCH ADSORPTION OF 4AAB ON XAD-7(3)

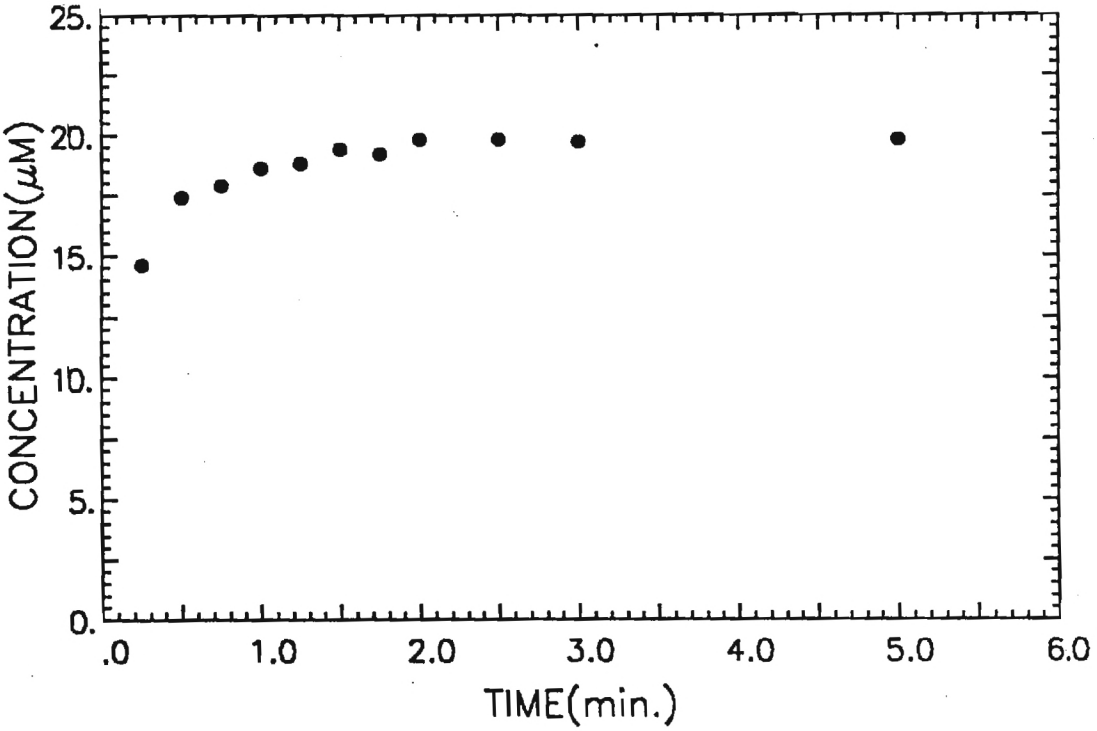

BATCH DESORPTION OF 4AAB FROM XAD-7(3)

Figure 24

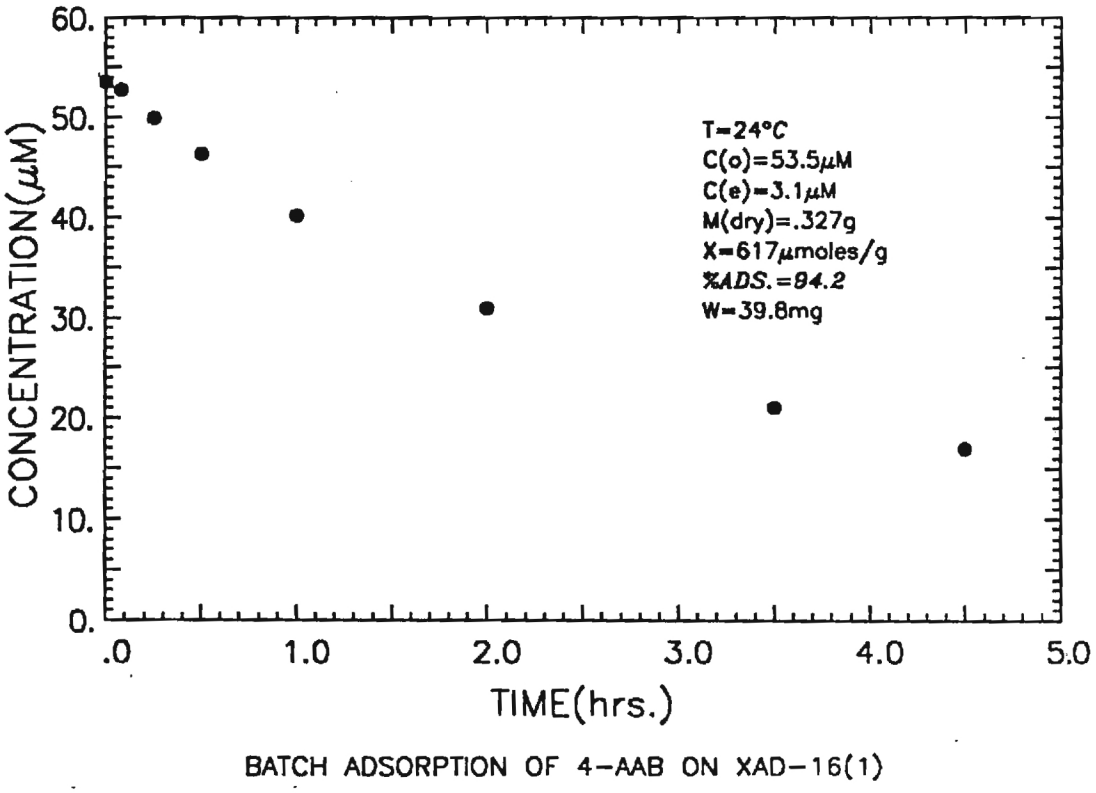

BATCH ADSORPTION OF 4-AAB ON XAD-16(1)

Figure 25

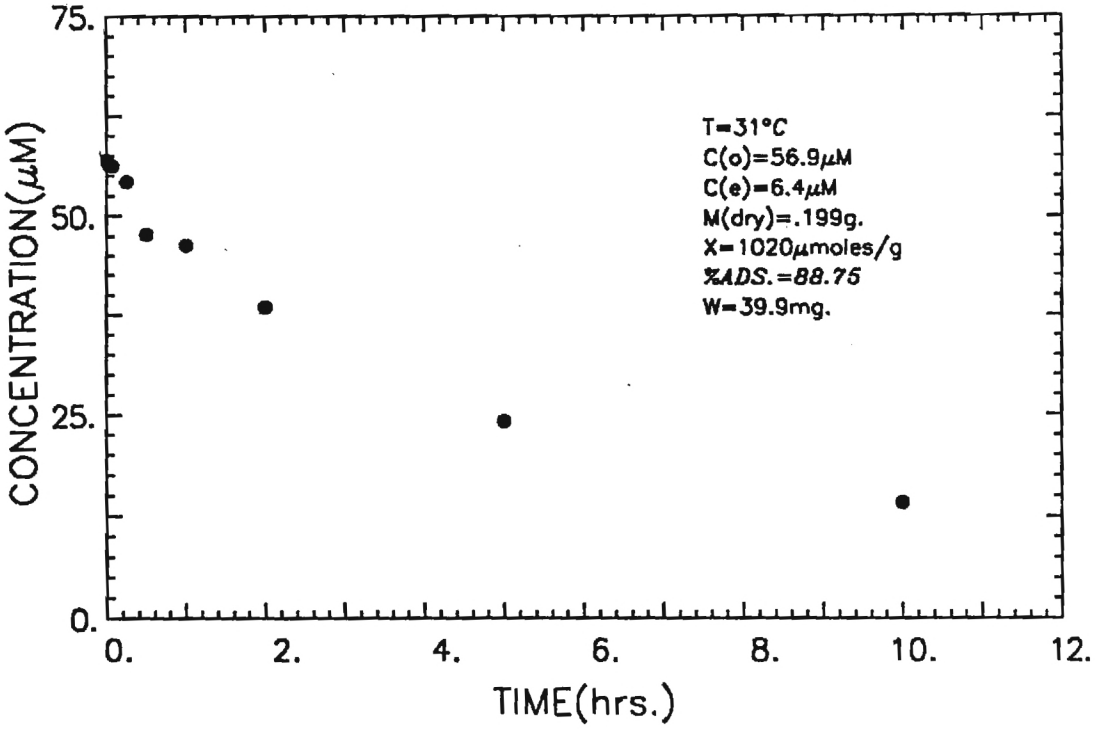

BATCH ADSORPTION OF 4AAB ON XAD-16(6)

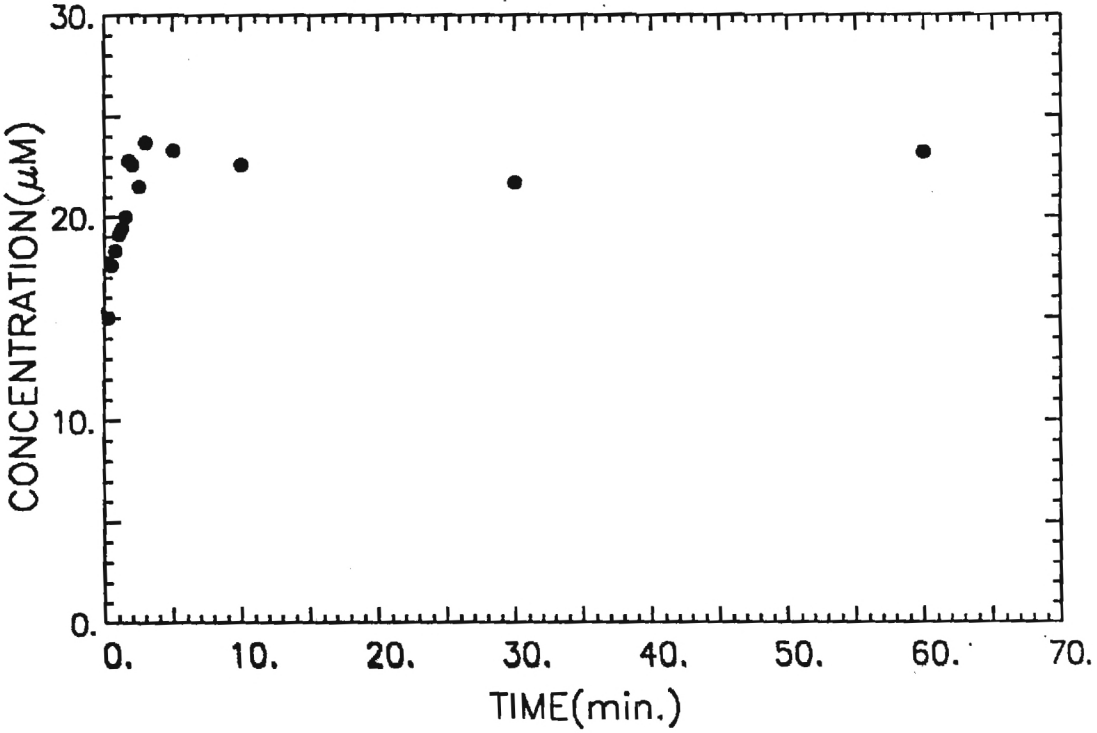

BATCH DESORPTION OF 4AAB FROM XAD-16(6)

Figure 26

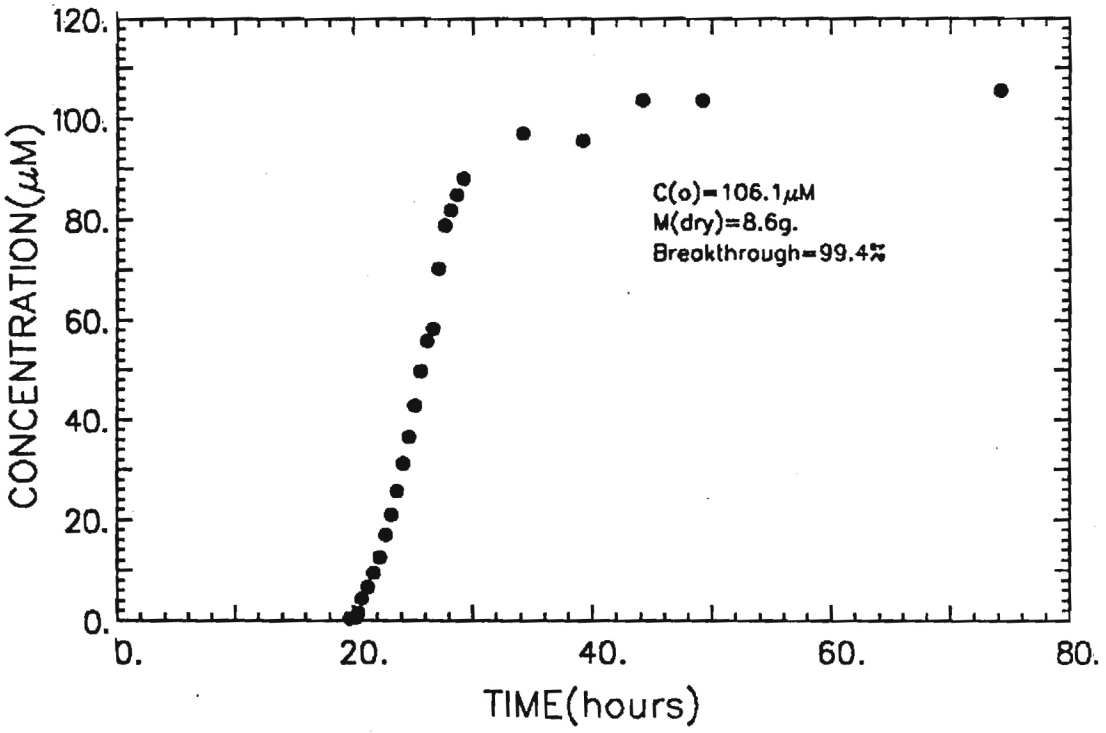

COLUMN ADSORPTION OF PNP ON XAD-16 (1)

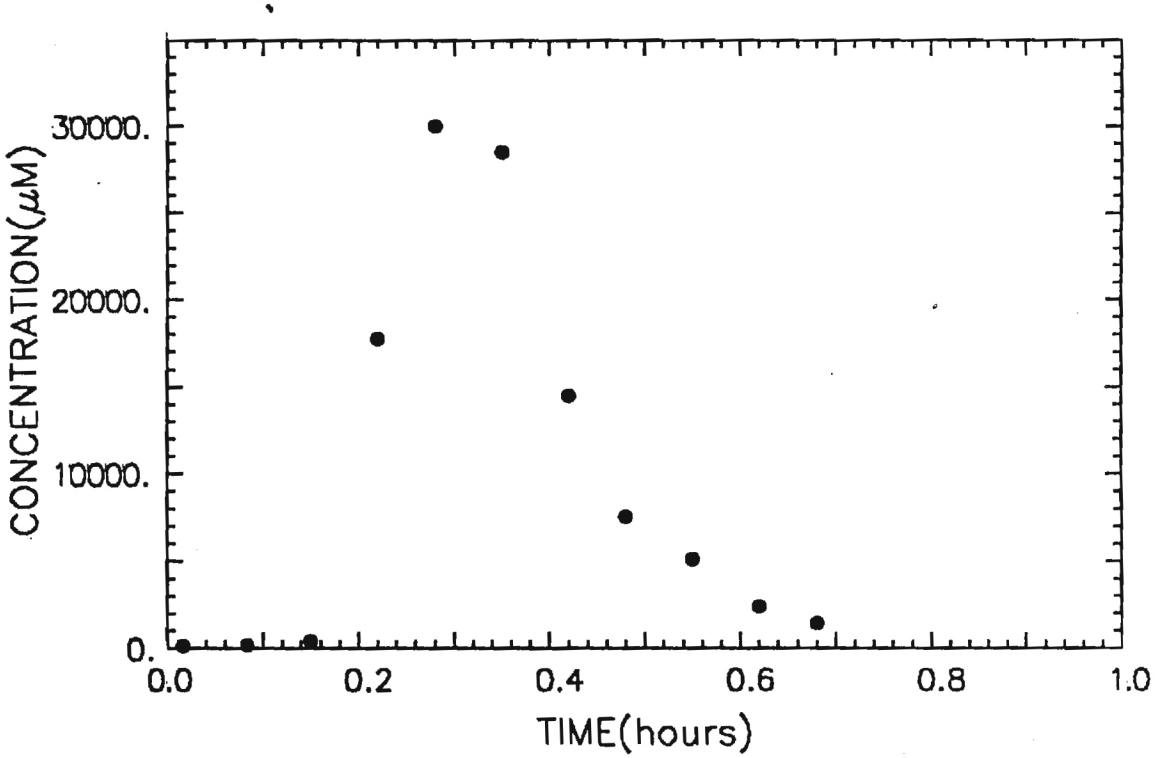

COLUMN DESORPTION OF PNP FROM XAD-16(1)

Figure 27

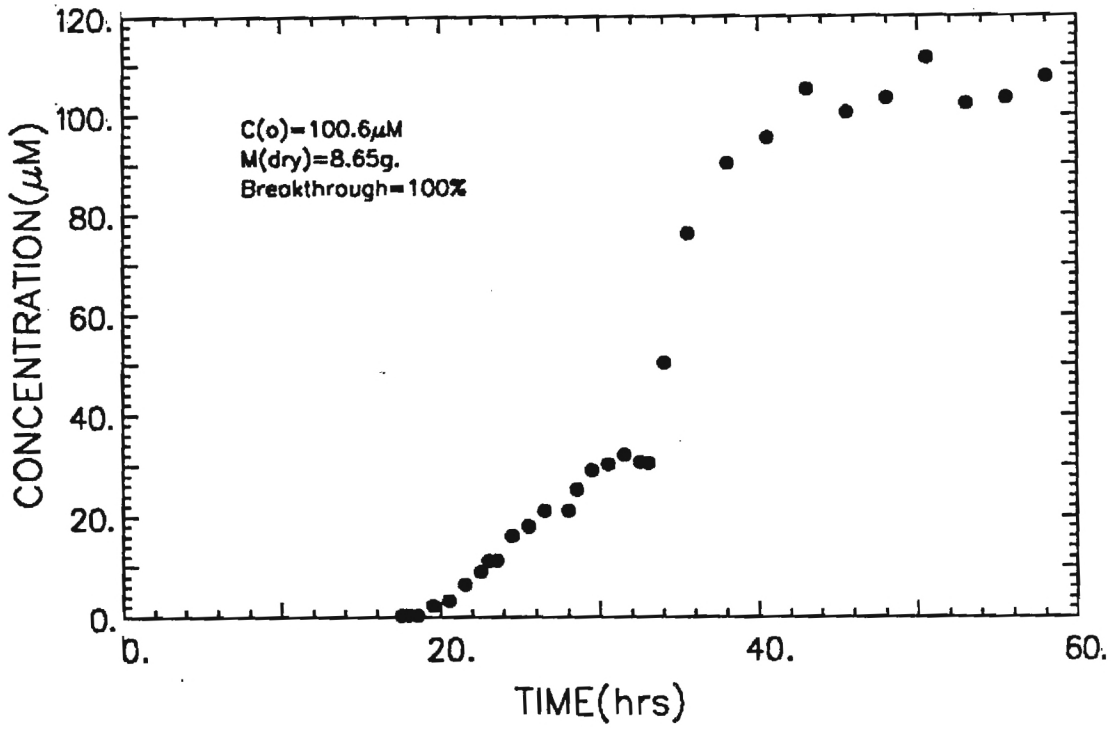

COLUMN ADSORPTION OF PNP ON XAD-16(2)

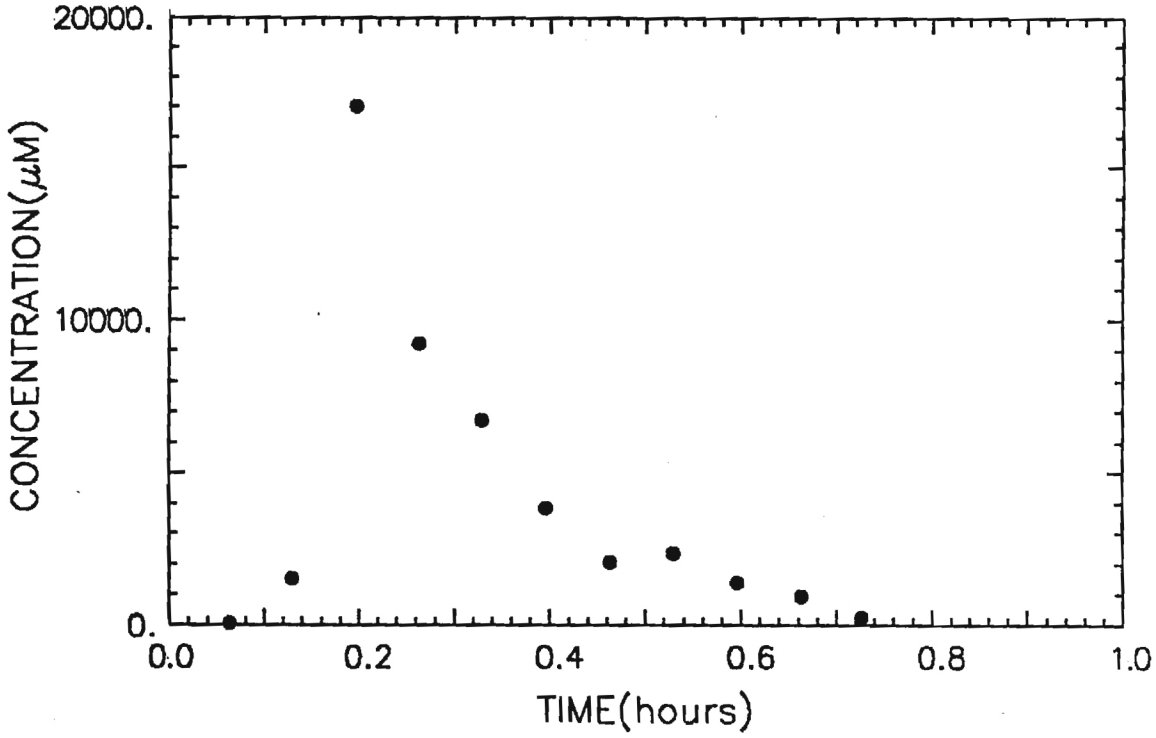

COLUMN DESORPTION OF PNP FROM XAD-16(2)

Figure 28

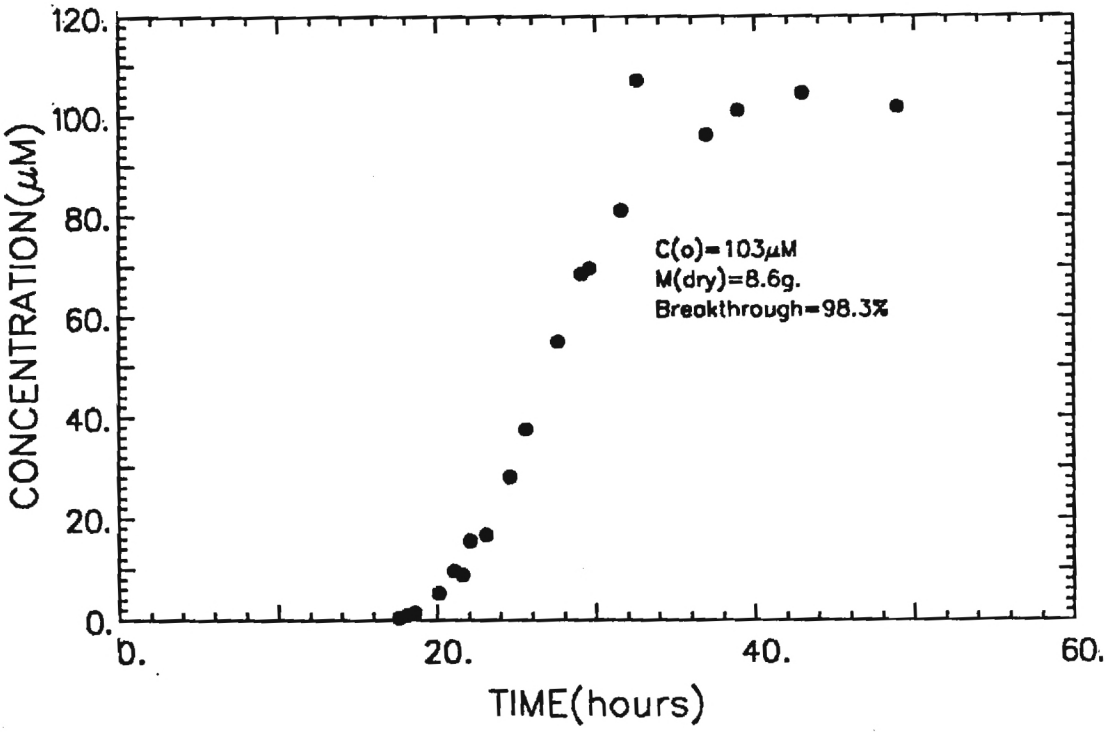

COLUMN ADSORPTION OF PNP ON XAD-16 (3)

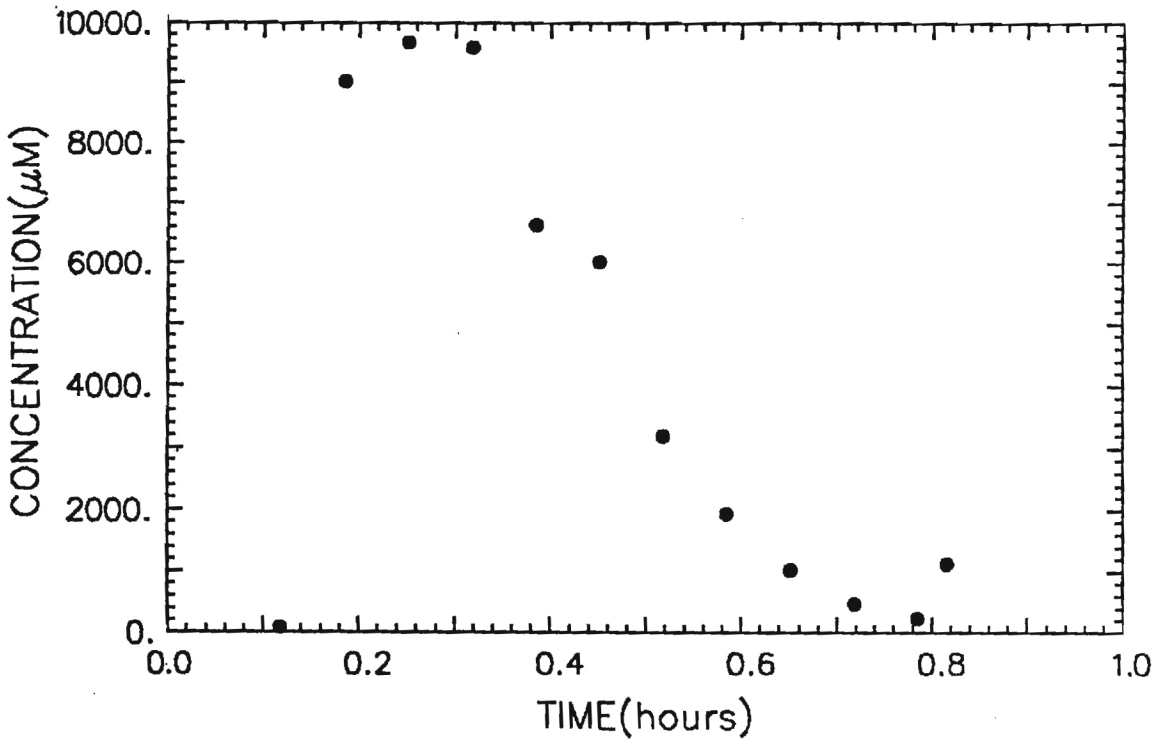

COLUMN DESORPTION OF PNP FROM XAD16(3)

Figure 29

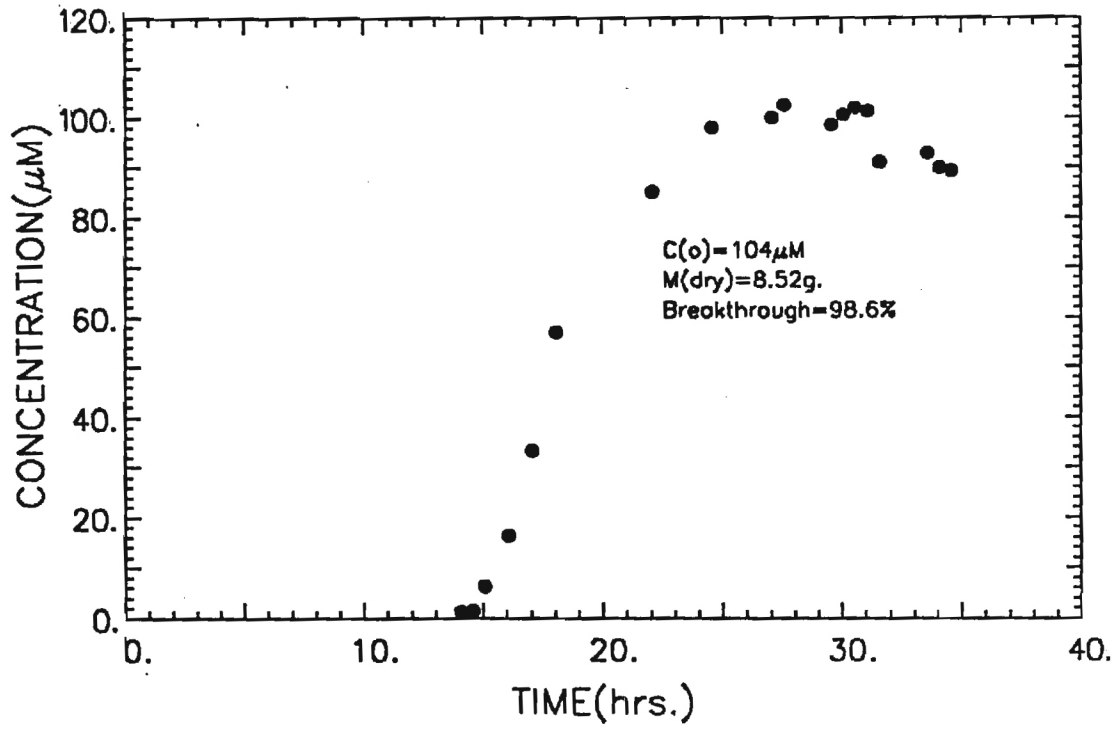

COLUMN ADSORPTION OF PNP ON XAD-16(4),pH=5

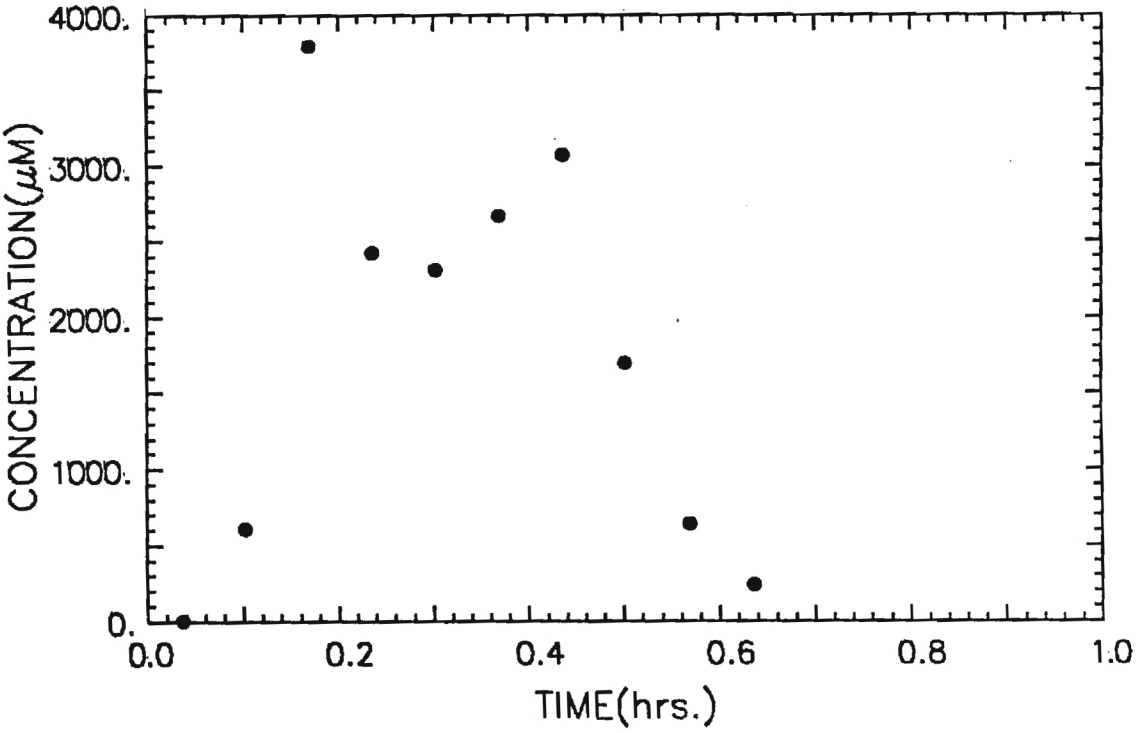

COLUMN DESORPTION OF PNP FROM XAD-16(4)

Figure 30

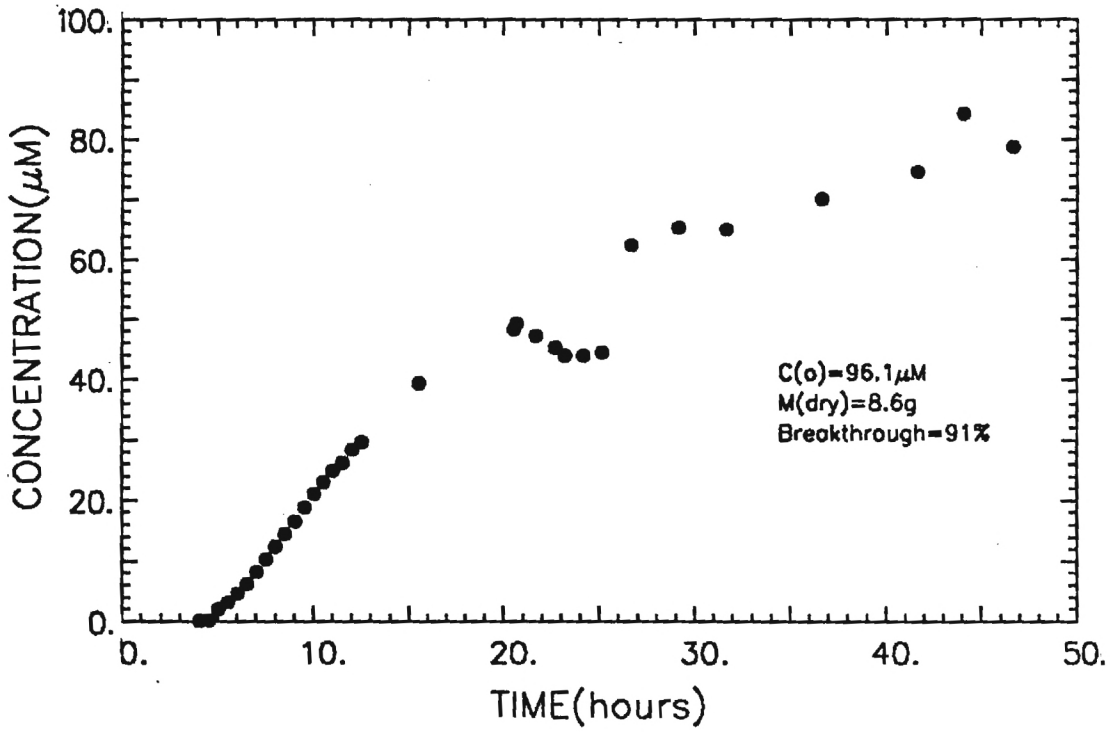

COLUMN ADSORPTION OF MO ON XAD-16 (1)

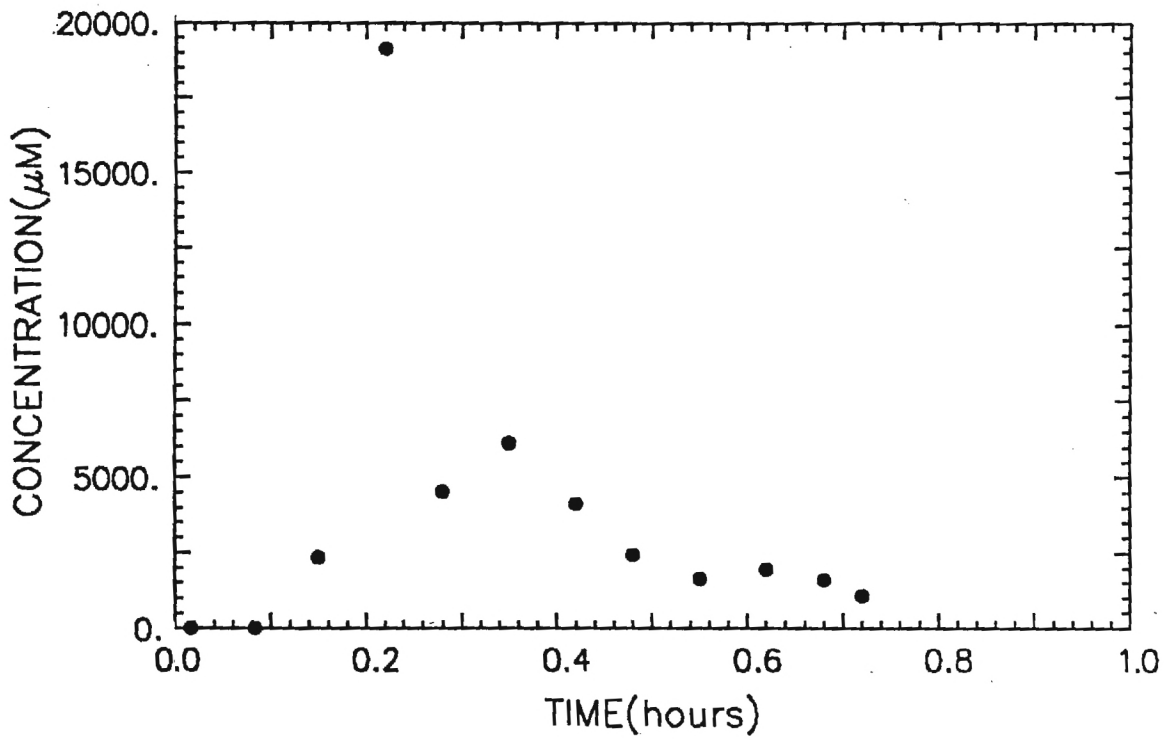

COLUMN DESORPTION OF M.O. FORM XAD-16(1)

Figure 31

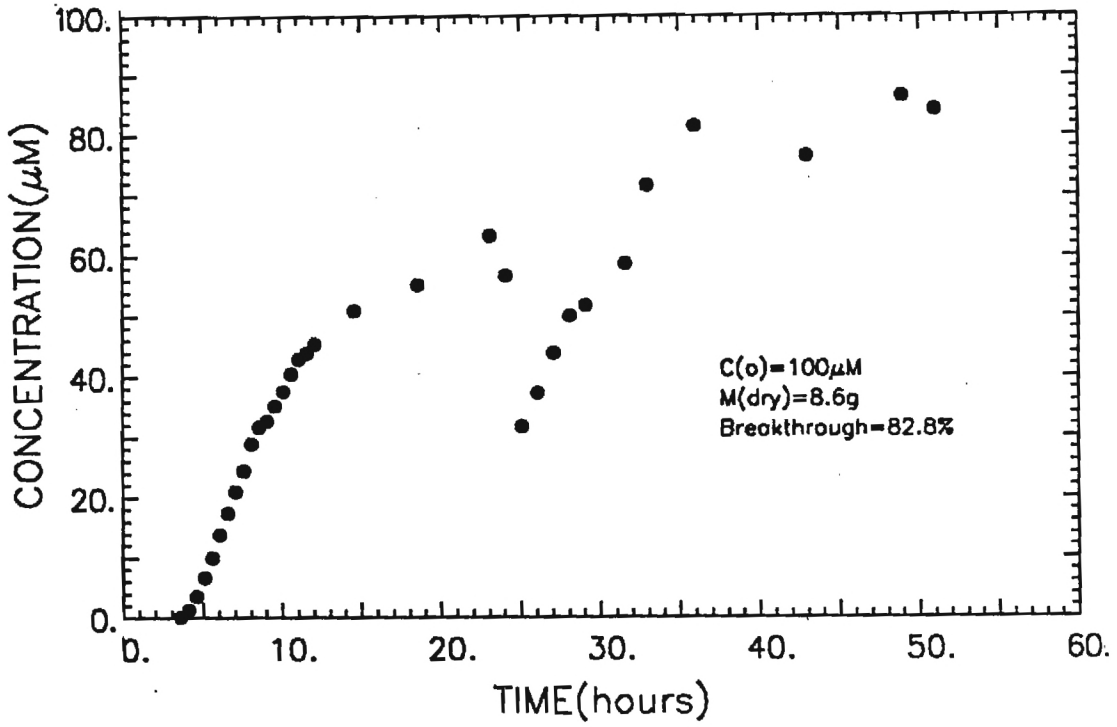

COLUMN ADSORPTION OF MO ON XAD-16(2)

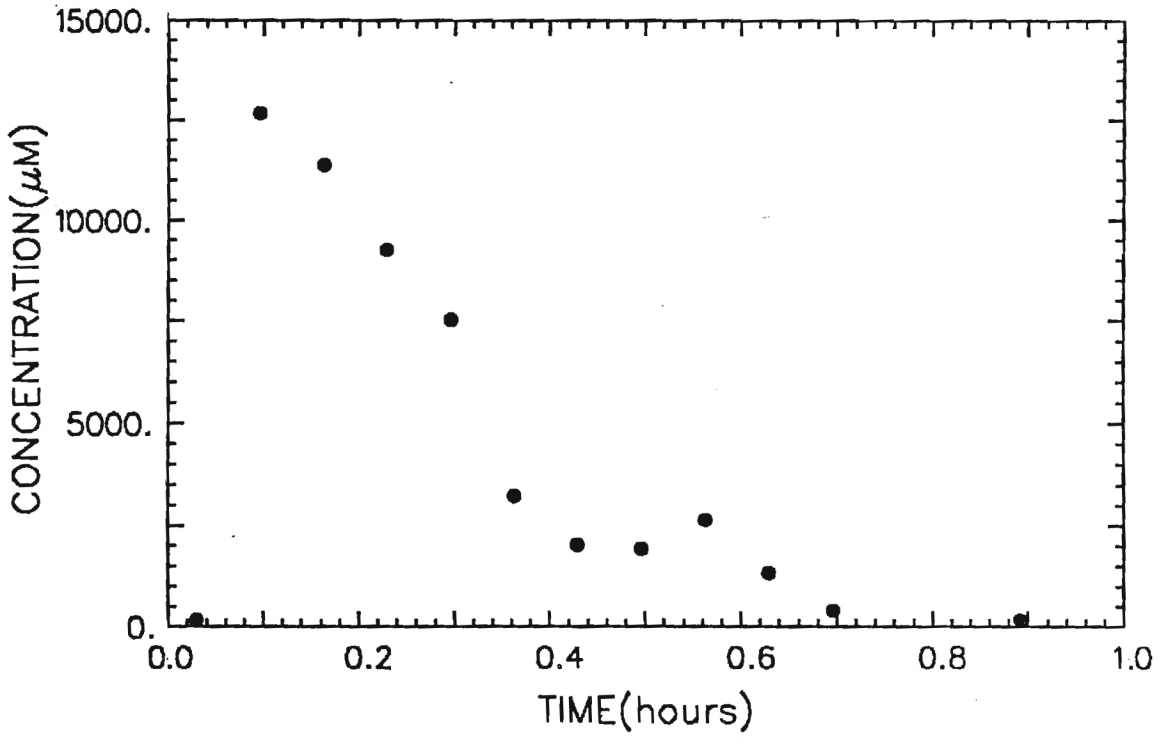

COLUMN DESORPTION OF M.O. FROM XAD-16(2)

Figure 32

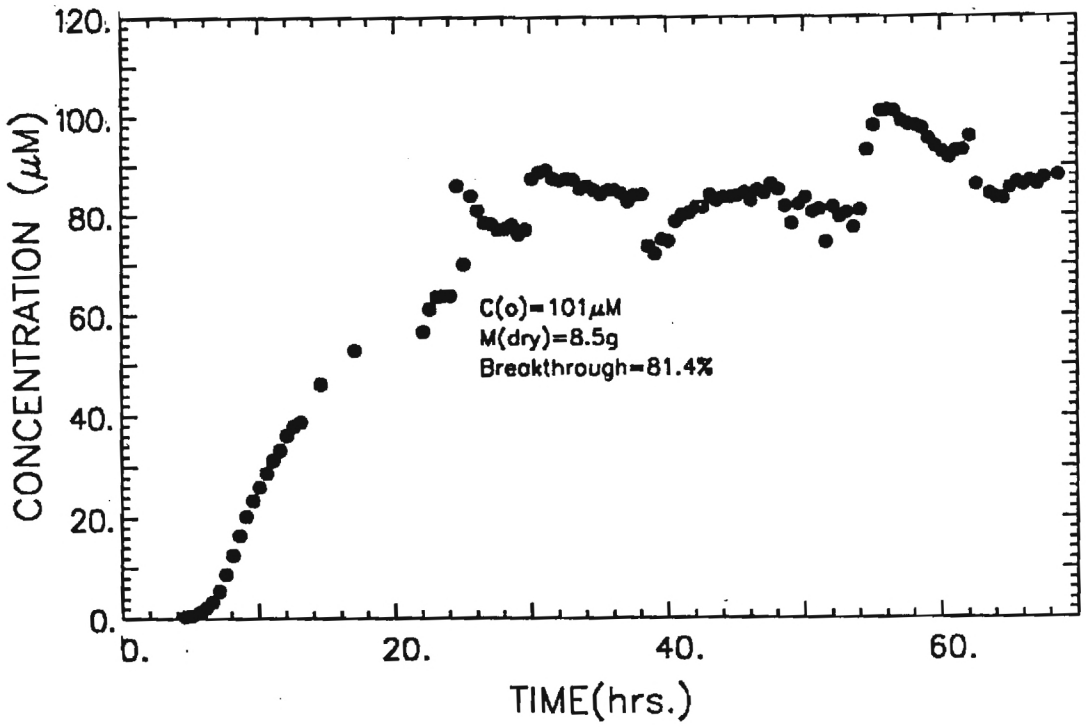

COLUMN ADSORPTION OF M.O. ON XAD-16(3)

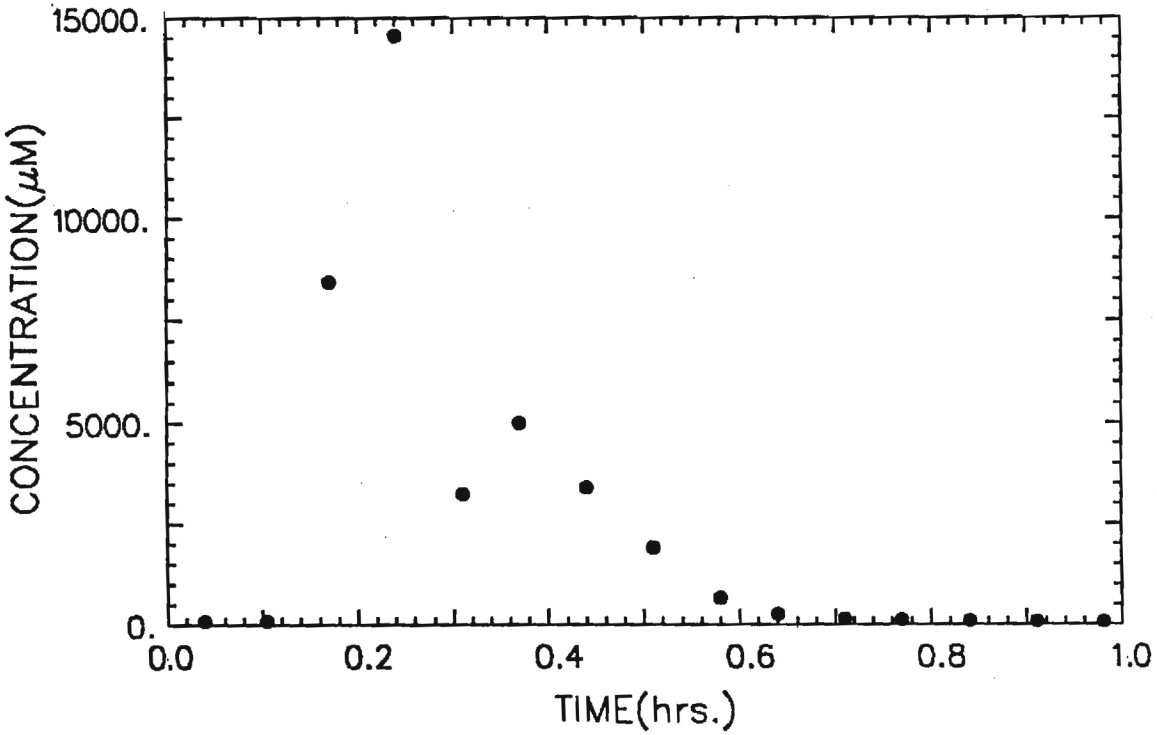

COLUMN DESORPTION OF M.O. FROM XAD-16(3)

Figure 33

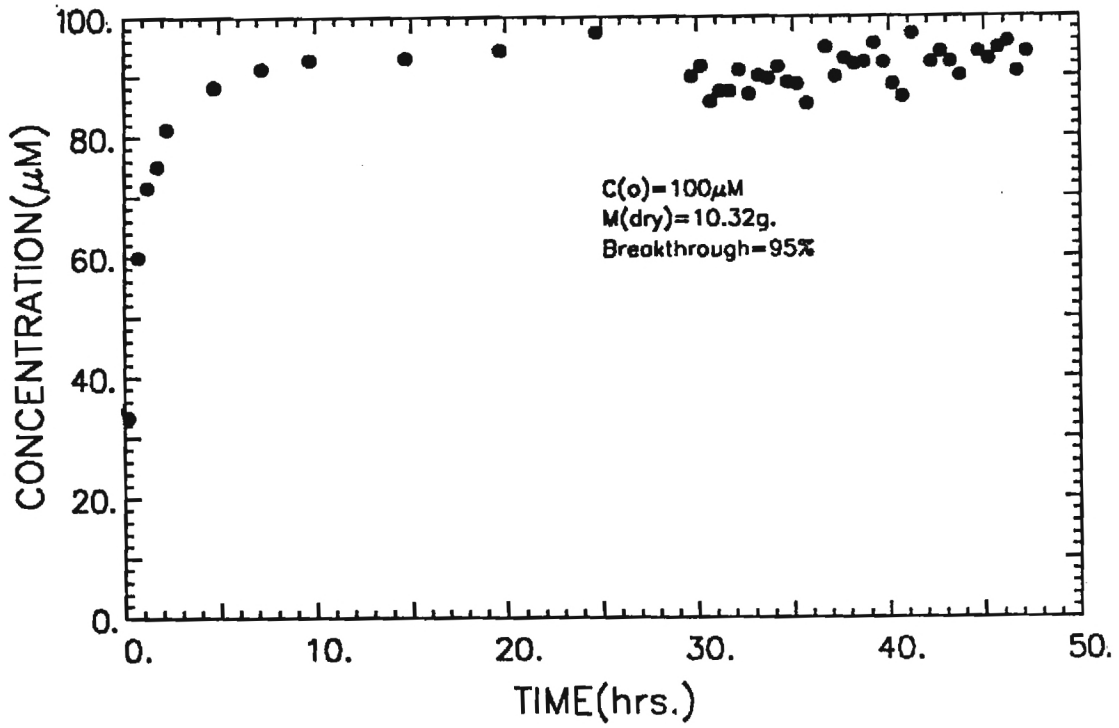

COLUMN ADSORPTION OF M.O. ON S-761

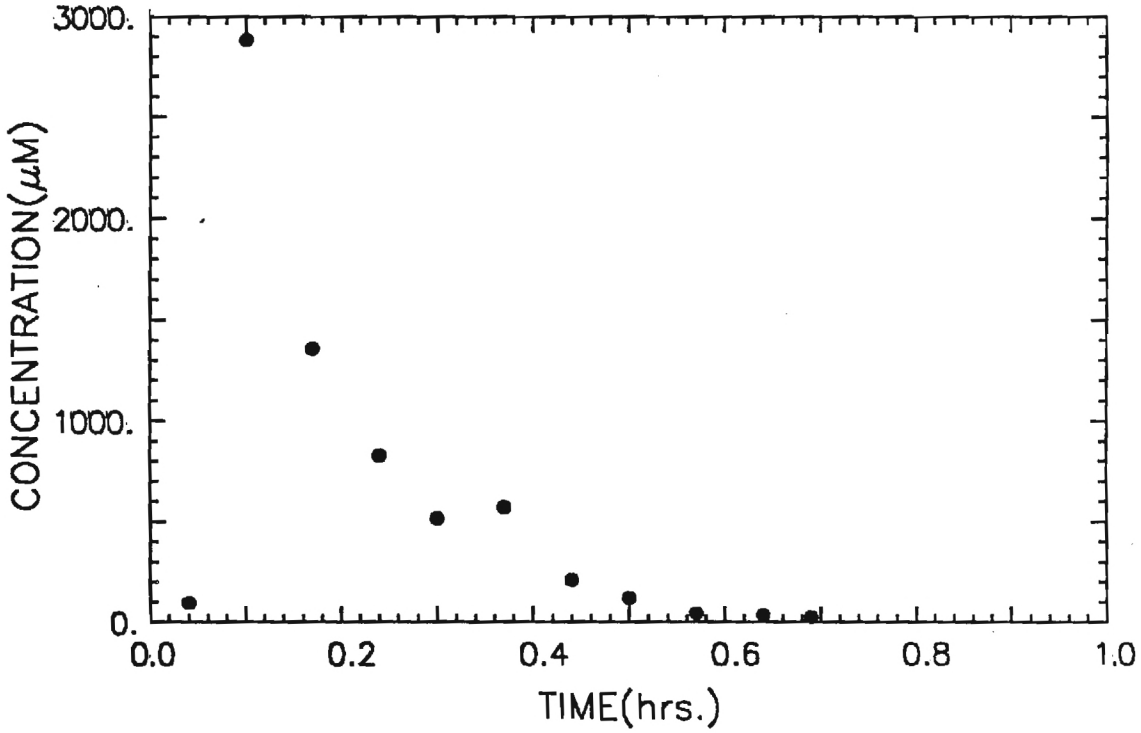

COLUMN DESORPTION OF M.O. FROM S-761

Figure 34

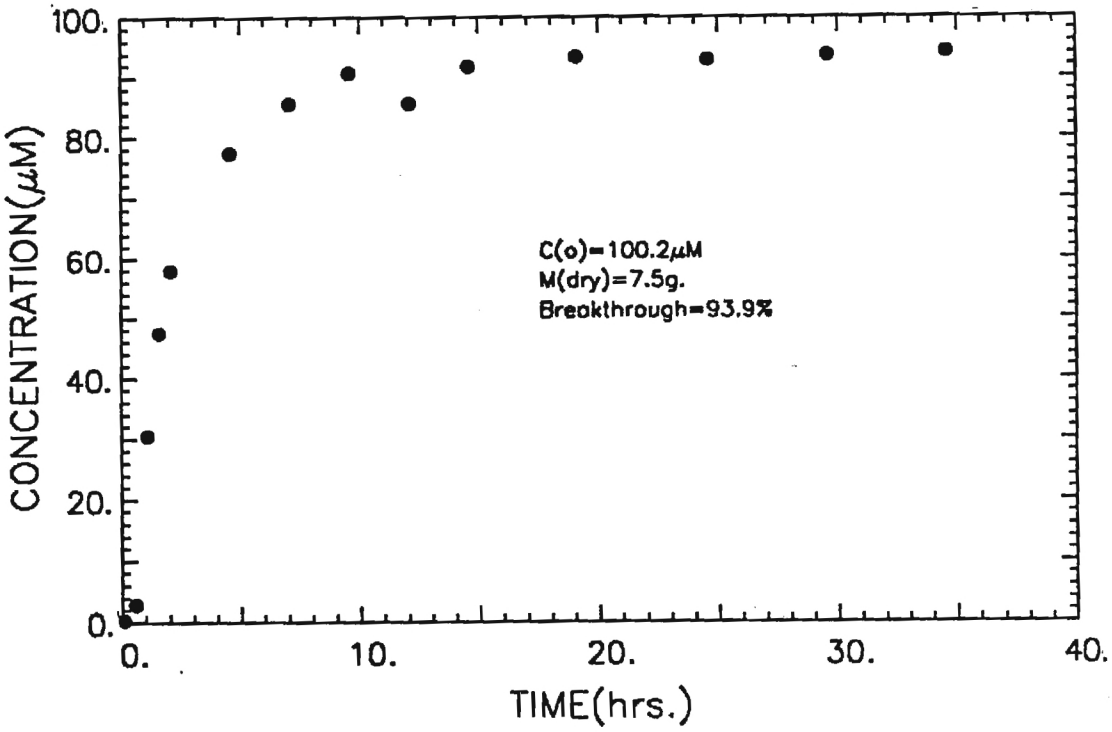

COLUMN ADSORPTION OF M.O. ON XAD-7

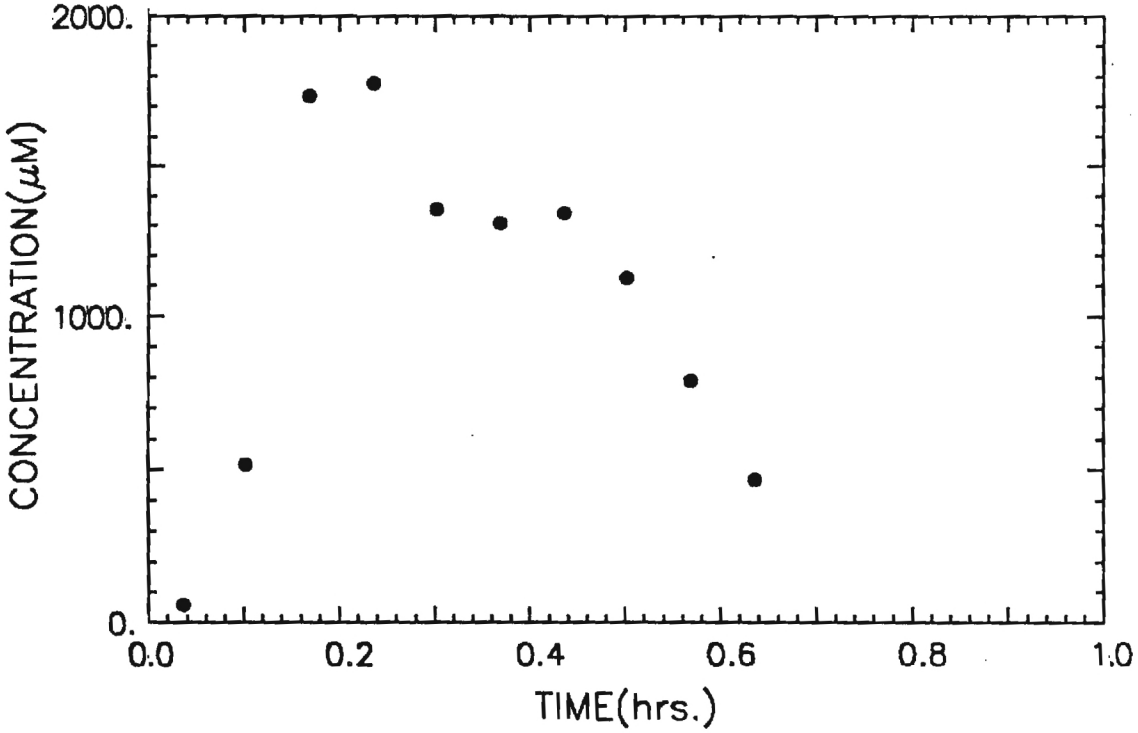

COLUMN DESORPTION OF M.O. FROM XAD-7

Figure 35

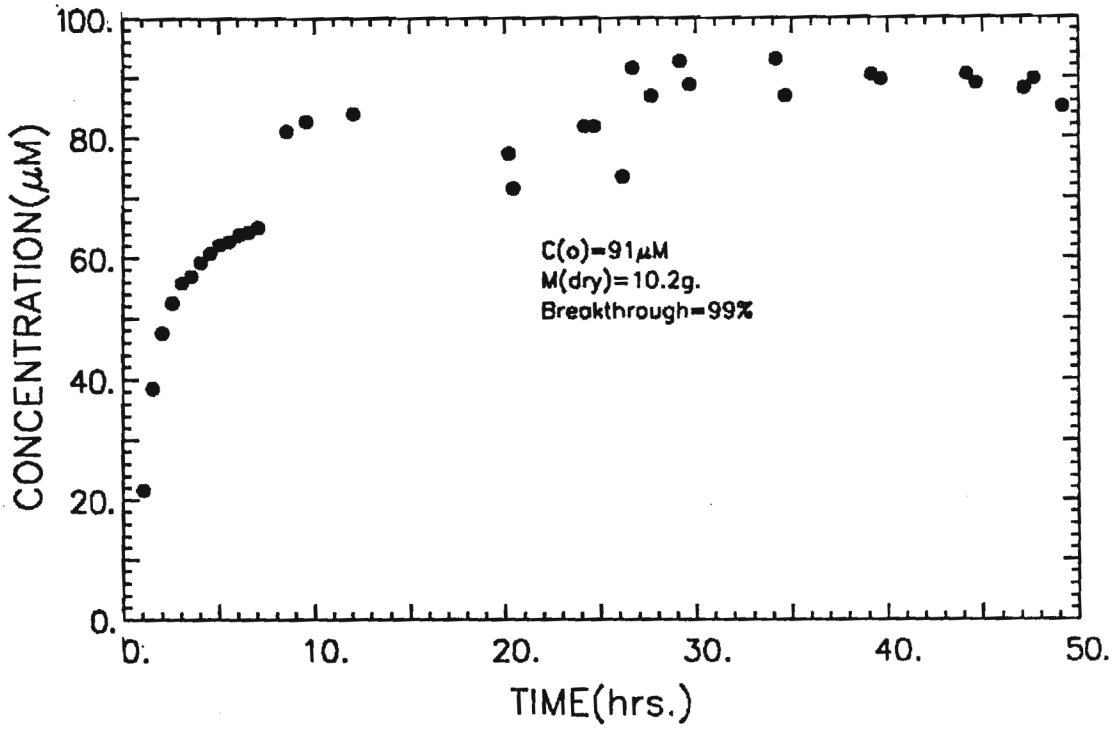

COLUMN ADSORPTION OF R40 ON XAD-16(1)

Figure 36

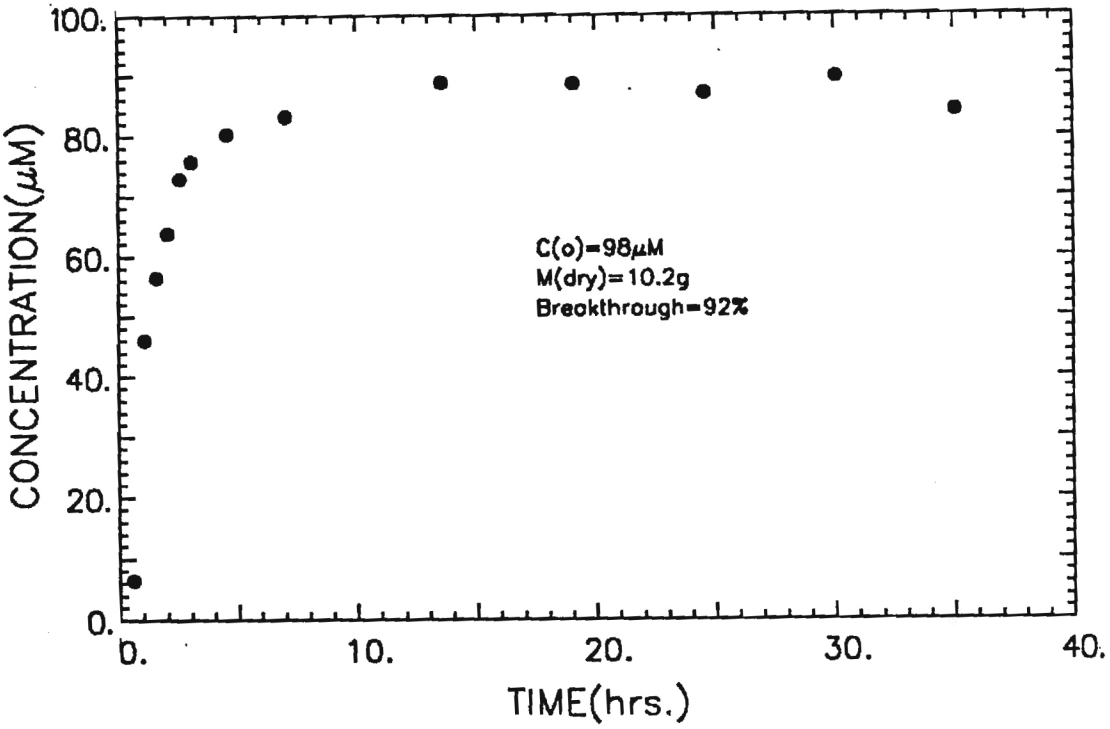

COLUMN ADSORPTION OF R40 ON XAD-16(2)

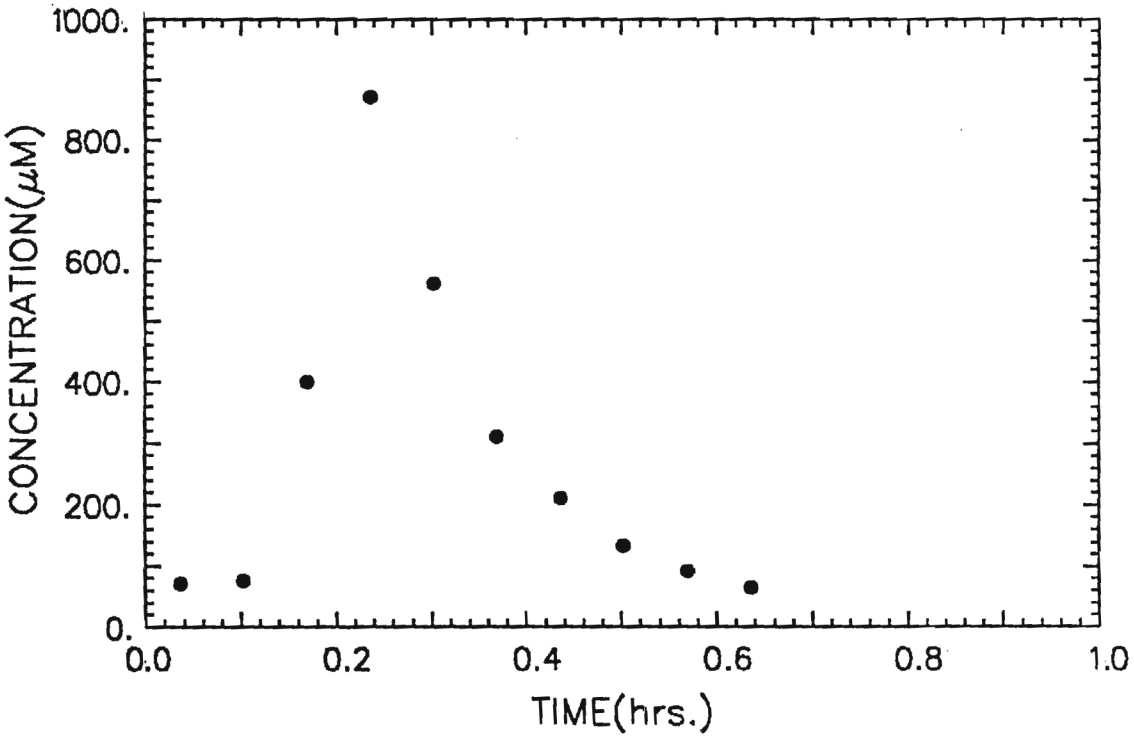

COLUMN DESORPTION OF R40 FROM XAD-16(2)

Figure 37

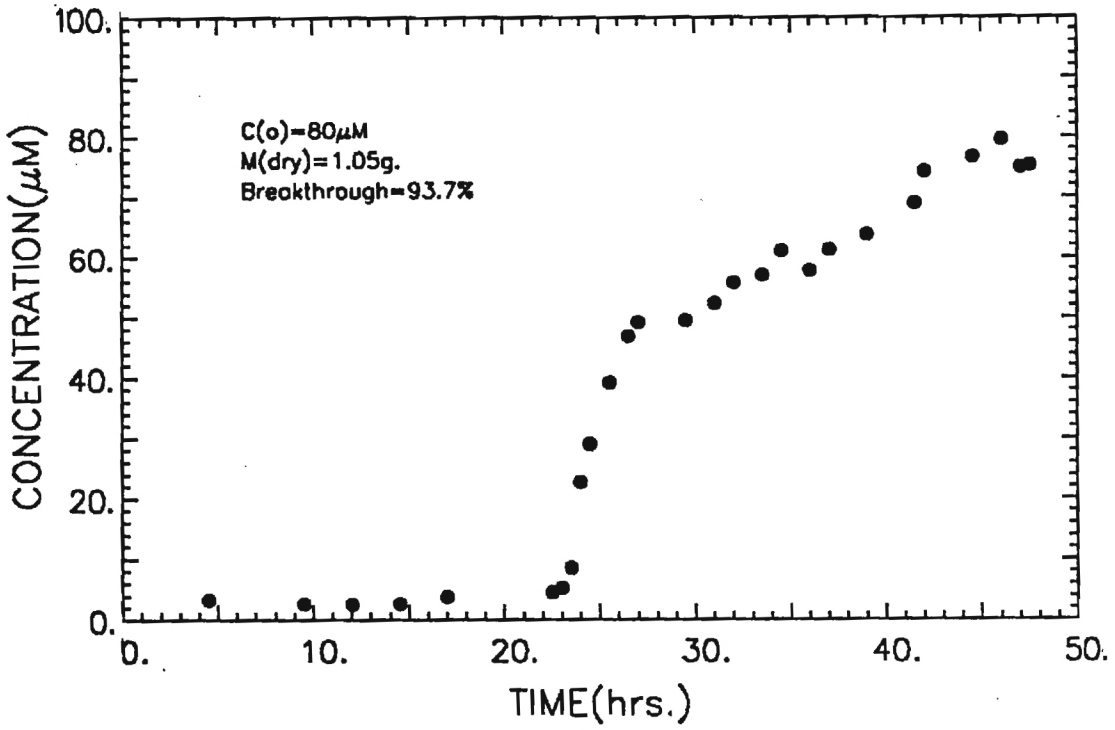

COLUMN ADSORPTION OF 4AAB ON XAD-7

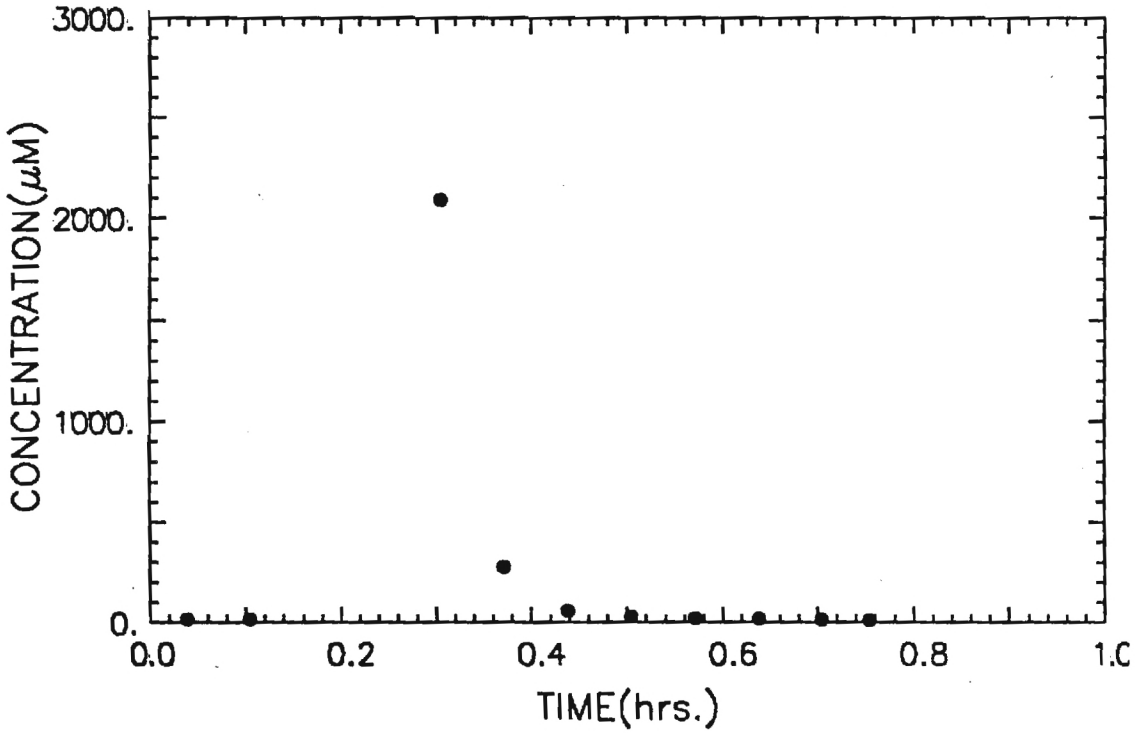

COLUMN DESORPTION OF 4AAB FROM XAD-7

Figure 38

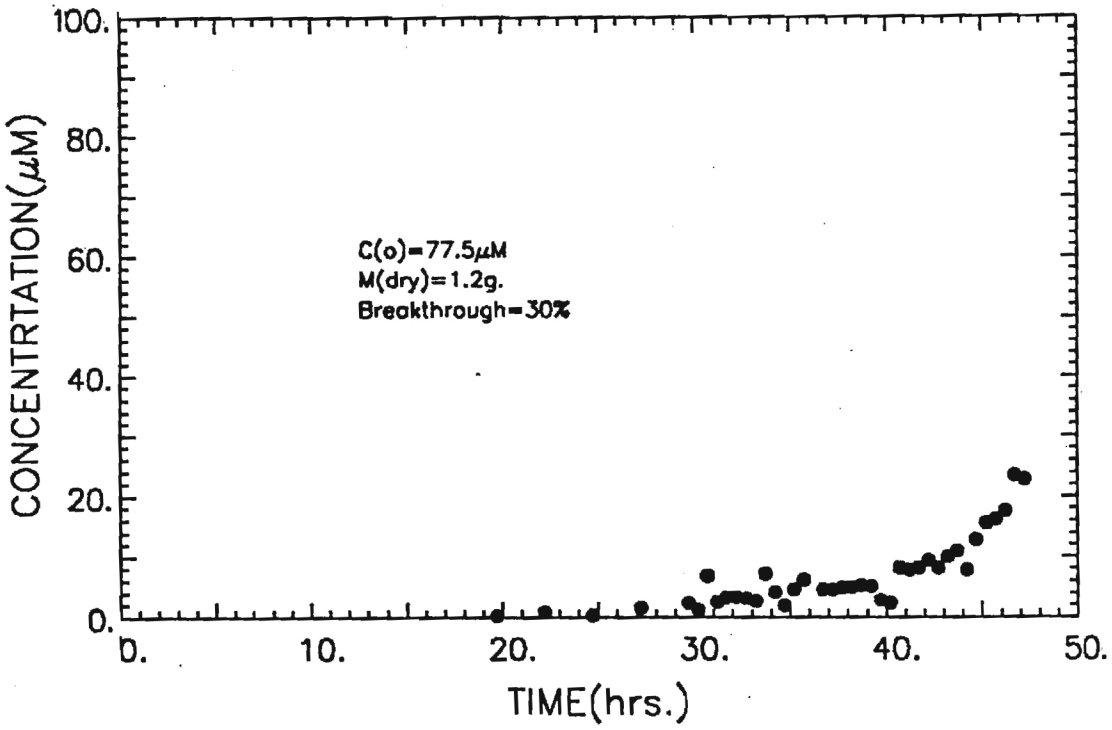

COLUMN ADSORPTION OF 4AAB ON XAD-16(1)

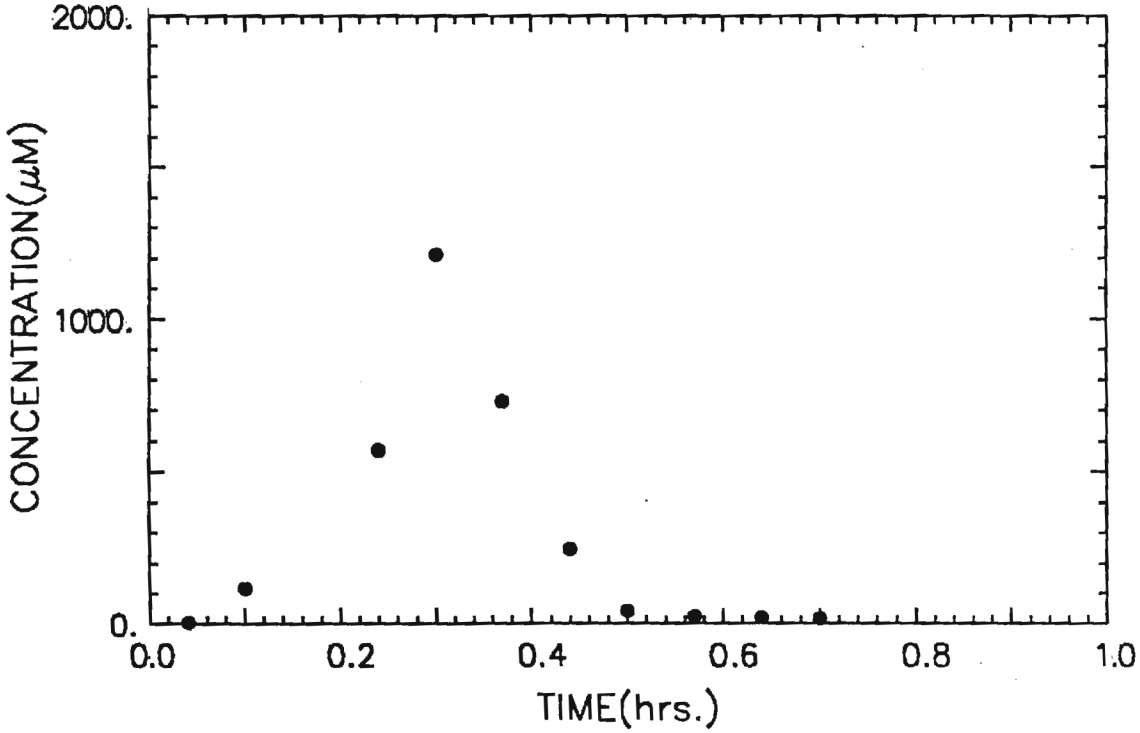

COLUMN DESORPTION OF 4AAB FROM XAD-16(1)

Figure 39

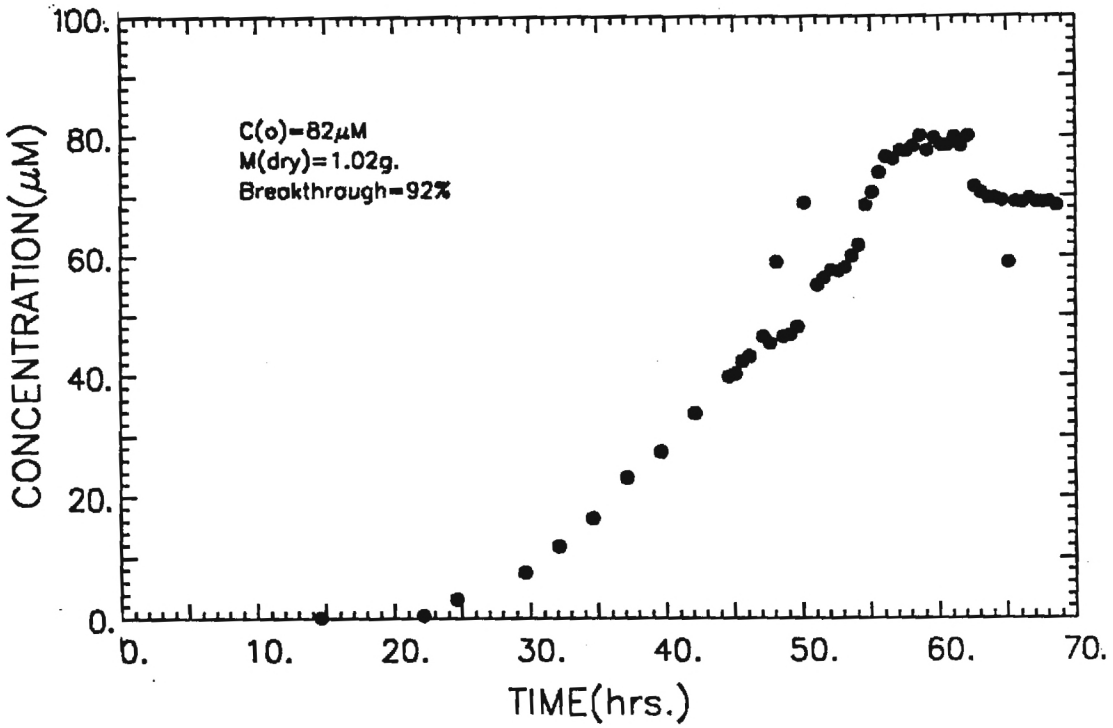

COLUMN ADSORPTION OF 4AAB ON XAD-16(2)

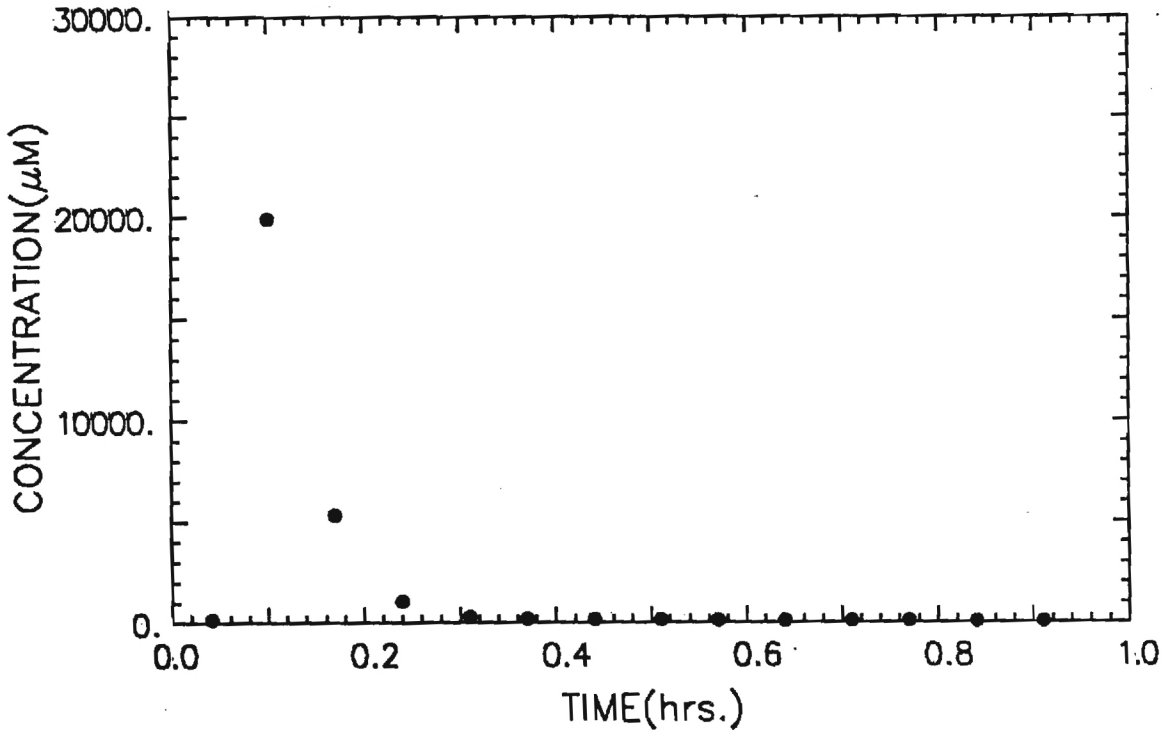

COLUMN DESORPTION OF 4AAB FROM XAD-16(2)

Figure 40

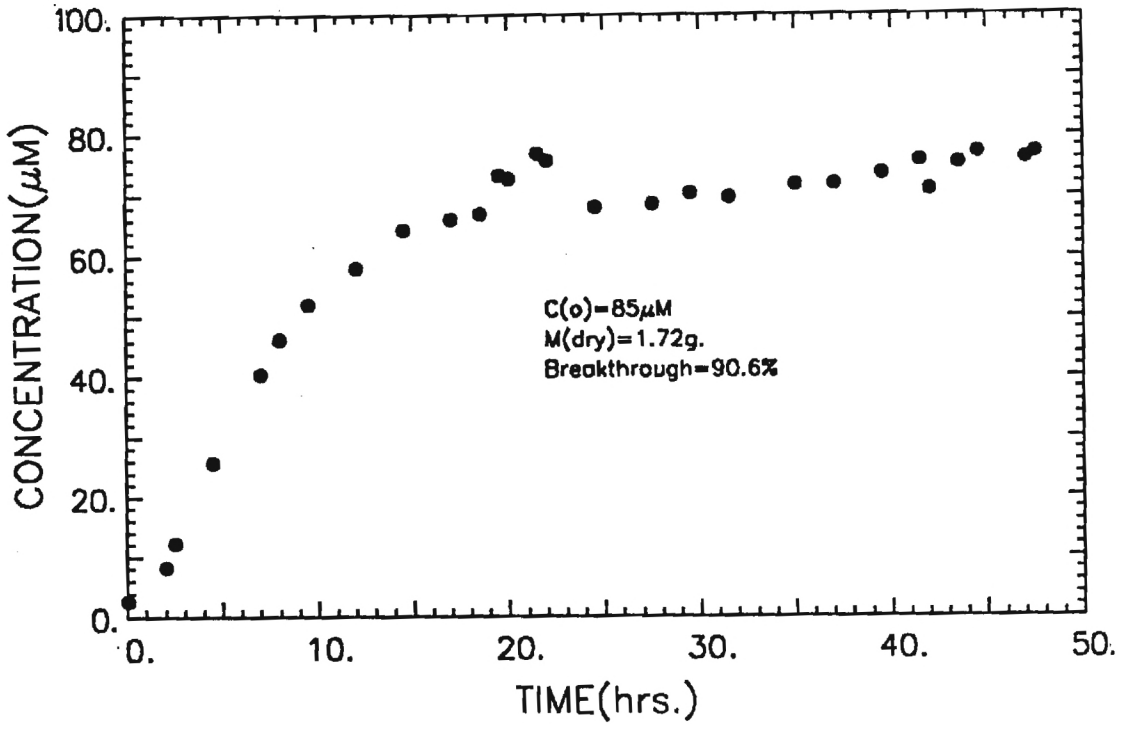

COLUMN ADSORPTION OF 4AAB ON S-761

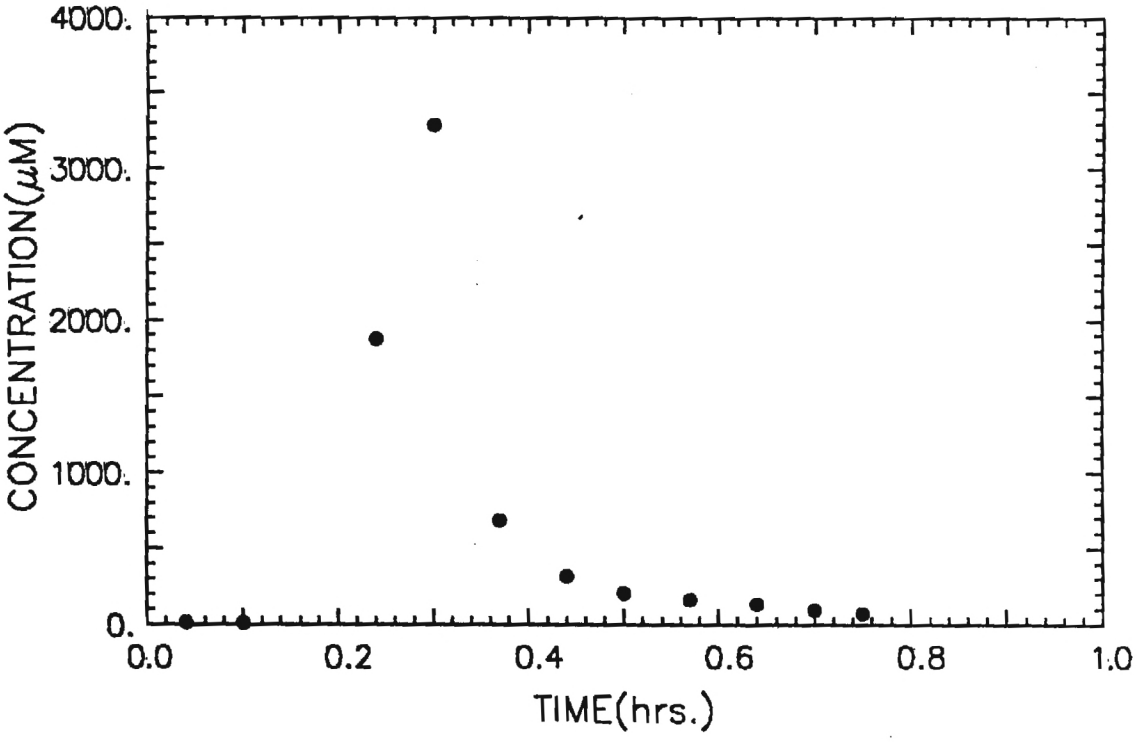

COLUMN DESORTION OF 4AAB FROM S-761

Figure 41

E-20-661

SCEGIT 88-101

DRAFT FINAL REPORT

ADSORPTION OF ORGANIC DYES ON SYNTHETIC RESINS FROM TEXTILE WASTEWATERS

Submitted to: U.S. Geological Survey
U.S. Department of the Interior

Grant Number: 14-08-0001-G-1070

Project Number E-20-661

Joseph P. Gould[1]
Byung R. Kim[2]
Jack H. Mizner, Jr.[3]
Kimberly A. Groff[4]

September 1987

[1]School of Civil Engineering, Georgia Institute of Technology
Atlanta, GA 30332
[2]Environmental Science Department, General Motors Research Laboratories,
Warren, MI 48090
[3]City of Atlanta, Bureau of Pollution Control, Division of Research
and Development, 2440 Bolton Road, NW, Atlanta, GA 30318
[4]Environmental Research and Technology, 696 Virginia Road,
Concord, MA 01742

TABLE OF CONTENTS

Table of Contents (continued)

LIST OF TABLES

LIST OF FIGURES

ABSTRACT

The adsorption of several water soluble synthetic dyes typical of those used in the textile industry and selected related compounds on synthetic adsorbent resins has been investigated. In the initial phases of this research, the adsorption of the compounds in batch systems on several resins was measured. On the basis of these studies, three resins, XAD-7, XAD-16 and S-761 were chosen for more extensive study.

The selected resins were used to develop detailed equilibrium and kinetic adsorption data in batch systems on the full range of selected dyes and dye related compounds. These resins were then used in column systems to assess the kinetics of adsorption in continuous flow applications. The columns were run to breakthrough levels equal to 90% or more of the influent concentrations.

Upon completion of the breakthrough studies, desorption studies were conducted using methanol as the regenerant solvent. In selected systems, resin columns were subjected to several cycles of adsorption followed by solvent regeneration. It was found that methanol had a substantial capacity for regeneration of these dye laden resins. In addition, it was found that, while the initial saturation of the resin resulted in loss of a fraction of capacity due in all probability to irreversible adsorption the remaining capacity was entirely recoverable thenceforth.

DISCLAIMER

Contents of this report were developed under a grant from the U.S. Geological Survey, Department of the Interior. However, the contents do not necessarily represent the policy of that agency and endorsement by the Federal Government should not be assumed.

Supported by the U.S. Geological Survey, Department of the Interior under award No. 14-08-0001-G-1070.

CHAPTER 1

INTRODUCTION

Among the most challenging problems in the environmental area is that associated with the discharge of wastewaters containing large quantities of synthetic organic dyes from textile dyeing operations. These synthetic dyes are, in many cases, largely resistent to conventional biological wastewater treatment and thus pass through wastewater treatment plants unchanged and are discharged thence to receiving bodies of water. This is of great concern since information regarding the impact of these complex organic compounds on the aquatic environment is essentially nonexistant. While techniques such as chlorination and ozonation have some potential for the destruction of the dyes by chemical oxidation, the latter process is likely to be prohibitively expensive when applied to the large volume flows characteristic of major fabric and carpet dyeing operations and the manufacture of paper products while former will certainly generate chlorination products which may be even more toxic and stable than the dyes themselves.

A treatment method which is free of the problems described above and thus quite attractive in this context is adsorption. Adsorption actually removes the dyes from solution rather than chemically modifying them, thereby avoiding problems associated with potential generation of toxic oxidation/chlorination production. From an economic standpoint, adsorption is, at first inspection, not very attractive due mainly to the high cost of typical adsorbents such as granular active carbon or adsorbent resins. In order to take advantage of the attractive features of adsorption it is necessary to develop facile methods of regenerating the adsorbent thereby permitting reuse of the most expensive component of the system, the sorbent. In this context, adsorbent resins are especially attractive. Unlike carbon, they can, to a large degree, be tailored during the manufacturing process to meet the precise requirements of a specific application. Their cost, however, makes regeneration even more necessary to render resin sorption economically feasible.

The report which follows describes the examination of resin adsorption of synthetic dyes and dye related organic compounds. In addition, the regeneration of the resins by organic solvent description will be investigated and the overall feasibility of resin sorption assessed.

CHAPTER 2

LITERATURE REVIEW

2.1 ADSORPTION PHENOMENA

2.1.1 Effect of Characteristics of Adsorbent on Adsorption

Synthetic resins are organic polymers which consist of basic matrices with some functional groups attached, as shown in Figure 1. They are classified, therefore, usually by type of matrix, functional group, and physical structure.

Resin Matrix -- The matrices of most resins are either aromatic ring-structured or aliphatic chain-structured. The most common aromatic structures are phenol-formaldehyde and styrene-divinylbenzene, as shown in Figure 1.

Functional Groups -- Functional groups, which are fixed ionic groups and responsible for ion exchange, are introduced by substitution during or after polymerization, or by starting with monomers that carry ionic groups. Depending on the type of functional group, the resin is classified as cation, anion exchangers, and nonionic. Cation and anion exchange resins exchange cations and anions, respectively, during the demineralization process, whereas nonionic resins do not possess this property. The functional groups of cation and anion exchange resins show various acid and base strengths, respectively. Thus, the resin is further classified as a strong-acid cation exchange resin, weak-acid cation exchange resin, strong-base anion exchange resin, or weak-base anion exchange resins. Examples are the strong-acid resin with sulfonate groups ($-SO_3^-$), the weak-acid resin with carboxylate groups ($-COO^-$), the strong-base resin with quaternary amine groups ($-NR_3^+$), and the weak-base resin with primary amine groups ($-NH_2$), as shown in Figure 1.

Nonionic resins are characterized only by their matrix, physical porosity, uniform pore size distribution, and high surface area. They have been developed mainly for the removal of organics by adsorption.

Physical Structure -- The physical structure of resins is differentiated, in general, by porosity, and surface area which are directly related to the degree of cross-linking. To describe the porosity of resins, the terms, "microporous," "macroporous," and "macroreticular," are used. Diameters of the micropores and the macropores are considered to be 20 Å or less and greater than 1000 Å, respectively. The pores of intermediate size are called transitional pores. "-Reticular" is a unique term to describe resins with special structures (for example, XAD series manufactured by Rohm and Haas). A granule of these resins consists of a large number of very small microspheres, fused together in a spherical agglomerate. Therefore, "-reticular" is used to differentiate between pores inside the microspheres and pores outside the microspheres. These outside pores, which exist within the gel structure formed by tiny microspheres, are called microreticular pores when their size is less than 10 Å, and called macroreticular pores when their size is larger than 200 Å. The intermediate pores are transitional pores.

The total surface area (internal and external) of resins is generally smaller than that of activated carbon which is on the order of 1000 sq meters

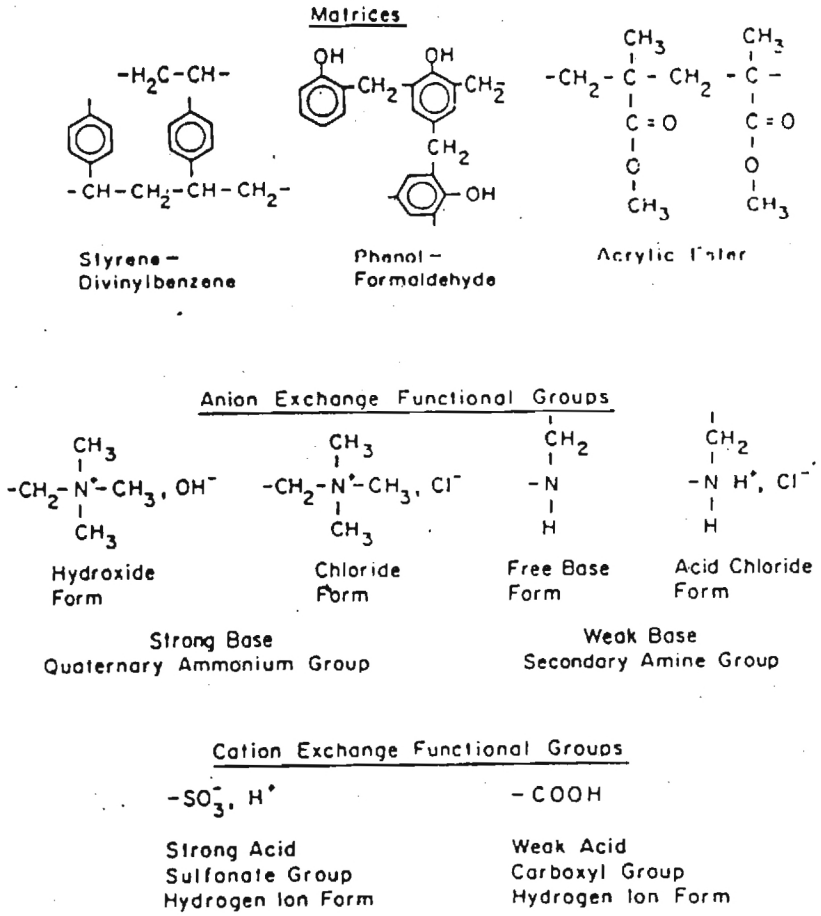

Figure 1. Matrices and Functional Groups of Commonly Used Synthetic Resins.

per gram of carbon (Process Design Manual, 1973), whereas the pore size of resins is larger than that of activated carbon (Gustafson and Paleos, 1971). Higher adsorption of proteins (size of virus) was reported on synthetic resins than on activated carbon (Foster, et al., 1977) probably due to larger pore opening of resins and thus more accessibility of internal surface area.

Organic solutes are, in general, removed by the resins, through two types of interactions; (1) between the solute and the resin matrix, and (2) between the solute and the functional groups. Adsorption on the resin matrix seems to be due to (1) London interaction between the solute and the matrix (Gasser and Kipling, 1960), (2) the dipole-dipole interactions between the polar solvent molecules and polar groups of the solute which tend to squeeze hydrocarbons out of the polar solution such as water (Helfferich, 1962), and (3) the inter- action of electrons between the aromatic rings of the matrix and the solute when the aromatic compounds are adsorbed on the aromatic type matrix (Gustafson and Paleos, 1971).

The mechanisms of organic removal by functional groups are known to be (1) ion exchange when the functional group is ionized and attracts counter ions of the solute, (2) hydrogen bonding between the hydrogen and the electro-negative atom, such as oxygen, nitrogen, halogen, or carbon, and (3) complex formation when the transition metals such as Cu are present as counter ions for the cation exchanger and make strong complexes with ammonia and organic amines. Cation exchange resin showed little capacity for removal of organics such as phenol (Chasanov, et al., 1956), and color and COD of secondary effluent (Rebhun and Kaufman, 1967). This seems to be due to the nature of organics in secondary effluent that was reported to be mostly anionic (Hunter, 1971). This was also supported by good performance of both strong- and weak-base anion exchange resins in removing the above organics (Anderson and Hansen, 1955; Rebhun and Kaufman, 1967; Kim, et al., 1976) and other anionic organics such as benzenesulfonate compounds (Abrams, 1966; Hinrichs and Snoeyink, 1976). The removal of these various benzenesulfonates was attributed mainly to the ion exchange mechanism where the solute and the amine functional group are both ionized.

Hydrogen bonding was speculated to be the major mechanism of adsorption of organic acids, such as phenol (Chasanov, et al., 1956; Kumagai and Kaufman, 1969) and p-nitrophenol (Kim, et al., 1976), on weak-base resins with amine functional groups, where the bonding seemed to occur between the nitrogen of the amine functional group and the hydrogen of the solute. The degree of ionization or protonation of the amine functional group, which could be estimated by the pK of the resin and the pH of solution, decreased the adsorption capacity, because the protonation appeared to block the bonding sites (Kim, et al., 1976; Kumagai and Kaufman, 1968). Ionization of the solute also decreased the capacity due to the loss of hydrogen of the solute. Therefore, it was observed that there was an optimal pH range for adsorption of phenol and p-nitrophenol, where the nonprotonated amine group and the nonionized solute coexist (Kim, et al., 1976; Kumagai and Kaufman, 1968).

Sorption of organic molecules on nonionic resins can be classified, in general, into two types: (1) a polar interaction between the hydrophilic portion of the solute molecule and the relatively hydrophilic surface of the resin such as aliphatic surface, and (2) a nonpolar interaction between the hydrophobic portion of the solute molecule and the hydrophobic surface of the

resin. The hydrophilicity of the resin surface depends on the polarity of the resin matrix.

Porosity, pore size, and surface area play an important role in competitive adsorption. The macroporous and/or macroreticular resins have been studied and used preferably for organic removal because organic molecules are much larger than inorganic molecules or metal ions, the removal of which was the main target for developing the traditional microporous resins.

Finally, the major advantage of using synthetic resins is that they can be manufactured with porosity, pore size, and surfaces of predetermined characteristics for a specific adsorption application.

2.1.2 Effect of adsorbates on Adsorption

The type of adsorbate, as characterized by size, shape, molecular weight, solubility, polarity, charge, affinity for the adsorption sites, and orientation at the adsorbent surface, influences adsorption characteristics.

The molar adsorption of larger solute molecules per unit weight of adsorbent is normally less than that of smaller ones when the orientation of molecules at the surface is parallel to the surface. For example, the carbon adsorption capacity for dodecylbenzenesulfonates was reported to be 40 percent of that for phenol (Morris and Weber, 1964), probably because a dodecyl-benzenesulfonate molecule took more adsorption sites than a phenol molecule did. Although this agrees with the theory of monolayer adsorption, this may not be true when multilayer adsorption occurs or when the orientation is normal to the surface.

The solubility of adsorbates also influences adsorption. In general, the less soluble material tends to be adsorbed more strongly (Adamson, 1967). For example, the anionic form of weak acids is more soluble than the neutral form. The adsorption of the neutral form of p-nitrophenol was higher than that of the anionic form (Jain and Snoeyink, 1973). This indicates that the pK_a of an adsorbate and the pH of a solution determine the form of the adsorbate and thus influence the adsorption. Furthermore, some adsorbates which are adsorbed at low pH will be desorbed at high pH. This is the reason why an alkaline solution such as sodium hydroxide solution can be used to regenerate spent synthetic resins. An organic solvent is also used to regenerate spent adsorbents because the solvent is selected such that the solubility of adsorbates in the solvent is higher than that in water.

The polarity of the adsorbate is also important. It is known that a nonpolar adsorbent, such as activated carbon and hydrophobic resins (aromatic nonionic resins), will preferentially adsorb the more nonpolar compounds from a polar solution such as water (Adamson, 1967). Adsorption of fatty acids by carbon (Adamson, 1967) and by hydrophobic resins (Gustafson and Paleos, 1971) increased in the order: formic acid, acetic acid, propionic acid, and butyric acid. The reverse was true when the fatty acids were adsorbed on a polar adsorbent (silica gel) from a nonpolar solution (toluene) (Adamson, 1967).

The molecular size, the pore size distribution, polarities of adsorbents and adsorbates, the orientation of the adsorbate on the surface, and the solubility of the adsorbate are all interrelated to one another in the

adsorption process, resulting in complex behavior.

2.1.2 Effect of Characteristics of Solution on Adsorption

The characteristics of the solution including pH, polarity, temperature, and other inorganic and/or organic species in the system also affect the adsorption of the solute of interest. The effect of pH and polarity on adsorption was discussed in the previous section along with the characteristics of adsorbates.

The adsorption of organics on carbon and synthetic resins is known to be exothermic as indicated by the greater adsorption of various organics on resins (Gustafson and Paleos, 1971) and of p-nitrophenol on carbon (Snoeyink, et al., 1969) at lower temperature. However, the net effect of temperature on the actual application of the adsorption system needs to be studied closely since decreased temperature increases the adsorption capacity but decreases the mass transfer rate through surface film and pore.

Other inorganic and organic species interfere with the adsorption of the solute of interest by competing for adsorption sites or changing the surface properties. Snoeyink, et al (1969) observed that the presence of 1 M NaCl at pH 10 enhanced the adsorption of p-nitrophenol. Randke and Jepsen (1982) found that the addition of salts improved adsorption of fulvic acids on activated carbon. This phenomenon was attributed to ion pair formation between metal ions, organic anions, salting-out effect, charge neutralization of organic anions and negative carbon surface by metal ions, and altered packing and orientation of adsorbed adsorbates due to the presence of metal ions. Interference of other organic compounds is also important because the adsorption system is more complex and, in effect, a multi-solute system. It was observed that adsorption isotherms in a mixture of organics were lower than those in corresponding single solute systems (McGuire and Suffet, 1978; Jain and Snoeyink, 1973; Herzing, et al., 1977). Isotherms in a bisolute system of n-butanol and 1,4-dioxane were lower than those in single solute systems at high equilibrium concentrations due to competition and became identical at low equilibrium concentrations probably due to the presence of sufficient adsorption sites which could prevent the competition (McGuire and Suffet, 1978). The relative competition among p-nitrophenol, p-bromophenol, and benzenesulfonate was studied by Jain and Snoeyink (1973). The interference of humic acid was also reported in adsorption of odor causing materials, 2-methylisoborneol and geosmin, on activated carbon (Herzing, et al., 1977).

2.2 ADSORPTION OF DYES

The treatment of textile wastewaters using adsorption has been studied by many researchers (Gardiner and Borne, 1978; McKay, 1978. 1979, 1980; McKay, et al., 1982a, 1982b; Roy and Volesby, 1978; Posey and Kim, 1983; Cross, et al., 1982). Gardiner and Borne (1978) discussed various processes (including adsorption) for treating textile wastewaters. Roy and Volesky (1978) presented various configurations of carbon adsorption systems used for treating textile wastewaters showing examples of several industrial textile wastewater treatment plants. The type of adsorbers, presented, were moving bed, fixed bed, and pulsed adsorbers. McKay, et al. (1978) compared various

adsorbents, including activated carbon, bleaching clay, silica, wood, peat, and alumina, with regard to adsorption of acid, direct, basic and dispersed dye compounds. They concluded that carbon had the highest adsorption capacity for dyes and that wood and peat were the cheapest adsorbents and silica one of the costliest although they did not consider regeneration of adsorbents and operational problems (e.g., flow patterns). McKay and his coworkers studies adsorption of basic dyes on carbon (1979) and adsorption of acid and direct dyes on chitin (1982a, 1982b). Posey and Kim (1983) and Cross, et al. (1982) studies solvent regeneration of activated carbon which was exhausted with various dyes. Posey and Kim showed that the recovery of adsorption capacity by using methanol was insufficient to offset the cost of methanol and, thus, the economics of solvent regeneration did not appear favorable by comparison with thermal regeneration.

By comparing different types of carbons derived from lignite and bituminous coal, DeJohn (1974) observed that high molecular weight dyes were adsorbed in the transitional pores whereas low molecular weight dyes were adsorbed in the micropores. Since surface area in the micropores is drastically reduced by thermal regeneration, the adsorption of dyes on bituminous coal-based carbon is likely to be affected significantly by thermal regeneration because of its extensive micropore structure. On the other hand, the adsorption of dyes on lignite-based carbon, because of its relatively larger pore structure, is less likely to be affected by thermal regeneration. DeJohn suggested that data based on virgin carbon could be used for removing high molecular weight dyes and that data based on reactivated carbon should be used for removing low molecular weight dyes.

2.3 REGENERATION USING SOLVENT EXTRACTION

Simplistically, the aspect of the adsorption process which lends validity to the idea of including desorption as a regenerative process is its reversible nature. As a dynamic process, adsorption is affected by a number of factors, as discussed earlier. Of primary importance among these factors is the effect of the regenerant on the behavior of a solute in an adsorbate/adsorbent/regenerant system. When a regenerant containing some solute is mixed with the solid phase, the solute redistributes itself between the adsorbent and the regenerant in order to minimize the total energy of the system. This redistribution is related primarily to the degree of solubility of the solute in the regenerant and the affinity of the solute for the adsorbent surface. The greater the attraction a solute has for the regenerant, the less likely it is to migrate to a surface or interface where is may be adsorbed.

In addition to the solubility, the distribution of the solute between the solution and the surface also depends on the interfacial tension of the solvent. The Gibbs free energy equation indicates that there will be positive adsorption (higher concentration of solute at the interface than that in the bulk solution) when the addition of solute molecules to a solvent results in a decrease of the interfacial tension of the solvent (Weber, 1972). Conversely, negative adsorption (desorption) occurs when the addition of solute molecules results in an increase of the interfacial tension. Therefore, desirable solvents for regeneration will be those which have lower interfacial tensions than that of water, because decreases of interfacial tensions of those

solvents will be less than that of water for the addition of the same number of solute molecules. This lesser degree of decrease will cause less positive adsorption in solvents than in water and also results in desorption of solute molecules (which are adsorbed in an aqueous system) if one of those solvents is used as a regenerant.

The type of regenerant required for extraction also depends on adsorption mechanisms previously described. If the principal mechanism for adsorption is ion exchange, the resins can be regenerated with the high concentration of neutral salt such as NaCl. This scheme can be explained by the difference of selectivities. The satisfactory elution of organics from RIA-904 (strong base resins with quaternary ammonium functional group) with NaCl was shown by Rebhun and Kaufman (1967).

Chasanov, et al. (1956) tried to use sodium hypochlorite (NaOCl) for regeneration of strong base quaternary anion exchange resins, but degradation of quaternary amine groups were observed.

Sodium hydroxide can be used as a regenerant, when organic acids are adsorbed on resins. Organic acids are anionic at high pH and more soluble than in the neutral forms at low pH. Another explanation for the success of sodium hydroxide as a regenerant can be derived from studies (Kumagai and Kaufman, 1968; Kim, et al., 1976) which indicated that there was drastically decreased adsorption of phenol and p-nitrophenol at high pH. Therefore, many organic compounds which are adsorbed at neutral pH can be eluted at high pH.

Adsorbed organics can be desorbed from synthetic resins by water soluble organic solvents such as low molecular weight alcohols and ketones which increase the solubility of the adsorbate. The organic solvent which has been used most frequently is methanol. The much smaller extend of adsorption of phenol from methanol than from water, which was studied by Anderson and Hansen (1955), allowed the regeneration of the resin Dowex 1 by methanol.

The efficiency of regeneration of styrene DVB resins was shown to be dependent on a solubility parameter ($cal^{0.5}/cm^{1.5}$) by Gustafson and Paleos (1971) which is the square root of the cohesive energy density (Gardon, 1966). The efficiency of organic solvents for regeneration can be ranked in increasing order as follows: methanol, ethanol, propanol, and acetone. The solubility parameters of those solvents decrease as anticipated.

The degree of regeneration depends on the degree of reversible adsorption. Irreversible adsorption reduces the adsorption capacity of resins with increasing number of cycles of adsorption - desorption. Therefore, irreversible adsorption needs to be studies as a function of adsorption - desorption cycles.

Solvent regeneration of activated carbon was studied by Chang and Savage (1981) on phenol removal, Loven and Huether (1970) on tar removal, Cross, et al. (1982) on dye removal, and Posey and Kim (1983) on dye removal. Although some researchers reported that solvent regeneration of activated carbon could be economical as compared with thermal regeneration in some cases (Himmelstein, 1974; Parmele, et al., 1981), solvent regeneration of dye -

laden activated carbon was, in some cases, costlier than thermal regeneration (Posey and Kim, 1983) due to relatively high degree of irreversible adsorption of organic dyes on carbon. Cross, et al. (1982) and Posey and Kim (1983) showed that most irreversible adsorption of dyes on carbon occurred during the first cycle.

2.4 ADSORPTION/DESORPTION KINETICS AND EQUILIBRIUM

So far, this discussion has been limited to the equilibrium condition in which the time that is required for an organic molecule to travel from bulk fluid (outside of adsorbent particle) to the adsorption site is not a factor.

In order to design an adsorption system, however, both adsorption kinetics and equilibrium capacity need to be determined because they determine the size of the carbon bed and the contact time based on given operational conditions, such as pH, temperature, flow rate, inflow concentrations of organic and inorganic species, and desired effluent concentrations of compounds of interest. When solvent extraction is used as a regeneration process, additional information on desorption kinetics and capacity is needed to determine the size of carbon bed (if there is loss of adsorption capacity during adsorption-regeneration cycles) and the amount of regenerant required.

2.4.1 Equilibria

Adsorption capacity is normally referred to in terms of the amount of adsorbate adsorbed at equilibrium. Isotherm equations are used to describe a functional relationship between adsorption capacity and equilibrium concentration. The equations, frequently used to fit isotherm data of single solute system, include the Langmuir equation (Adamson, 1967), the Freundlich equation (Adamson, 1967), and the equations which were developed based on the ideal adsorbed solution (IAS) theory by Radke and Prausnitz (1972) and by Jossens, et al. (1978). Extension of the isotherm equations to multi-solute systems was also attempted (Adamson, 1967, Butler, 1930; Jain and Snoeyink, 1973; Radke and Prausnitz, 1972). Fritz and Schlunder (1981) indicated that the IAS theory was the theoretically most sound method for prediction of multisolute adsorption equilibria.

2.4.2 Kinetics

Since both adsorption and desorption kinetics work similarly in reversible adsorption except for the direction of mass flow, only adsorption kinetics will be discussed.

In general, adsorption kinetics show that the rate of adsorption is influenced by temperature, carbon particle size, molecular size of adsorbates, mixing of solution, characteristics of solvent, and concentrations of adsorbates, whereas equilibrium studies demonstrate that the ultimate adsorption capacity is influenced by temperature, pH, characteristics of solvent and concentrations of adsorbates and other solutes.

Increased temperature results in increased mass transfer rate through both the film on the surface of carbon particle and the carbon pore, although

it decreases equilibrium adsorption capacity.

The carbon particle size determines the length of pore that the adsorbate has to travel through. Thus, a smaller size will give the smaller pore diffusion resistance. However, the use of a smaller particle size should be evaluated carefully due to the higher head loss or pumping cost in the actual operation. The adsorption capacity is not influenced by the particle size because the external surface area is relatively negligible when compared to the internal surface area.

The molecular size of the adsorbate determines the diffusivity of the molecule and thus controls the diffusion. The porosity and tortuosity of carbon also influence the effective diffusivity in the pore (Satterfield, 1970). Higher diffusivity of a molecule in the pore is obtained with smaller molecular size, less tortuosity, and greater porosity. Mixing in bulk fluid either in a batch or packed-bed reactor is important to determine the film diffusion resistance on the carbon particle surface. Increased mixing will compress the film thickness and thus results in decreased film resistance and increased adsorption rate.

The characteristics of the solvent affect the diffusivity of the adsorbate and thus the kinetics.

The concentration gradients of the adsorbate that exist in the carbon pore and along the packed-bed reactor determines the diffusion and dispersion fluxes, showing the dynamic nature of the adsorption process.

Knowledge of only the equilibrium condition (i.e., isotherms) does not provide an accurate description of a breakthrough curve from a packed-bed reactor because mass transfer resistance frequently plays a major role and thus the equilibrium condition between the bulk concentration (outside the adsorbent particle) and the adsorption sites (inside the adsorbent particle) does not exist at any time except after complete breakthrough. Since the concentration of the adsorbate in a pore is not measurable, mathematical models have been developed to describe the relationship between conditions inside and outside of the adsorbent particles, which involves descriptions of the pore and film diffusion resistances and the dynamic equilibrium conditions in the pore. Various models have been developed to predict the performance of backed-bed reactors which remove organics and inorganics. Keinath (1975) developed a packed-bed model by using a linear driving potential approximation in describing the diffusion phenomena in the pore. Hsieh, et al. (1977) used the similar approach to develop a packed-bed model for multicomponent adsorption systems. More recent attempts have been made to incorporate more detailed description of intraparticle diffusion into packed-bed models. Adsorption of some phenolic compounds and benzene sulfonate compounds on carbon have been modeled for batch and packed-bed reactors using the pore-surface diffusion concept (Crittenden and Weber, 1978). Adsorption of two alcohols on carbon (Liapis and Rippin, 1978) and reduction of free chlorine (Suidan, et al., 1977) and combined chlorine (Kim, et al., 1978; Kim and Snoeyink, 1980) by carbon were modeled based on the pore-bulk diffusion concept. Merk, et al. (1981) and Fritz, et al. (1981) compared both modeling approaches using bisolute systems and indicated that both approaches adequately predicted breakthrough curves of bisolute systems with litter differences in equilibria and diffusive properties. However, the pore-surface

diffusion approach was inadequate in predicting adsorption rates of relatively weakly adsorbed solutes because the approach could not describe the chromatographic separation of adsorbed solutes in pore. Since adsorption kinetics are rather complex, most models need to be solved by various numerical methods, such as the lumped parameter method (Keinath, 1975), the finite difference method (Crittenden and Weber, 1977; Suidan, et al, 1977; Kim, et al., 1977; Fritz, et al., 1981; Merk, et al., 1981), and the method of weighted residuals (Kim, et al., 1978; Kim and Snoeyink, 1980; Thacker, et al., 1981; Liapis and Rippin, 1978).

Although these models can be used to predict the performance of the packed-bed reactor, isotherm equations and other model coefficients in the model need to be determined and verified experimentally by means of isotherm studies under various conditions, batch kinetic tests, and packed-bed tests before being used to design adsorption systems. The experimental conditions should cover the range of interest in the actual application as fully as possible so that the model coefficients will be meaningful for all practical ranges and the degree of extrapolation from the model will be minimized.

Desorption kinetics during solvent regeneration can be described similarly if the adsorption isotherm of the compound of interest in regenerant is known. To design an adsorption system with a solvent regeneration scheme, a mathematical model which includes the descriptions of equilibria and kinetics for adsorption and desorption need to be developed. The use of the model will result in an optimal design of the carbon bed and an efficient use of regenerant.

CHAPTER 3

MATERIALS AND METHODS

3.1 ADSORBENTS

3.1.1 Adsorbent Characteristics

Several resins were screened to determine which were best suited for the removal of dye compounds from water. These adsorbents were selected to permit investigation of a range of different combinations of resin classes and matrices. The important properties of these resins are shown in Table 1. Resins A-7, A-191, and S-761 were obtained from Diamond Shamrock. The remaining resins were obtained from Rohm and Haas.

3.1.2 Adsorbent Conditioning

Resins were shipped dry and contained preservatives to control bacterial and mold contamination. Before use it was necessary to condition the resins by hydration, removal of preservatives, and adjustment of pH. The first step in this process was to soak the resins in deionized water. The hydrated resins were then transferred to glass columns and backwashed with deionized water at a bed expansion of 75-100% to remove fines. Following this procedure, the resins were conditioned according to manufacturers specifications. Each of the resin classes required different conditioning procedures, described below.

a. Anion Exchange Resins

Each of the anion exchange resins was conditioned according to the following procedure:

-Two bed volumes of 1.5N NaOH were pumped through the column over a 20 minute period.

-The resin was rinsed free of caustic soda by pumping 5 bed volumes of deionized water through the column over a 20 minute period.

-Two bed volumes of 2N HCl were pumped through the column over a 20 minute period.

-The resin was rinsed free of acid by pumping 5 bed volumes of deionized water through the column over a 30 minute period.

-The above procedure was repeated.

-Methanol was pumped through the column until all UV absorbing species are eliminated from the effluent. To determine this point a UV absorbance spectra were run on a Beckman 26 Recording UV/VIS Spectrophotometer. When the effluent spectrum matched that of pure methanol, the methanol wash was discontinued and the resin was considered free of impurities.

TABLE 1. SUMMARY OF RESIN CHARACTERISTICS

Resin	Matrix	Class	Particle Size (A)/ Mesh Range	Density (g/cc)	Functional Group	Surface Area (m^2/g)	Avg. Pore Diameter (A)
A-7 aromatic	phenolic	weak base anionic	16-50	1.12	polyfunctional amine	-	-
A-191 aliphatic	styrene-DVB	strong base anionic	-	-	quartenary amine	-	-
IRA-93 aromatic	styrene-DVB	weak base anionic	0.46 mm	1.04	polystyrene polyamine	-	-
A-200 aromatic	styrene-DVB	strong acid cationic	0.49 mm	1.26	sulfonic acid	-	-
DP-1 aliphatic	methacrylic acid-DVB	weak acid cationic	0.45 mm	1.17	carboxylic acid	-	-
XAD-2 aromatic	polystyrene	adsorbent	20-60	1.09	none	160	225
XAD-7 aliphatic	acrylic ester	adsorbent	20-60	1.05	none	450	90
XAD-8 aliphatic	acrylic ester	adsorbent	20-60	1.02	none	800	100
XAD-16 aromatic	polystyrene	adsorbent	20-60	1.02	none	300	90
S-761 aromatic	phenolic	adsorbent	16-50	1.11	hydroxyl	100	300

-Five bed volumes of deionized water were pumped through the column over a 30 minute period.

-The resin was converted to the hydroxide form by pumping two bed volumes of 1.5N NaOH through the column over a 30 minute period.

-Deionized water was pumped through the column until the effluent pH was below 9.0.

-Refrigerate resins until use.

b. Cation Exchange Resins

Each of the cation exchange resins was conditioned according to the following procedure.

-Two bed volumes of 2.0N HC1 were pumped through the column over a 20 minute period.

-The resin was rinsed free of acid by pumping 5 bed volumes of deionized water through the column over a 30 minute period.

-Two bed volumes of 1.5N NaOH were pumped through the column over a 20 minute period.

-The resin was rinsed free of caustic soda by pumping 5 bed volumes of deionized water through the column over a 30 minute period.

-The resin was removed from the column and boiled in deionized water for 30 minutes. Return the resin to the column.

-Methanol was pumped through the column until all UV absorbing species are removed. Determine this point as above for anion exchange resins.

-Five bed volumes of deionized water were pumped through the column over a 30 minute period.

-The resin was converted to the chloride form by pumping 2.0N HC1 until the effluent pH is above 4.0.

-Store resins in refrigerator until use.

c. Adsorbent Resins

Each of the adsorbent resins was conditioned according to the following procedure.

-Resins were placed in a Soxhlet Extraction Apparatus and extract with methanol for 24 hours.

-The resin was removed from the Soxhlet Extraction Apparatus and placed in a glass laboratory column. Deionized water was pumped through the column until methanol was completely rinsed from the resin. To determine this point the absorbance of the effluent at 220 nm was monitored. At this wavelength

the absorbance of methanol was maximized while the absorbance of water was minimized. Washing with deionized water continued until the absorbance was less than 0.01 units.

-Store resin in refrigerator until use.

3.1.3 Experimental Preparation of Adsorbents

Prior to experimentation each resin was equilibrated to the desired pH of the experiment. A quantity of resin was mixed with deionized water and the pH was adjusted by the addition of acid or base, as needed. When the desired pH was maintained for a period of 24 hours with no acid or base addition, the resin was assumed to be equilibrated at the desired pH.

Following pH adjustment, aliquots of the resin were transferred to centrifuge tubes and spun in an International Clinical Centrifuge, Model CL, at maximum speed for 10 minutes. A quantity of resin was weighed for use in experiments. These wet weights were converted to dry resin weight using the percent moisture of the resin, determined from the procedure described below.

3.1.4 Percent Moisture Determination

All resins used in isotherm, and batch and column kinetic experiments were sampled to determine the percent moisture of the resin used in the experiment. This was necessary to convert the weight of the wet resin to dry weight, the parameter used to express resin mass.

The procedure for this determination is as follows:

- One or two samples of the resin to be used were taken. In instances where the same resin was used for several simultaneous experiments, two samples were removed.

- The samples were placed in Gooch crucibles of known weight, previously dried at 100°C for at least 24 hours, and weighed (= wet weight).

- The crucibles, plus samples, were placed in a 100°C oven and dried for at least 24 hours.

- The crucibles were then removed from the oven and re-weighed (= dry weight).

- During transport of the crucibles and at all times, except the actual weighing process, the crucibles were kept in dessicators to insure that the sample and crucible weight were accurate.

- Percent moisture was calculated as follows:

$$\% \text{ moisture} = \left(1 - \frac{\text{dry wt. - crucible wt.}}{\text{wet wt. - crucible wt.}}\right) \times 100 \qquad (1)$$

- The dry weight of the resin was calculated as follows:

$$\text{dry weight} = \text{wet wt.} \; (100 - \% \text{ moisture}) \times 100 \qquad (2)$$

The range of values of percent moisture for all resins used in this study are presented in Table 2. In cases where sample estimates were not available (i.e., spillage, leakage of resin from crucible) these average percent moisture values were applied to obtain dry resin weight.

3.2 ADSORBATES

3.2.1 Adsorbate Properties

The physical-chemical properties of the dye compounds chosen for this study are summarized in Table 3. From the variety of organic dyes available, eight compounds were selected, based on the following criteria. The compounds selected were relatively water soluble, commercially available in a relatively pure form, contained an azo group, possessed a relatively simple underlying structure with comparable functional groups, and were easy to analyze by spectrophometric techniques. All compounds, except the two food dyes, were reagent grade chemicals purchased from Aldrich Company. The two food dyes, FD&C red #40 and FD&C yellow #6, were obtained as samples from Ferguson and Jenkins Company.

An elemental analysis of these compounds was conducted on an F&M Model 185 CHN Analyzer. Results from these analyses are contained in Table 4. Excluding the percent in 4-azoaminobenzene, 4-hydroxyaminobenzene, and methyl orange, theoretical and measured results matched fairly well.

3.2.2 Quantification of Adsorbate Concentration

All dye concentrations were quantified by measuring sample absorbance on one of two spectrophotometers, a Beckman Model 26 Recording Spectrophotometer, or a Coleman Model 46 Spectrophotometer. For water based samples the pH was adjusted, as necessary, to insure the presence of the desired ionic species, the absorbance was measured, and then converted to concentration by correlating that reading with a previously determined calibration curve. For methanol based samples, no pH adjustment was necessary. Absorbance was measured and converted to concentration as above.

This quantification was straightforward except during the early stages of column desorption. Because the methanol regeneration cycle followed immediately after the adsorption cycle, early desorption samples were suspected of contamination by water. To determine the degree of contamination UV/VIS spectra of the first five desorption samples were run. In all instances the wavelength of maximum absorption of the samples was indistinguishable from that of the dye in pure methanol. Therefore, concentration was determined using the methanol calibration curves.

3.2.3 Calibration Curves

Calibration curves were prepared for all dyes used in this study according to Beer's Law relationship. Curves were developed for each dye dissolved in water and methanol. Both Beckman and Coleman model spectrophoto-

TABLE 2. PERCENT MOISTURE OF SYNTHETIC RESINS

XAD-16		XAD-7		S-761	
Experiment	% Moisture	Experiment	% Moisture	Experiment	% Moisture
PC161	65.22	PB7	68.05	PC761	58.22
	64.98	MB71	68.1	PC762	56.46
PC165	65.78		67.5	MB76	56.3
MB162	65.82	MB73	68	AB76	56.53
	65.32		67.9		
RB161	63.8	RB7	69.4		
	63.9		69.4		
RB162	65.16	AB71	70.06		
AB161	64.3		70.2		
AB162	65.21	AB72	69.86		
AB166	64.47	AB73	70.44		
MRB161	64.91	MRB7	72.56		
	65.06		73.6		
VB16	64.1	YB7	68.3		
HB16	64.3		71.5		
		HB7	69.97		
			69.89		
$\bar{X}$ = 64.82		$\bar{X}$ = 69.69		$\bar{X}$ = 56.88	
n = 15		n = 17		n = 4	
$S_{\bar{X}}$ = 0.64		$S_{\bar{X}}$ = 1.69		$S_{\bar{X}}$ = 0.9	

TABLE 3. SUMMARY OF DYE CHARACTERISTICS

Compound	Molecular Weight (mole/g)	Purity (%)	Solubility	pKa
 Methyl Orange (MO) $C_{14}H_{14}N_3SO_3Na$	327.25	95	very soluble	3.63
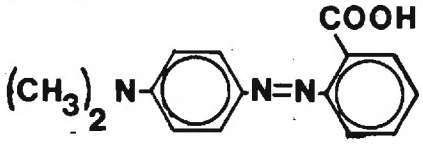 Methyl Red (MR) $C_{15}H_{15}N_3O_2$	269.31	95	soluble	2.5 9.95
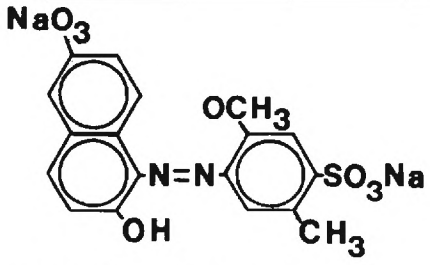 FD&C Red No. 40 (R40) $C_{18}H_{14}N_2S_2O_8Na_2$	496.44	91	very soluble	<1.04 >10.09
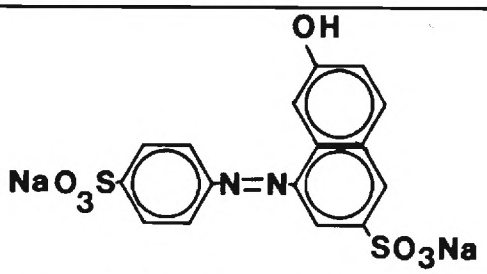 FD&C Yellow No. 6 (Y6)	452.38	92	very soluble	<1.03 >8.98
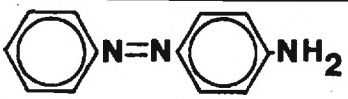 4-Azoaminobenzene $C_{12}H_{11}N_3$	197.24		slightly soluble (.01 g/L)	11.12
 4-Hydroxyazobenzene $C_{12}H_{10}N_2O$	198.23		slightly soluble (.01 g/L)	9.38
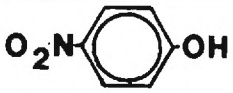 Paranitrophenol $C_6H_5NO_3$	139.11		soluble	7.15

TABLE 4. ELEMENTAL ANALYSIS OF DYE COMPOUNDS

Compound	Percent C		Percent N		Percent H		Σ
	Theoretical	Measured	Theoretical	Measured	Theoretical	Measured	(meas.)
4-Aminoazobenzene	73.06	83.80	21.31	24.3	5.63	4.82	112.92
4-Hydroxyazobenzene	72.70	74.70	14.13	14.64	5.09	4.69	94.03
4-Phenylazobenzoic Acid	69.01	58.3	12.38	11.70	4.46	4.49	74.49
Methyl Red	61.84	61.94	14.43	14.30	4.85	4.37	80.61
Methyl Orange	51.36	42.40	12.84	11.18	4.32	3.85	57.43
FD&C Yellow 6	42.48	41.80	5.19	5.98	2.23	2.12	49.9
FD&C Red 40	43.55	41.07	5.64	5.20	2.85	3.37	49.64

meters were used in this study, based upon availability and operability. In most cases, calibrations were performed on both spectrophotometers. To avoid inherent analytical errors the samples from a single experiment were measured on only one of these instruments.

a. Water Calibration Curves

For compounds with known pKa values, calibration was straightforward. Duplicate solutions of known concentration were prepared and adjusted such that one of the pairs had a pH well above the pKa and the other had a pH well below the pKa of the dye to be calibrated. A sample of each of these solutions was scanned over the ultraviolet and visible light range to determine the form of the compound that resulted in maximum absorbance. The wavelength at which this occurred was λ_{max}.

For compounds in which the pKa could not be found in the literature (phenylazobenzoic acid, methyl orange, FD&C Yellow #6, and FD&C Red #40), it was determined experimentally, according to the procedures in Snoeyink and Jenkins (1980). For each of these compounds, solutions of identical concentration were prepared. The pH of these solutions was adjusted to cover the desired range of pH values and samples of these solutions were scanned over the ultraviolet/visible light range. The pKa was determined by shifts in absorbance as a function of pH. These scans are contained in Appendix 1. Methyl orange has two pKa's, one at 3.63, and the other at pH > 11.0. Since pH 11.0 is beyond the range of this study, further quantification was unnecessary. FD&C Red #40 and FD&C Yellow #6 also have pKa's outside the pH range of this study. For FD&C Red #40 no change in absorbance occurred between pH 1.03 and pH 8.98. For FD&C Yellow no change in the spectrum occurred between pH 1.04 and pH 10.1. It was impossible to determine the pKa of phenylazobenzoic acid. The wavelength of maximum absorbance (λ_{max}) was determined for these three compounds by the procedure described above.

Given λ_{max} and the ionic species which produced maximum absorbance, calibration curves were prepared. For each dye, approximately 10 aqueous solutions of varying concentration, adjusted to the proper pH, were prepared. The concentrations were chosen such that the absorbance spanned the range between 0.1 and 1.8 A. The absorbances of these solutions were measured and correlated with concentration, according to Beer's Law using linear regression. A summary of these results is presented in Table 5.

b. Methanol Calibration Curves

For each dye approximately 10 methanol solutions of varying concentrations were prepared such that the absorbance range of these solutions fell between 0.1 and 1.8 A. No pH adjustment was necessary. Absorbance was measured at λ_{max} and correlated with concentration according to Beer's Law. Table 5 contains a summary of these results.

3.3 ISOTHERM EXPERIMENTS

Isotherm experiments were conducted using methyl orange and para-nitrophenol in combination with the following resins: A-7, A-191, A-200, IRA-93, DP-1, XAD-2, XAD-7, XAD-8, XAD-16, and S-761. The resin and dye solution was

TABLE 5. SPECTROMETRIC CALIBRATION DATA

Solute	Solvent	Spec.	Max	E	Y Int	r	n
PNP	water	PE	400	17,476	.0168	.998	
PNP	water	B	400				
PNP	methanol	B	307	10,585	-.009	.9999	11
PNP	methanol	PE	307	10,184	-.099	.9998	11
MO	water	PE	510	42,416	.0065	.9999	11
MO	water	B	510	47,150	-.0039		
MO	methanol	PE	425	27,944	.0054	.9997	10
MO	methanol	B	425	28,500	.0029		
MR	water	B	425	19,410	-.0085		
ED40	water	PE	500	22,368	.029	.9996	9
ED40	water	B	500	23,508	.0089	.9999	5
ED40	methanol	PE	505	22,093	.039	.9998	11
ED40	methanol	B	505	22,172	.0105	.9998	12
EL6	water	PE	485	22,340	.0057	.9999	9
EL6	water	B	485	22,034	.0105	.9999	5
EL6	methanol	B	480	17,762	.0053	.9999	12
AAB	water	PE	495	6,988	.0067	.997	11
AAB	water	B	495	8,610			
AAB	methanol	PE	382	102,506	.025	.997	11

added to batch reactors (125 mL glass bottles fitted with teflon-lined screw caps) and mixed using a horizontal shaft rotary contactor. Each contractor held 32 bottles and was rotated at 2 rpm. Temperature was controlled by placing the contactors in a Freas, Model 815, Low Temperature Incubator. Temperature was maintained at 22°C $\pm$ 0.5°C.

Isotherm adsorption studies were carried out by adding equal amounts of resin to varying concentrations of the adsorbate. Resins were prepared according to Section 3.1. Aliquots of the resin were weighed and added to bottles, which contained deionized water adjusted to the proper pH. Stock solutions of the dyes were prepared and adjusted to the proper pH. Various volumes of deionized water were removed from the bottles and replaced with equal volumes of the stock solution. A blank, containing 125 mL of dye solution, intermediate in the range of experimental concentrations, with no resin, was prepared to check for microbial degradation. Batch reactors were then mixed until equilibrium was reached.

The time needed to attain equilibrium was determined by two independent procedures. Concurrently with early isotherm experiments, several bottles of equal adsorbate and adsorbent concentration were prepared. Bottles were removed at daily intervals and the absorbance of the remaining solution was measured. When the difference between successive absorbance readings was less than 1.0%, it was assumed that equilibrium had been attained. The time to reach this point was less than three days in all cases. In addition, batch kinetic experiments, conducted as a part of this study (see Section 3.4) indicated that equilibrium was achieved within a contact period of 24 to 26 hours. Therefore, in each isotherm experiment, a contact period of at least 3 days was maintained.

Once equilibrium was attained, the bottles were removed from the mixer, and the resin was settled. Aliquots of the solution were removed and analyzed by UV/VIS Spectrophotometry to determine the residual concentration of the adsorbate.

Results form these experiments were used to calculate the absorbed solid phase concentrations according to the following equation.

$$q = (C_i - C_e)/M \qquad (3)$$

where: q = moles adsorbed/gram of resin
C_i = initial adsorbate concentration
C_e = equilibrium adsorbate concentration
M = dry weight of resin

These values were used to construct adsorption isotherms.

3.4 BATCH KINETIC EXPERIMENTS

3.4.1 Experimental Apparatus

Batch Kinetic Experiments were conducted in continuously stirred 4 liter batch reactors, designed to minimize evaporation and provide easy access for sampling, pH adjustment, and temperature control (Figure 2). The basic

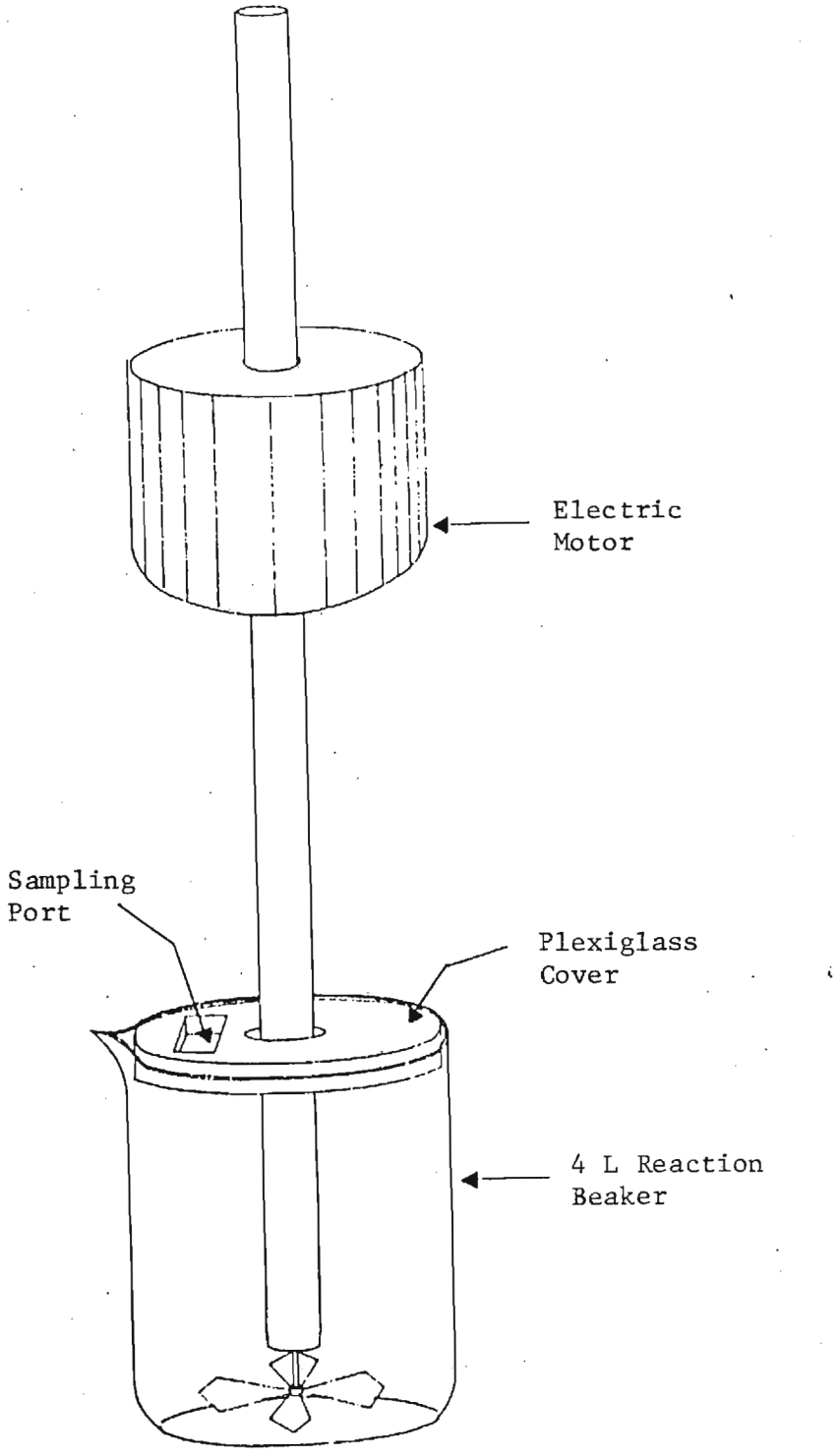

Figure 2. Batch Kinetic Experimental Appartus.

unit of this system is a 4 liter Pyrex beaker. Fitted to the top of the beaker is a circular cover cut from 1/4 inch plexiglass and notched to fit snugly within the beaker. Cut into this cover is a rectangular access port with rounded corners. A top for the access port was constructed by gluing two pieces of 1/4 inch plexiglass together. The lower piece was cut to fit snugly within the access port, while the upper piece, but slightly larger, completely covered the port, providing a tight seal. A 1/4 inch hole was drilled in the center of the reactor cover to accommodate the stirring rod.

A stirring rod, 1/4 inch in diameter, with three blades was used to mix the contents of the reactor. The stirrer was turned by a laboratory motor, mounted onto a ring stand using standard laboratory clamps.

Prior to the beginning of an experiment parafilm was placed between the reaction beaker and the cover to insure a tight fit and to prevent evaporation. Parafilm was used to cover the lip of the beaker, the only portion not fitted by the cover.

Adsorption and desorption samples were taken with a 10 mL pipet fitted with a pipet tip to prevent removal of resin particles. This tip was made by placing a piece of 100 micron Nitex netting between two pieces of hard plastic tubing. This tip was placed over the pipet tip, allowing samples to be taken without interrupting the reaction. Good results were obtained by this method. Liquid samples, uncontaminated by resin particles, were easily collected.

3.4.2 Initial Adsorption Experiments

Initial Adsorption refers to those experiments in which virgin resin particles were used to adsorb dye from an aqueous solution. The procedure for these experiments is described below.

- Four liter batches of solution were prepared as follows: The total quantity of dye required was dissolved in deionized water in a 2 liter volumetric flask. This volume was poured into the reaction beaker. The volumetric flask was refilled with 2 liters of deionized water and poured into the reaction beaker.

- Approximately 0.04 g of $NaHCO_3$ (0.01 g/L) was added to each dye solution to provide buffer capacity. This was necessary because of problems with pH control observed in early experiments.

- The batch reactor apparatus was assembled, the solution was mixed, and the pH was adjusted to the desired experimental value.

- The resin was weighed according to the procedure described in Section 3.1.3 and added to the reaction beaker through the access port. Resin addition began at 10 seconds before the beginning of the experiment (time = 0) and continued for approximately 10 seconds after time zero.

- Samples were taken at the following intervals: 2, 5, 15, 30, 60, 120 minutes, and as necessary thereafter.

- Temperature and pH were measured at the time of sample collection, and, as necessary between samples. pH was adjusted, if needed, to the

intended value by addition of acid or base. Temperature was not controlled.

- Mixing speed was adjusted visually to suspend the resin particles in solution, while at the same time preventing air entrapment.

- Except for sample collection, temperature measurement, and pH measurement/adjustment, the access port was covered to prevent evaporation and contamination.

3.4.3 Desorption Experiments

Following adsorption, the dye was desorbed into methanol. The same reactor that was used for the adsorption cycle was used for the desorption cycle. These experiments were conducted according to the following procedure.

- Following the termination of the adsorption cycle, the reactor was disassembled, and the stirring rod as washed with deionized water to remove any adhering resin particles.

- The dye solution was decanted from the beaker taking care not to lose any resin particles. When this became difficult, the remaining solution was removed by pipetting with a 25 mL pipet fitted with a sampling tip.

- The experimental apparatus was reassembled, and 2 liters of methanol poured into the beaker at approximately 10 seconds prior to time zero.

- Samples were taken at the following intervals: 15, 30, 45, 60, 75, 90, 120, 300 seconds; 15, 30, 60 minutes; and, as necessary thereafter. Temperature was recorded at the time of sampling.

3.4.4 Secondary Absorption Experiments

In these experiments the resin used had already been subjected to at least one absorption/desorption cycle. The studies were conducted to investigate the potential of reusing resins and to quantify any losses in adsorption or desorption capacity. The procedure described below begins at the end of the initial desorption cycle.

- The second dye solution was prepared in a 4 liter beaker as described in Section 3.4.1.

- The desorption run was terminated, the reactor disassembled, and the stirrer rinsed.

- The methanol was decanted by slowly pouring off the solution, taking care not to lose any of the resin particles. When that was no longer possible, the remaining methanol was removed by pipetting with a pipet fitted with a sampling tip.

- The reactor was reassembled and the same procedure and sampling scheme followed as for the initial adsorption experiments.

3.5 COLUMN KINETIC EXPERIMENTS

3.5.1 Experimental Apparatus

Continuous flow exhaustion and subsequent in situ solvent regeneration studies were conducted using an arrangement of four upflow columns, operated in parallel. Components of this system were built onto two laboratory benches (Figure 3). The system was designed with the following features in mind:

- Easy replenishment of the feed solution without interruption of experimentation.
- Automatic operation and sample collection.
- Collection of effluent for flow determination.
- Easy switch over between adsorption and desorption cycles.

The feature most responsible for the successful operation of this system, the column pressure regulator (Model , Sears and Roebuck Co.), was not originally designed into it, but was added to correct a problem encountered in the early stages of experimentation. This problem, the formation of gas bubbles in the column during the desorption cycle, caused much frustration, and significant delay, and deserves comment. After the first adsorption runs were performed successfully on the experimental system, regeneration of the resin with methanol was attempted. Upon initiation of the desorption cycle, gas bubbles began to form within the resin bed. These bubbles continued to form as the experiment proceeded, aggregating to form larger bubbles, which eventually caused short circuiting and head loss in the column, and a breakdown of the resin bed. This resulted in poor and incomplete regeneration and problems with pumping of methanol. In an experiment with methyl orange and XAD-16, although a regenerant volume of six times the original adsorbate solution volume was passed through the column, significant dye remained on the resin. This was less than an ideal situation, and causes were investigated. An analysis of the gas within the column indicated a composition identical with air. Since testing of other possible regenerants confirmed methanol as the most efficient, a solution to this problem was necessary. After much investigation, the following explanation was postulated. During adsorption, dissolved air, in addition to solute molecules, was adsorbed onto the resin. As methanol was passed through the resin, air was desorbed and entrapped in pockets within the column. To correct this problem, each column was placed under enough pressure to keep the desorbed gas in solution. A pressure regulator and control valve were installed on the effluent side of each column. By maintaining pressure at 2 atmospheres, no further air binding problems were encountered.

Chromoflex glass columns (Kontes Glass Co., Vineland, NJ) were used for the resin reactors. Two different column sizes were used (Figure 4). In the majority of the experiments a straight column, 2.5 cm in internal diameter, 20 cm long, with the ends fitted with Deldrin fittings and Viton "O" rings (Kontes Glass Co., Vineland, NJ) was used. Because only a small amount of resin was needed to adsorb the dye 4-aminoazobenzene, a smaller diameter column was chosen for studies with this sorbate. This was done to insure sufficient resin depth to prevent short circuiting. This column, 2.5 cm in internal diameter at the ends, 1.25 cm in internal diameter in the middle, accepted the same fittings as the larger column, and was interchangeable in the experimental system. Each column was packed with resin, sandwiched

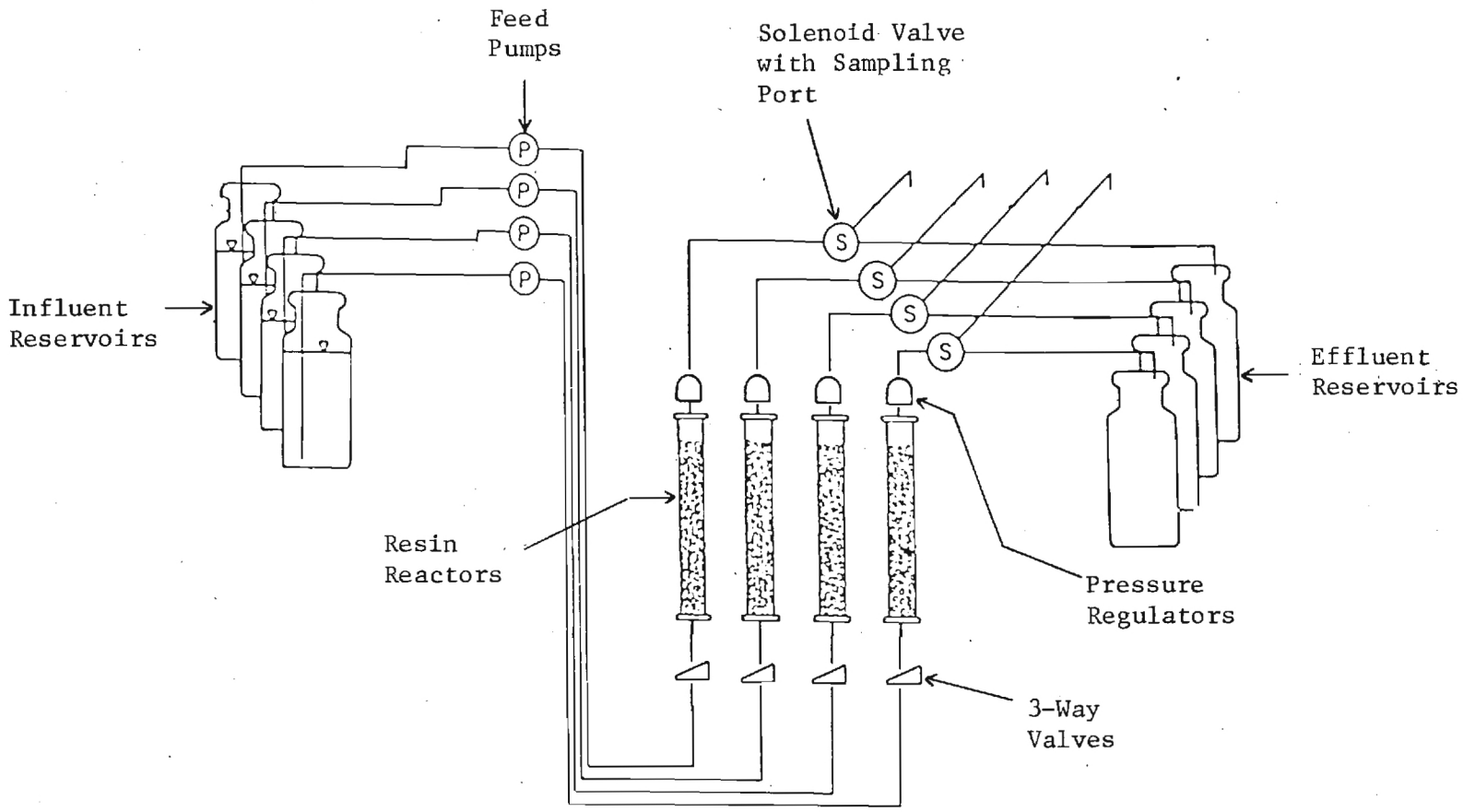

Figure 3. Column Kinetic Experimental Apparatus.

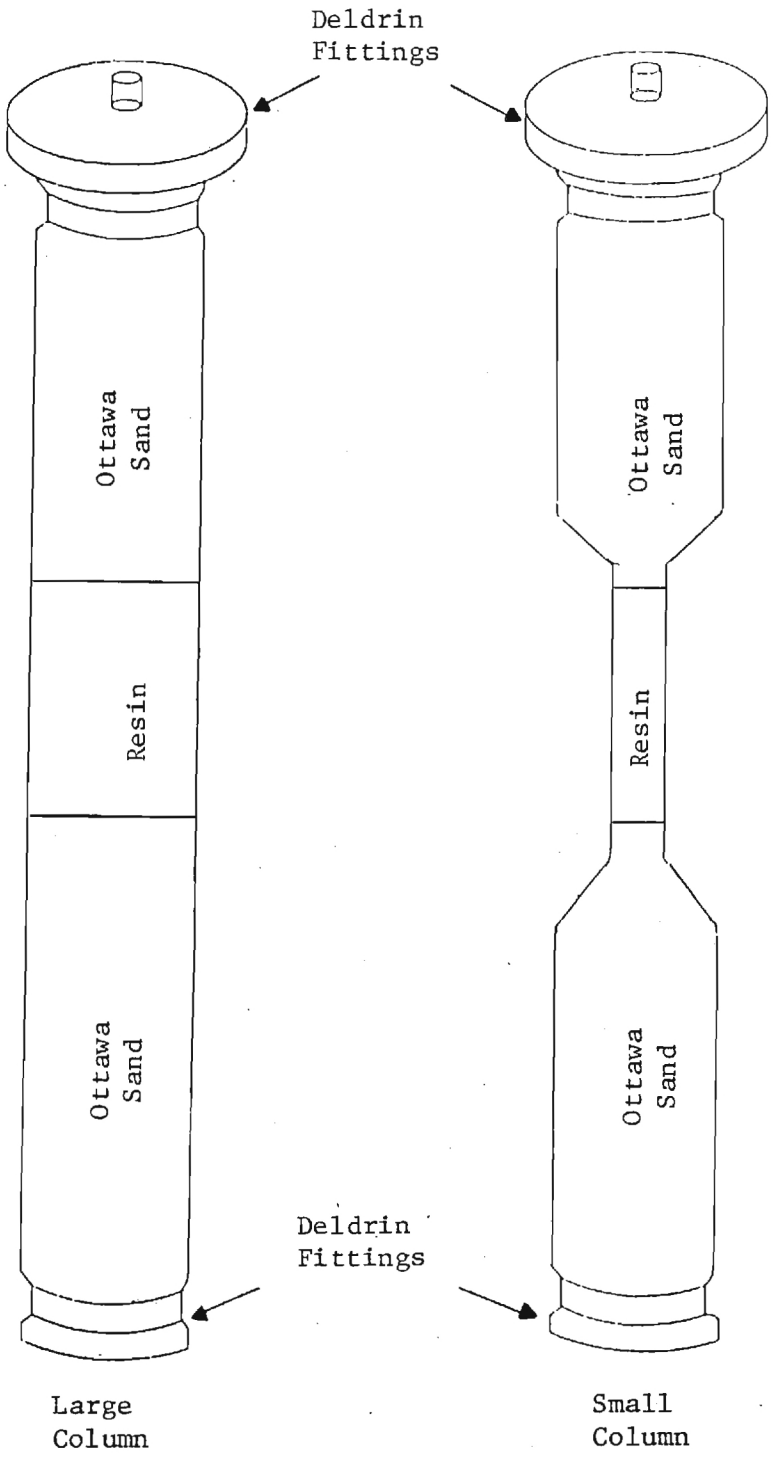

Figure 4. Chromoflex Glass Column Reactors.

between layers of Ottawa sand. This was done first, to produce a uniform flow distribution into the resin bed, and, second, to hold the resin particles, which have low specific gravities, in the column. The influent and effluent lines were constructed from 0.483 cm copper tubing. All fittings and valves were purchased from SWAGELOCK.

The feed solution was pumped from the influent reservoir to the columns using positive displacement laboratory pumps (Model RP-650, Fluid Metering Inc., Oyster Bay, NY), fitted with 1/4 inch drives (Model RP-G6, Fluid Metering Inc., Oyster Bay, NY). The arrangement of the influent and replacement reservoirs permitted easy, non-interrupted replenishment of the feed solution. A replacement reservoir was placed above the influent reservoir, and the replacement was siphoned into the influent using a length of plastic tubing. Prior to each column influent a 1/4 inch internal diameter three-way brass valve (Model Number B-43xS4, Whitey Company, Oakland, CA), was installed in the feed line. This permitted the feed line to be purged prior to the beginning of an experiment, insuring that the solution entering the column was of the specified composition, undiluted and uncontaminated by the previous experimental solution.

A three-way solenoid valve (Model 8220A89, Automatic Switch Company, Florham, NJ) was placed in the influent line of every column. These valves were synchronized with a fraction collector (Model 1205, Research Specialties Co., Richmond, CA) by an electronic timer in order to provide automatic sampling of the effluent from each column with time. A series of integrated circuits was employed to maintain a system that exhibited a time-synchronized sampling scheme. The effluent from each column flowed to the waste reservoir until the in-line solenoid valve was activated to divert the effluent to a sample tube. The sample tubes were held on a fraction collector which also interfaced with the sampling sequence via the electronic timer. Following a brief period of time during which the effluents lines were purged of solution which remained in the system from the previous sampling period, the fraction collector rotated to allow a clean sample to be dispensed into another tube. The solenoid valve was automatically shut off at the appropriate time and the fraction collector was pulsed to rotate again so as to provide an empty tube for the subsequent sampling sequence. For a detailed description and schematic diagram of the system, see Cross et al., 1982.

3.5.2 Initial Column Adsorption Experiments

As previously described, initial column adsorption experiments were those experiments in which virgin resin particles were used to adsorb dyes from an aqueous solution. The procedure for these experiments is described below.

- Dye solution was prepared in 18 liter aliquots in graduated glass carboys (reservoirs), calibrated in liters. For each experiment, two reservoirs of solution were prepared. Dye was added to the reservoir and dissolved in a few liters of deionized water. The reservoir was then filled to the 18 liter mark with deionized water.

- Approximately 0.18 g of $NaHCO_3$ (0.01 g/L) was added to each dye solution to provide buffer capacity. This was necessary because of problems with pH variability encountered in earlier experiments.

- The solution was mixed, and the pH was adjusted to the experimental value. This was a lengthy process, often requiring two days, as the reservoirs had to be mixed by hand between pH measurements and acid/base additions.

- The laboratory columns were assembled and deionized water, previously adjusted to the experimental pH, was pumped for one hour through the system to flush out residues from previous experiments.

- The column tops were removed and the columns were packed with Ottawa sand, previously washed in deionized water, and synthetic resin, prepared and weighed according to the procedures described in Section 3.1.3.

- The tops of the column were replaced and the entire system was flushed with deionized water (pH adjusted) for at least one hour.

CHAPTER 4

RESULTS AND DISCUSSION

4.1 ISOTHERM EXPERIMENTS

Results from the isotherm screening experiments, in which methyl orange and paranitrophenol were used to screen the ten potential resins, are shown in Figures 5 and 6. Table 6 contains the Freundlich isotherm constants from these experiments. The Freundlich, or van Bemmelan equation (Freundlich, 1926) has the general form:

$$q_e = KC^{1/n} \qquad (4)$$

where: q_e = surface coverage
K,n = constants
C = final concentration

The Freundlich equation is basically an empirical one, but is useful as a means for data description. Data are usually fitted to the logarithmic form of the equation.

$$\log q_e = \log K + 1/n \text{ Log } C \qquad (5)$$

The intercept is roughly an indicator of sorption capacity and the slop, 1/n, of adsorption intensity.

In general, performance based on resin class followed the order: anionic > adsorbent > cationic. From these results, in conjunction with the resin matrix, four resins, A-7, XAD-16, XAD-7, and S-761, were chosen for further study. Resin A-7, a weak base, anion exchanger with a phenolic matrix, was chosen because of it's high adsorption capacity. It was decided, however, not to use A-7 in batch and column kinetic studies due to complexities in pH control and removal of solute through an ion exchange mechanism as well as adsorption. The remainder of the resins chosen were adsorbent resins, each with a different matrix. Resin XAD-16, with a polystyrene matrix, performed best, followed by XAD-7, with an acrylic ester matrix, and S-761, with a phenol formaldehyde matrix.

The isotherm data collected for all dye compounds and the four selected resins are shown in Figures 7 through 18. Resin A-7 appeared to be the best resin for the removal of p-nitrophenol, methyl orange, methyl red, red 40 and yellow 6. For compounds which exist in the ionized form, such as methyl red, methyl orange, red 40 and yellow 6, it was likely that an ion exchange mechanism prevailed in the removal process. However, for a neutral compound, such as p-nitrophenol, the dominant mechanism was most likely physical absorption. XAD-16 adsorbed 4-aminoazobenzene and phenylazobenzoic acid more strongly than the other resins. XAD-7 and XAD-16 exhibited the highest adsorption capacity for 4-hydroxyazobenzene. Red 40 and yellow 6 were the least adsorbable compounds on all resins except A-7. This could possibly be attributed to the higher solubility of the red 40 and yellow dyes in comparison to the other dyes. The effectiveness of A-7 may be due to ion exchange with

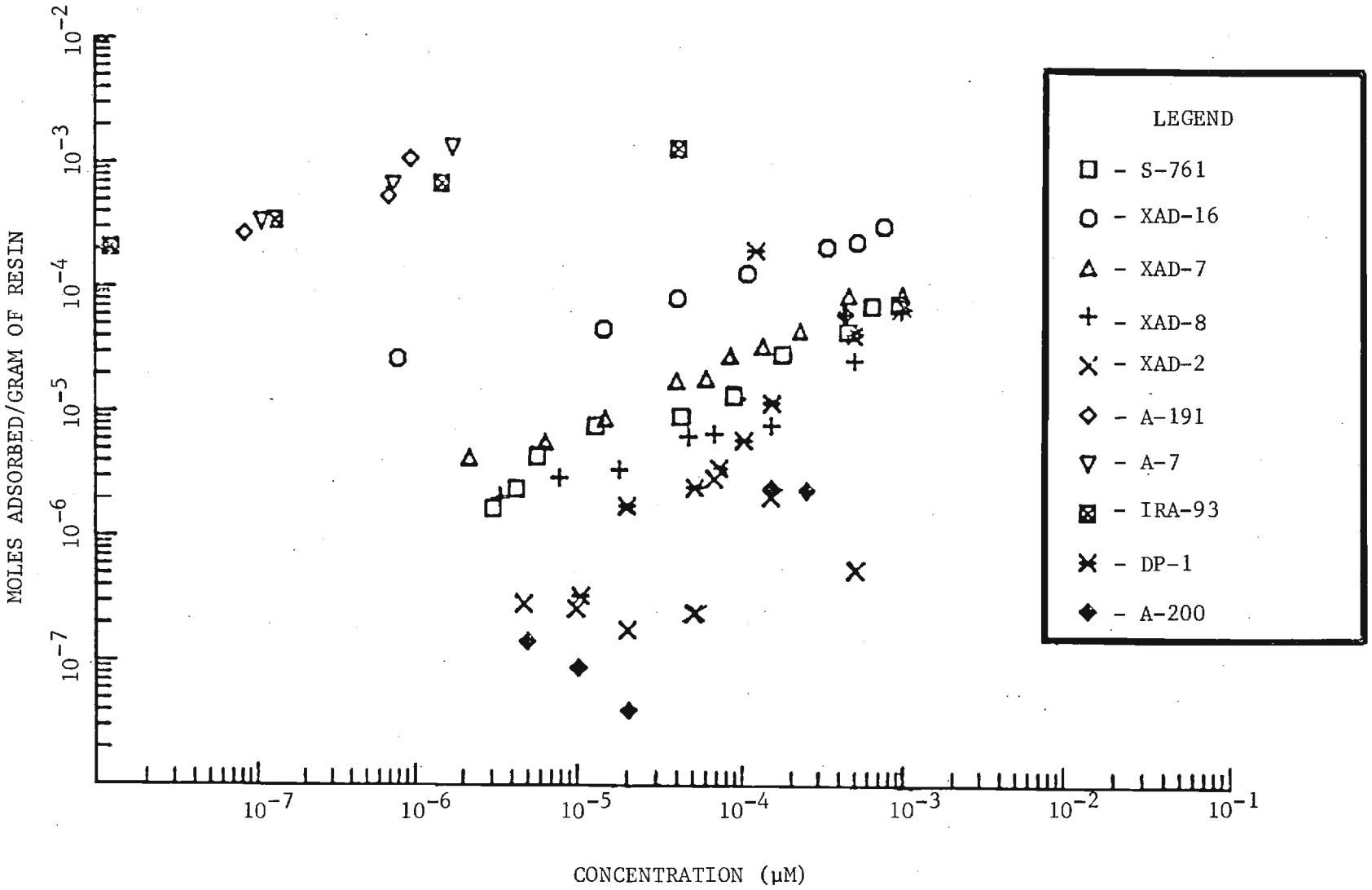

Figure 5. Adsorption Isotherms for Methyl Orange, pH 5.0.

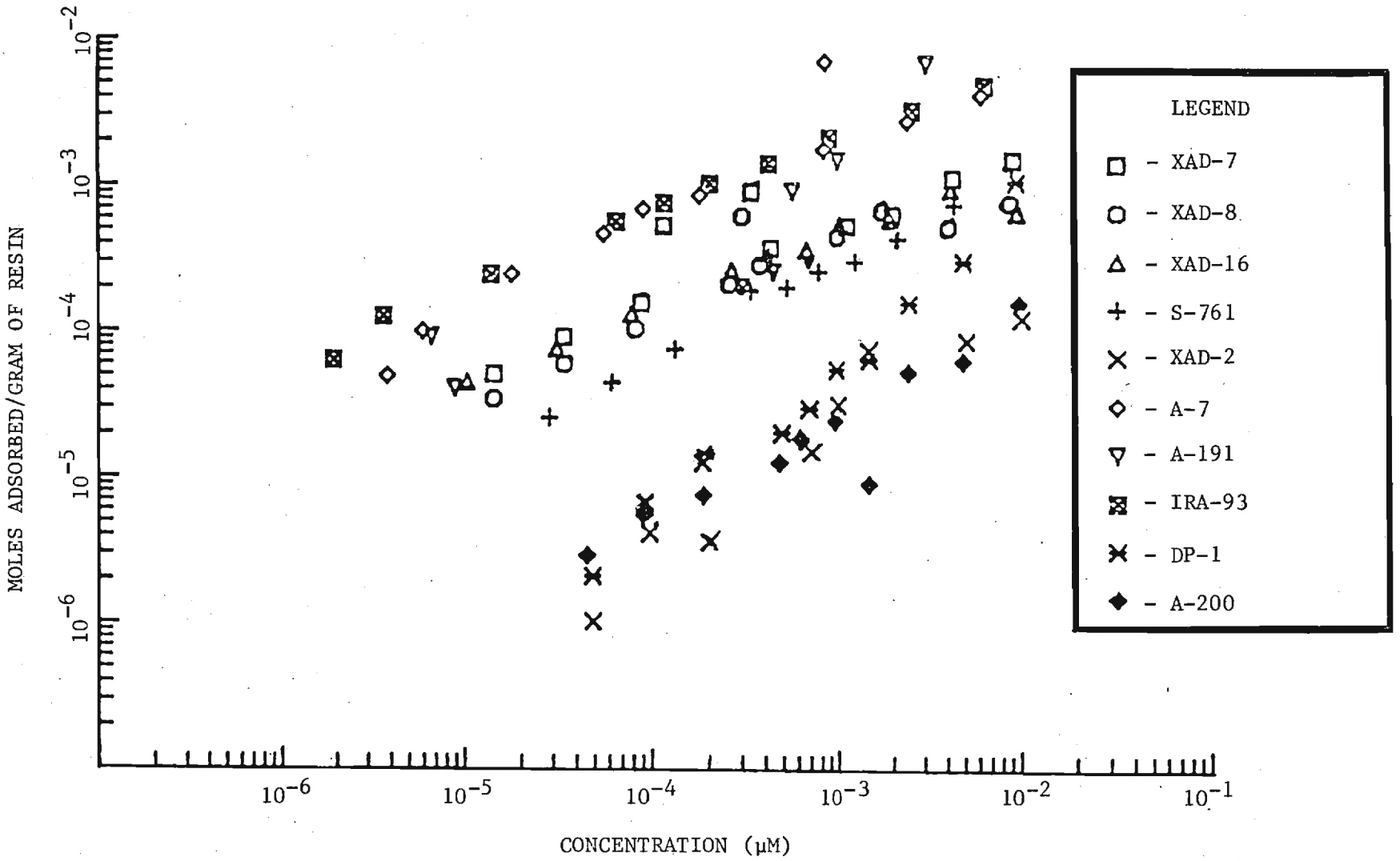

Figure 6. Adsorption Isotherms for P-nitrophenol, pH 5.0.

TABLE 6. FREUNDLICH CONSTANTS FROM ISOTHERM EXPERIMENTS FOR RESIN SCREENING

Dye	Resin	Data Pts.	r	K	n	pH
MO	A-7	3				
MO	A-191	3	.9193	.6541	2.08	
MO	IRA-93	4	.997	.014	4.29	
MO	A-200	6	.882	.319	.763	
MO	DP-1	9	.832	.436	.852	
MO	XAD-8	9	.956	.0022	1.733	
MO	XAD-7	10	.991	.0047	1.814	
MO	XAD-16	7	.983	.004	2.68	
MO	XAD-2	7	.521	1.99E-5	2.77	
MO	S-761	10	.986	.006	1.608	
PNP	A-7	6	.982	.125	1.688	
PNP	A-191	10	.857	.051	1.679	3.94
PNP	A-191	10	.916	.046	2.56	10.32
PNP	IRA-93	10	.996	.083	1.901	
PNP	A-200	10	.937	.0024	1.48	
PNP	DP-1	10	.991	.139	.89	
PNP	XAD-8	10	.918	.0127	2.016	5.86
PNP	XAD-8	8	.812	.211	.788	9.1
PNP	XAD-7	10	.902	.018	2.066	5.1
PNP	XAD-7					9.47
PNP	XAD-16	10	.971	.0099	2.197	5.23
PNP	XAD-16	10	.926	.036	1.141	
PNP	XAD-2	10	.981	.0152	1.408	
PNP	S-761	10	.995	.0317	1.485	5.16
PNP	S-761	5	.31	.0004		9.15

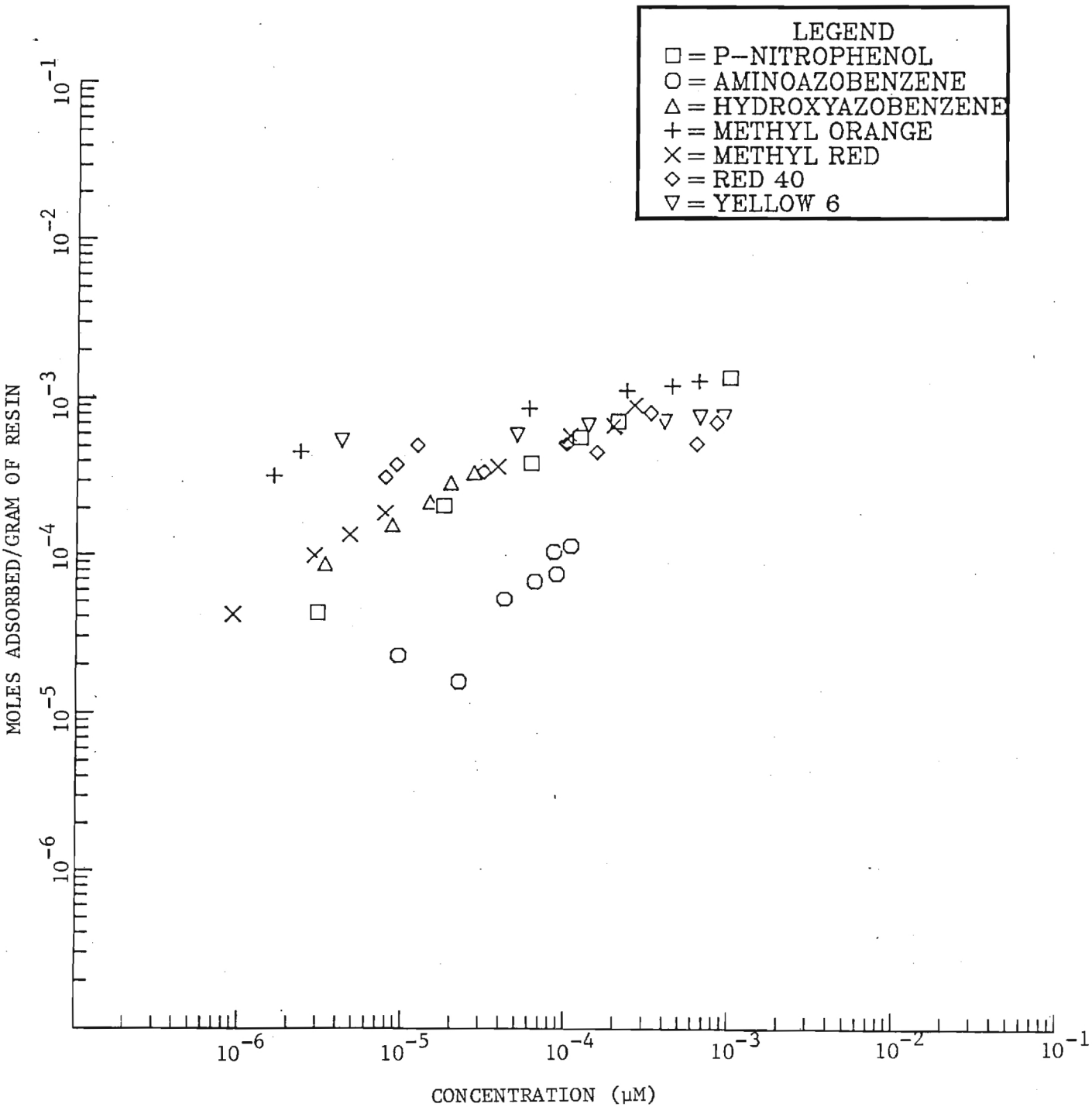

Figure 7. Adsorption Isotherms on Resin A-7.

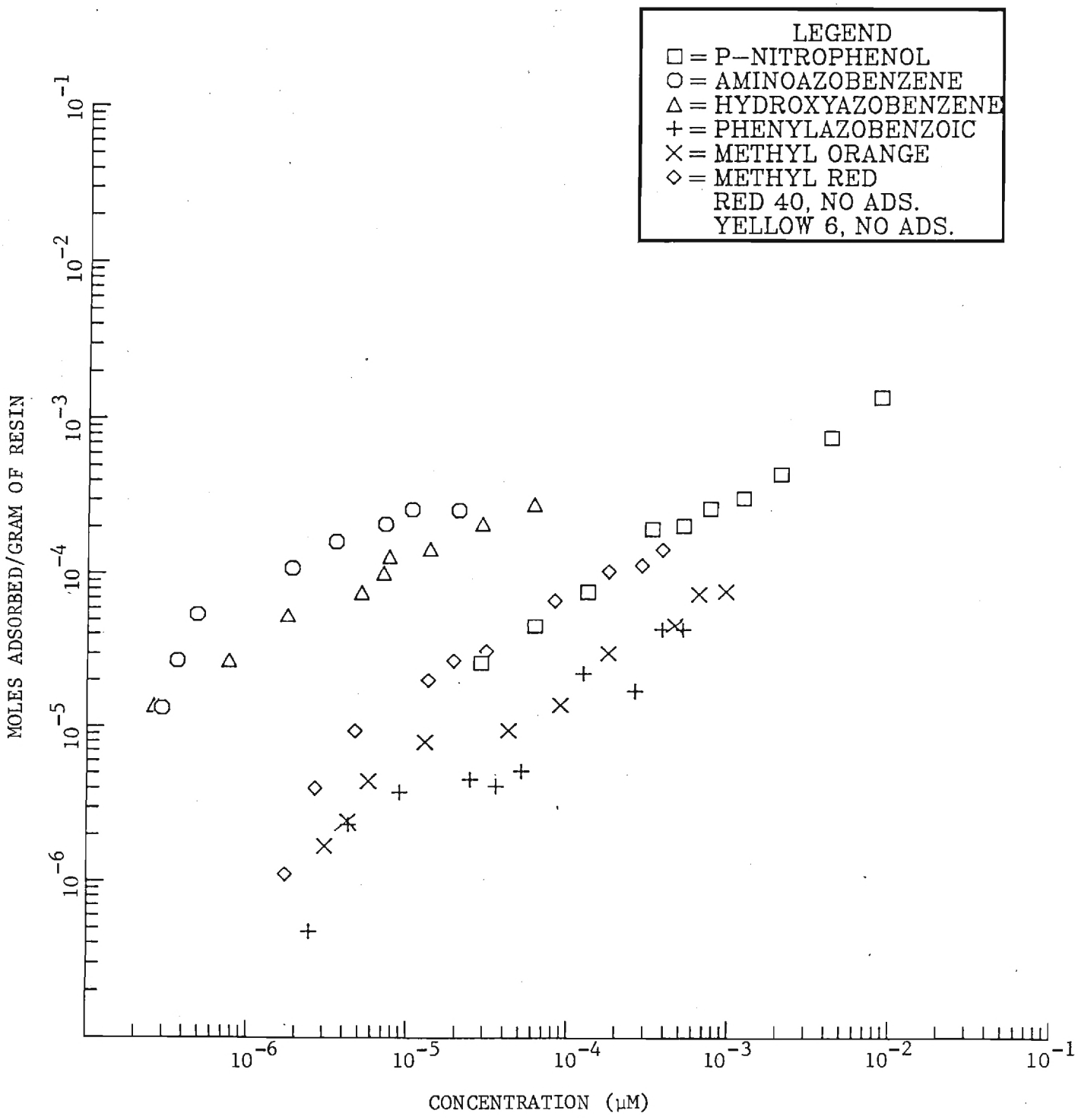

Figure 8. Adsorption Isotherms on Resin S-761.

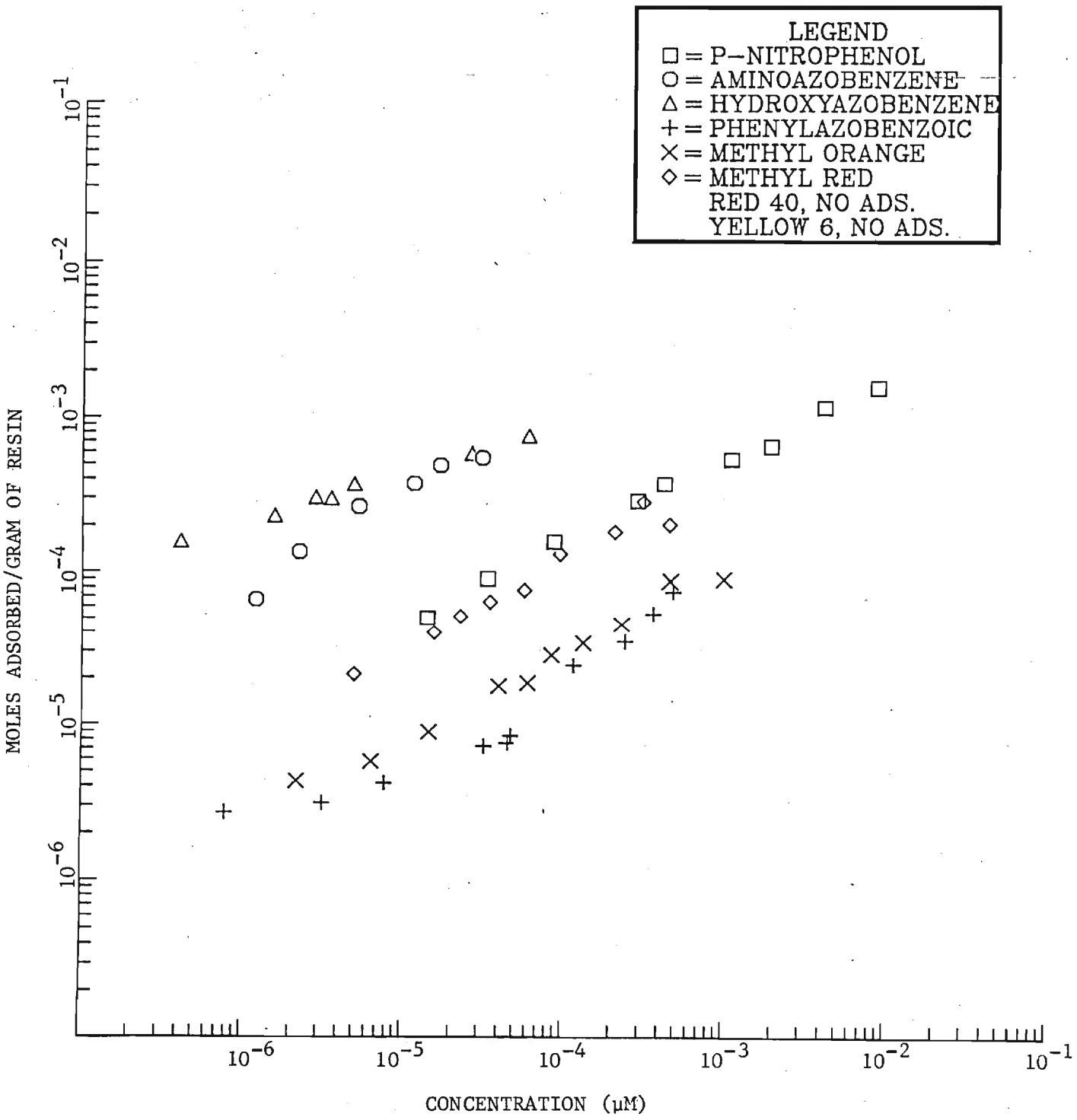

Figure 9. Adsorption Isotherms on Resin XAD-7.

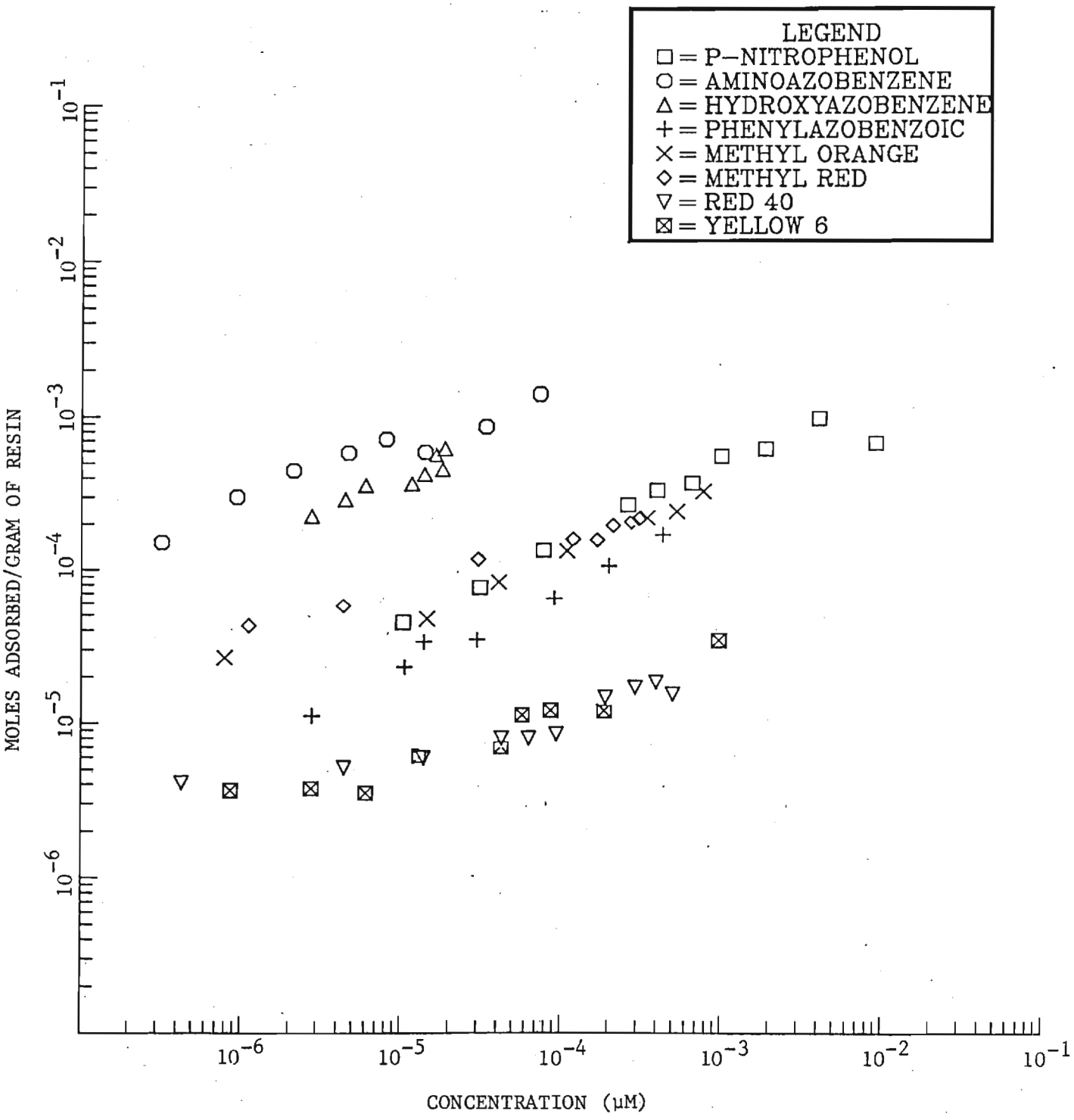

Figure 10. Adsorption Isotherms on Resin XAD-16.

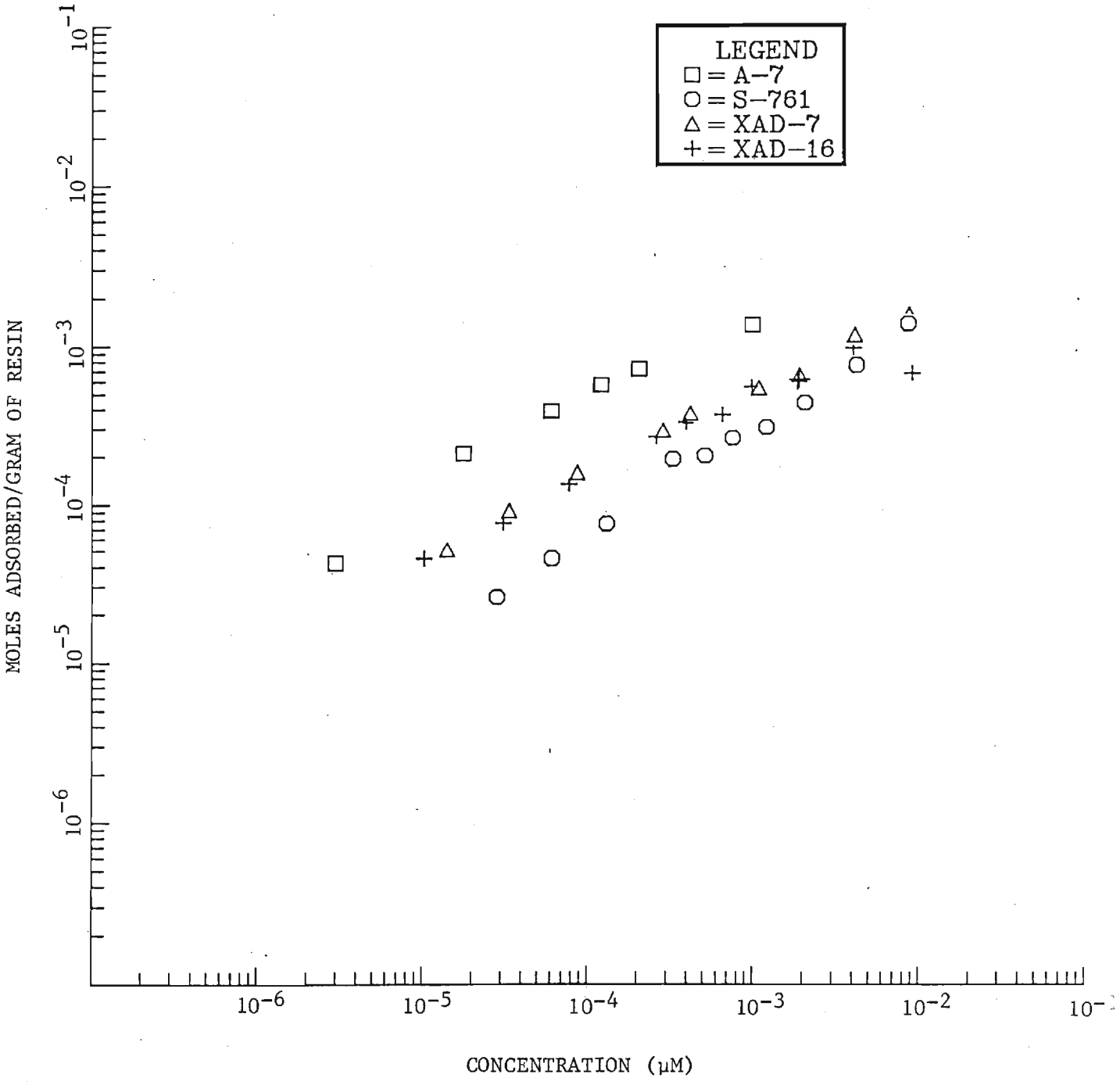

Figure 11. Adsorption Isotherms for P-nitrophenol pH=5.0.

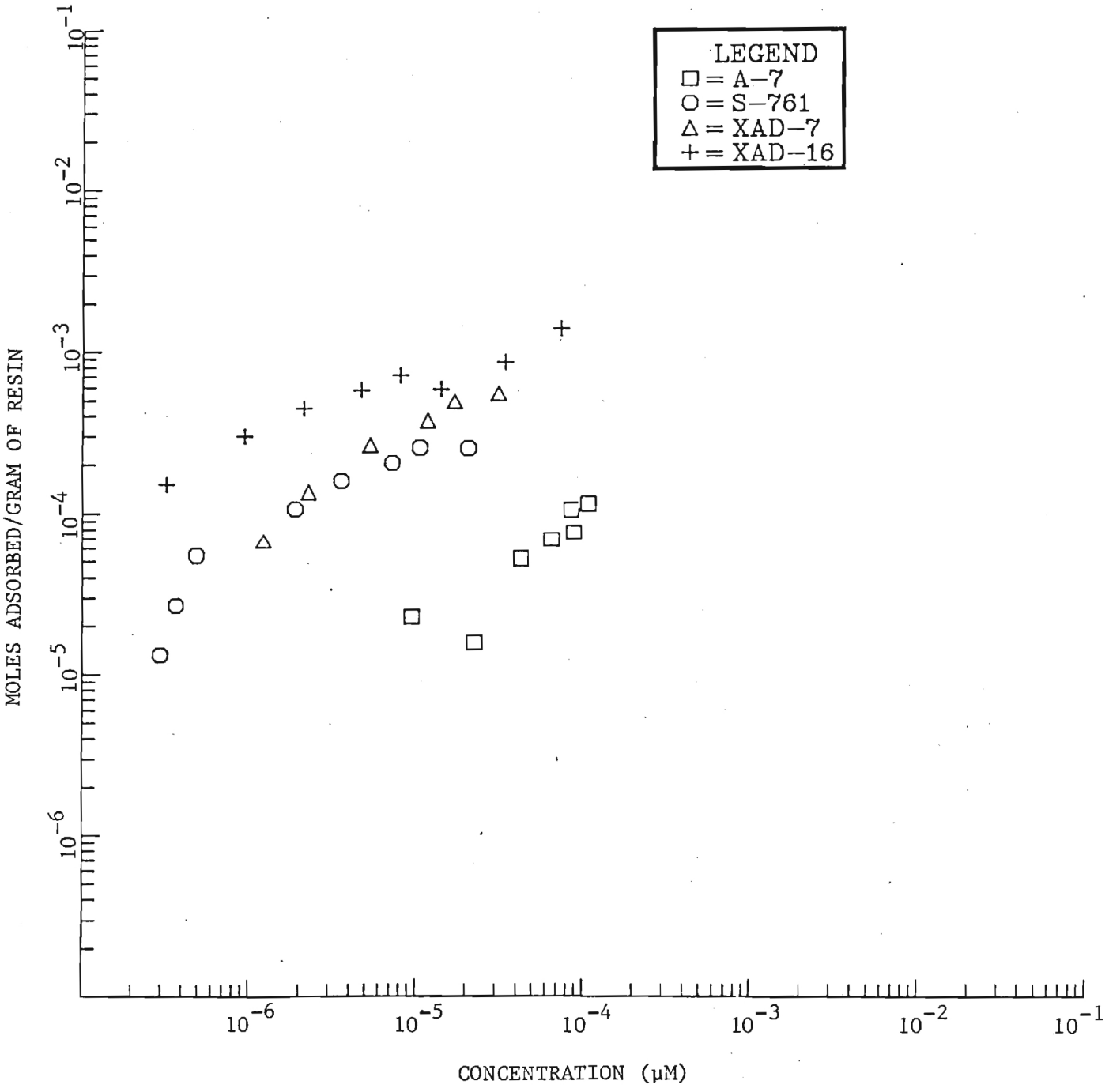

Figure 12. Adsorption Isotherms for 4-Aminoazobenzene pH=6.0.

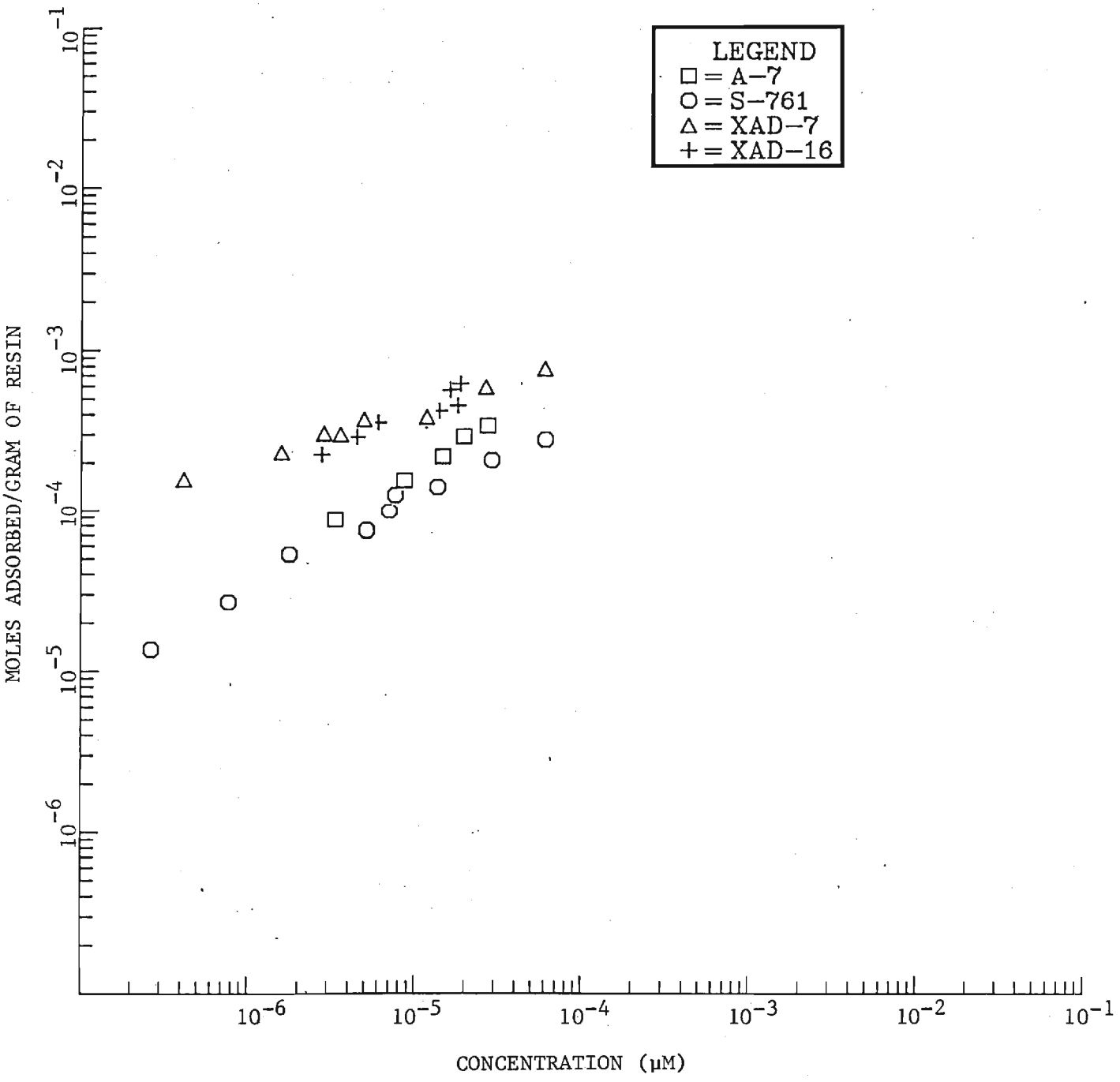

Figure 13. Adsorption Isotherms for 4-Hydroxyazobenzene pH=6.0.

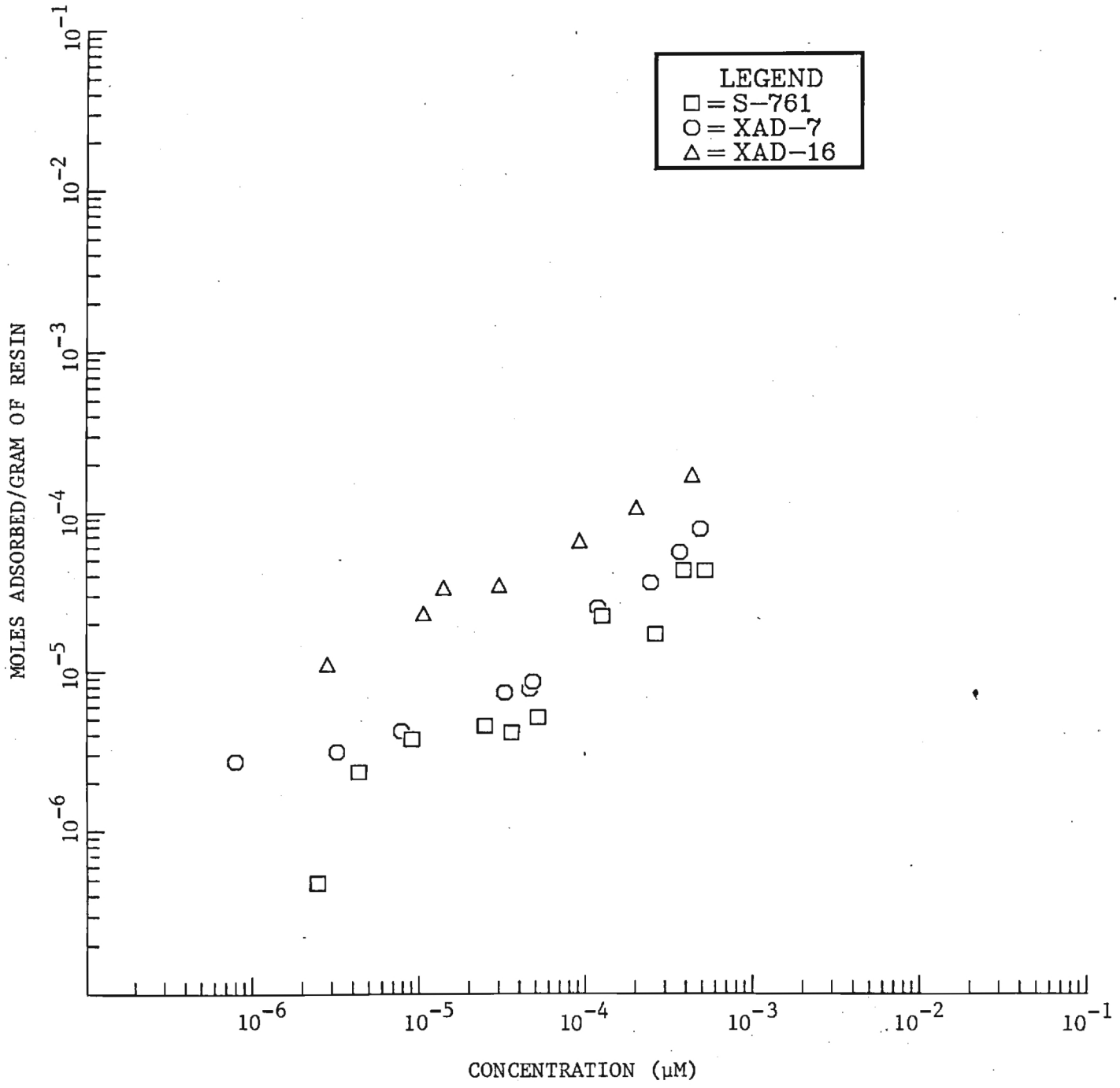

Figure 14. Adsorption Isotherms for Phenylbenzoic Acid pH=8.5.

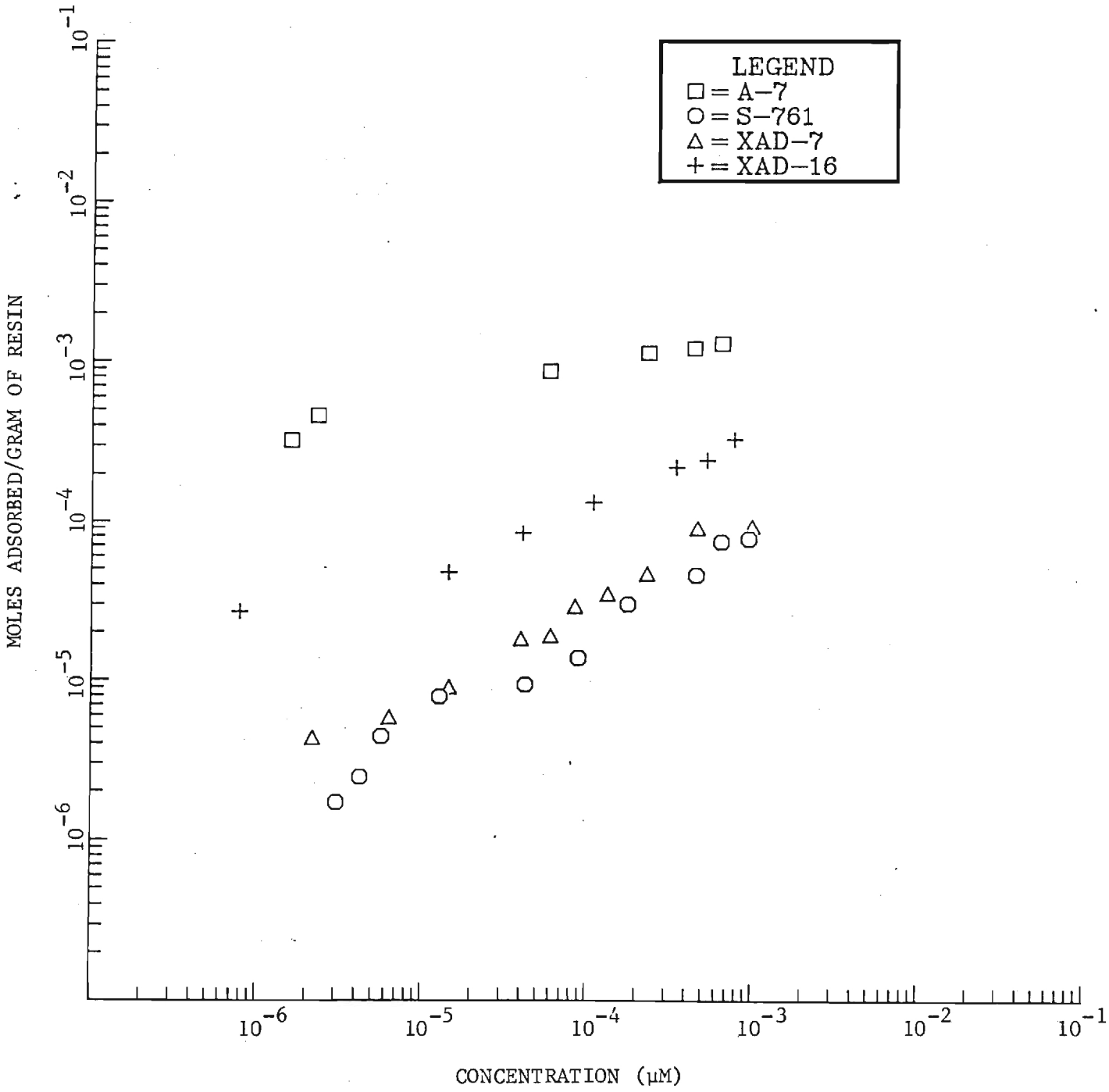

Figure 15. Adsorption Isotherms for Methyl Orange pH=6.0.

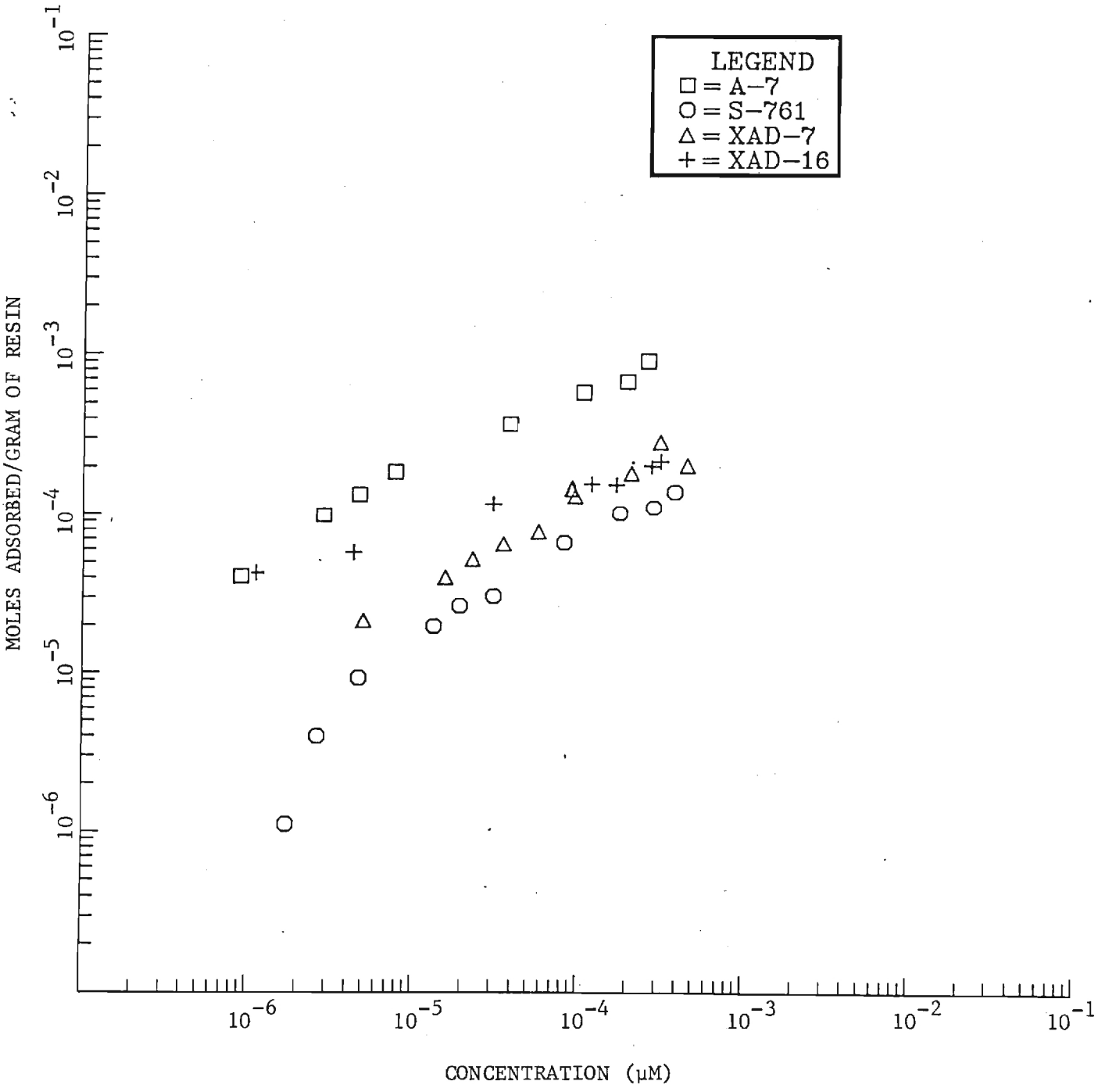

Figure 16. Adsorption Isotherms for Methyl Red pH=6.0.

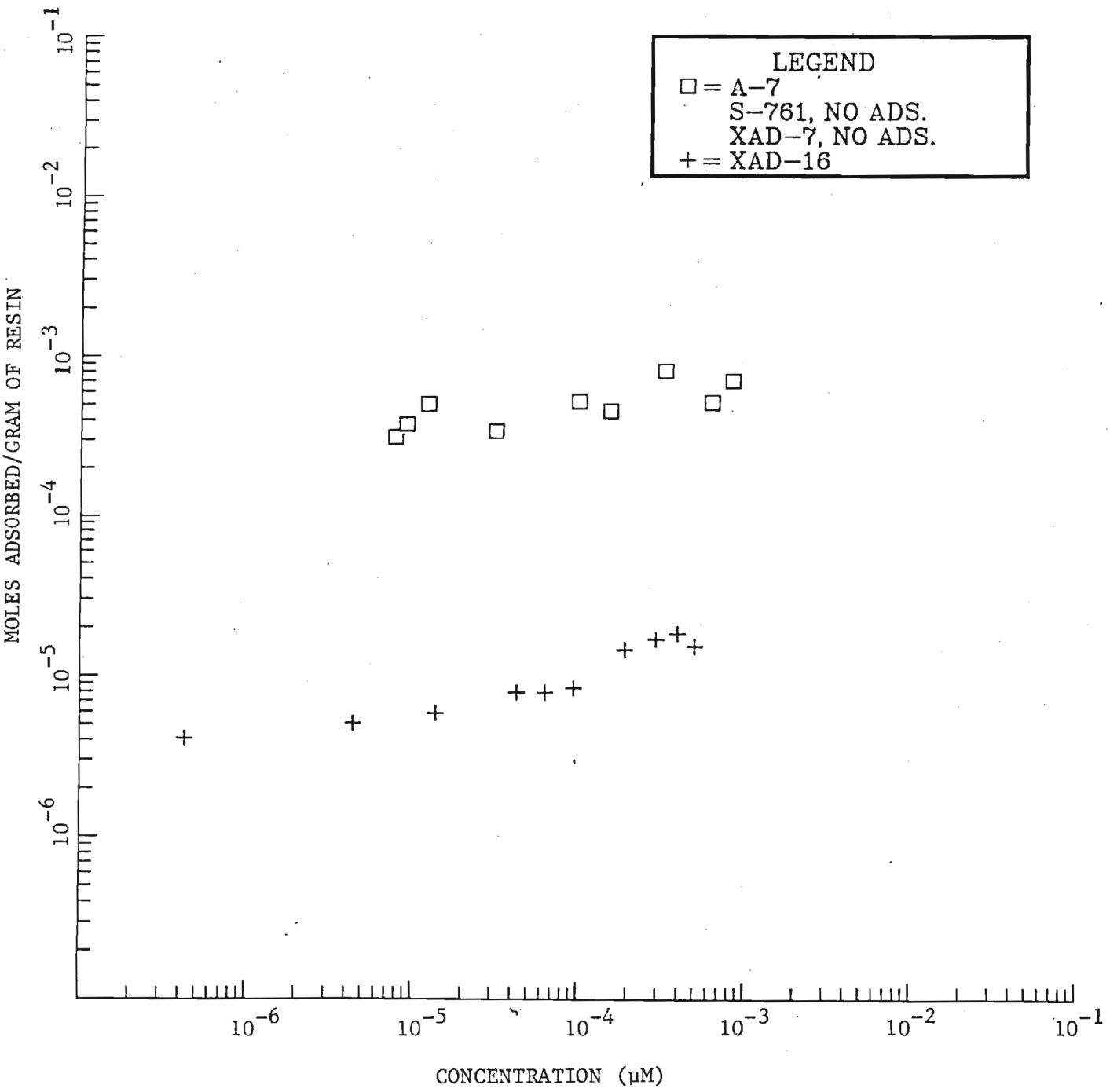

Figure 17. Adsorption Isotherms for FD&C Red 40 pH=6.0.

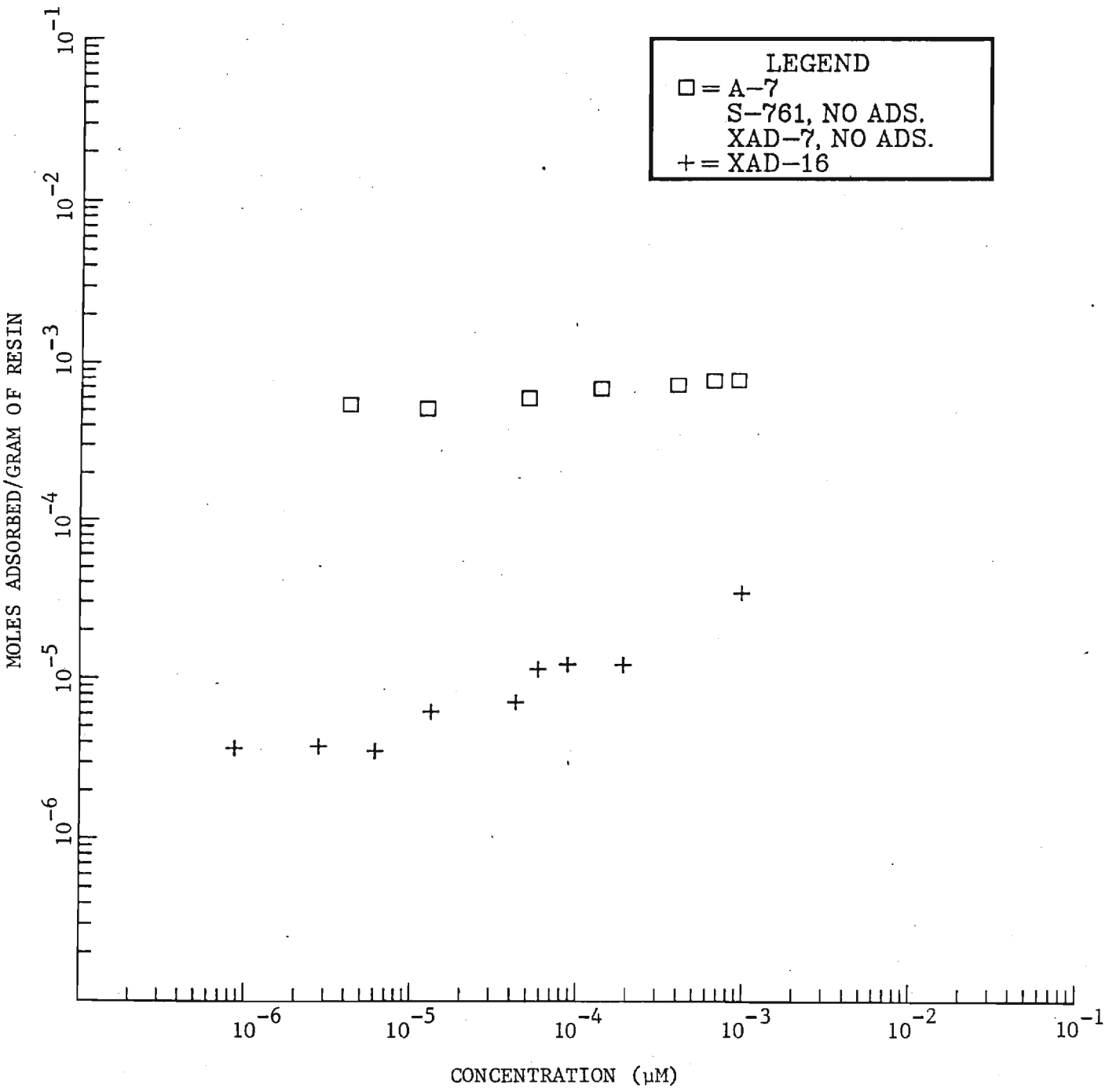

Figure 18. Adsorption Isotherms for FD&C Yellow 6 pH=6.0.

the sulfonic acid functional groups present in red 40 and yellow 6.

The same order of adsorption affinity was observed in both S-761 and XAD-7. 4-aminoazobenzene and 4-hydroxyazobenzene were adsorbed most strongly followed by p-nitrophenol, methyl red, methyl orange, and phenylazobenzoic acid. Neither red 40 nor yellow 6 adsorbed on S-761 or XAD-7. XAD-16 followed a similar pattern with 4-aminoazobenzene and 4-hydroazobenzene being adsorbed in the largest quantity and methyl orange, methyl red, phenylazobenzoic acid, and p-nitrophenol, adsoring in the same region. The most poorly adsorbed compounds on XAD-16 were red 40 and yellow 6. All the compounds adsorbed similarly on A-7 with the exception of 4-aminoazobenzene. 4-aminoazobenzene did not adsorb well due to the positive charge on the compound at the pH studied.

4.2 BATCH KINETIC EXPERIMENTS

Batch kinetic experiments were performed with p-nitrophenol, methyl orange, methyl red, red 40, yellow 6, 4-aminoazobenzene, and 4-hydroxyazobenzene in combination with the following resins: XAD-2, XAD-7, XAD-8, XAD-16, and S-761. Only a few experiments were performed with XAD-1 and XAD-8 in the early part of this study. Because they were poor performers they were not used further. Because of similarities in adsorption of methyl orange and methyl red, yellow 6 and red 40, and 4-aminoazobenzene and 4-hydroxyazobenzene one of each of these pairs was chosen for intensive study. The dyes chosen were methyl orange, red 40 and 4-aminoazobenzene. p-nitrophenol was also included.

A total of 40 adsorption experiments was successfully completed. Twenty-four of these were followed by a subsequent desorption run. Four experiments, using the resin XAD-16 in combination with methyl orange, p-nitrophenol, red 40, and 4-aminoazobenzene, were conducted to investigate the changes in adsorption capacity during successive adsorption and desorption cycles. For each dye, three adsorption/desorption cycles were conducted.

Plots of all experimental data are contained in Appendix 2. A summary of the results from these experiments are contained in Table 7. Methods used to calculate these values are described below. Also contained in this Table are acronyms used to denote the particular experiment. These acronyms will be used as shorthand notation throughout this report.

4.2.1 Calculation of Experimental Results

Percent Adsorbed (% A):

$$\%A = \frac{C_o}{C_e} \times 100 \qquad (6)$$

where: C_o = initial solution concentration (moles/L)
C_e = final solution concentration (moles/L)

Mass Adsorbed (W_A)

TABLE 7. SUMMARY OF BATCH KINETIC EXPERIMENTS

Acronym	Resin	Dye	M (g)	C_o (μM)	C_e (μM)	W_A, W_D (mg)	%A, %D	Teq.	T (°C)	X (moles/g) $x10^{-6}$
PB7	XAD-7	PNP	4.57	101	22.1	44.1	78.2-A	15 hr.	27	69
PBD7	XAD-7	PNP	4.57			41.7	92.7-D			
PB161	XAD-16	PNP	4.96	101	20.9	44.4	79.2-A	20 hr.	25	64.3
PBD161	XAD-16	PNP	4.96							
PB162	XAD-16	PNP	4.96	101	18.7	45.6	81.4-A	18 hr.	26	66
PBD162	XAD-16	PNP	4.96							
PB163	XAD-16	PNP	4.96	13.9	1.5			22 hr.	27	
PBD163	XAD-16	PNP	4.96							
PB164	XAD-16	PNP	4.96	101	19.5	45.1	80.7-A	20 hr.	27	65.7
PBD164	XAD-16	PNP	4.96							
PB165	XAD-16	PNP	4.63	104	22.5	45.1	78.3-A	25 hr.	26.5	70.1
PBD165	XAD-16	PNP	4.63			57.3	>100			
PB761	S-761	PNP	6.23	70.9	34.2	20.4	51.8-A	25 hr.	28	23.6
PBD761	S-761	PNP	6.23							
PB762	S-761	PNP	6.52	97.6	55.7	23.3	42.9-A	25 hr.	29	25.7
PBD762	S-761	PNP	6.52							
MB71	XAD-7	MO	4.91	24.7	15	12.7	39.3-A	49 hr.	25	7.9
MB72	XAD-7	MO	4.29	24.7	18.8	7.72	23.9-A	50 hr.	26	5.5
MB73	XAD-7	MO	1.09	10.5	8.63	2.41	17.8-A	50 hr.	22	6.74
MB74	XAD-7	MO		25.9	9.2	21.9	64.5-A	60 hr.	28	
MBD74	XAD-7	MO				20.9	95.6-D			
MB8	XAD-8	MO	6.58	24.9	21.1	4.97	15.3-A	15 hr.	25	2.31
MB161	XAD-16	MO	1.88	24.8	8.24	21.67	66.8-A	80 hr.	28	35.3
MB162	XAD-16	MO	4.92	93.2	8.62	110.7	90.8-A	80 hr.	25	68.8
MBD162	XAD-16	MO	4.92			105	94.85-D			
MB163	XAD-16	MO	4.92	99.8	17.2		982.7-A	80 hr.	28	67
MBD163	XAD-16	MO	4.92			118	>100-D			
MB164	XAD-16	MO	4.92	137	25.5	146.3	81.4-A	80 hr.	27.5	91
MBD164	XAD-16	MO	4.92			179.9	>100-D			
MB76	S-761	MO	10.94	24.7	9.0	20.5	63.4-A	50 hr.	28	5.73
MBD76	S-761	MO	10.94			24.5	>100-D			

TABLE 7. (Continued)

Acronym	Resin	Dye	M (g)	C_o (μM)	C_e (μM)	W_A, W_D (mg)	%A, %D	Teq.	T (°C)	X (moles/g) $x10^{-6}$
RB161	XAD-16	R40	4.8	18.7	11.6	14.1	38-A	80		5.92
RB162	XAD-16	R40	6.18	16.8	4.7	24.1	72.1-A	80	25.5	7.86
RBD162	XAD-16	R40	6.18			8.9	36.9-D			
RB163	XAD-16	R40	6.18	18.4	12.2	12.3	33.7-A	80	27	4.01
RBD163	XAD-16	R40	6.18							
RB164	XAD-16	R40	6.18	19.7	13.5	12.3	31.5-A	80	27	4.01
RBD164	XAD-16	R40	6.18			9.92	80.6-D			
AB71	XAD-7	4AAB	.47	66.1	16.7	39.1	74.9-A	23	26	422
AB72	XAD-7	4AAB	.407	60	15.2	35.34	74.6-A	20		
ABD72	XAD-7	4AAB	.407	0	18	7.08	10-D			
AB73	XAD-7	4AAB	.38	57	13.2	35.5	76.8-A	20 hr.	30	456
ABD73	XAD-7	4AAB	.38	0	19.9	7.84	10.d-D			
AB161	XAD-16	4AAB	.327	53.5	3.1	39.8	94.2-A	26	24	617
ABD161	XAD-16	4AAB								
AB162	XAD-16	4AAB	1.82				100-A	30	25	
ABD162	XAD-16	4AAB	1.82							
AB163	XAD-16	4AAB	1.82	136	0		100-A	30	26	
ABD163	XAD-16	4AAB	1.82							
AB164	XAD-16	4AAB	1.82	50.4	0		100-A	25	27	
ABD164	XAD-16	4AAB	1.82	0	44.5					
AB165	XAD-16	4AAB	.17					30	28	
AB166	XAD-16	4AAB	.199	56.9	6.4	39.9	88.8-A	33 hr.	31	1015
ABD166	XAD-16	4AAB	.199	0	22.5	8.87	22.2-D			
AB76	S-761	4AAB	.652	63	7.34	43.9	88.3-A	70 hr.	26.5	341
ABD76	S-761	4AAB	.652			4.93	11.2-D			

$$W_A - (C_o - C_e) \times 4L \times (M.W.)/1000 \quad (7)$$

where: M.W. = The molecular weight of the compound studied
4L = the volume of the adsorption reactor
1000 = a conversion factor from grams to milligrams

W_A is expressed as mg of dye adsorbed

Mass Desorbed (W_B)

$$W_B = C_e \times 2L \times (M.W.)/1000 \quad (8)$$

where: 2L = The volume of the desorption reactor

(C_o the initial concentration is always zero, as pure methanol was added to the reactor).

W_B is expressed as mg of dye desorbed.

Percent Desorbed (% D)

$$\% D = W_A/W_B \times 100 \quad (9)$$

X (= moles of dye adsorbed/g of resin)

$$X = \frac{(C_o - C_e) \times 4L}{M} \quad (10)$$

Teq

This parameter was determined graphically and by examination of the data. It represents the earliest time at which the final equilibrium concentration was attained.

4.2.2 Validation

Because of the length of time required for each experiment and the number of experiments conducted using different combinations, a statistical validation of reproducibility was impossible. However, in several instances experiments were conducted using the same resin-dye pair at similar values. Examples are MB71 and MB72; AB71 and AB73; AB161 and AB166.

In addition it was necessary to produce comparable results between isotherm and batch kinetic studies to demonstrate consistency in adsorption throughout the study. Since different individuals conducted these experiments, this was particularly important. Because each point on an adsorption isotherm represents in effect, a continuously stirred batch reactor, this is easily done. For each batch kinetic experiment sorbate uptake, X, was calculated and, using the measured final concentration, compared to that predicted by the adsorption isotherm. In all cases the uptake from batch studies fell within the range of experimental error of isotherm. An example of this type of comparison is shown in Figure 19 for the adsorption of 4AAB, MO, and R40 on XAD-16.

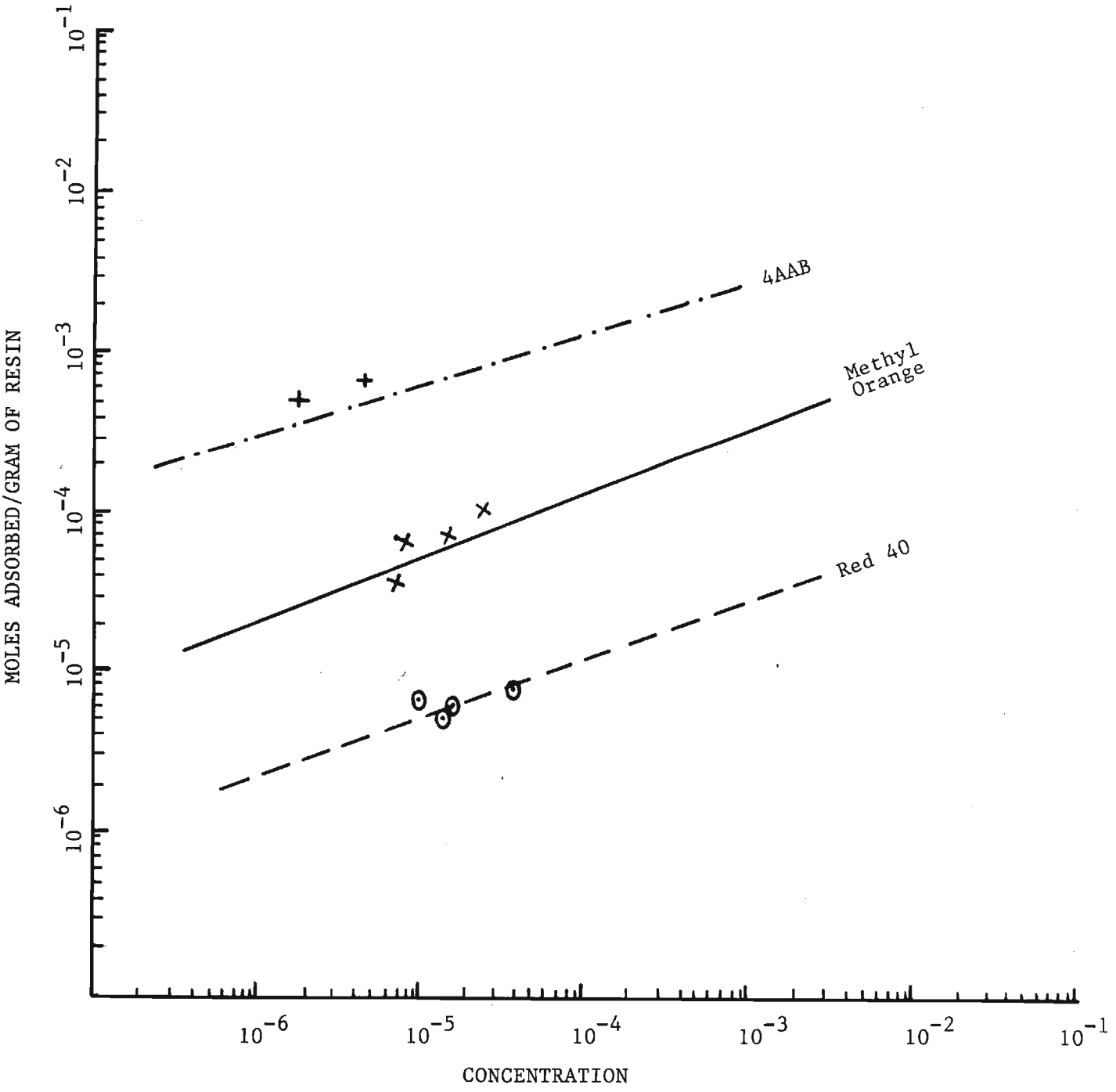

Figure 19. Comparison of Isotherm and Batch Kinetic Results.

4.2.3 Adsorption of Dye Compounds onto Synthetic Resins

Direct comparisons of the adsorption behavior of synthetic dyes is difficult because variable experimental parameters. In general, experiments were designed to remove between 70 and 90% of the dye in solution. Where possible, solution concentrations were kept constant with respect to individual dyes, but often were varied to satisfy the percent removal consideration. In the figures that follows, single experiments were selected for illustration to show trends on the basis of their similarity in percent adsorbed and initial dye concentration. Resin weight tended to vary widely.

4.2.3 a) 4-aminoazobenzene

4-aminoazobenzene was adsorbed more strongly than any of the dyes studies. This is likely due to the fact that it is relatively insoluble in water, and tends to preferentially seek any solid surface. It was adsorbed most strongly onto the resin XAD-16 ($X = 6\text{-}10 \times 10^{-4}$ moles/g), followed by XAD-7 ($X = 45.\times 10^{-4}$ moles/g), then S0761 ($X = 3.4 \times 10^{-4}$ moles/g). The shapes of the adsorption curves are similar with adsorption onto XAD-7 proceeding most rapidly (Figure 20). XAD-16 and S-761 are aromatic resins, while XAD-7 is an aliphatic resin. Obviously, the "like attracts like" rule does not apply here. Additionally, 4AAB is a small molecule and should not be limited by diffusion into any of the pores. The most straightforward explanation for this behavior appears to be related to simply to surface area. The surface areas for XAD-16, SAD-17, and S-761 are 800, 450 and 300 m^2/g, respectively. These values are nearly proportional to the experimental estimates of X. It would appear that the strongly hydrophobic molecule, 4AAB, showed little preference for a particular surface, but simply occupied the available area of the solid surface.

4.2.3 b) Methyl Orange

Methyl orange absorbed most strongly onto XAD-16 ($X\text{-}7.0 \times 10^{-5}$ moles/g) followed by S-761 ($X = 5.9 \times 10^{-6}$ moles/g) and XAD-7 ($4\text{-}8 \times 10^{-6}$ moles/g). The shapes of the adsorption curves again appear similar (Figure 21). The apparent difference in the initial adsorption between XAD-16 and the other resins was a result of the fact that the initial concentration for the XAD-16 experiment was nearly 100 μM, while the initial concentrations for the XAD-7 and S-761 experiments was approximately 25 μM.

That XAD-16 had the greatest capacity to adsorb methyl orange is no surprise. XAD-16 is an aromatic resin with the greatest surface area of any of the resins tested. That XAD-7 and S-761 have nearly the same capacity requires explanation. Methyl orange should have a greater affinity for the aromatic resin, S-761 than for XAD-7. However, XAD-7 has more than 4 times the surface area of S-761. Although a poorer surface for adsorption, the greater surface area of XAD-7 makes it a comparable resin for the adsorption of methyl orange.

4.2.3 c) Paranitrophenol

The resins XAD-7 and XAD-16 showed nearly identical capacity for the adsorption of paranitrophenol ($X = 6.9 \times 10^{-5}$ and 7×10^{-5} moles/g, respectively). The resin S-761 showed much less capacity ($X = 2.6 \times 10^{-5}$ moles/g) (Figure 22).

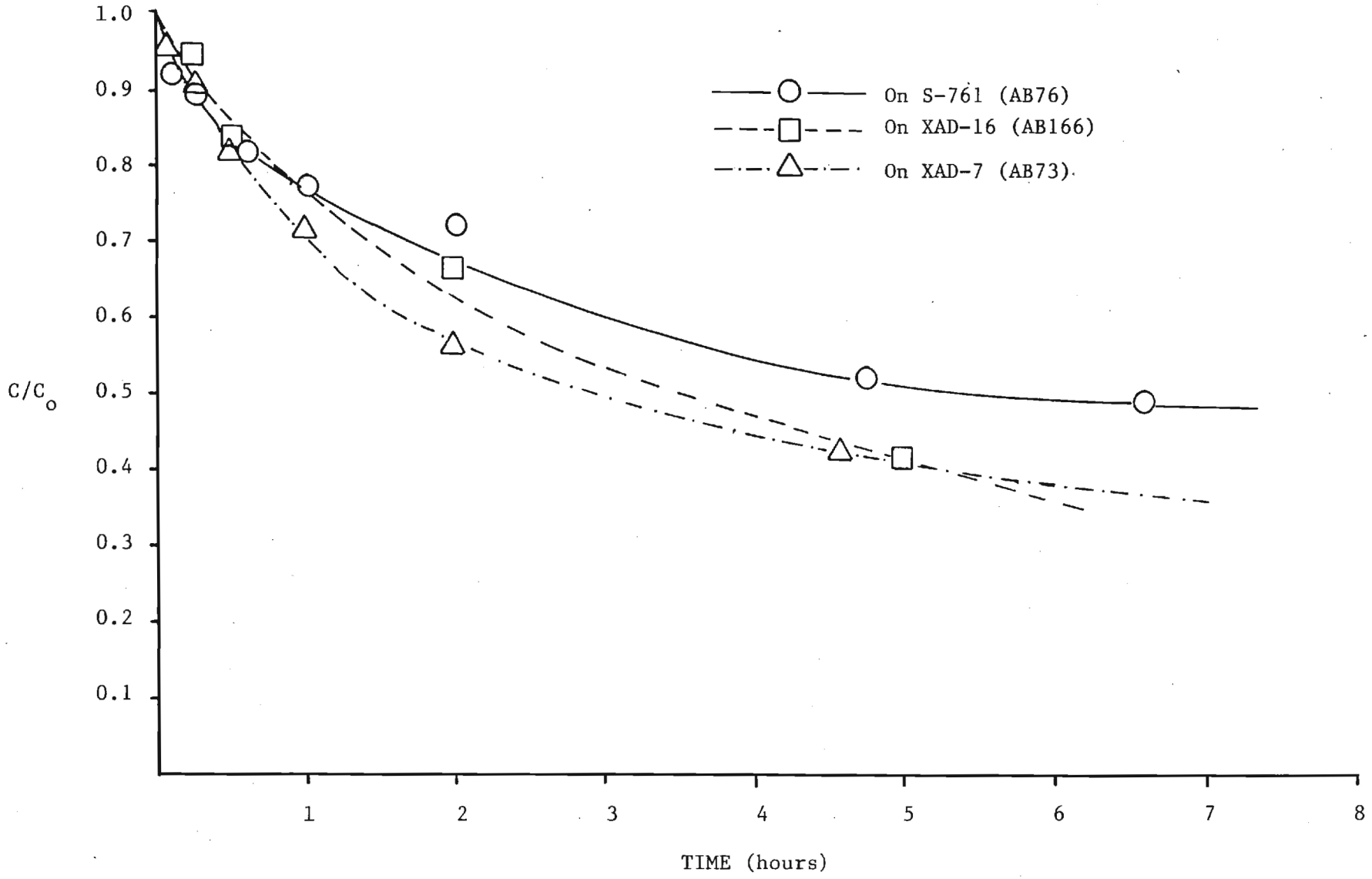

Figure 20. Batch Adsorption of 4-aminoazobenzene.

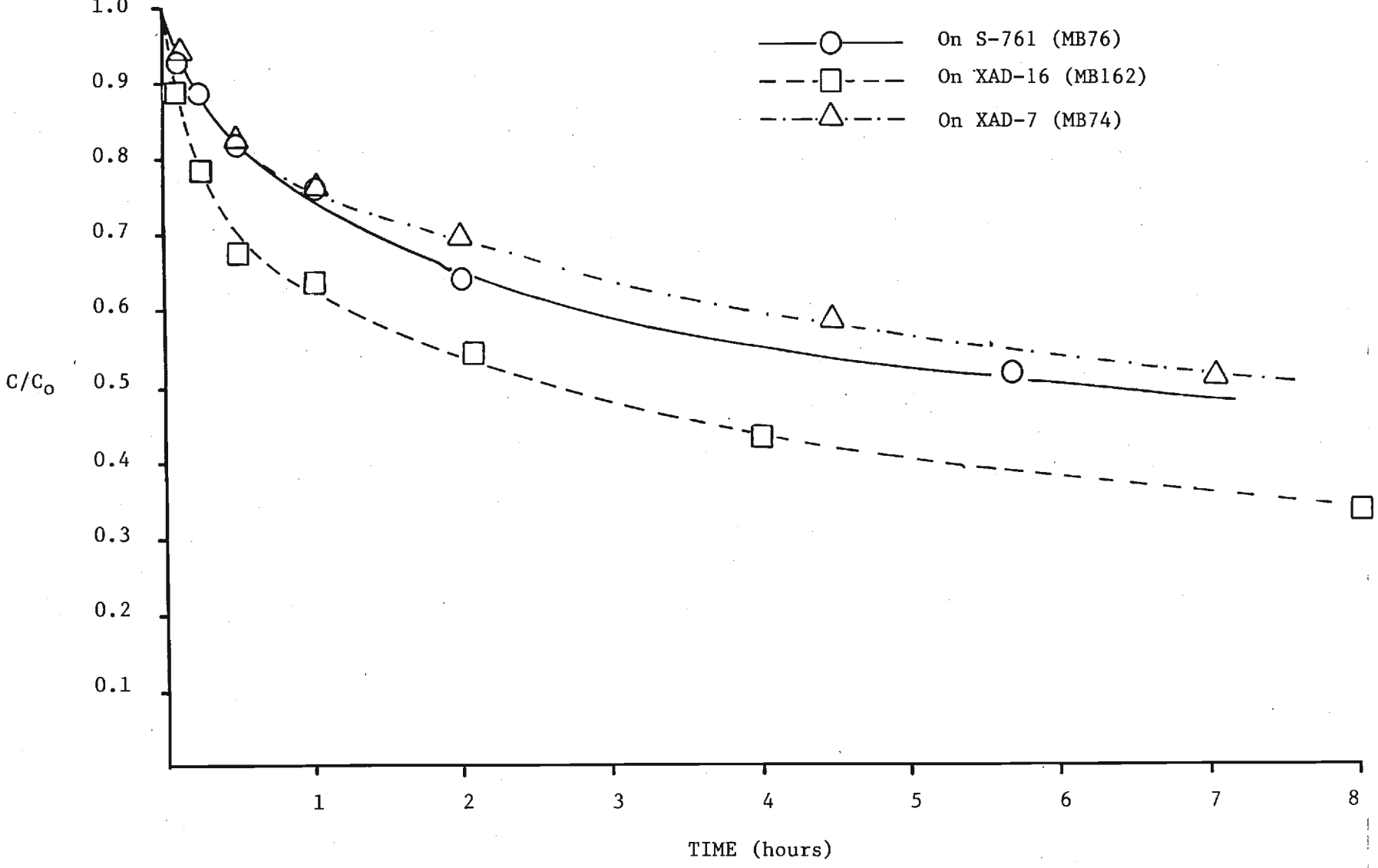

Figure 21. Batch Adsorption of Methyl Orange.

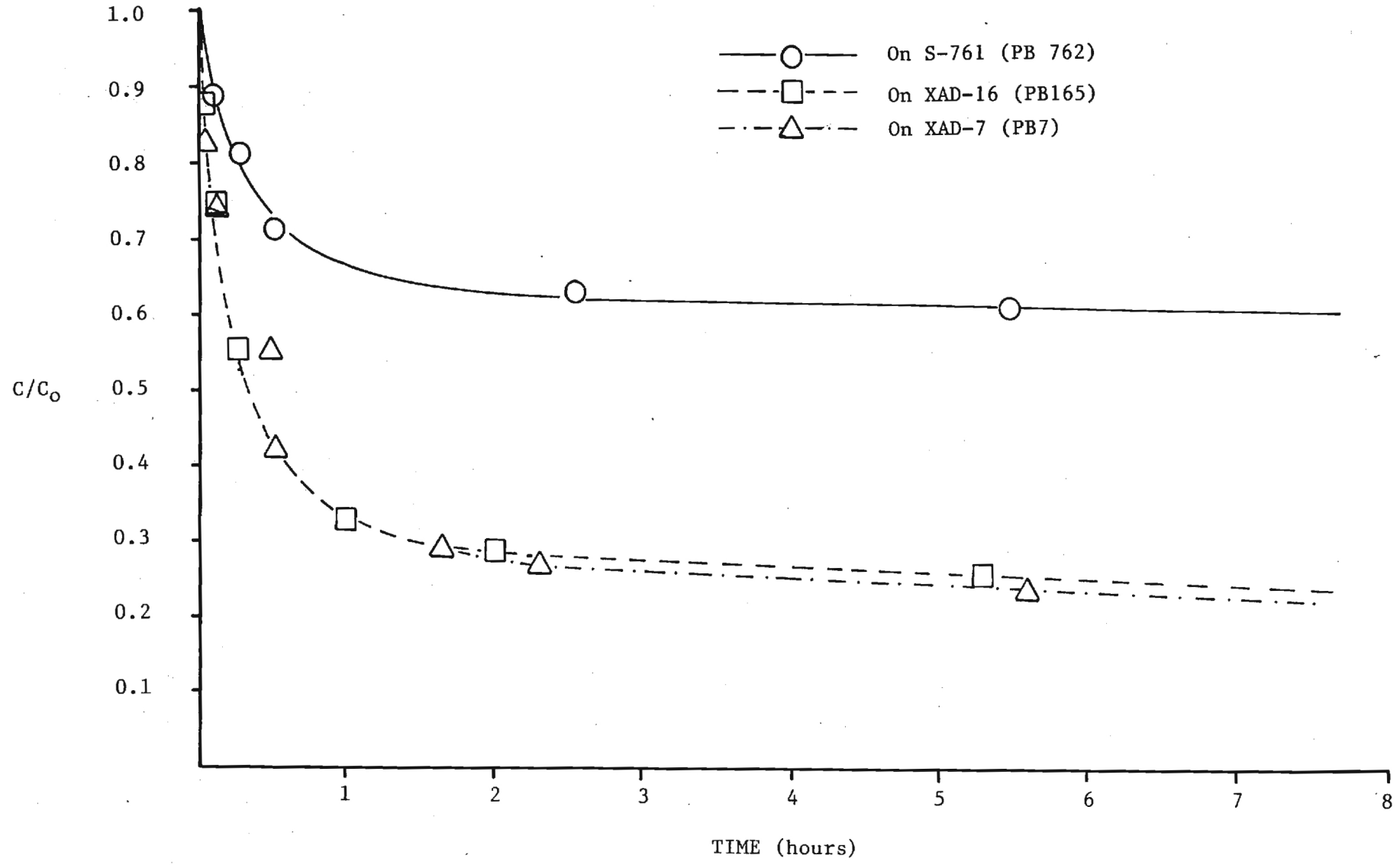

Figure 22. Batch Adsorption of p-nitrophenol.

The same amount of XAD-7 and XAD-16 resin was used (4.57 and 4.62 g (dry weight), respectively, while 6.52 g (dry weight) of S-761 was added to the reaction chamber. The initial concentration was approximately 100 μM in all cases.

That XAD-7 adsorbed more PNP than S-761 can be explained using an argument parallel to that of 4.2.3 b) for methyl orange, suggesting again, that surface area was more important than surface characteristics. This, however, did not explain the similar capacities of XAD-7 and XAD-16. XAD-16 has the preferred surface characteristics and a greater surface area. In this case, the aromatic compound, p-nitrophenol, had a greater affinity for an aliphatic surface than for an aromatic surface.

4.2.4 Desorption of Dye Compounds from Synthetic Resins

The ease with which dyes were removed from synthetic resins followed the order: paranitrophenol > methyl orange > red 40 > aminoazobenzene. XAD-16 appears to be the resin most easily regenerated, followed by XAD-7 and S-761. In retrospect, excessive regenerant was added to the batch reactor in experiments involving paranitrophenol and methyl orange. This resulted in 100% desorption in nearly all cases.

4-aminoazobenzene, the least soluble and most readily absorbed dye was the least desorbable. This is to be expected in terms of solubility. That red 40, the most soluble dye, was also difficult to desorb, stands in contrast to the above generalization. The reason for this phenomenon may be due to its poor solubility in methanol, or to a chemical interaction between red 40 and the resin surface.

In all cases equilibrium was reached rapidly, within the first 5 minutes.

4.2.5 Adsorption Capacity After Successive Adsorption/Desorption Cycles

Four experiments were conducted to observe the effect that successive adsorption/desorption cycles have an absorption capacity. One of these experiments, 4AAB on XAD-16, failed. Too much resin was added to the initial run, resulting in complete adsorption. Desorption and adsorption cycles were conducted, but due to rapid adsorption and poor desorption, little information was gained. The other experiments were successfully completed and demonstrated the different effect that individual dyes have on loss of adsorption capacity.

4.2.5 a) Methyl Orange

Figure 23 is a plot of the data from experiments with methyl orange and XAD-16. Capacity for adsorption decreased between the first and the second cycle (90.8% to 82.7%), but remained essentially the same for the third cycle (81.4%). This is in agreement with results obtained by Cross, et al. (1982) using activated carbon and organic dyes. In the first two adsorption cycles, the value of X remained the same (initial concentrations = 93 and 100 μM, respectively). In the third cycle, the initial concentration was increased to 173 μm. This resulted in an increase in the value of X (from 68 to 91), but the percent of this concentration adsorbed decreased. The increase in initial

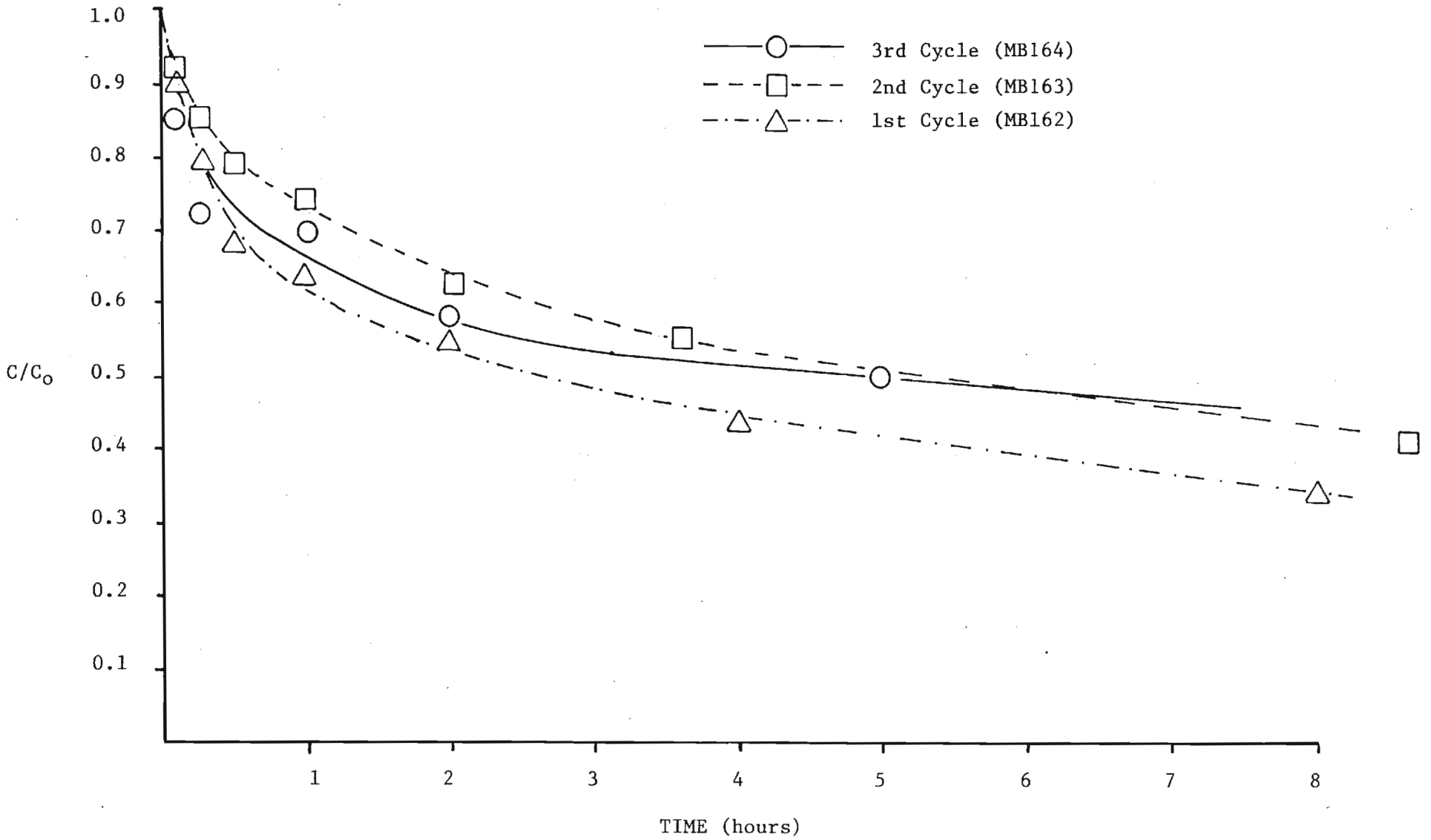

Figure 23. Sequential Batch Adsorption of Methyl Orange on XAD-16.

concentration increased the driving force for adsorption, as reflected by the results. The capacity for adsorption lost due to successive cycles, however, remained the same after the initial cycle at about 10% with no further loss of capacity observed.

4.2.5 b) Red 40

Figure 24 is a plot of the data from experiments with Red 40 and XAD-16. The observation that most of the adsorption capacity is lost after the initial cycles, with remaining cycles contributing little loss, is most apparent in this series of experiments. Initially 72% of the dye was adsorbed. This capacity decreased to 33.7% and 31.5% at the second and third cycles. The value of X decreased between the first and second cycles and remained the same thereafter.

4.2.5 c) Paranitrophenol

Adsorption of paranitrophenol appeared to be completely reversible when methanol was used as a regenerant. In this set of experiments, four successive cycles were run. The reason for the fourth cycle was due to an error in the third cycle. A concentration much less than that specified was added to the reactor. The experiment was carried out, however, and the correct solution concentration was used for the fourth cycle.

No decrease in absorption capacity occurred. The percentage of the dye absorbed was 79.2 in the first cycle and 86.7 in the fourth.

4.2.6 Capacity Versus Rate of Adsorption

The parameter X, the moles of compound adsorbed per gram of resin, is a measure of the capacity of a particular resin for a solute. Because it is measured at equilibrium, it is only indicative of the affinity of a solute for a solid surface, and does not account for the speed at which the overall process takes place. In other words, assuming the actual process of a solute adsorbing onto a surface is instantaneous, it ignores the time it takes to bring the solute to the resin surface, and the process responsible for it (bulk, pore and film diffusion). To get an idea of the rate at which the adsorption process takes place, T_{eq}, the time at which equilibrium conditions were achieved, was calculated. Table 8 ranks the various experiments in terms of T_{eq} and X.

In these experiments mixing energy was sufficient to keep all resin particles in suspension. As a result bulk diffusion could be ignored. Film diffusion could also be ignored. Concentration was measured in the bulk solution, therefore, once a particle entered a pore it was effectively removed from solution. The differences in Table 8 between T_{eq} and X ranking can be addressed in terms of pore diffusion. The parameters which affect pore diffusion most strongly are pore diameter and size of the solute.

The resin S-761 had the largest pore diameter, followed by XAD-8, XAD-7 and XAD-16. Red 40 had the largest molecular weight of the molecules studied, followed by methyl orange, p-nitrophenol, and 4-aminoazobenzene.

From Table 8 it can be seen that, with the exception of run MB8, methyl

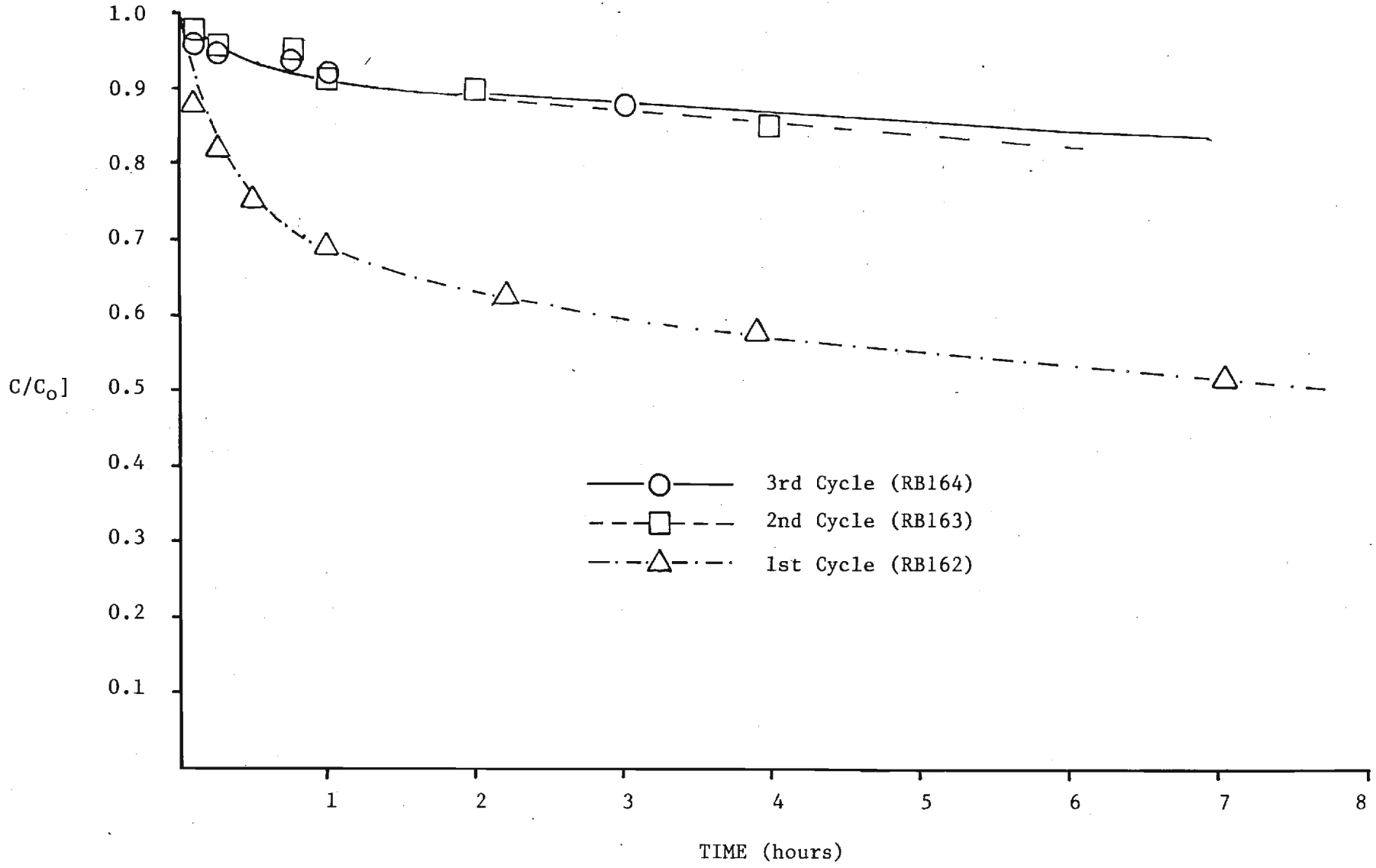

Figure 24. Sequential Batch Adsorption of Red 40 on XAD-16.

TABLE 8. RANKING OF BATCH KINETIC EXPERIMENTS BY X (moles ads/g) AND TIME TO EQUILIBRIUM

T eq (low to high) in hours		X (high to low) in moles ads/g of resin
PB7	15	AB166
MB8		AB161
*PB162		AB73
PB161		AB71
*PB164	15-20	AB76
AB73		*MB164
AB72		PB165
*PB163		PB7
PB165		MB162
AB71	20-25	*MB163
PB761		*PB162
PB762		*PB164
AB164		PB161
AB161		MB161
AB162	25-35	PB762
AB163		PB761
AB165		*PB163
AB166		MB71
MB71		RB162
MB72	45-60	MB73
MB73		RB161
MB74		MB76
MB161		MB72
MB162		*RB163
*MB163		*RB164
*MB164	>80	MB8
RB161		
*RB162		
*RB163		

*Denotes successive cycle in adsorption/desorption set of experiments.

orange and red 40 took the longest time to reach equilibrium. XAD-8 has a relatively large surface area so that, in the case of MB8, the reaction was not limited by pore diffusion. Paranitrophenol, achieved equilibrium rapidly on all resins, while 4-AAB was intermediate in behavior.

In comparing the resins XAD-7 and XAD-16 it can be seen that equilibrium was reached more quickly on XAD-7, but XAD-7 has a slightly smaller pore diameter (90 A versus 100 A). However, XAD-16 has a much greater surface area (800 m^2/g versus 450 m^2/g). While the rate of pore diffusion is of the same magnitude, the reaction on XAD-16 proceeds for a longer time because of the greater number of adsorption sites available.

4.3 COLUMN KINETIC EXPERIMENTS

Column kinetic experiments were performed with p-nitrophenol, methyl orange, Red 40, and 4-aminoazobenzene in combination with the following resins: S-761, XAD-7, and XAD-16. A total of 16 column adsorption studies was completed. Column desorption experiments were successfully completed on 15 of these. Two experiments, using the resin XAD-16 in combination with p-nitrophenol and methyl orange, were conducted to investigate the loss of adsorption capacity with successive adsorption and desorption cycles.

Plots of all experimental data are contained in Appendix 3. A summary of the results from these experiments is contained in Table 9. Also contained in this table are acronyms used to denote the particular experiment. These acronyms will be used as shorthand notations throughout this report. Methods used to calculate the values in this table are described below.

4.3.1 Calculation of Experimental Results

Flow Rate, FR (L/hr)

Flow rates of adsorbate and regenerant through the column were determined in two methods: (1) measurement of volumes of individual samples, and (2) measurement of volumes in effluent reservoir.

(1) Volume of individual samples ($F.R._{(S)}$) - The sample collection period was two minutes (30 seconds for the pruge cycle, and 90 seconds for sampling cycle). At the end of the experiment, the volume of representative samples was measured. The flow rate was calculated by dividing this volume by the length of the sample period. This rate was converted to L/hr and used in later calculations. This flow rate estimate was essentially instantaneous, in that it measured the flow rate over discrete short intervals during the experiment, and indication of the variation in flow rates. It is designated as $F.R._{(2)}$.

(2) Volume accumulated in effluent reservoir ($F.R._{(C)}$) - At the end of the experiment the volume in the effluent reservoir was measured (V_C). The period of time that the column effluent flowed into the effluent reservoir (T_C) was calculated by subtracting the total sampling time (T_S) from the length of the experiment (T_T). The total sampling time (T_S) was calculated as the product of the number of samples and the sampling collection period (2 min). This flow rate estimate was an average value for the entire experiment.

TABLE 9. SUMMARY OF COLUMN ADSORPTION EXPERIMENTS

Acronym	Resin	Dye	M (g)	Time (hrs.)	Cumulative Flow (L)	C_o (μM)	%B, %D	W_A, W_D (mg)
PC161	XAD-16	PNP	8.67	74.5	35.7	106.1	99.5-B	187.9
PCD161	XAD-16	PNP	8.67	20.2	-	-	-	-
PC162	XAD-16	PNP	8.67	52.5	18.0	100.65	100.4-B	222.86
PCD162	XAD-16	PNP	8.67	3.45	1.38	-	69.9-D	156
PC163	XAD-16	PNP	8.67	50.9	29.34	103.34	98.7-B	232.9
PCD163	XAD-16	PNP	8.67	4.3	1.61	-	72.1-D	167.88
PC164	XAD-16	PNP	8.67	34.6	23.4	104.35	95.8-B	214.5
PCD164	XAD-16	PNP	8.67	4.7	-	-	-	-
PC76	S-761	PNP	9.7	47.2	27.44	104	98.1-B	85.5
PCD76	S-761	PNP	9.7	8.2	4.25	-	77-D	64.4
MC7	XAD-7	MO	7.93	34.6	21.9	100.46	98.1-B	8.3
MCD7	XAD-7	MO	7.93	-	-	-	-	-
MC161	XAD-16	MO	8.57	44	23.3	96.1	87.7-B	376.7
MCD161	XAD-16	MO	8.57	107.83	32.9	-	>100-D	396
MC162	XAD-16	MO	8.57	50.9	30.3	99.7	84.5-B	472.1
MCD162	XAD-16	MO	8.57	71.07	25.5	-	>100-D	-
MC163	XAD-16	MO	8.95	68.6	37.9	100.8	87.2-B	439.7
MCD163	XAD-16	MO	8.95	17	6.48	-	79.3-D	348.6
MC76	S-761	MO	11.22	48.2	29.7	100.2	93.9-B	106.4
MCD76	S-761	MO	11.22	8.2	4.12	-	79.4-D	84.5
RC161	XAD-16	R40	10.13	49.7	-	90.9	89.8-B	-
RC162	XAD-16	R40	10.45	34.6	21.2	-	-	184.76
RCD162	XAD-16	R40	10.45	-	-	-	-	-
AC7	XAD-7	4AAB	1.19	47.5	26.75	79.9	94.1-B	255.2
ACD7	XAD-7	4AAB	1.19	6.75	2.13	-	7.9-D	20.34
AC161	XAD-16	4AAB	1.24	47.2	26.53	77.5	30-B	651.3
ACD161	XAD-16	4AAB	1.24	8.2	3.69	-	14.9-D	97.26
AC162	XAD-16	4AAB	1.07	68.6	38.78	80.22	-	419.1
ACD162	XAD-16	4AAB	1.07	17.04	7.35	-	40.2-D	168.54
AC76	S-761	4AAB	1.79	47.5	33.7	85	-	160.67
ACD76	S-761	4AAB	1.79	6.75	7.36	-	>100-D	172.05

Cumulative Flow (V_t)

Cumulative flow was the total volume of adsorbate or regenerant passed through the column during an experiment. It was determined using one of the flow rate estimates above.

Mass Adsorbed, W_A (mg)

The total mass adsorbed at any particular time during an adsorption cycle was determined using the following equation:

$$W_A = \sum_{i}^{n} [C_o - (\frac{C_{s_i} + C_{s_{i+1}}}{2})][M.W.][1000][t_{i+1} - t_i][FR] \qquad (11)$$

where: C_o = influent concentration
C_s = the concentration of the effluent same, in moles/L
MW = molecular weight of the compound (g/mole)
1000 = conversion factor from g to mg
t = time at which sample was collected
FR = flow rate from one of the methods above.

The most accurate determination of W_A used $FR_{(s)}$ in the above equation. In cases where this estimate was not available, $FR_{(c)}$ was substituted.

These calculations were performed on an IBM Personal Computer using LOTUS, 1-2-3, Software. An example of an adsorption spreadsheet is contained in Appendix 4.

This method is most easily visualized by referring to a plot of cumulative mass of sorbate in the effluent versus cumulative flow (Figure 25). In this figure the area under the curve represents the total mass which passed through the column. If the total outlined rectangle on the figure is unity, then total mass absorbed is represented by 1 - $\int$ area under curve, indicated by the shaded portion.

Mass Desorbed, W_D(mg)

The total mass desorbed at any particular time during a desorption cycle is determined from the following equation:

$$W_D = \sum_{i}^{n} (C_{s_i} + C_{s_{i+1/2}}) (1000) (t_{i+1} - t_i) (FR) \qquad (12)$$

where: C_s = effluent sample concentration (moles/L)
t = time of corresponding sample
1000 = conversion from g to mg
FR = flow rate from one of the above methods.

As in the above case, the most accurate determination of W_D uses $FR_{(2)}$ in the above equation. In cases where this estimate was not available, $FR_{(c)}$ was substituted.

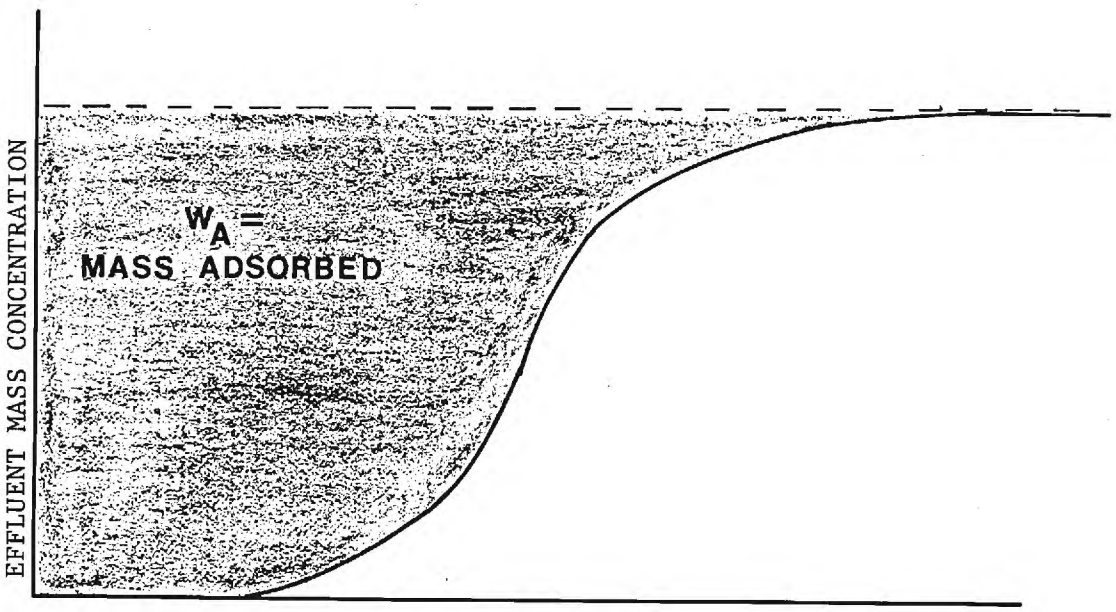

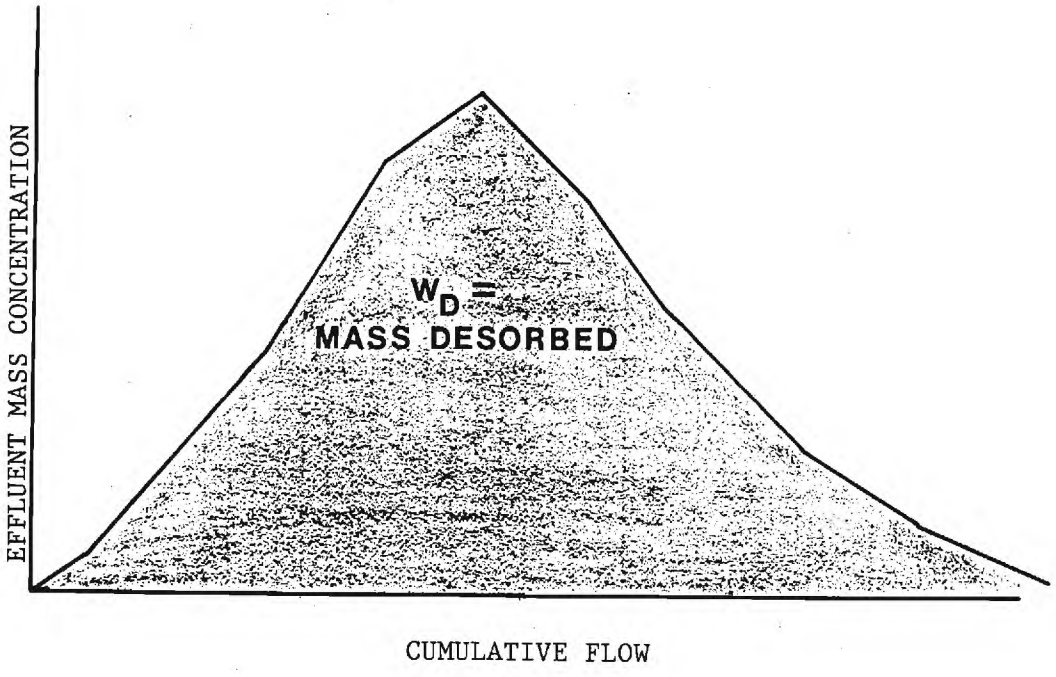

Figure 25. Visual Representation of Mass Absorbed and Desorbed in Column Kinetic Experiments.

These calculations were performed on an IBM Personal Computer using LOTUS 1-2-3 software. An example of a desorption spreadsheet is contained in Appendix 4.

Percent Breakthrough (%B):

$$\% B = C_o/C_e \times 100 \quad (13)$$

where: C_o = influent concentration
C_e = final effluent concentation

This value is indicative of the degree of saturation of the adsorption column

Percent Desorption (%D):

$$\%D = W_A/W_D \times 100 \quad (14)$$

This value represents the mass of compound desorbed at equilibrium, and is indicative of the amount of solute irreversibly adsorbed.

4.3.2 Adsorption of Dye Compounds onto Synthetic Resins

Column adsorption experiments were conducted according to the procedure outlined in the Materials and Methods section. The resultant breakthrough curves were of typical S-shape with the time for the initial breakthrough and the attainment of column saturation, indicative of the adsorption characteristics previously determined. Figures 26 through 29 are typical breakthrough curves.

The adsorption of PNP onto XAD-16 (Figure 28) produced the most ideal breakthrough curve. p-nitrophenol was not detected in the effluent until 15 hours had elapsed. Thereafter, the concentration increased rapidly up to 25 hours when saturation was reached. The adsorption of Red 40 onto XAD-16 (Figure 27) was typical the other extreme. Initial breakthrough occurred almost immediately, and after about 15 hours saturation conditions had been attained. The adsorption of 4AAB (Figure 26) and methyl orange (Figure 29) illustrate intermediate behavior.

According to the batch kinetic results XAD-16 had approximately equal capacities for the adsorption of methyl orange and para-nitrophenol. The column adsorption curves, however, were very different. Initial breakthrough occurred much sooner and the time required to saturate the resin was much larger for methyl orange. This reflected a difference in the rates of adsorption. With approximately equal flow rates, incomplete removal of the solute occurred in the adsorption of methyl orange due to the slower rate of diffusion into the pores. Early breakthrough of the sorbate resulted.

These curves also illustrate a phenomenon commonly observed during this study, a cyclic variation of the effluent concentration as the resin became saturated. Initial attempts were made to correlate these fluctuations with variability in flow rates. However, during the third adsorption of methyl orange onto XAD-16 (Figure 28), the flow rate was maintained within 5% and could not account for the variation in effluent concentration. No conolusive explanation can be advanced at present for this phenomenon.

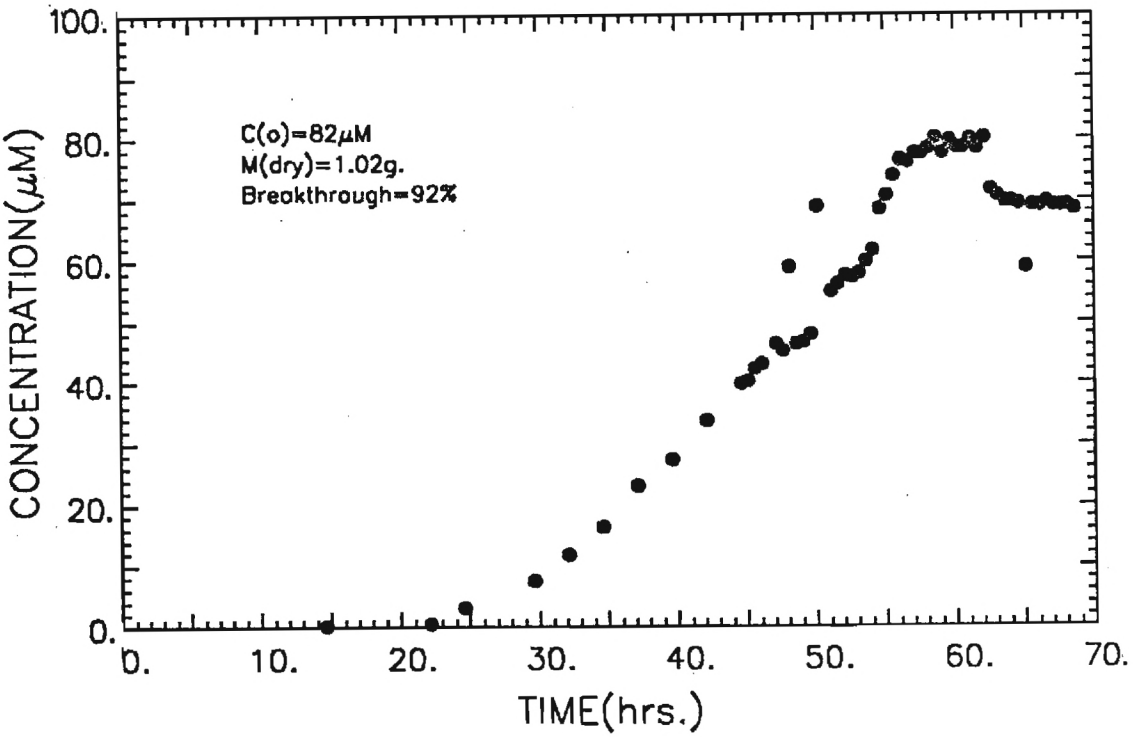

Figure 26. COLUMN ADSORPTION OF 4AAB ON XAD-16(2)

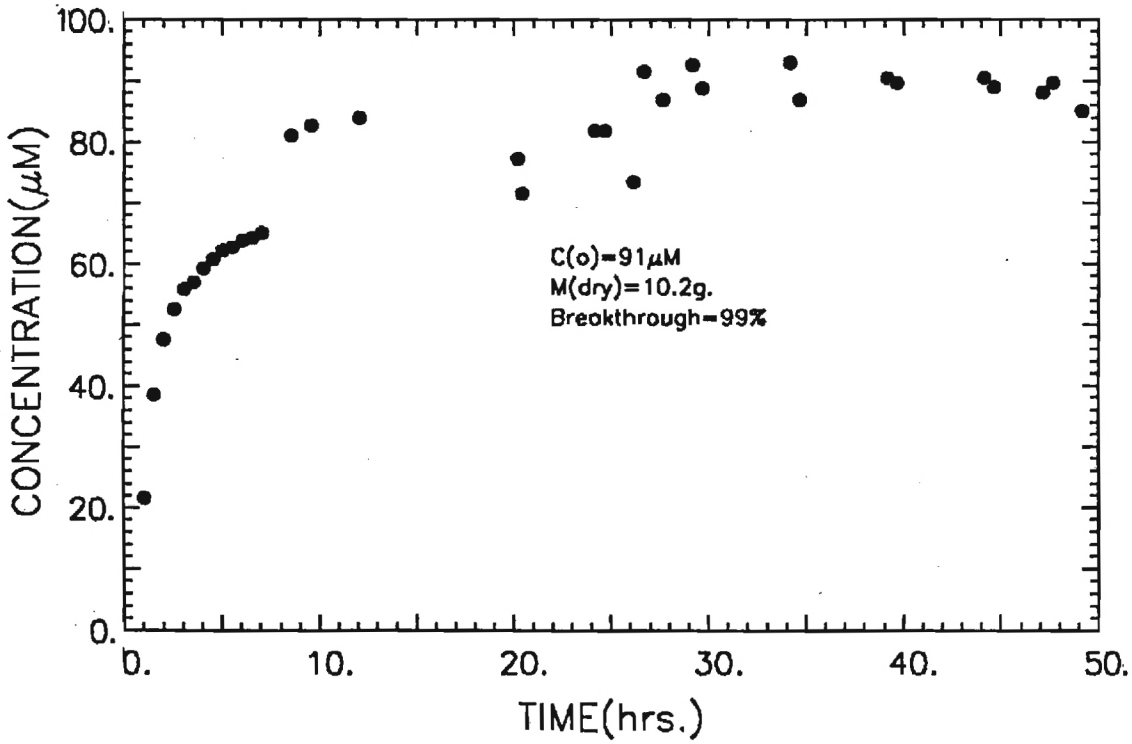

Figure 27. COLUMN ADSORPTION OF R40 ON XAD-16(1)

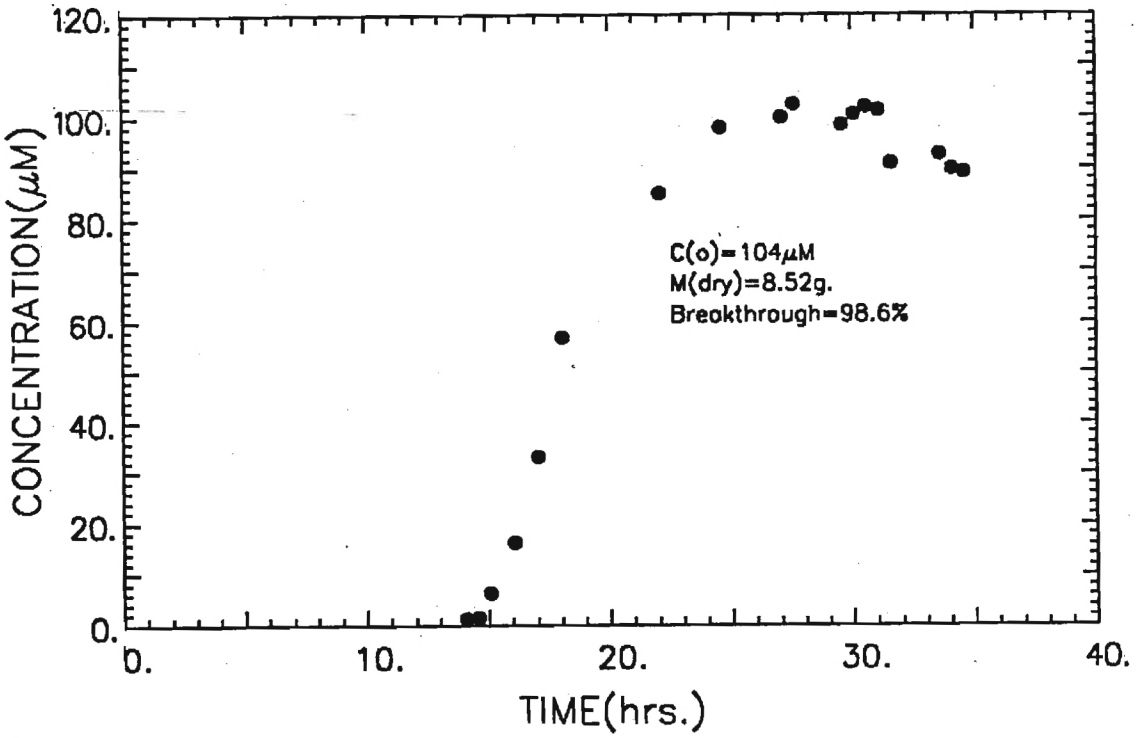

Figure 28. COLUMN ADSORPTION OF PNP ON XAD-16(4),pH=5

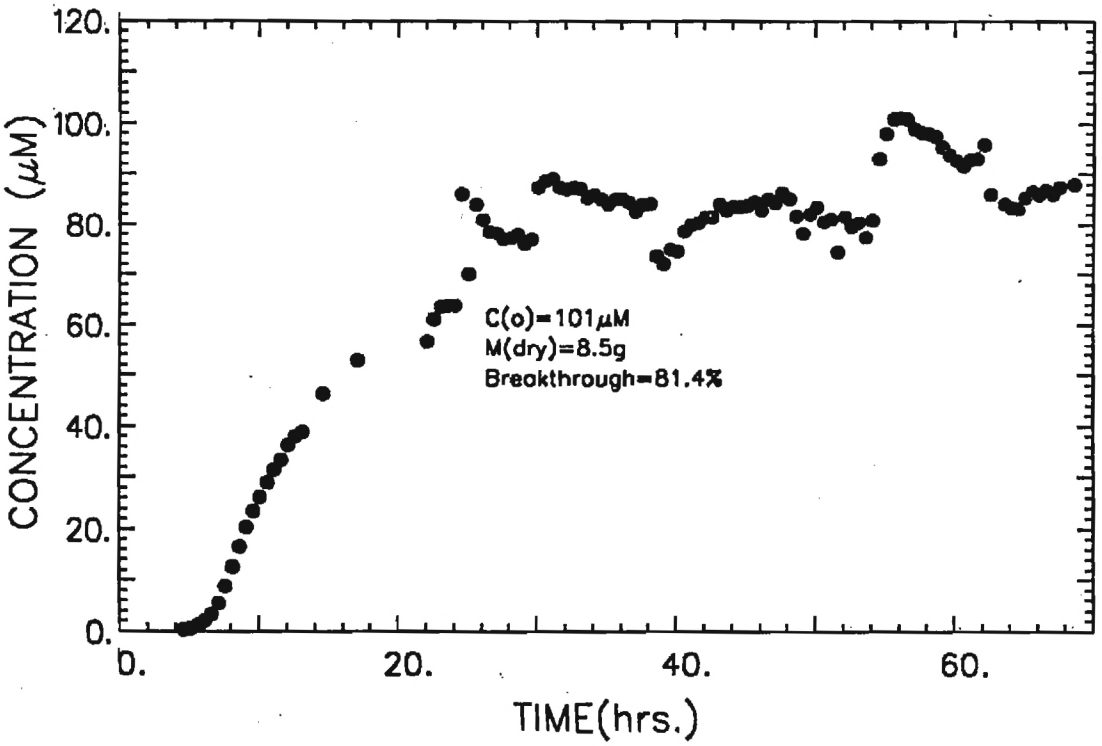

Figure 29. COLUMN ADSORPTION OF M.O. ON XAD-16(3)

Figure 30 is a plot of cumulative mass absorbed versus cumulative flow for selected combinations of resins and dyes. It illustrates the general trends noted earlier. Care must be taken in interpreting this figure because the weight of the compound adsorbed is presented on the Y axis. For example, although the amount adsorbed during run AC162 appears lower than in the case of MC163, the adsorption capacity (moles adsorbed/g of resin) is greater in the first case. Keeping this in mind the following can be deduced from this figure, adsorption onto XAD-16 was greatest on a mass basis of the resins studied. This was followed by XAD-7, then S-761; of the compounds studied, 4-aminoazobenzene was adsorbed most strongly; methyl orange and p-nitrophenol absorbed about equally, and Red 40 to the least extent. The shape of the curves should also be noted. The straight line portions of the curves at low total flow indicate complete adsorption of the compound within the resin bed. A decreasing slope from that point corresponds to initial breakthrough of the dye. Subsequent decreases in the slope of the line indicate approach to saturation. When the slope equals zero, saturation has been achieved.

4.3.3 Desorption of Dye Compounds from Synthetic Resins

Column desorption experiments were conducted according to the procedure outlined in the Materials and Methods section. Figures 31 through 34 represent the desorption of the dye and resin combinations already discussed in Section 4.3.2, and are typical of the desorption curves from all column desorption experiments. Desorption occurred rapidly (within about 45 minutes) in all cases. Thereafter, small amounts of material were desorbed over much longer time intervals.

Figure 35 is a plot of the cumulative mass adsorbed versus cumulative flow for the same set of experiments presented in Figure 30. The percentages of dye desorbed for these experiments are presented in Table 10.

TABLE 10. PERCENT OF SORBATE DESORBED

Run	% Desorbed
MCD 163	79
MCD 76	80
PCD 163	72
PCD 76	77
ACD 163	40
ACD 7	8
ACD 76	100
RCD 162	22

It is significant that for p-nitrophenol and methyl orange the percent desorption was essentially idential, regardless of the resin. This indicates that solute/regenerant interaction predominated over the solute/resin surface interaction with a considerable degree of reversible adsorption present. Desorption of 4-aminoazobenzene was strongly dependent on the resin involved. Desorption of 4AAB from XAD-7 was only 8%, while desorption from S-761 was essentially complete. This agrees qualitatively with the observed preference

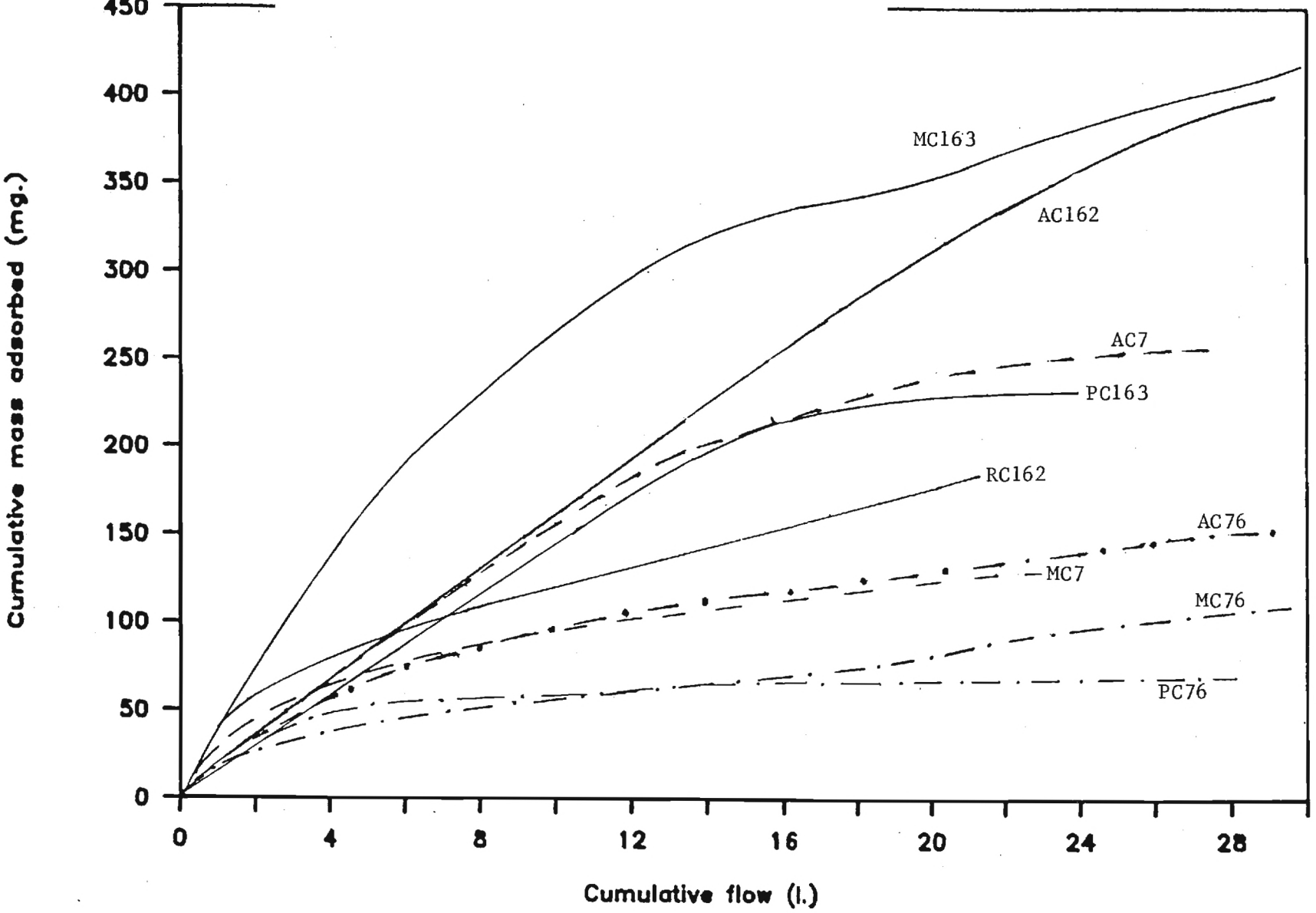

Figure 30. Column Adsorption of Selected Combinations of Dyes and Resins.

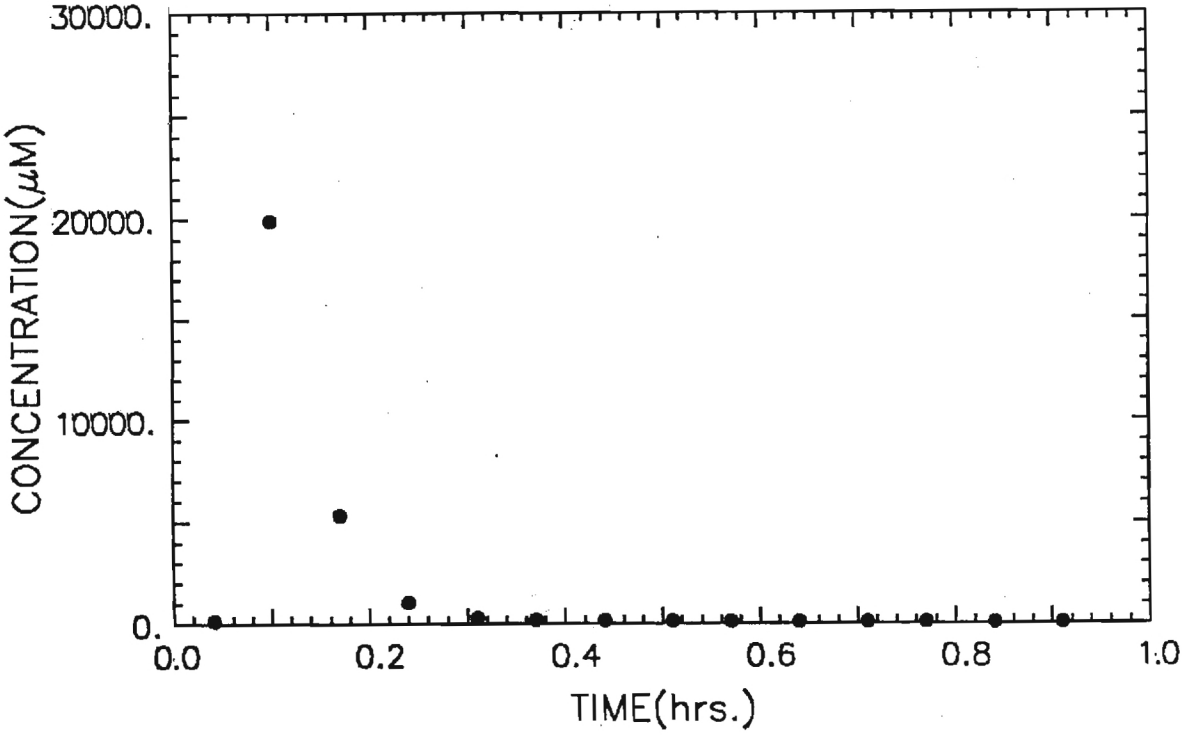

Figure 31. COLUMN DESORPTION OF 4AAB FROM XAD-16(2)

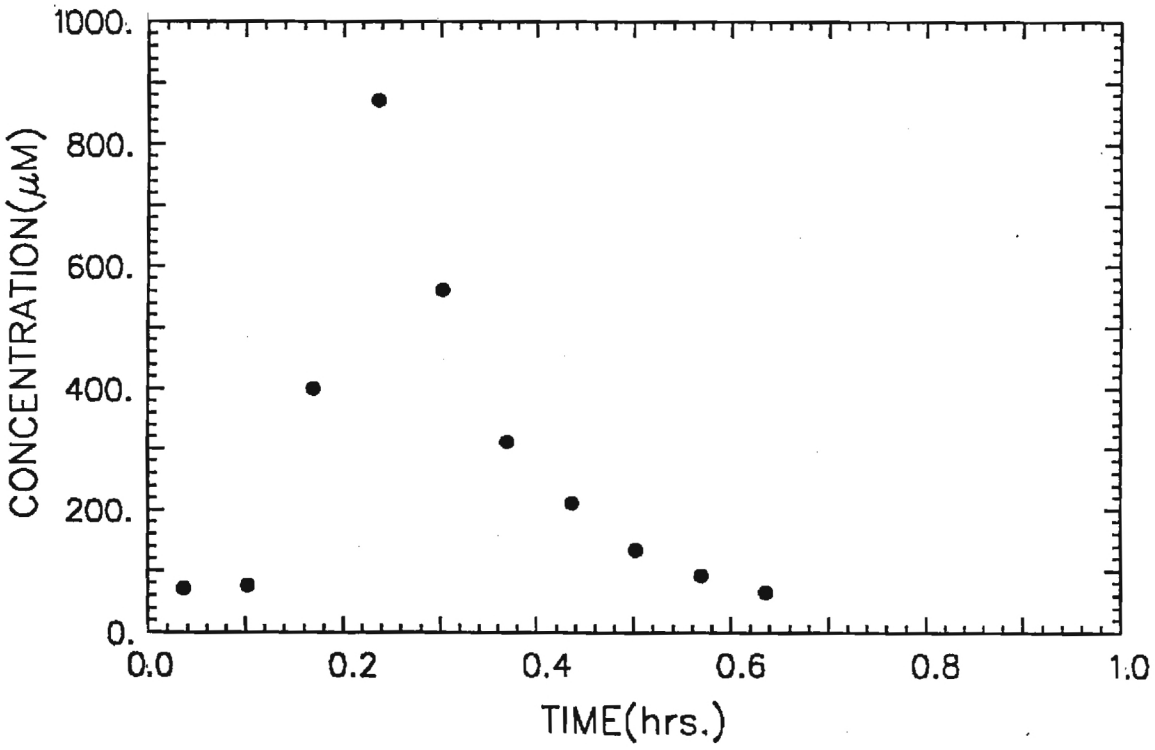

Figure 32. COLUMN DESORPTION OF R40 FROM XAD-16(2)

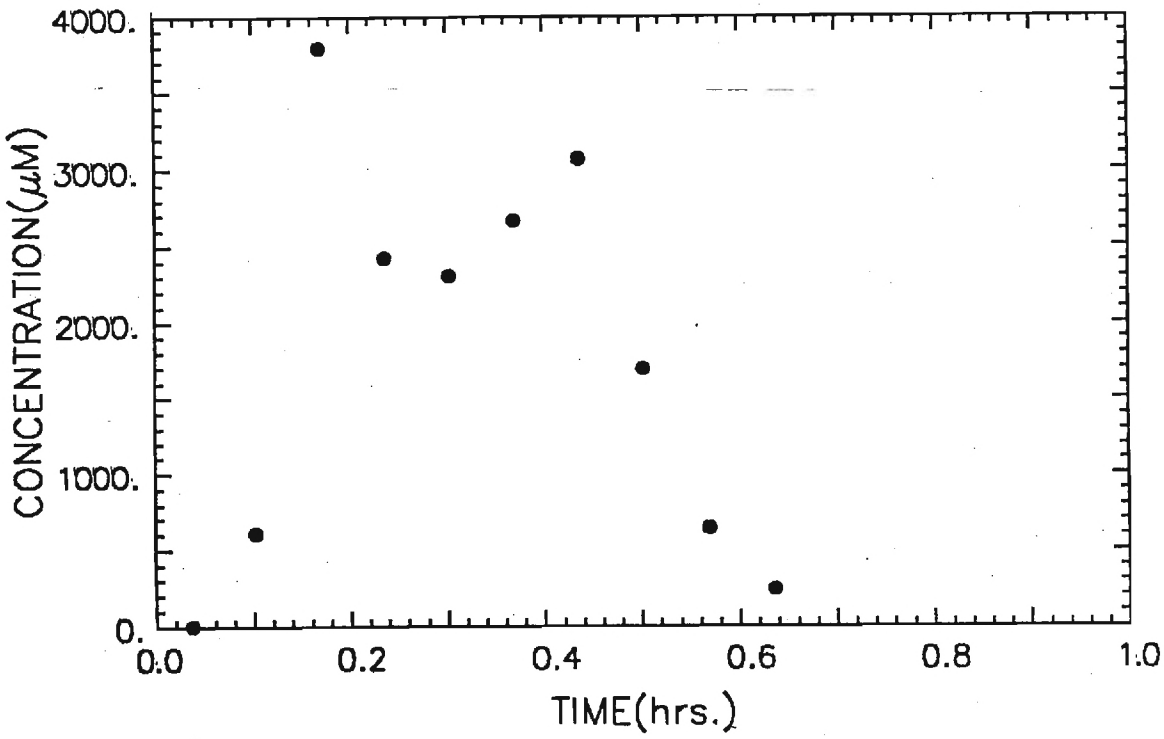

Figure 33. COLUMN DESORPTION OF PNP FROM XAD-16(4)

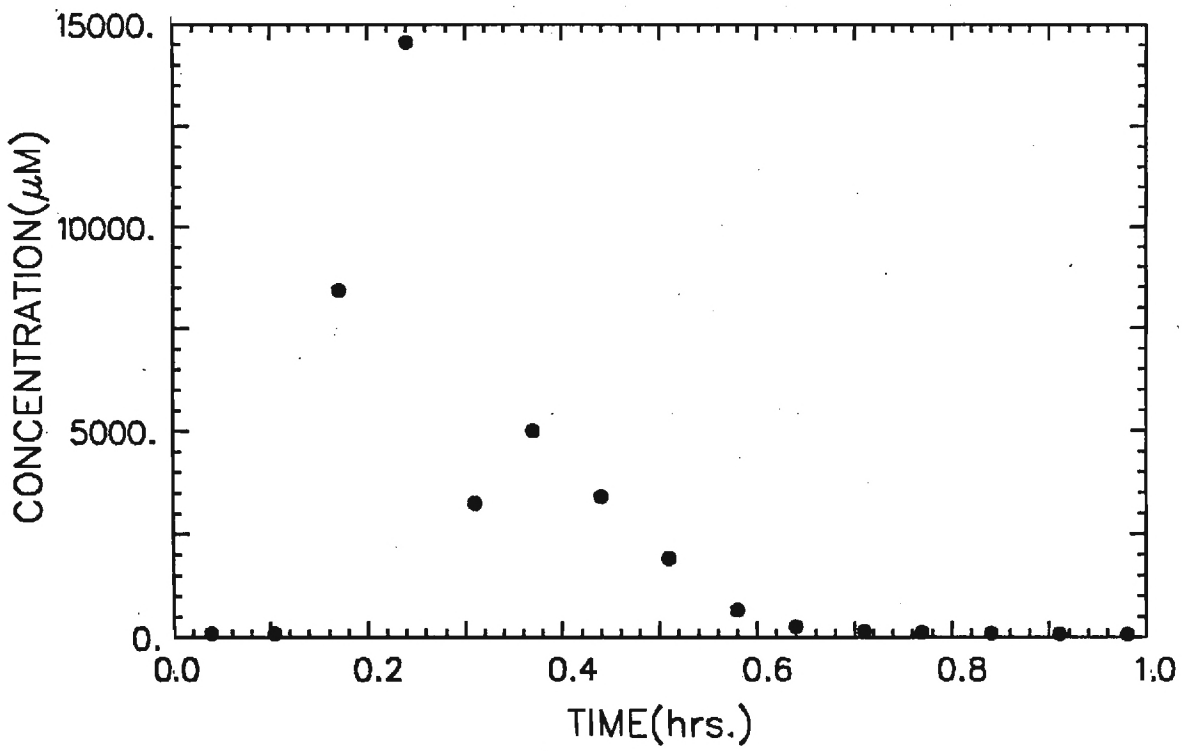

Figure 34. COLUMN DESORPTION OF M.O. FROM XAD-16(3)

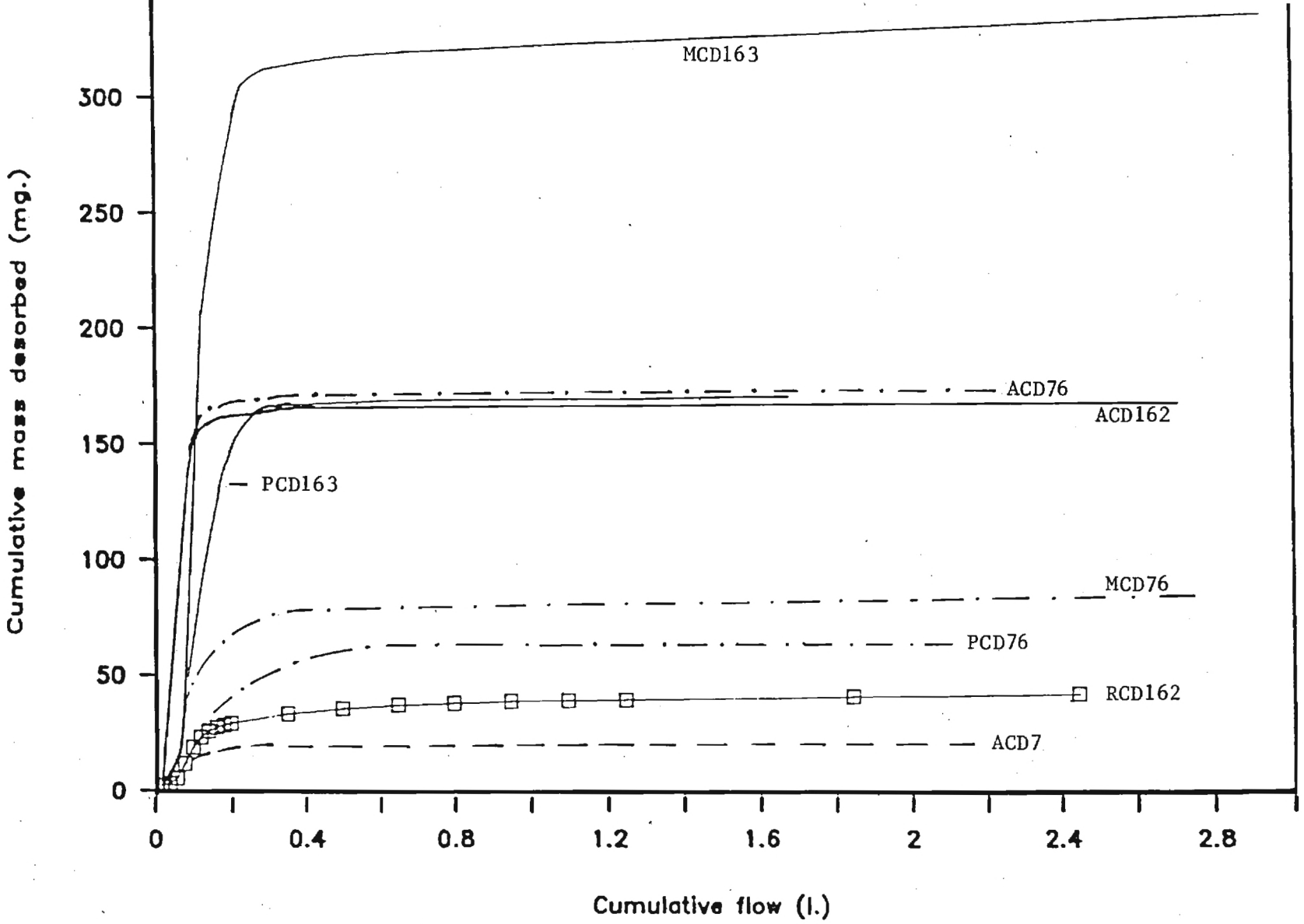

Figure 35. Column Desorption of Selected Combinations of Dyes and Resins.

of adsorption of 4AAB onto XAD-7 over S-761 if it can be assumed that the most strongly absorbed material will be the hardest to desorb. Desorption from XAD-16, which absorbed 4AAB most strongly, however, was intermediate at 40%. Desorption of Red 40 from XAD-16 was poor, as was adsorption onto the resin. Clearly some degree of irreversible sorption of dye had occurred in these systems.

4.3.4 Loss of Adsorptive Capacity in Column Systems

Two experiments were conducted to investigate the loss of adsorptive capacity with successive adsorption/desorption cycles. Three cycles were run on paranitrophenol and XAD-16, and two cycles were run on methyl orange and XAD-16. The experiments were cnducted early in this study when methodology was still being developed. As a consequence, the results are quantitatively inconclusive, but some general qualitative statements can be made. Each of the experiments will be discussed below.

The first regeneration cycle for PNP and XAD-16 (PCD161) was conducted for over 20 hours and the flow rate was not accurately recorded, so that the total amount of material desorbed is now known. However, from the desorption curve (see Appendix) it is estimated that desorption was close to 100%. the length of time the experiment was conducted does not represent a practical application because the uantity of solvent required would not be cost-effective. The second and third adsorption cycles (PCD162, PCD163) were conducted for shorter periods of time (5 and 9 hours) and cumulative flows (1.38 and 1.61 L). The percent desorbed was 69.9 and 72.1 percent, respectively. This indicates a loss in adsorption capacity of about 30 percent.

Both regeneration cycles (MCD161, MCD162) for MO and XAD-16 were conducted for very long periods of time (108 and 71 hours) with high cumulative flows (32.9 and 30.3). The results indicated that greater than 100 percent of the adsorbed material was regenerated. Most of the material was desorbed within the first hour. The large volume of methanol passed through the column likely resulted in an overestimate of the material desorbed. Analytical measurements of low concentrations are less accurate, and interferences from impurities more significant at this stage. The effect is cumulative resulting in greater than 100% adsorption. In a third experiment with methyl orange and XAD-16 (MCD163) only 6.5 L of methanol was used to regenerate the resin. This resulted in 79.4 of the material being desorbed.

These results indicate that theoretically all adsorbed materials can be subsequently desorbed in a column system if enough regenerant is added. This, of course, is not practical. However, since most of the material was adsorbed within one hour, desorption of organic dyes from synthetic resins appears to be a feasible and realistic option.

CHAPTER 5

CONCLUSIONS

Adsorption of textile related organic dyes onto synthetic resins and their subsequent desorption was studied by conducting isotherm, batch kinetic and column kinetic experiments.

The resin XAD-16 was the best adsorbent for all compounds studies, followed by XAD-7 and S-761. The least soluble compound, 4-azoaminobenzene, was the most strongly absorbed, but was poorly desorbed. Methyl orange and p-nitrophenol were absorbed strongly and desorbed well. Red 40, a very water soluble compound adsorbed poorly, and was difficult to desorb.

The adsorption capacity of a resin for a dye was primarily a function of solubility and compound/surface interaction. The rate of adsorption appeared to be related primarily to the molecular size of the compound and the pore diameter of the resin.

Desorption was rapid, being substantially complete within 5 minutes in batch experiments and within 45 minutes for column experiments. The percentage of the adsorbed material which was desorbed, however, varied greatly.

While it is feasible to consider synthetic resins as an alternative technology to remove organic dyes from wastestreams specific considerations must be addressed. In particular research needs to be conducted on the larger more complex commercial dyes to determine their adsorption characteristics. The most effective adsorbent in this study, XAD-16, has a relatively small pore diameter and may not be preferable for larger compounds.

The best application would be one where specific wastestreams, containing only one, or a few, related compounds at relatively high concentrations can be segregated. In complex wastestreams, different compounds will be removed at different rates and to different degrees. Excess resin would be required to achieve acceptable effluent quality, resulting in unused capacity. Regeneration, likewise, will vary with respect to both the compound adsorbed and the adsorbent. For an isolated wastestream, however, the system could be designed much more efficiently.

Solvent regeneration of adsorbed organic dyes using methanol was highly effective. The rate of desorption was rapid and only small volumes of methanol were required. This is the most attractive feature of using synthetic resins as adsorbents. The desorbed solution might then be treated (i.e., distillation) to recover both the solvent and, if economically feasible, the desorbed solute.

CHAPTER 6

ACKNOWLEDGMENTS

The authors express their gratitude to those individuals who provided assistance during the various phases of this research project. Dr. Wendall Cross provided invaluable help and advice in the design and operation of the Batch and Column Experimental systems. Four undergraduate students, Keith Ross, Bill Farrell, Camelia Merati, and Azadeh Nezhat, worked in the laboratory and helped conduct batch and column experiments. Henrietta Bowman and Elaine Sharpe typed the manuscript.

REFERENCES

Abrams, I. M., "Removal of Anionic Sufactants from Liquids," Patent No. 3,232,867, U.S. Patent Office (1966)

Adamson, A. W., Physical Chemistry of Surface, Second Edition, Interscience Publishers, N. Y. (1967)

Andersen, R. E. and Hansen, R. D., "Phenol Sorption on Ion Exchange Resins," Ind. Eng. Chem., 47,72 (1955)

Butler, J. A. V. and Ockrent, C., "Studies in Electrocapillarity, III," J. Phys. Chem., 34,12 (1930)

Chang, C. H. and Savage, D. W., "Investigations of Solvent-Regenerable Carbon-Sulfur Compounds for Phenol Removal in a Packed Column," Env. Sci. Tech., 15, 201 (1981)

Chasanov, M. G., Kunin, R., and McGarvey, F., "Sorption of Phenol by Anion Exchange Resin," Inc. Eng. Chem., 48, 305 (1956)

Crittenden, J. C. and Weber, W. J., Jr., "Predictive Model for Design of Fixed-Bed Adsorbers: Parameters Estimation and Model Development," J. Env. Eng. Div., ASCE, 104, 185 (1978)

Cross, W. H., Suidan, M. T., Rollor, M. A., Kim, B. R., and Gould, J. P., "Organic Solvent Regeneration of Granular Activated Carbon," ERC 08-82, School of Civil Engineering, Georgia Institute of Technology, Atalnat, Georgia, a report submitted to Environmental Resources Center, Georgia Institute of Technology (1982)

DeJohn, P. B., Proceedings of the 29th Industrial Waste Conference, Purdue University, Lafayette, Ind. (1974)

Foster, D. H., Engelbrecht, R. S., and Snoeyink, V. L., "Application of Weak Base Ion Resins for Removal of Proteins," Env. Sci. and Tech., 11,1 (1977)

Fritz, W. and Schlunder, E. U., "Competitive Adsorption of Two Dissolved Organics onto Activated Carbon - I, Adsorption Equlibria," Chem. Eng. Sci., 36, 721 (1981)

Fritz, W., Merk, W., and Schlunder, E. U., "Competitive Adsorption of Two Dissolved Organics onto Activated Carbon -II, Adsorption Kinetics in Batch Reactors," Chem. Eng. Sci., 36, 731 (1981)

Gardon, "Encyclopedia of Polymer Science and Technology," Interscience Publishers, New York (1966)

Gardiner, D. K. and Borne, B. J., "Textile Waste Waters: Treatment and Environmental Effects," J. Soc. Dyers Colourists, 94, 339 (1978)

Gasser, C. G. and Kipling, J. J., " The Effect of Surface Complexes on Adsorption from the Liquid Phase by Carbon Black," Proceedings of the Fouthe Conference on Carbon, Part i, p. 55-61, Pergamon Press, London and New York (1960)

Gustafson, R. L. and Paleos, J., "Interactions Responsible for the Selective Adsorption of Organics on Organic Surfaces," Chapter 10, Organic Compounds in Aquatic Environments, Faust, S. D. and Hunter, J. V. (Eds.), Dekker, New York (1971)

Herzing, D. R., Snoeyink, V. L., and Wood, N. F., "Activated Carbon Adsorption of the Ordorous Compounds 2-Methylisoborneol and Geosmin,: J> Amer. Water Works Assoc., 69,4 (1977)

Himmelstein, K. J., Fox, R. D.K and Winter, T. H., "In_Place Regeneration of Activated Carbon Used in Industrial Waste Treatment," Water, 70, 310 (1974)

Hinrichs, R. L. and Snoeyink, V. L., "Sorption of Benzenesulfonates by Weak-Base Anion Exchange Resins," Water Research, 10,79 (1976)

Hsieh, J. S. C., Turian, R. M., and Tien, C., "Multicomponent Liquid Phase Adsorption in Fixed Bed," AIChE J., 23, 263 (1977)

Hunter, J. V., Chapter 4, "Organic Compounds in Aquatic Environments," Faust, S. D. and Hunter, J. V. (Eds.), Dekker, New York (1971)

Jain, J. S. and Snoeyink, V. L, "Competitive Adsorption from Bisolute Systems on Active Carbon," J. Water Poll. Control Fed., 45, 2463 (1973)

Jossens, L., Prausnitz, J. M., Fritz, W., Schlunder, E. U., and Meyers, H. L., "Thermodynamics of Multisolute Adsorption from Disolute Aqueous Solutions," Chem. Eng. Sci., 33, 1097 (1978)

Keinath, T. M., "Modeling and Simulation of the Performance of Adsorption Contactors," In: Mathematical Modeling for Water Pollution Control Processes, pp. 1-66, T. M. Keinath and M. Wanielista, eds., Ann Arbor, Michigan (1975)

Kim, B. R., Schmitz, R. A., Snoeyink, V. L., and Tauxe, G. W., "Analysis of Models for Dichloramine Removal by Activated Carbon in Batch and Packed-Bed Reactors Using Quasilinearization and Orthogonal Collocation Methods,: Water Research, 12, 317 (1978)

Kim, B. R., Snoeyink, V. L., and Saunders, F. M., "Adsorption of Organic Compounds by Synthtic Resins," J. Water Poll. Control Fed., 48, 120 (1976)

Kim, B. R., Snoeyink, V. L., and Schmitz, R. A., "Removal of Dichloramine and Ammonia by Granular Carbon," J. Water Poll. Control Fed., 50, 122 (1977)

Kumagai, J. S. and Kaufman, W. J., "removal of Organic Contaminants - Phenol Sorption by Activated Carbon and Selected Macroporous Resins," SERL Report No. 68-8, Berkeley: Sanitary Engineering Research Lab., University of California (1968)

Liapis, A. I. and Rippin, D. W. T., "The Simulation of Binary Adsorption in Activated Carbon Columns Using estimates of Diffusional Resistance within the Carbon Particles Derived from Batch Experiments," Chem. Eng. Sci., 33, 593 (1978)

Loven, A. W. and Huether, C. H., "Activated Carbon in Treating Industrial Wastes," presented at the Amer. Chem. Soc. 159th National Conference, Houston, Texas (1970)

McGuire, M. J. and Suffet, I. H., "Adsorption of Organics from Domestic Water Supplies," J. Amer. Water Works Assoc., 70,11 (1978)

McKay, G., "Basic Dye Adsorption Activated Carbon," Water, Air, and Soil Poll. (Neth.), 12, 307 (1979)

McKay, G., Otterburn, M. S., and Sweeney, A. G., The Removal of Colour from Effluents Using Various Adsorbents: Some Preliminary Economic Considerations," J. Soc. Dyers Colourists, 94, 357 (1978)

McKay, G., Blair, H. S., and Gardiner, J. R., "Adsorption of Dyestuffs onto Chitin. I. Equilibrium Studies," J. Applied Polymer Science, 27, 3043 (1982a)

McKay, G., Blari, H. S., and Gardiner, J. R., "Adsorption of Dyestuffs onto Chitin. External Mass Transfer Processes," J. Applied Polymer Science, 27, 4251 (1982b)

Merk, W., Fritz, W., and Schlunder, E. U., "Competitive Adsorption of Two Dissolved Organics onto Activated Carbon - III, Adsorption Kenetics in Fixed Beds," Chem. Eng. Sci., 36, 743 (1981)

Morris, C. J. and Weber, W. T., Jr., "Removal of Bilolgically Resistant Pollutants from Waste Waters by Adsorption," Proceedings of First Int. Conf. On Water Pollution Research, London, Pergamon Press, London, Vol. 2 (1964)

Parmele, C. S., Alperin, E. S., and Jurgen, H. E., "Nondestructive Regeneration of Activated Carbon - A Viable Chemical Engineering Technology," presented at the Annual Meeting of the American Institute of Chemical Engineers, new Orleans, Louisiana (1981)

Posey, R. J. and Kim. B. R., "Solvent Regeneration of Activated Carbon," presented at the 56th WPCF conference, Atlanta, GA (1983)

Radke, C. J. and Prausnitz, J. M., "Adsorption of Organic Solutes from Dilute Aquous Solution on Activated Carbon," Ind. and Eng. Chem. Fundamentals, 11, 445 (1972)

Rebhun, M. and Kaufman, J., "Removal of Organic Contaminants, Sorption of Organics by Synthetic Resions and Activated Carbon," SERL Rept., No. 67-9, San. Eng. Res. Lab., Univ. of California, Berkeley, Calif. (1967)

Roy, C. Nad Volesby, B., "Activated Carbon Adsorption Process for Purification of Textile Wastewater," Textile Chemist and Colorist, 10, 94 (1978)

Satterfield, C. N., Mass Transfer in Heterogeneous Catalysis, MIT Press, Cambridge, MA and London (1970)

Snoeyink, V.L., and Jenkins,D. Water Chemistry, John Wiley and Sons, New York, New York, 1980

Snoeyink, V. L., Weber, W. J., Jr., and Mark, H. B., "Sorption of Phenol and Nitrophenol by Active Carbon," Env. Sci. and Tech. 3, 918 (1869)

Suidan, M. T., Snoeyink, V. L., and Schmitz, R. A., "Rudiction of Aqueous HOCl with Granular Activated Carbon," J. Env. Eng. Div., ASCE, 103, 677 (1977)

Thacker, W. E., Snoeyink, V. L., and Crittenden, J. C., "Modeling of Activated Carbon and Coal Gasification Char Adsorbents in Single Solute and Bi-Solute Systems," Research Report No. 161, Water Resources Center, Univ. of Illinois at Urbana-Champaign (1981)

Weber, W. J., Jr., Physicochemical Processes from Water Quality Control, p. 203, Wiley-Interscience (1972)

APPENDIX 1

Determination of pK_a for Dye Compounds

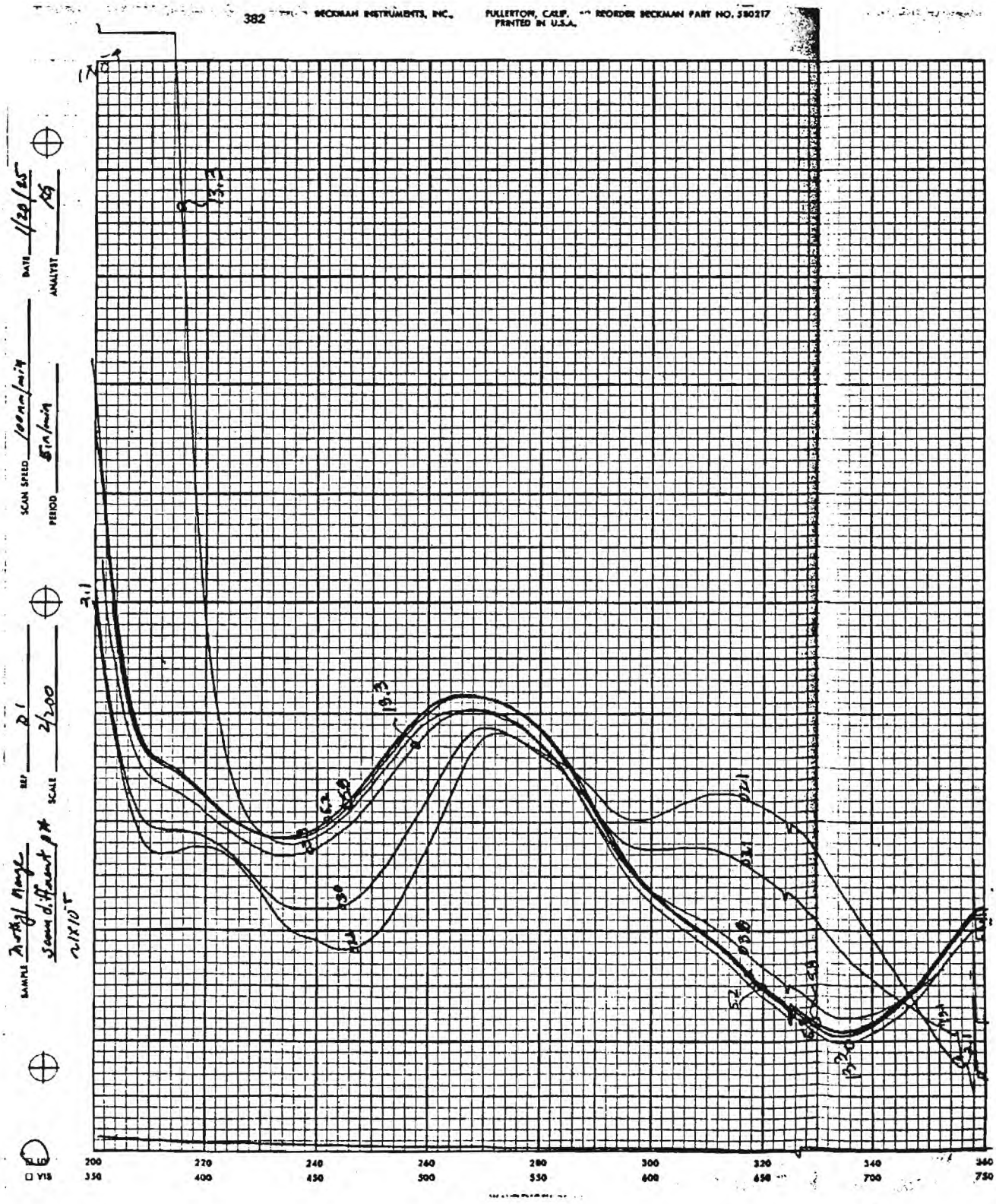

Figure A1-1. Spectrophotometric Determination of pKa for Methyl Orange (1).

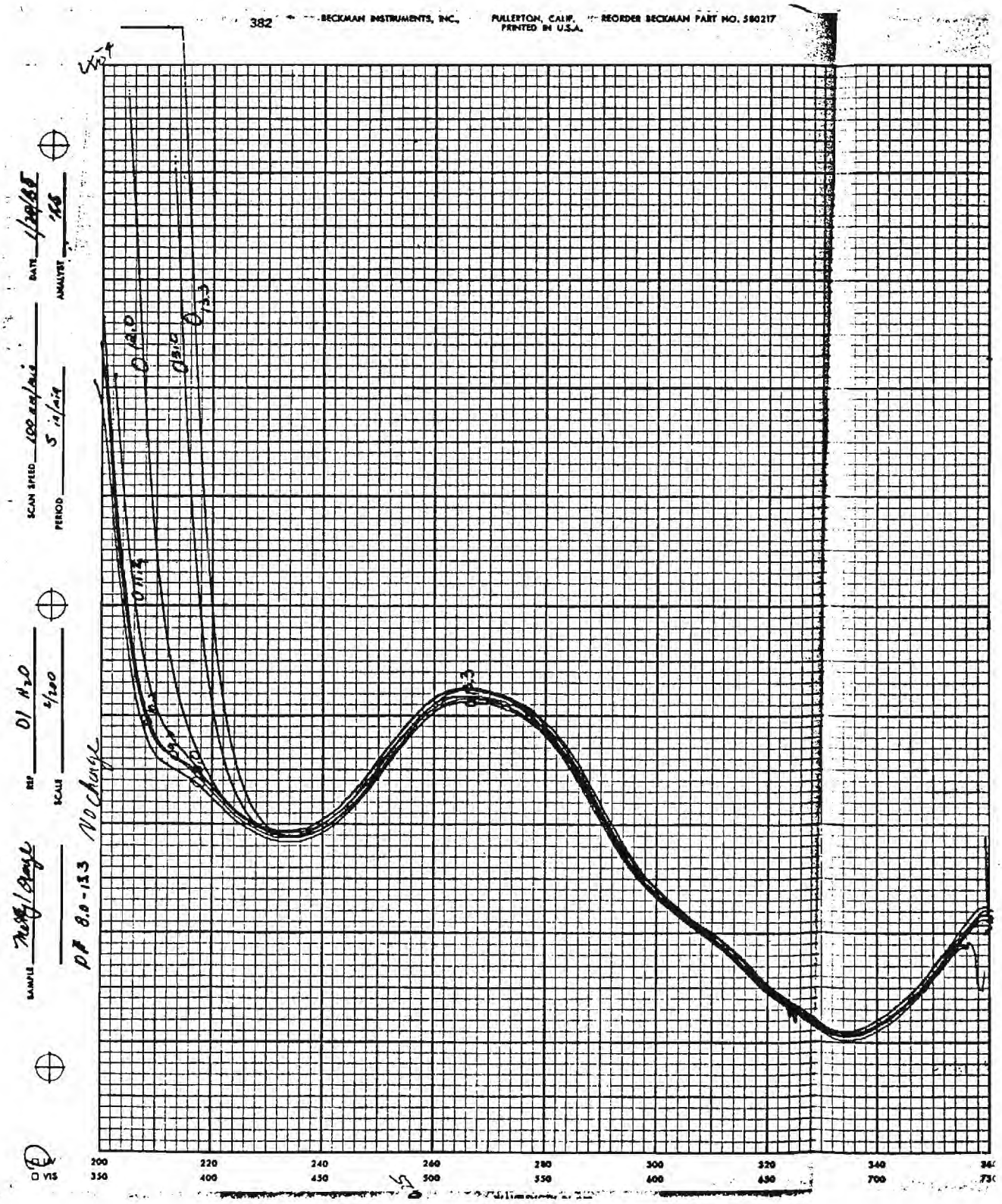

Figure A1-2. Spectrophotometric Determination of pKa for Methyl Orange (2).

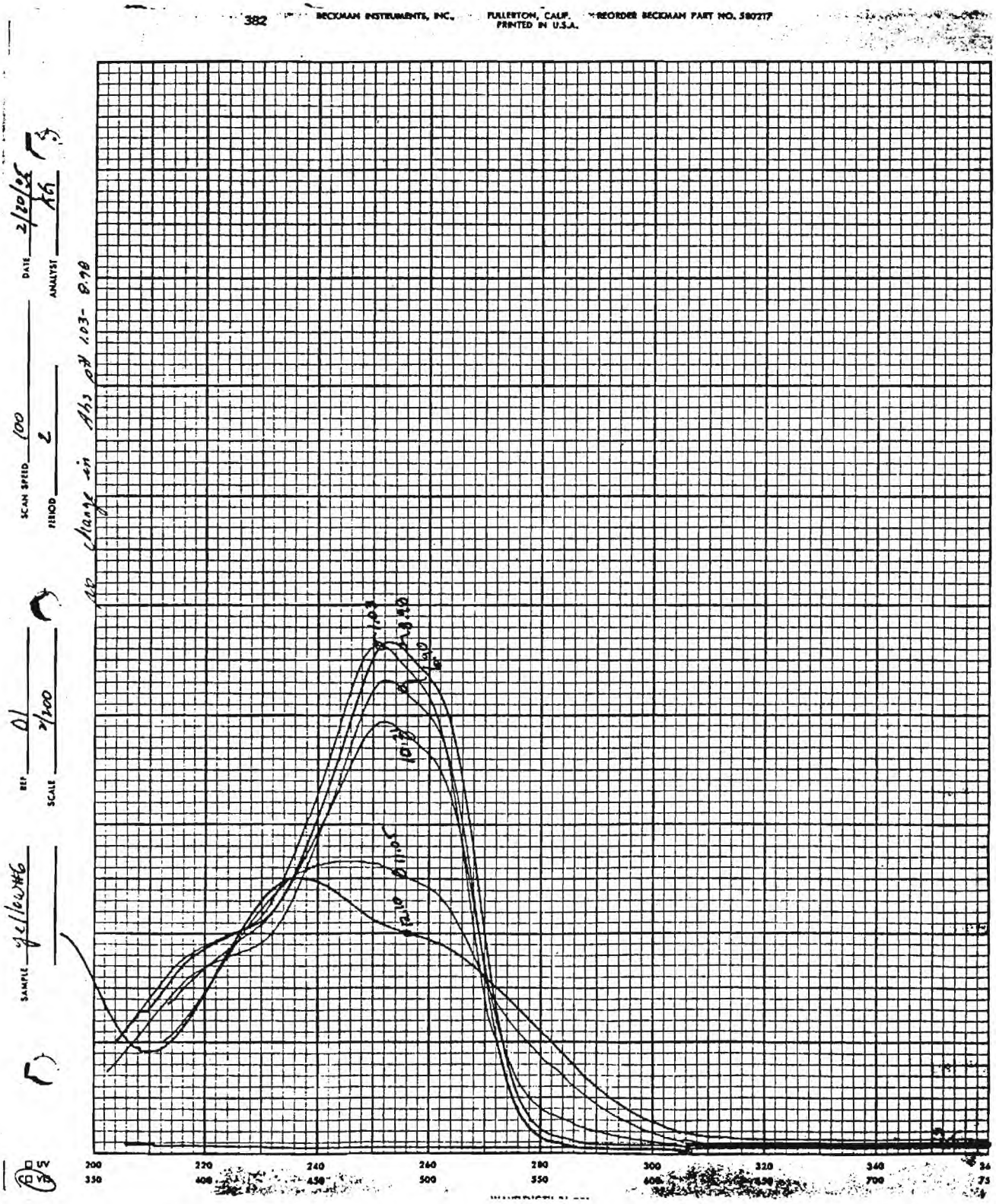

Figure A1-3. Spectrophotometric Determination of pKa for FD&C Yellow No. 6 (1).

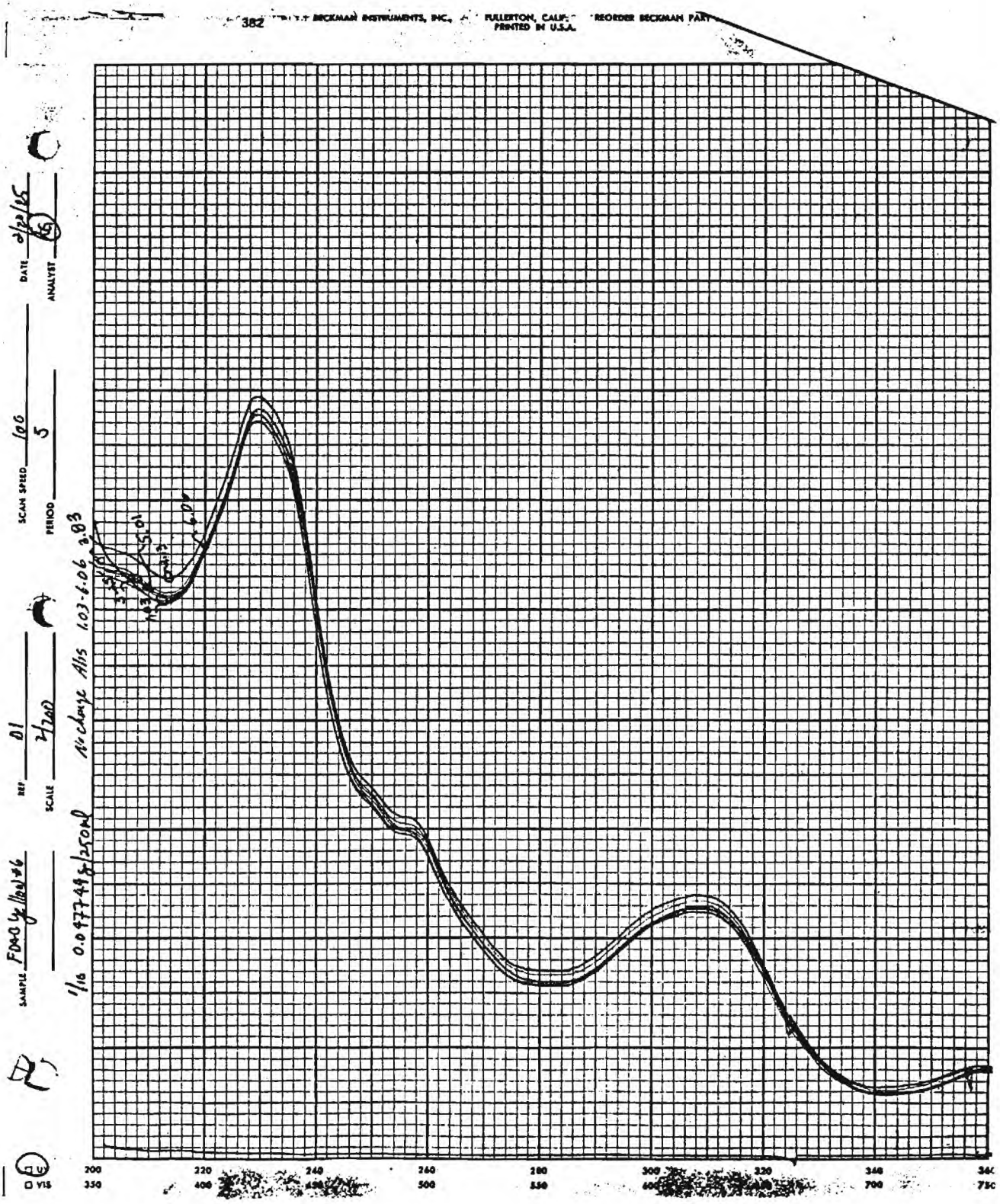

Figure A1-4. Spectrophotometric Determination of pKa for Yellow FD&C No. 6 (2).

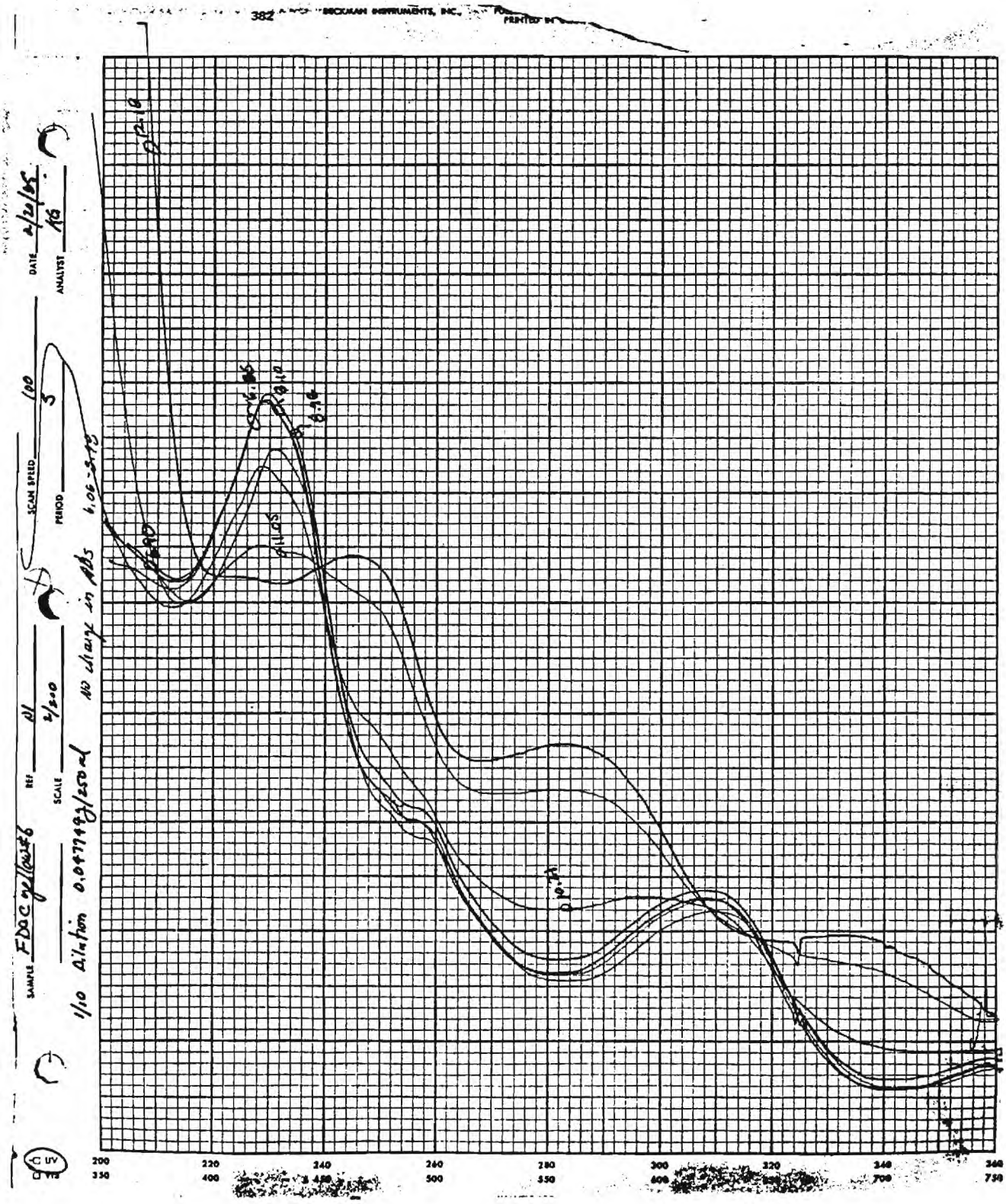

Figure A1-5. Spectrophotometric Determination of pKa for FD&C Yellow No. 6 (3).

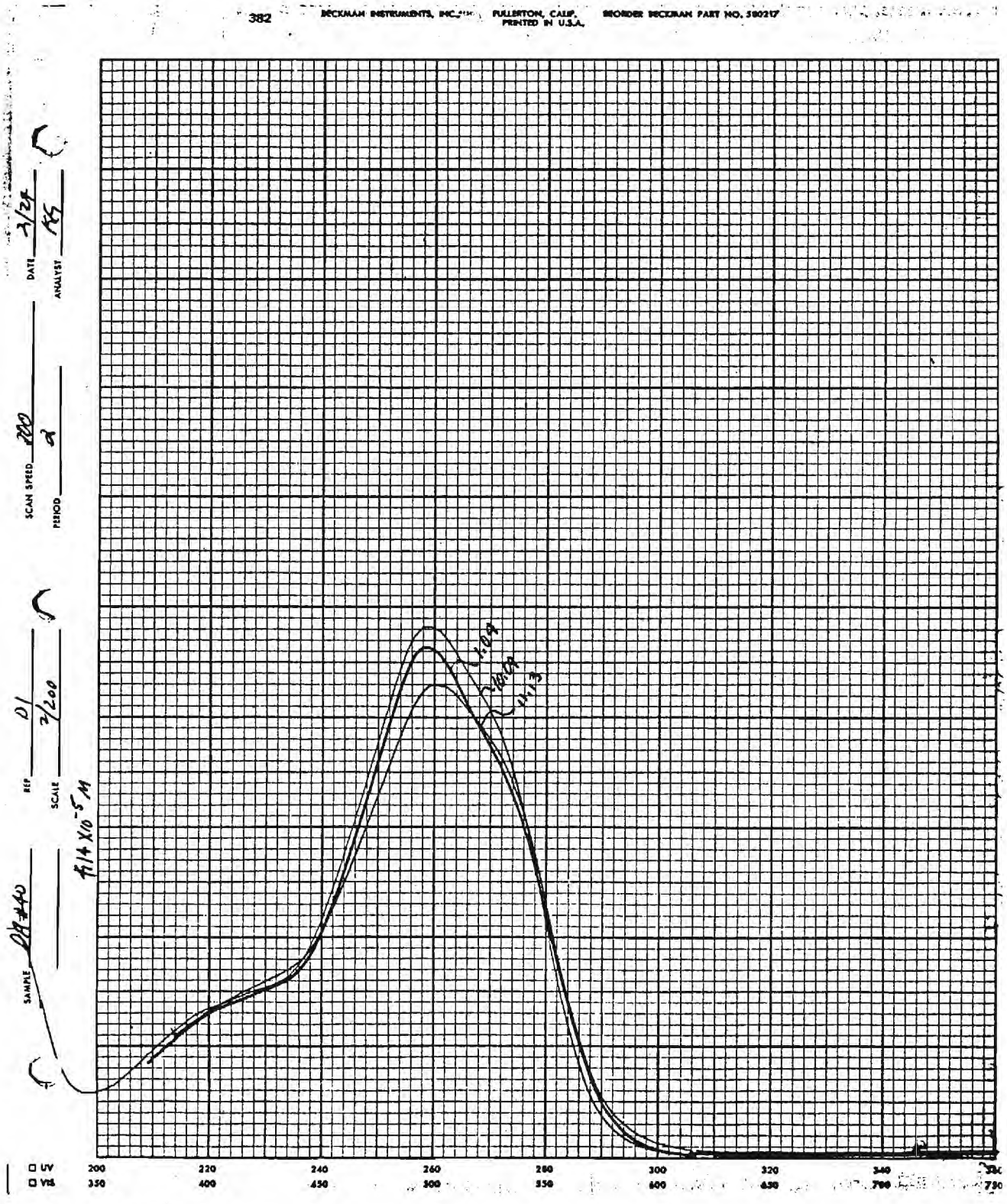

Figure A1-6. Spectrophotometric Determination of pKa for FD&C Red No. 40 (1).

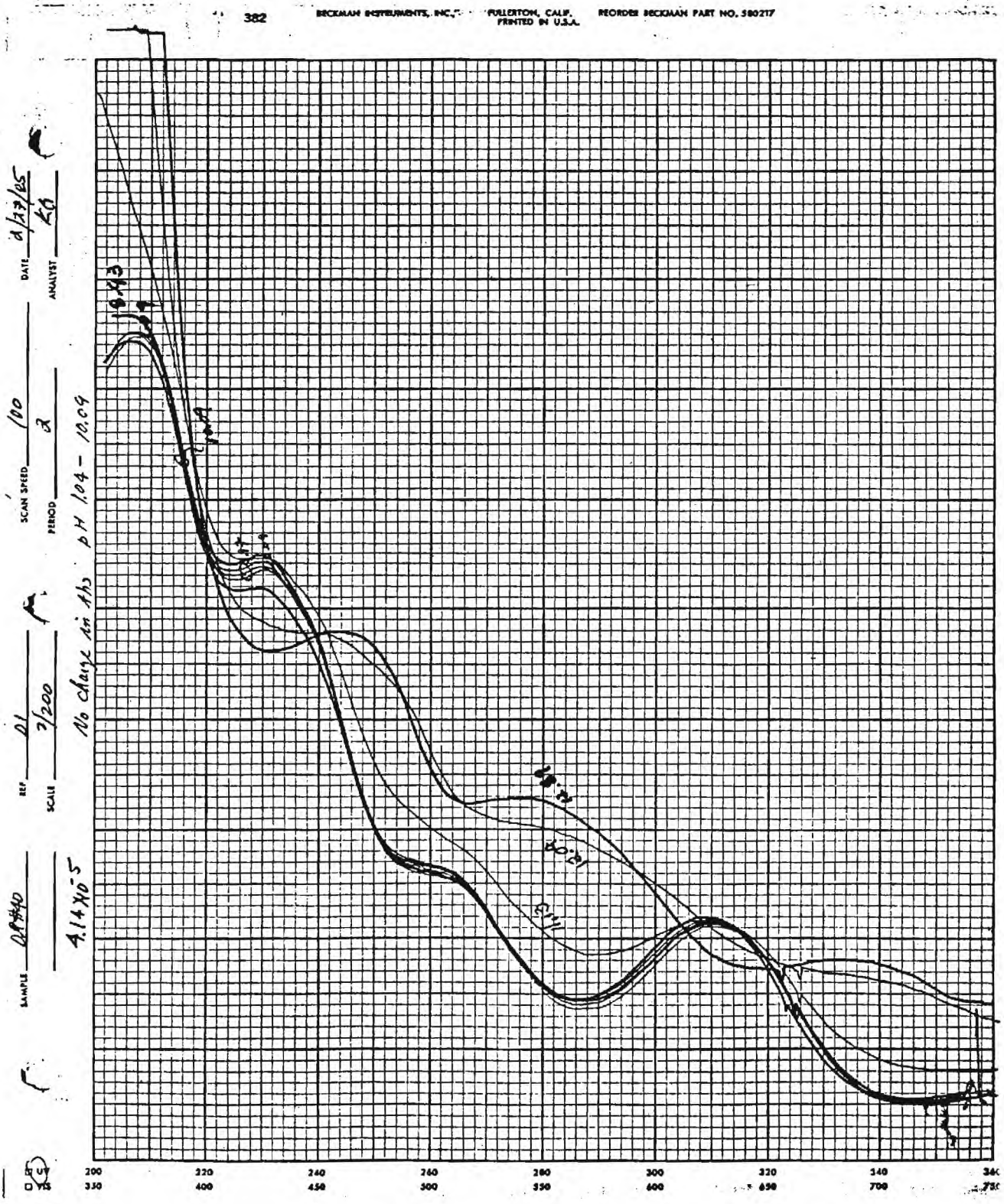

Figure A1-7. Spectrophotometric Determination of pKa for FD&C Red No. 40 (2).

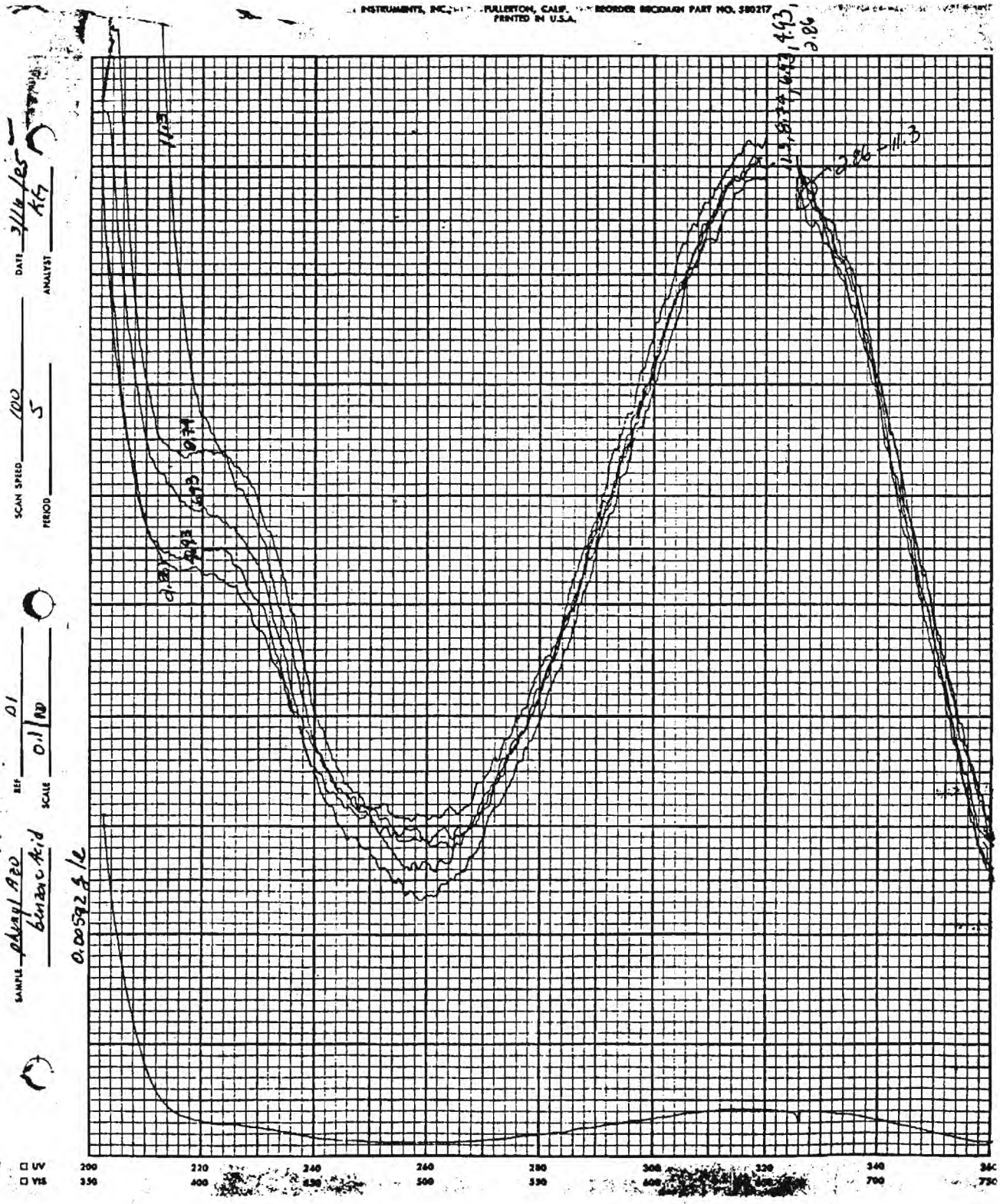

Figure A1-8. Spectrophotometric Determination of pKa for Phenylazobenzoic Acid.

APPENDIX 2

Batch Kinetic Adsorption and Desorption Curves

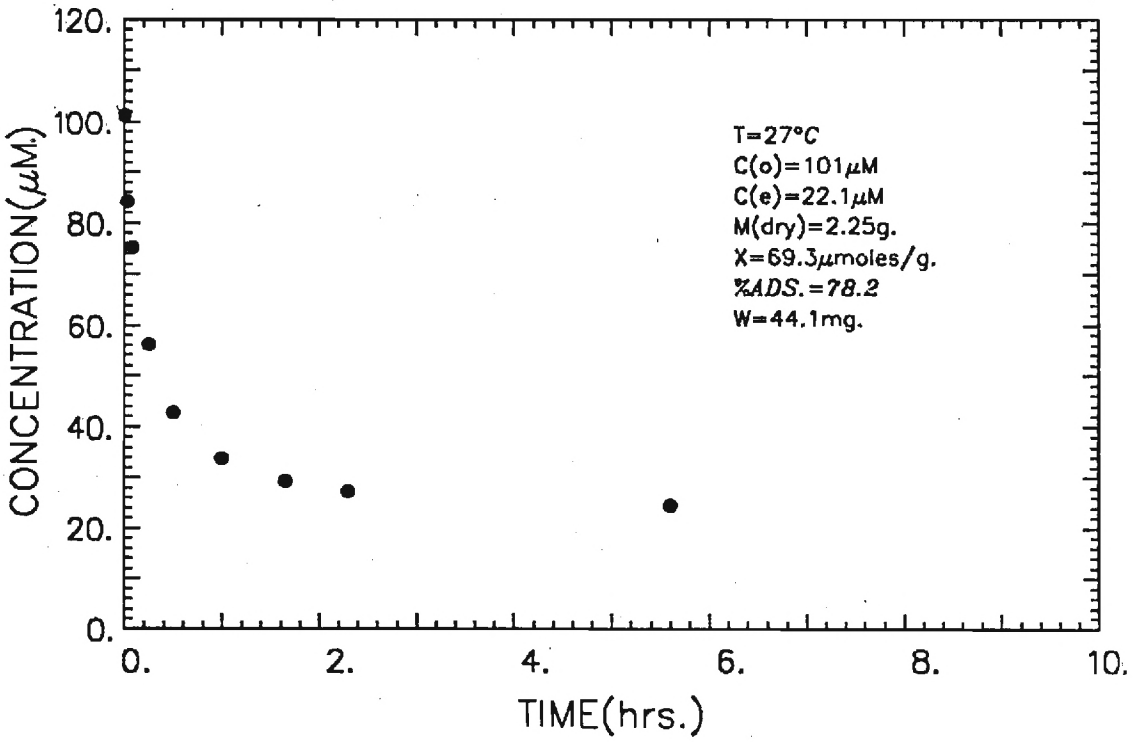

Figure A2-1. BATCH ADSORPTION OF PNP ON XAD-7

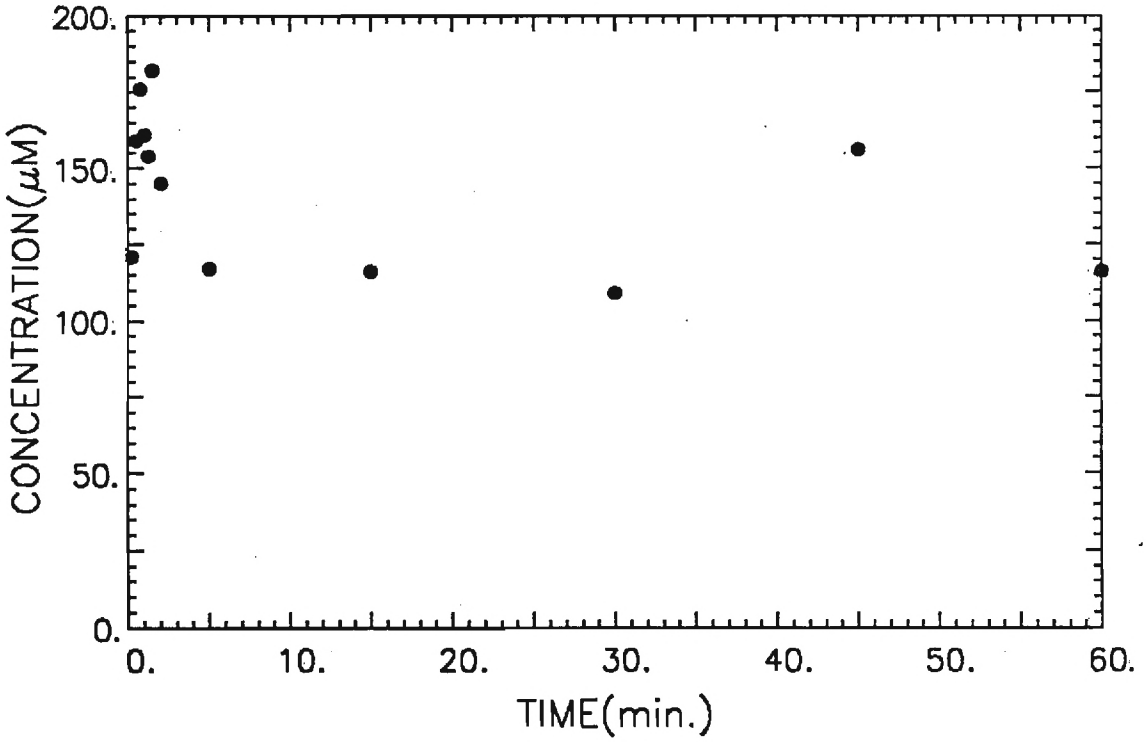

Figure A2-2. BATCH DESORPTION OF PNP FROM XAD-7

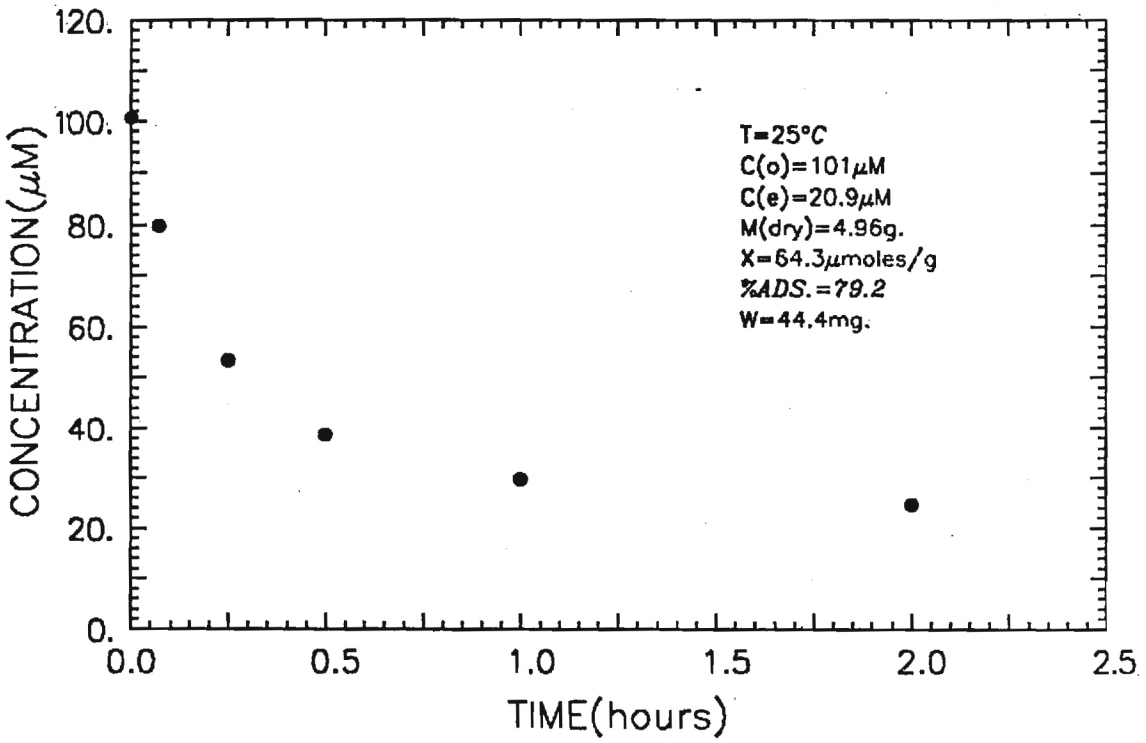

Figure A2-3. BATCH ADSORPTION OF PNP ON XAD-16(1)

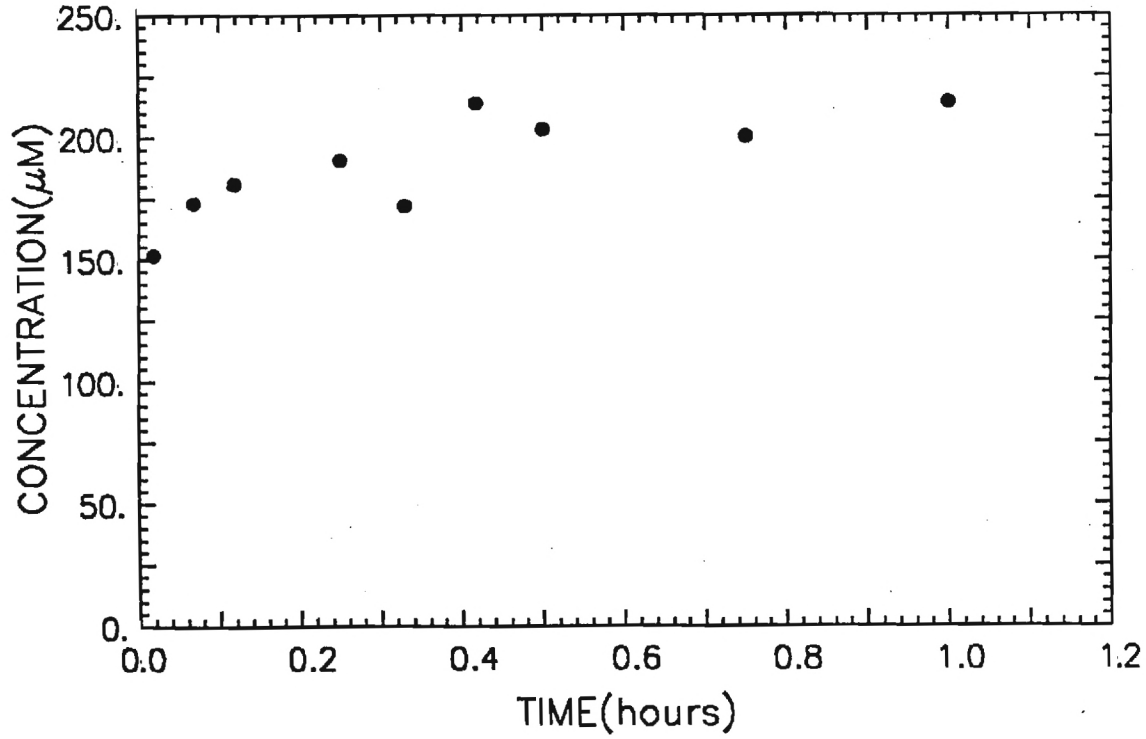

Figure A2-4.BATCH DESORPTION OF PNP FROM XAD-16(1)

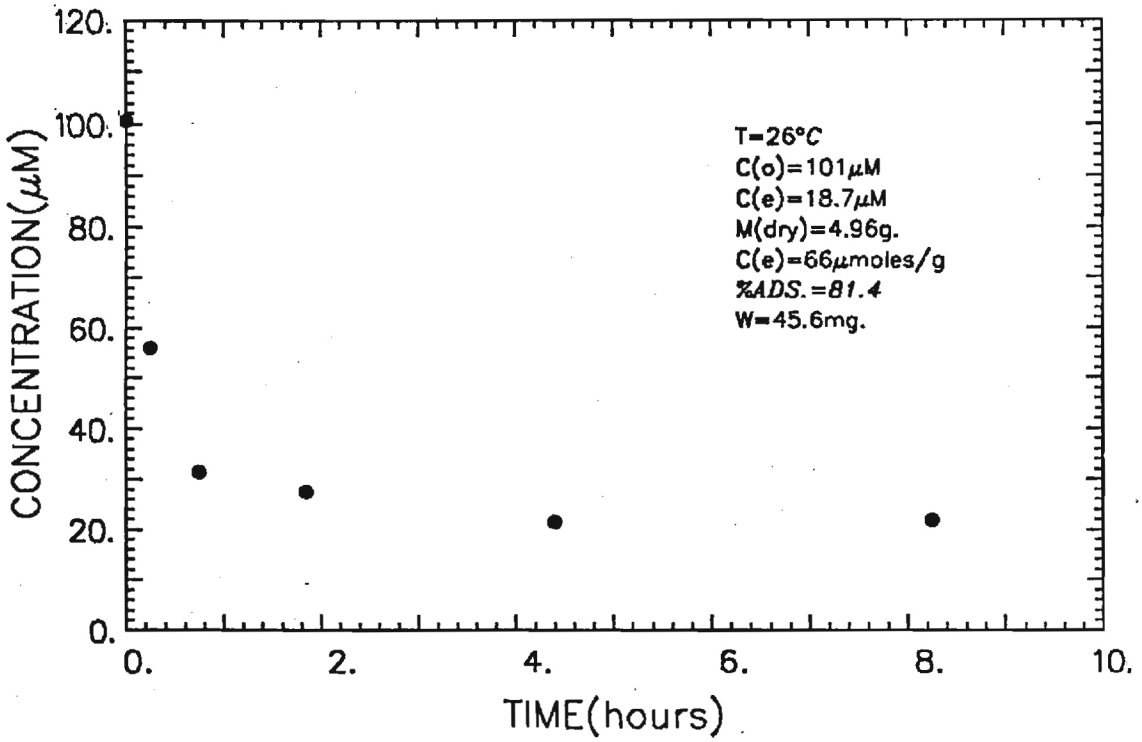

Figure A2-5. BATCH ADSORPTION OF PNP ON XAD-16(2)

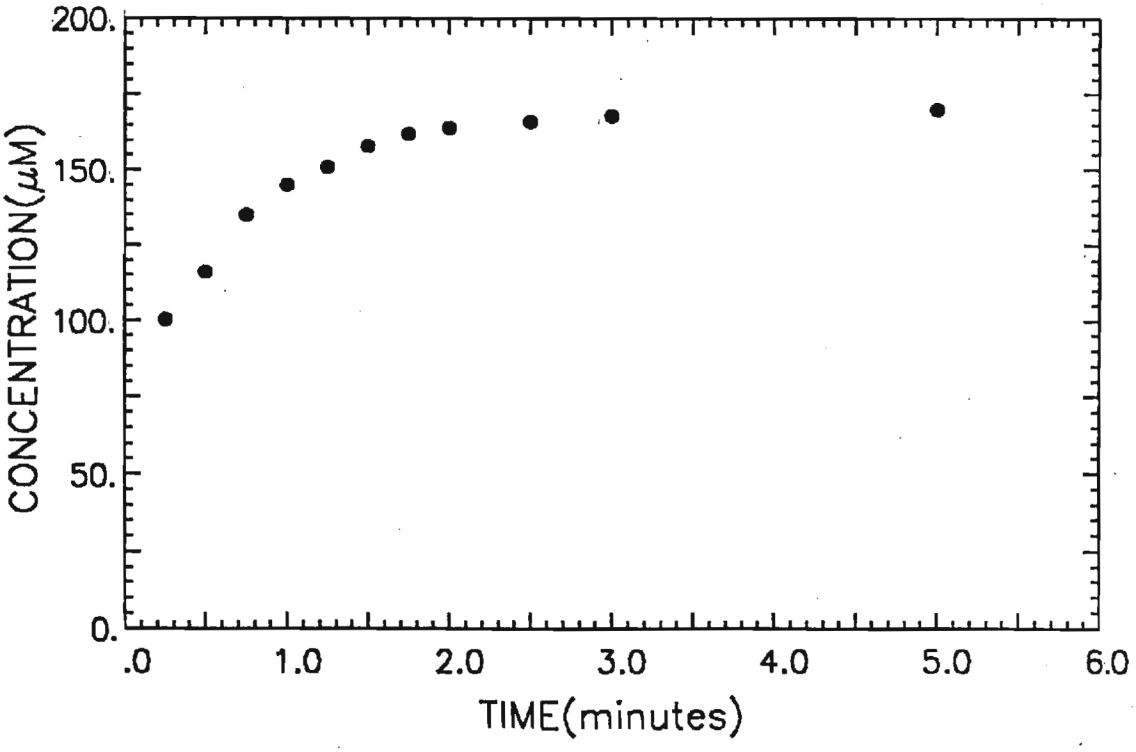

Figure A2-6. BATCH DESORPTION OF PNP FROM XAD-16(2)

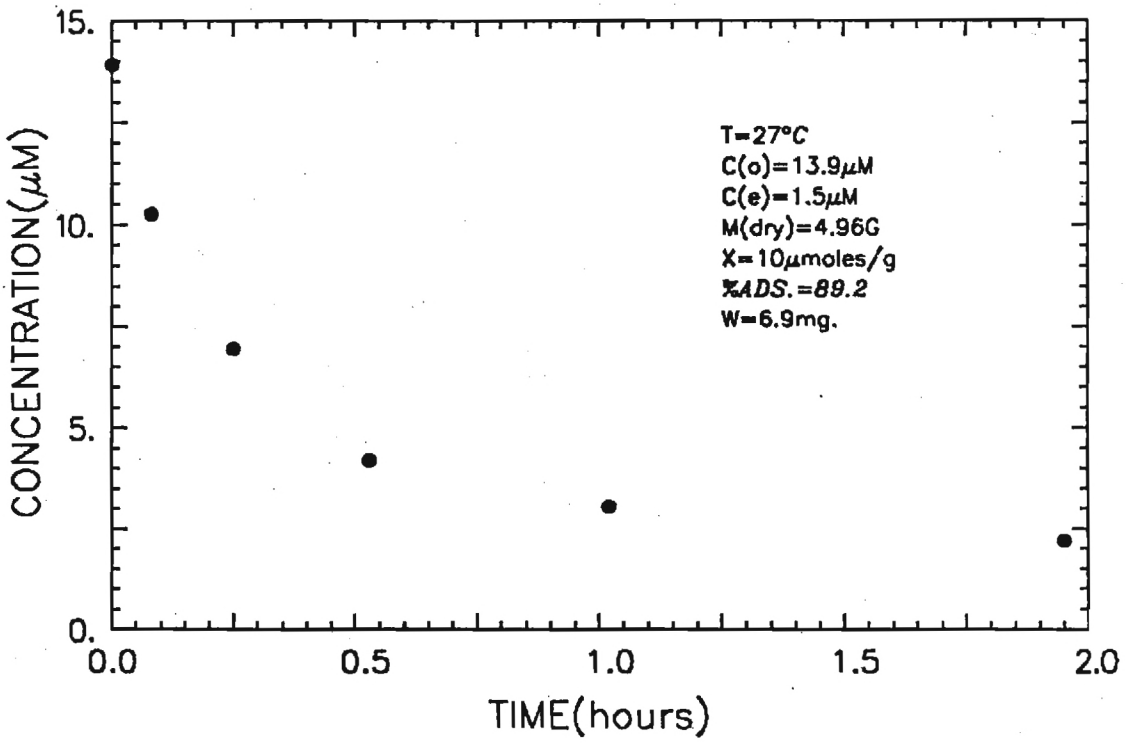

Figure A2-7. BATCH ADSORPTION OF PNP ON XAD-16(3)

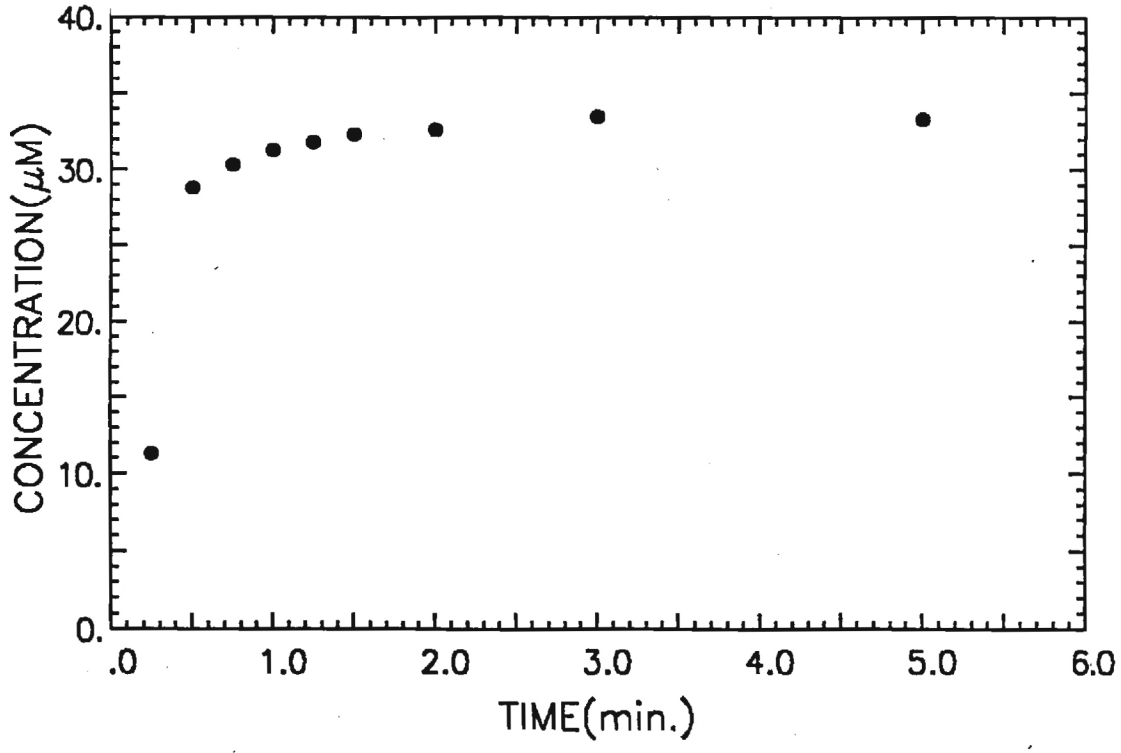

Figure A2-8. BATCH DESORPTION OF PNP FROM XAD-16(3)

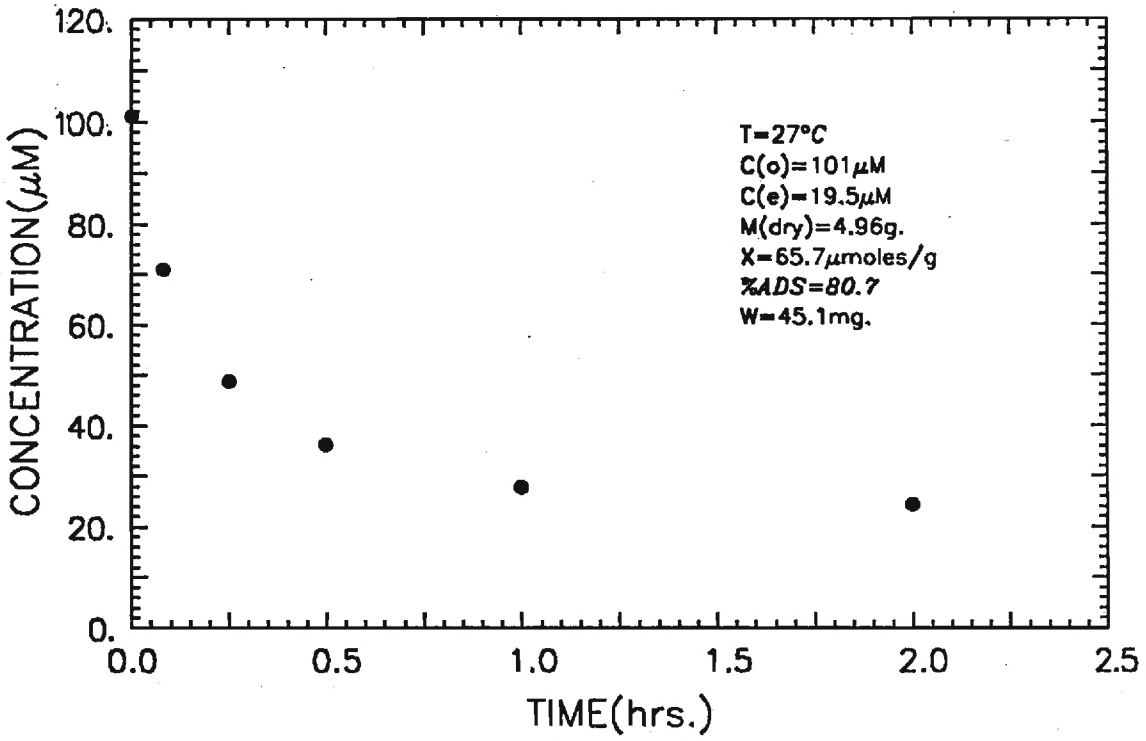

Figure A2-9. BATCH ADSORPTION OF PNP ON XAD-16(4)

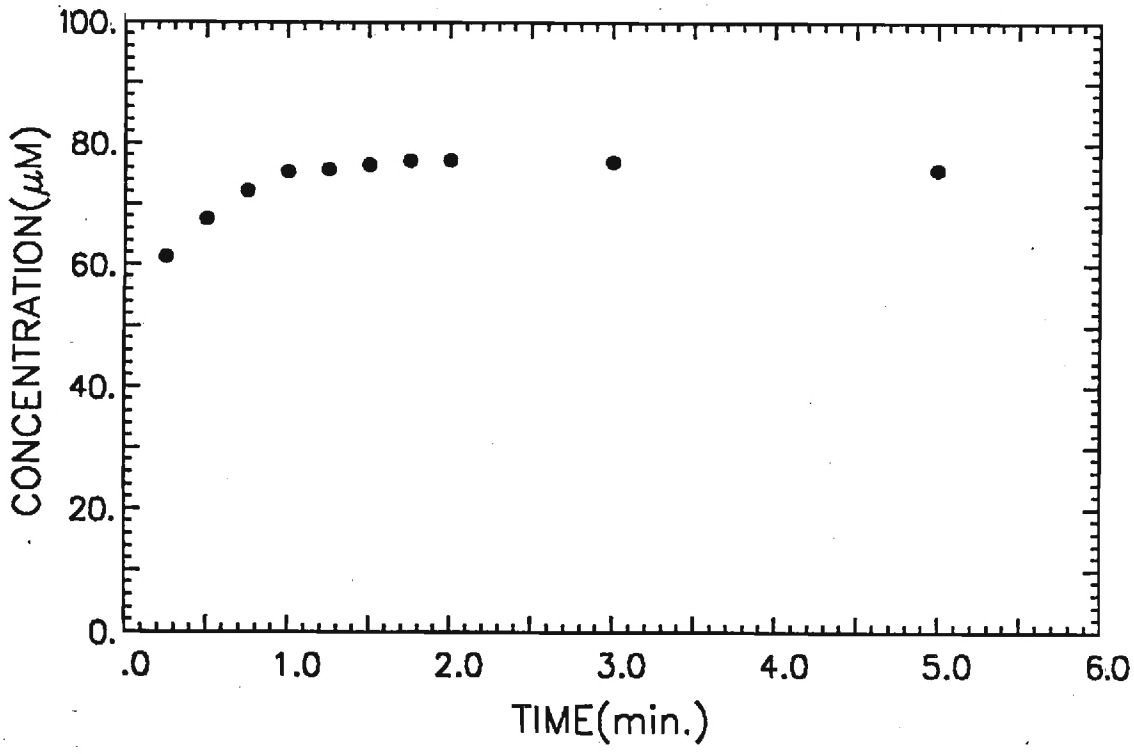

Figure A2-10. BATCH DESORPTION OF PNP FROM XAD-16(4)

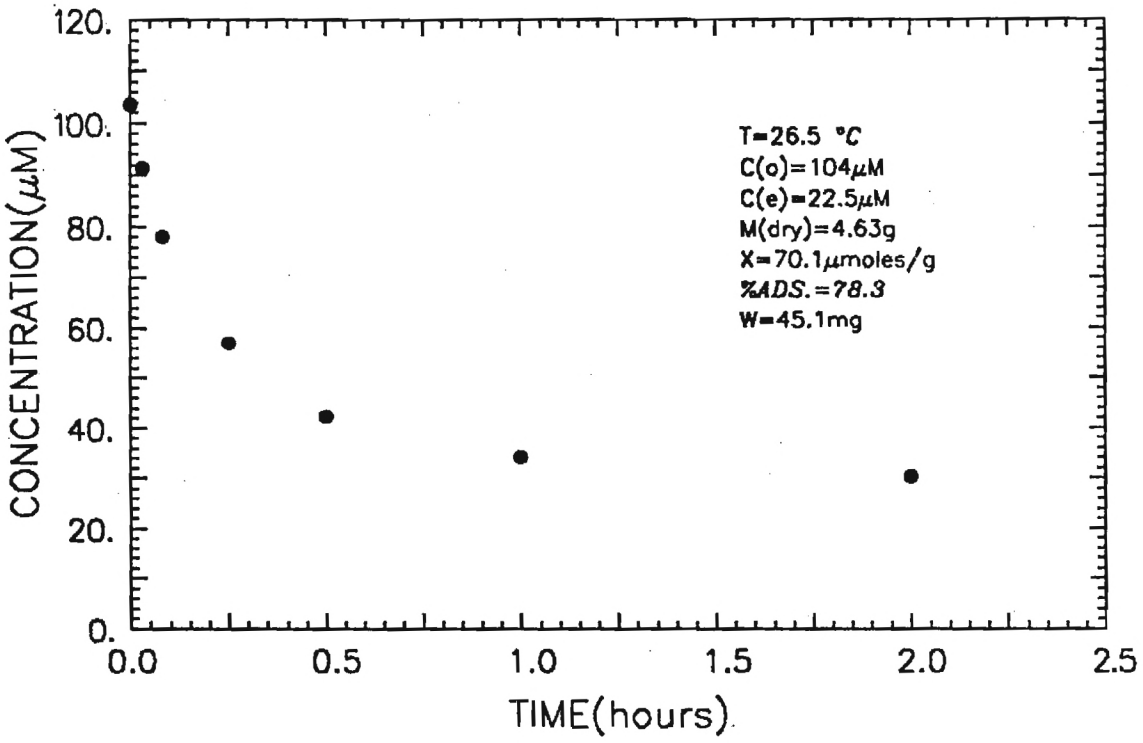

Figure A2-11. BATCH ADSORPTION OF PNP ON XAD-16(5)

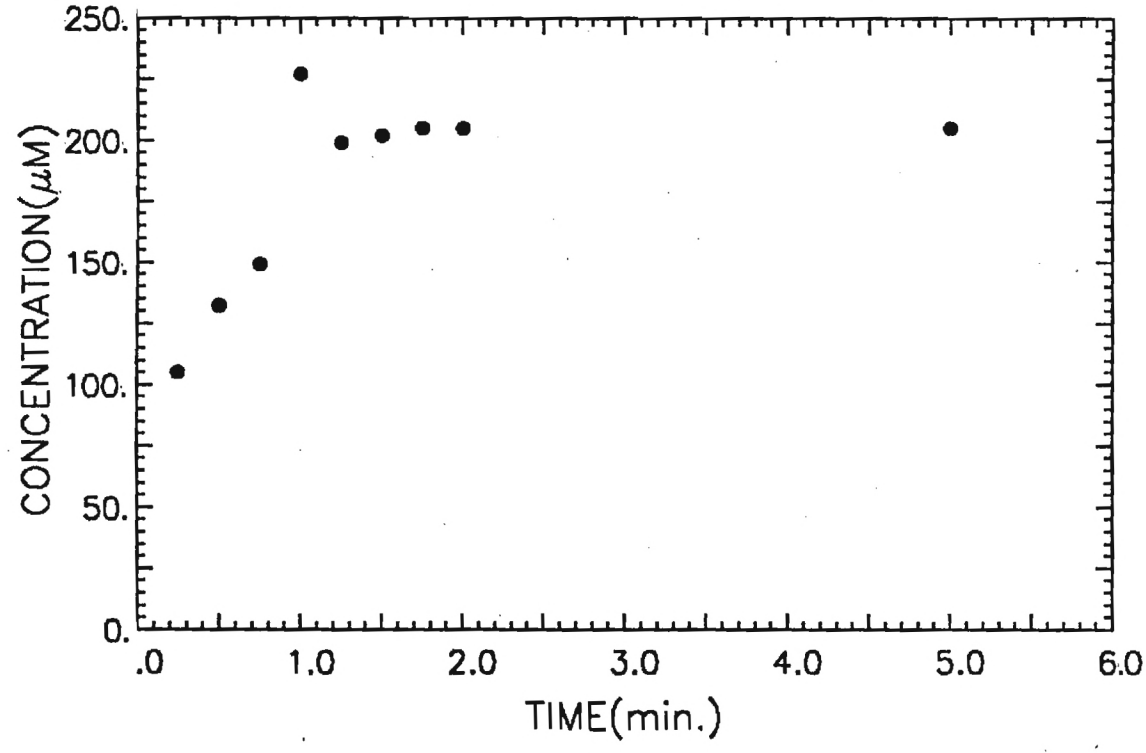

Figure A2-12. BATCH DESORPTION OF PNP FROM XAD-16(5)

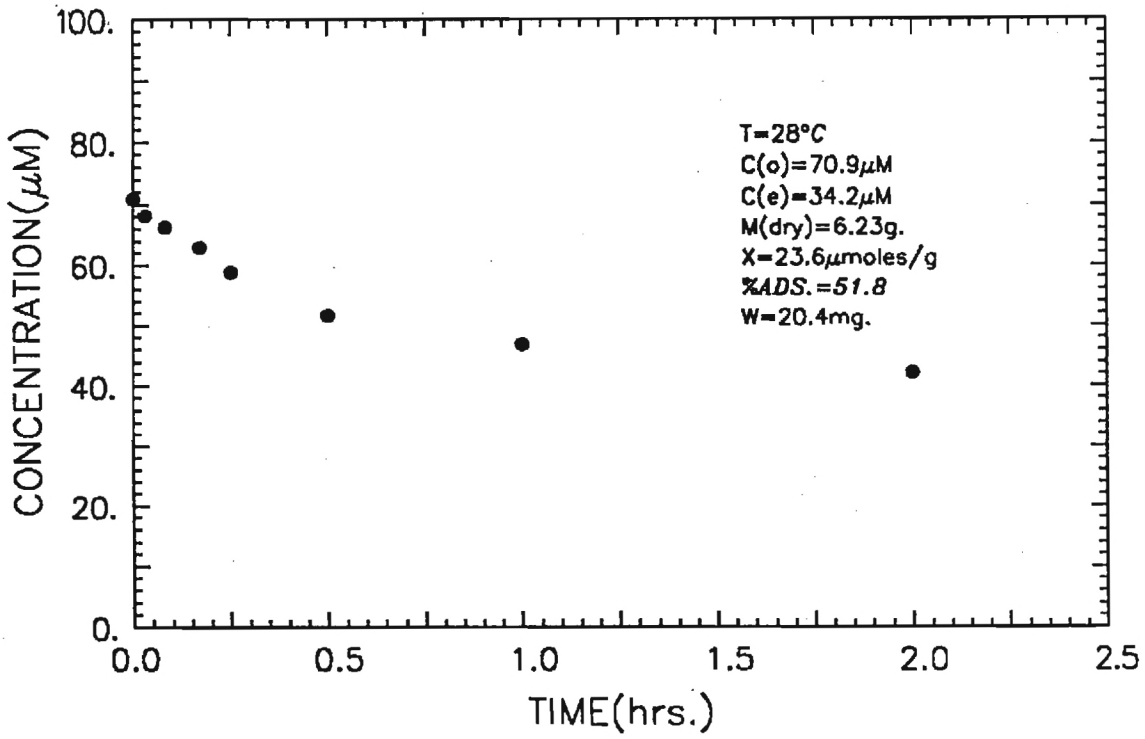

Figure A2-13. BATCH ADSORPTION OF PNP ON S-761(1)

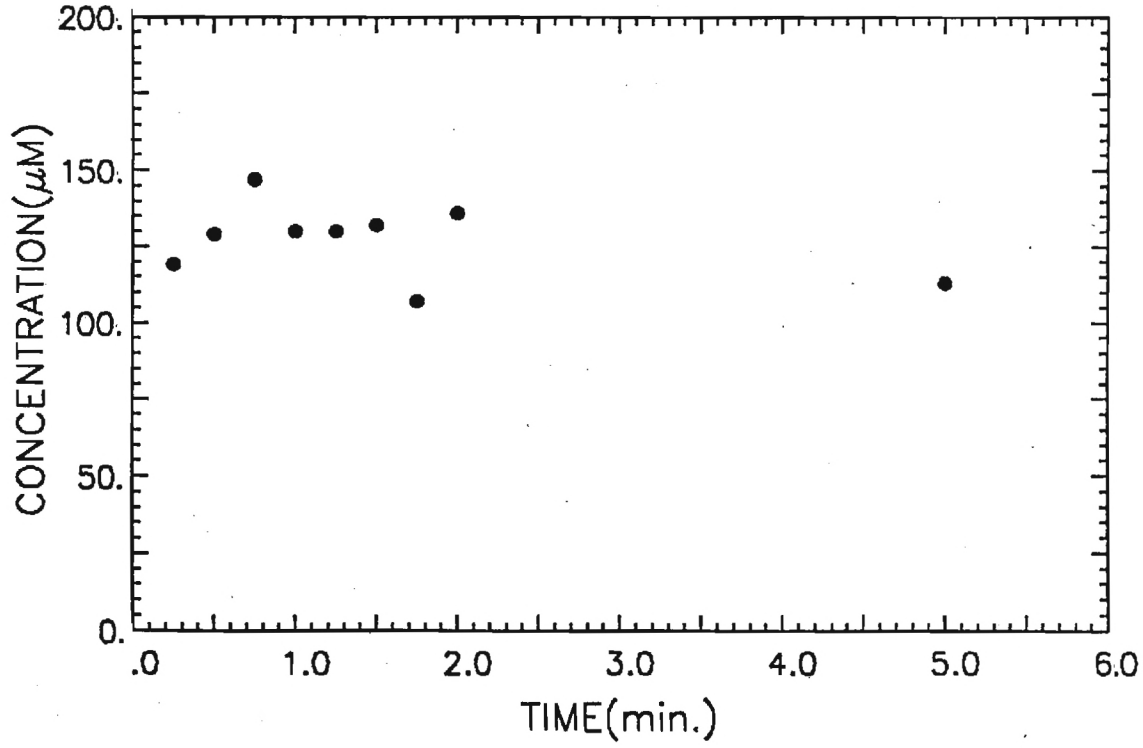

Figure A2-14. BATCH DESORPTION OF PNP FROM S-761(1)

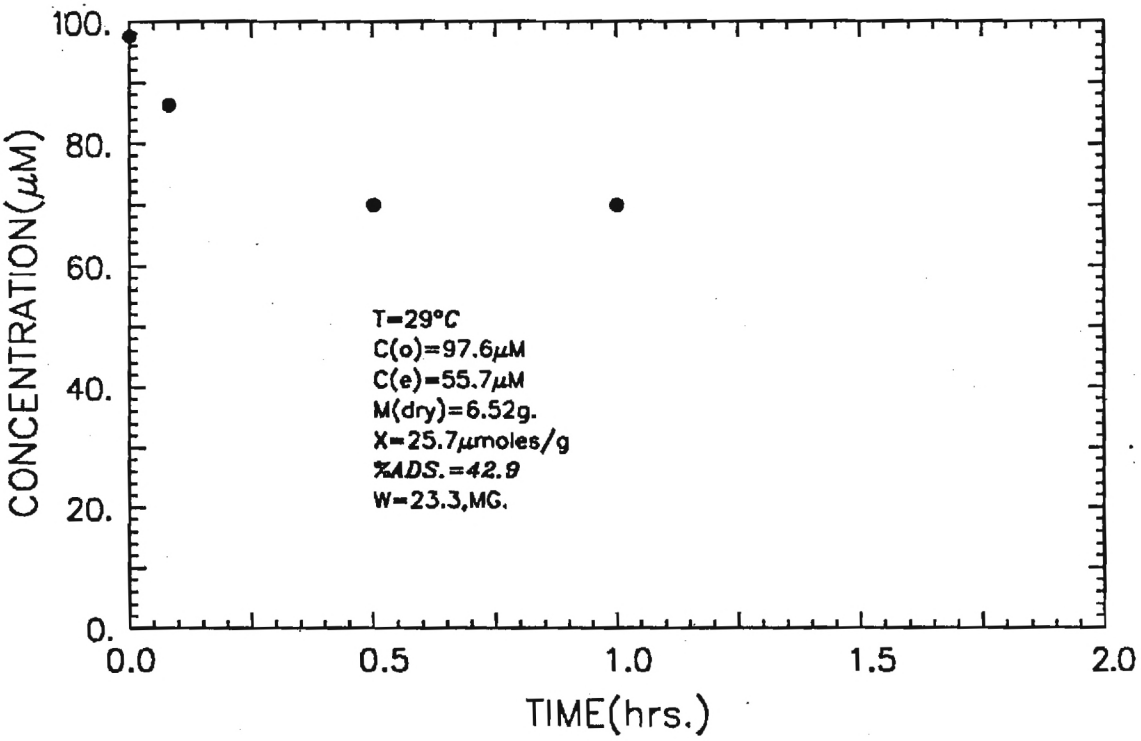

Figure A2-15. BATCH ADSORPTION OF PNP ON S-761(2)

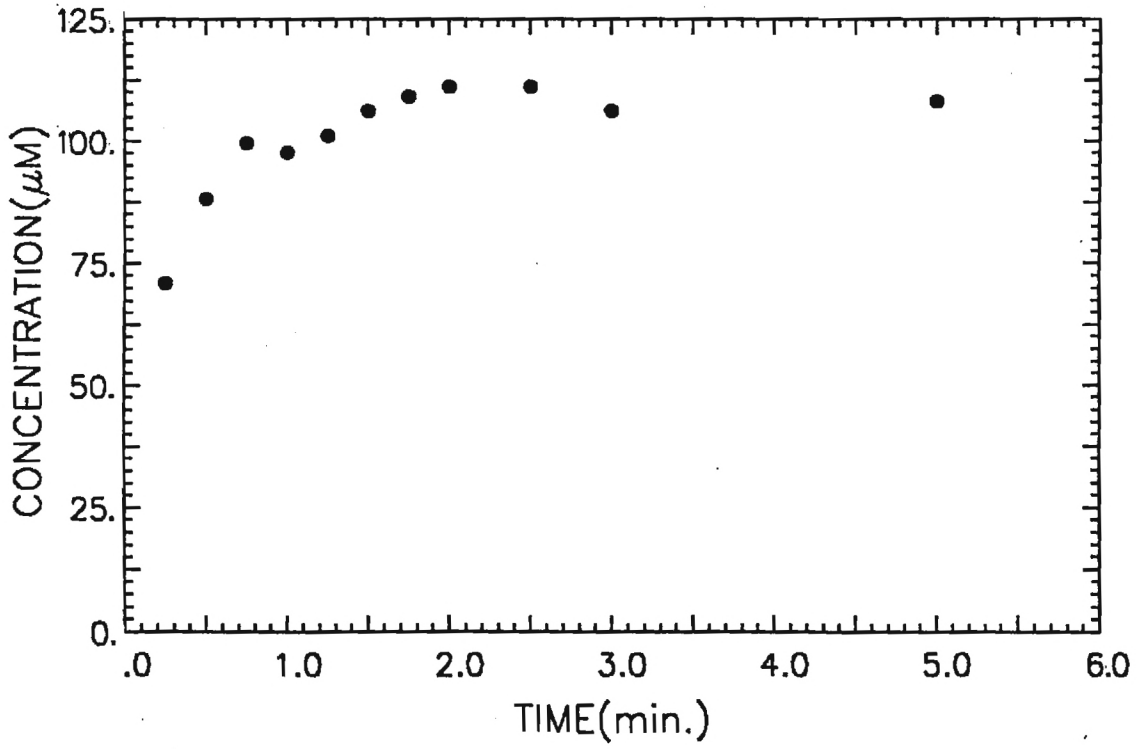

Figure A2-16. BATCH DESORPTION OF PNP FROM S-761(2)

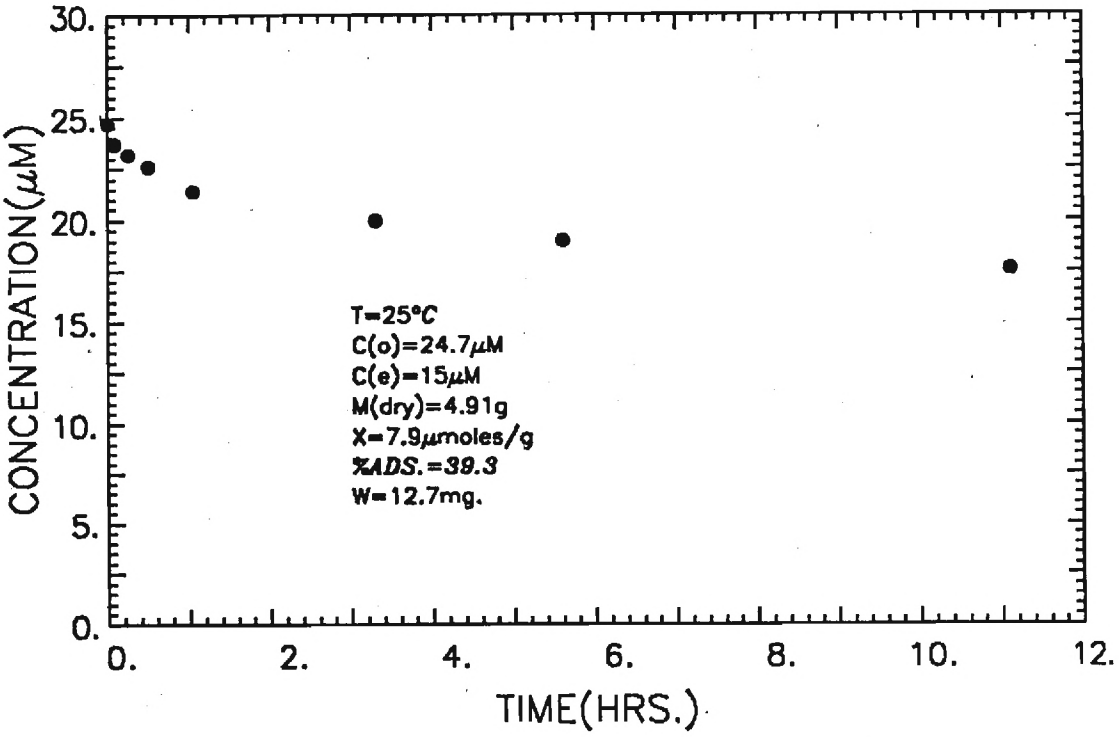

Figure A2-17. BATCH ADSORPTION OF M.O. ON XAD-7(1)

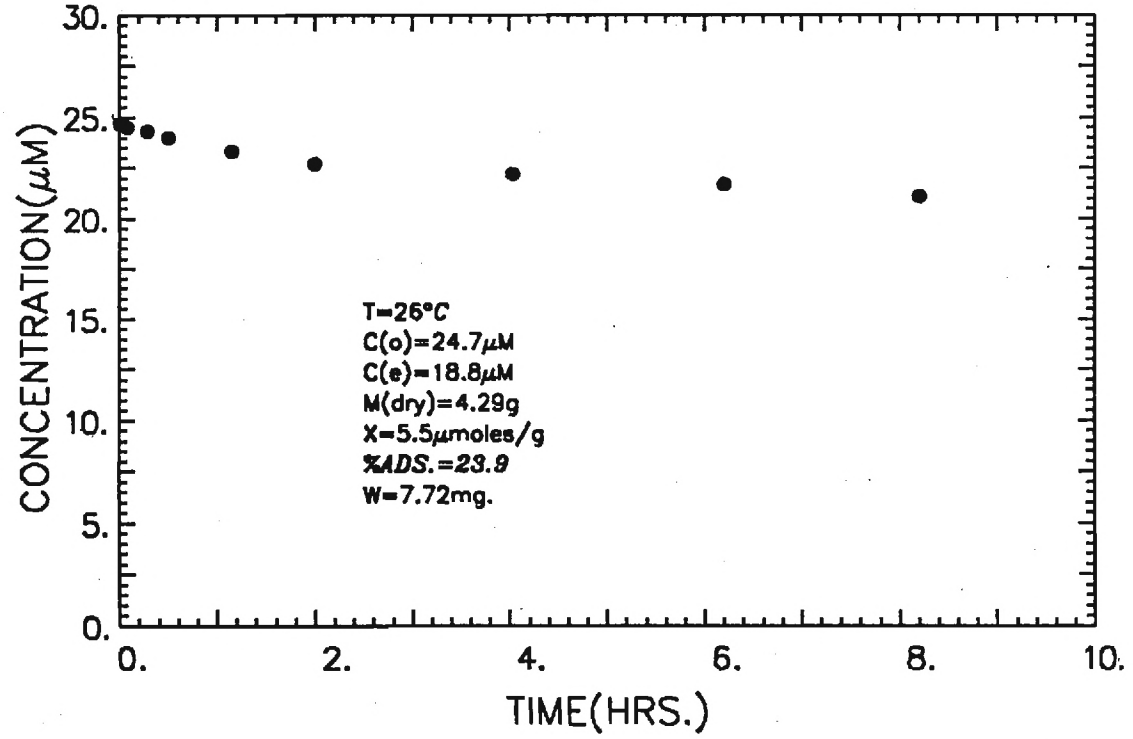

Figure A2-18. BATCH ADSORPTION OF M.O. ON XAD-7(2)

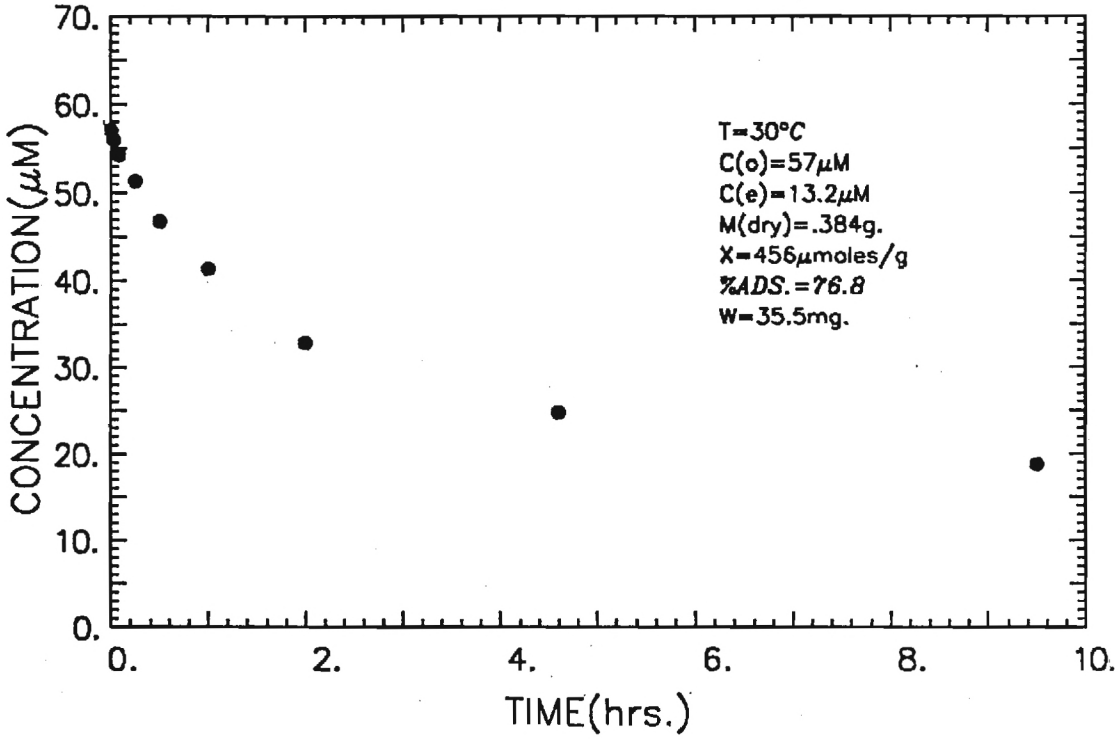

Figure A2-19. BATCH ADSORPTION OF 4AAB ON XAD-7(3)

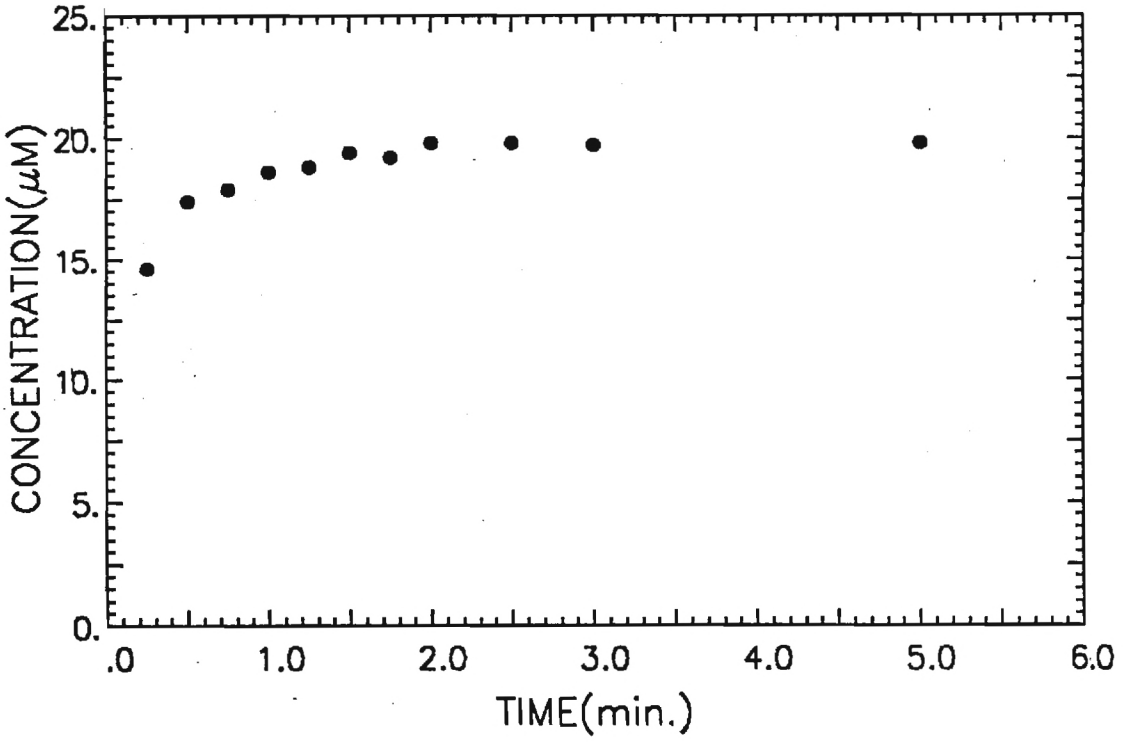

Figure A2-20. BATCH DESORPTION OF 4AAB FROM XAD-7(3)

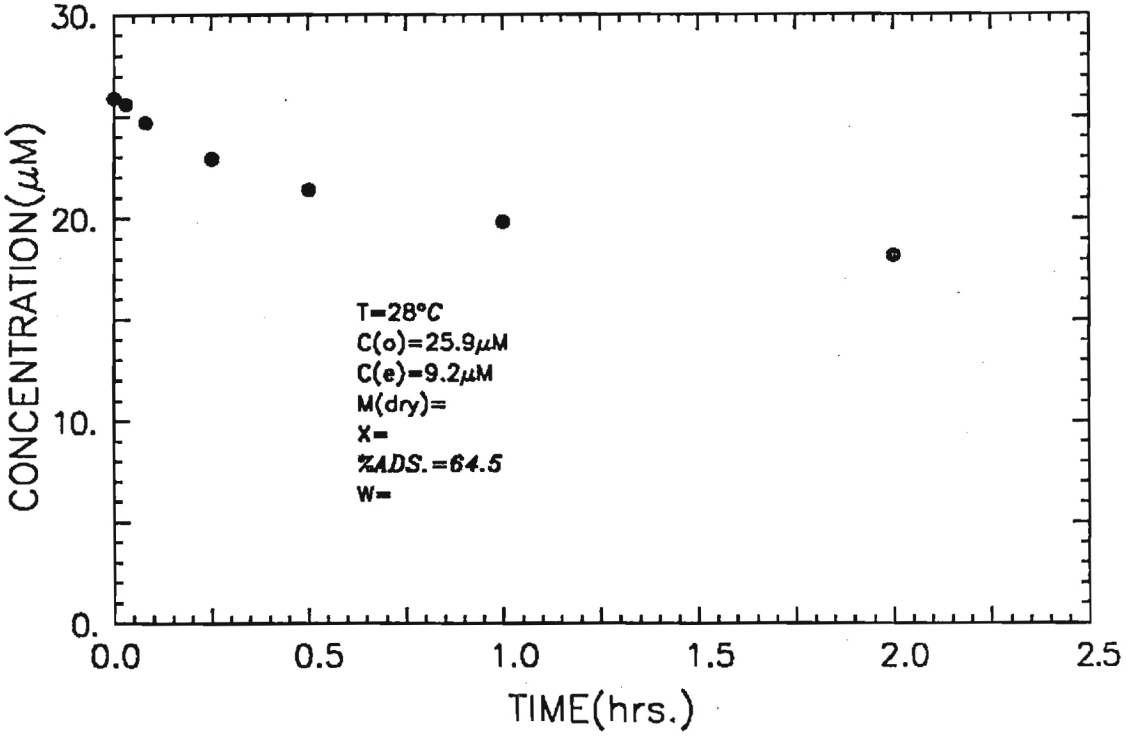

Figure A2-21. BATCH ADSORPTION OF M.O. ON XAD-7(4)

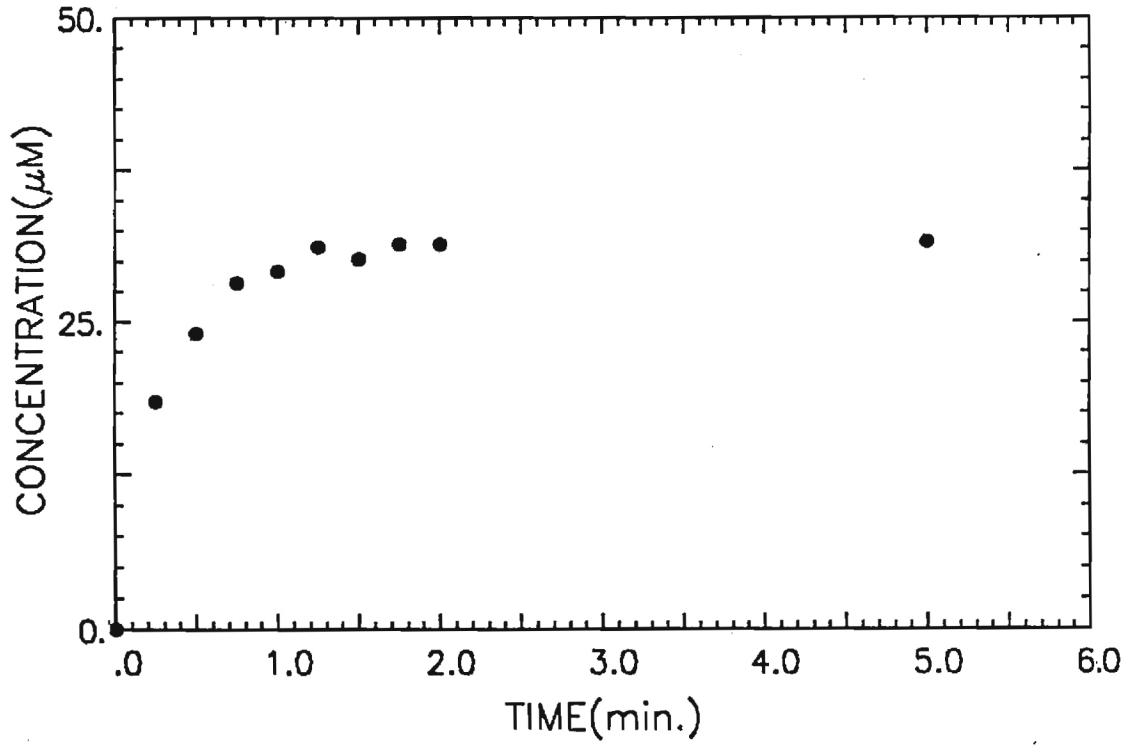

Figure A2-22. BATCH DESORPTION OF M.O. FROM XAD-7(4)

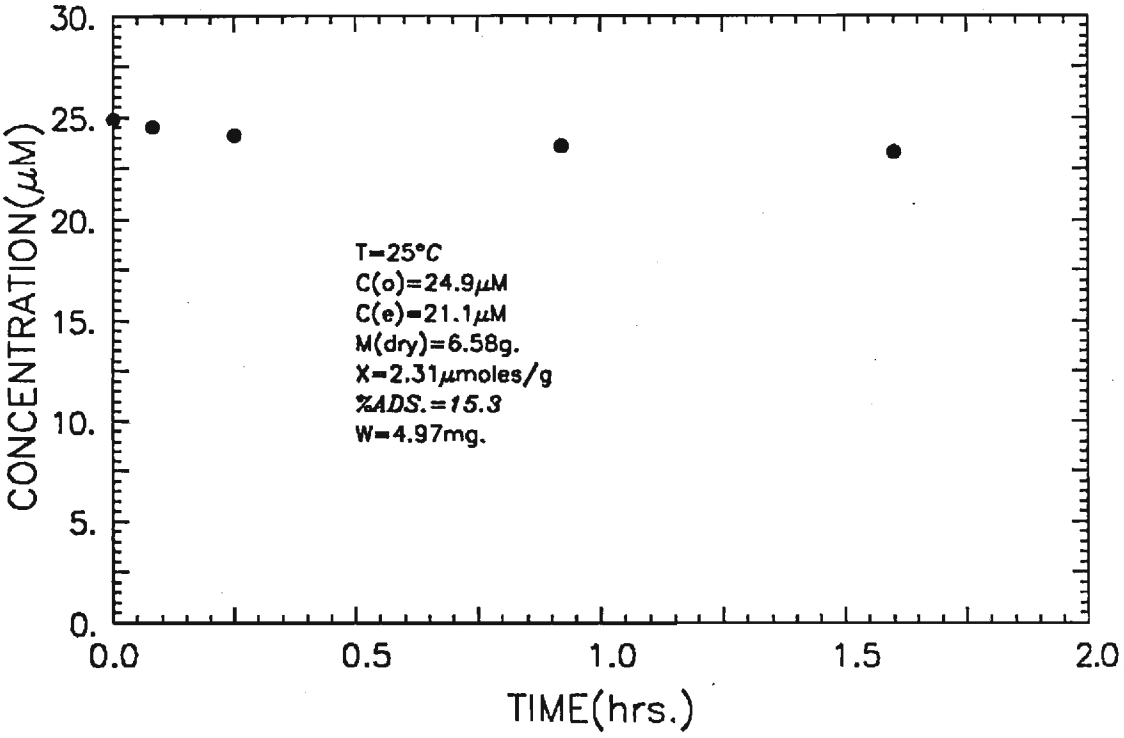

Figure A2-23. BATCH ADSORPTION OF M.O. ON XAD-8

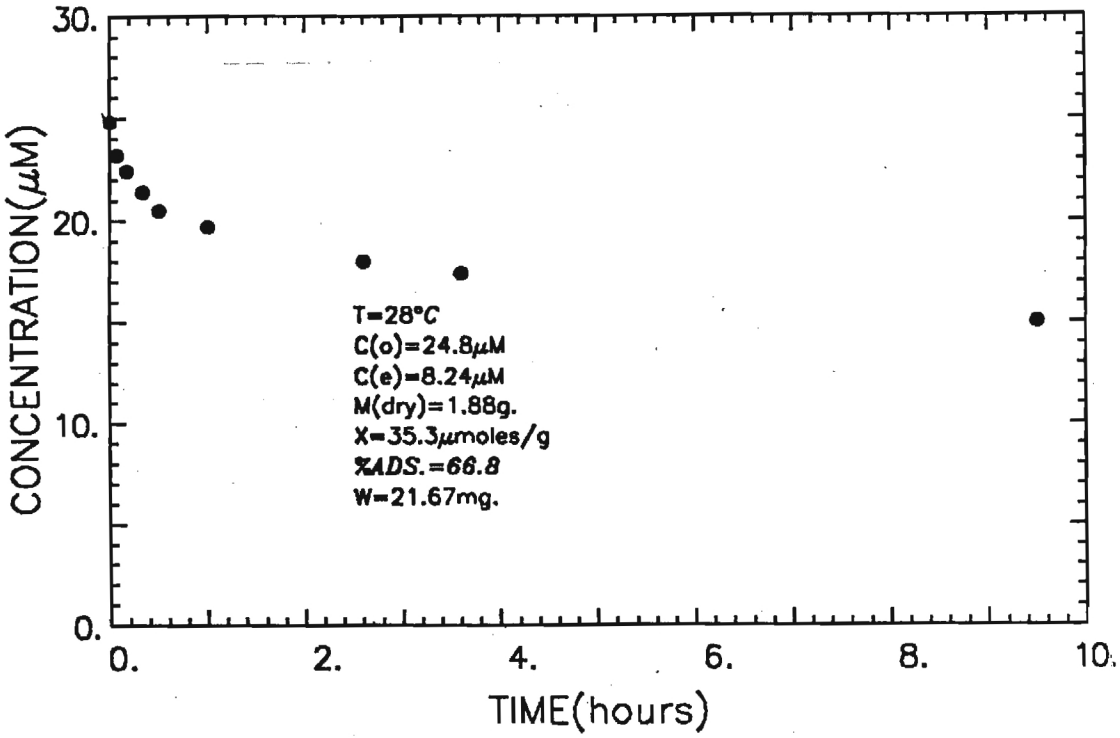

Figure A2-24. BATCH ADSORPTION OF MO ON XAD-16 (1)

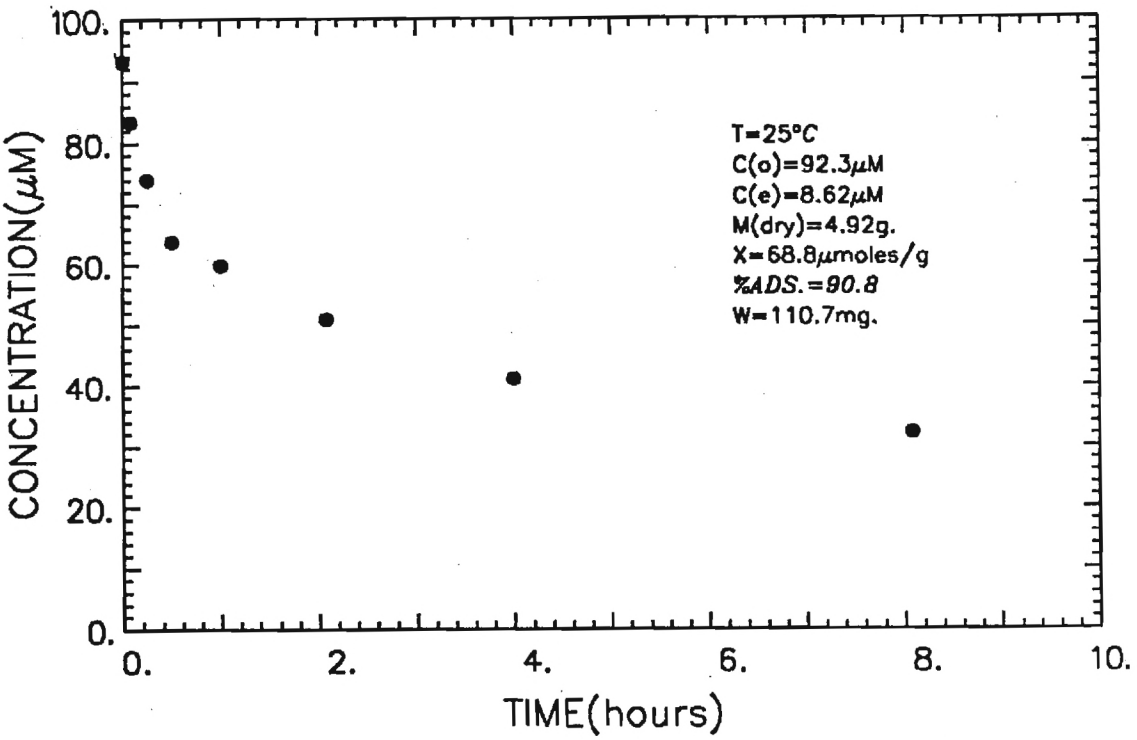

Figure A2-25. BATCH ADSORPTION OF MO ON XAD-16 (2)

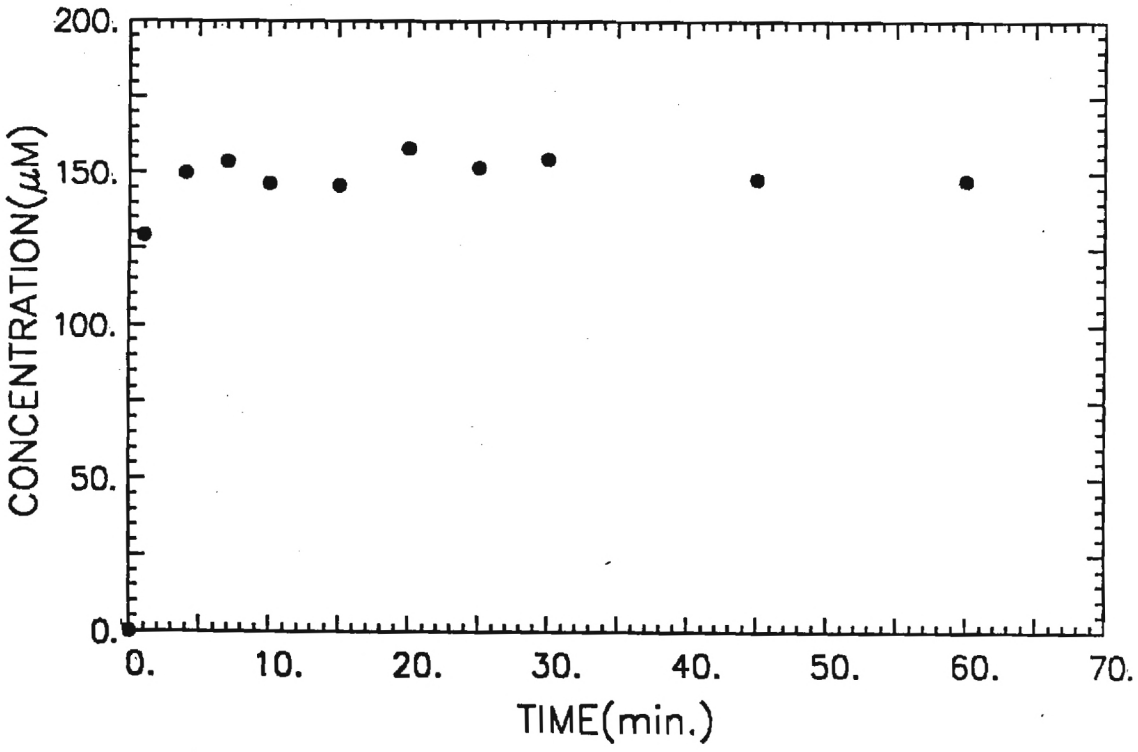

Figure A2-26. BATCH DESORPTION OF M.O. FROM XAD-16(2)

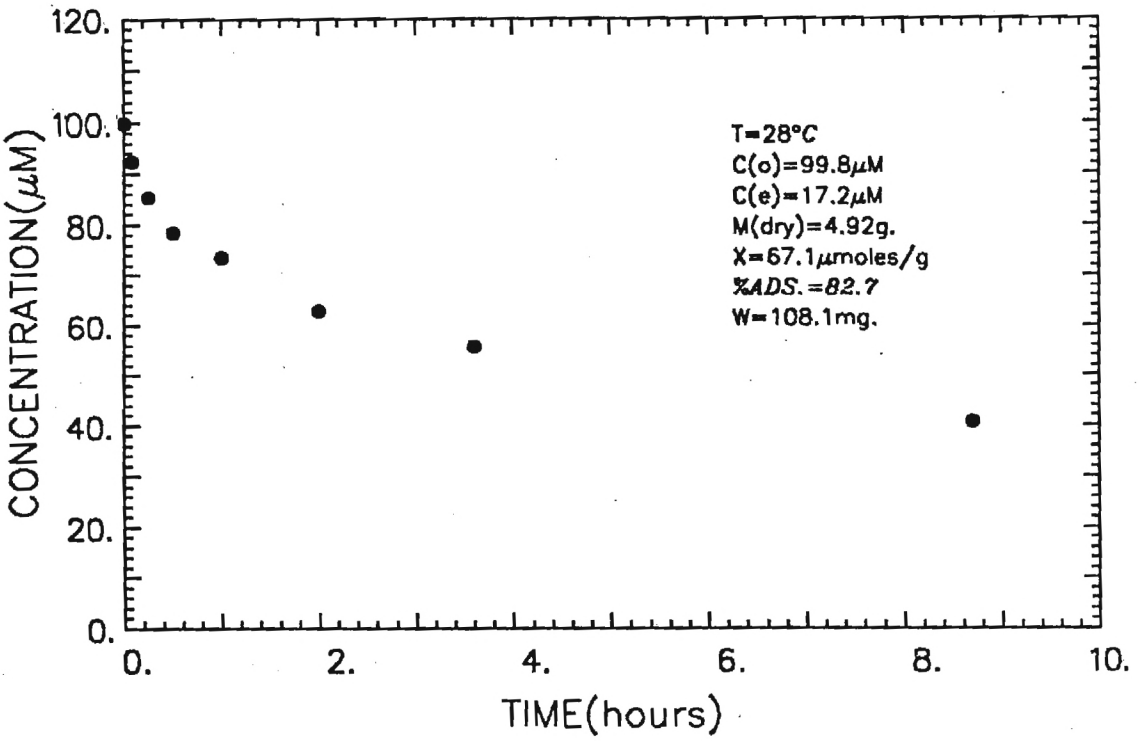

Figure A2-27. BATCH ADSORPTION OF MO ON XAD-16 (3)

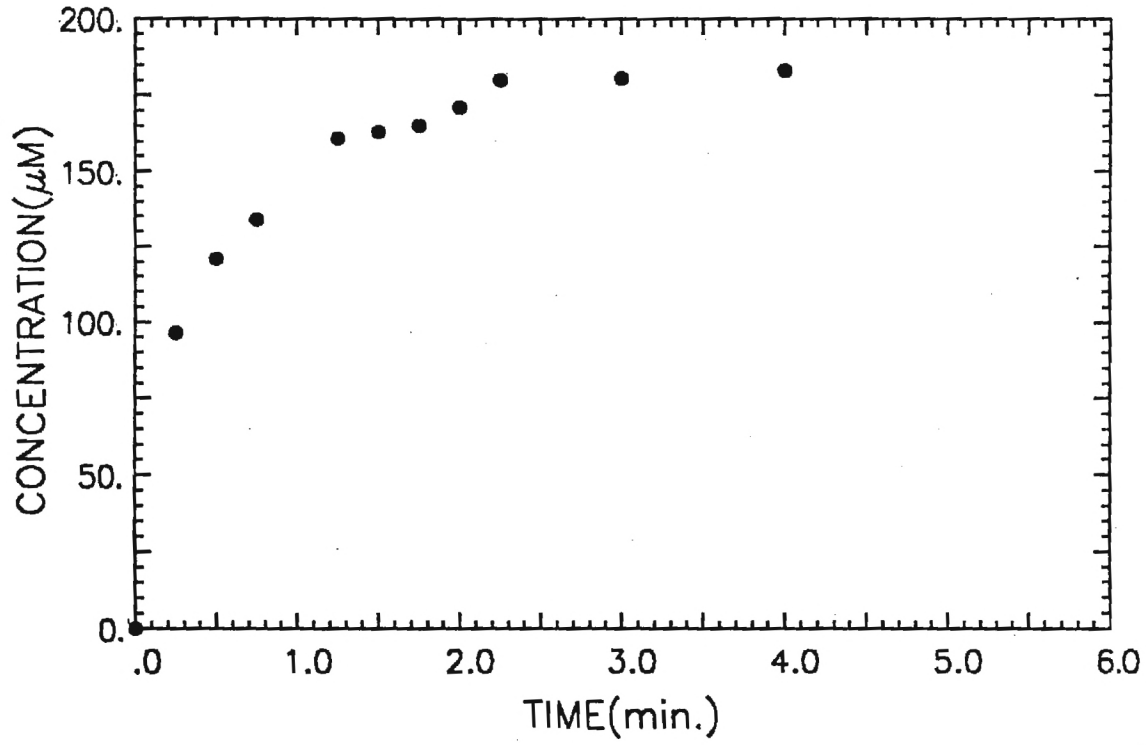

Figure A2-28. BATCH DESORPTION OF M.O. FROM XAD-16(3)

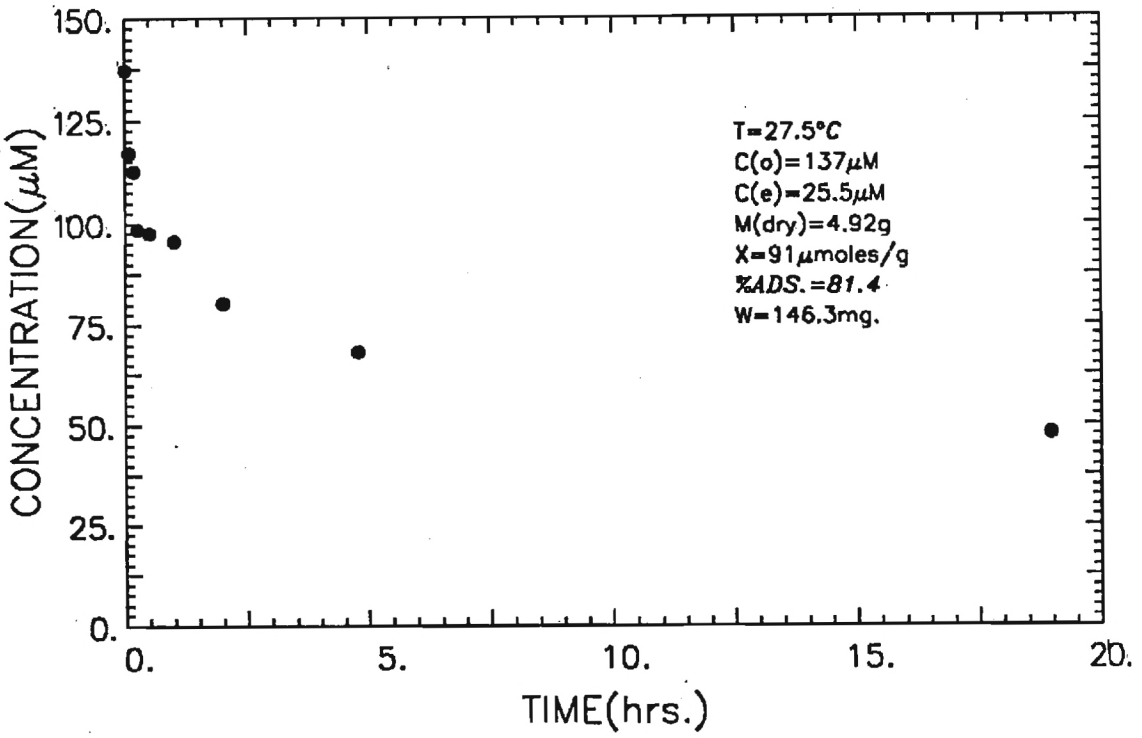

Figure A2-29. BATCH ADSORPTION OF M.O. ON XAD-16(4)

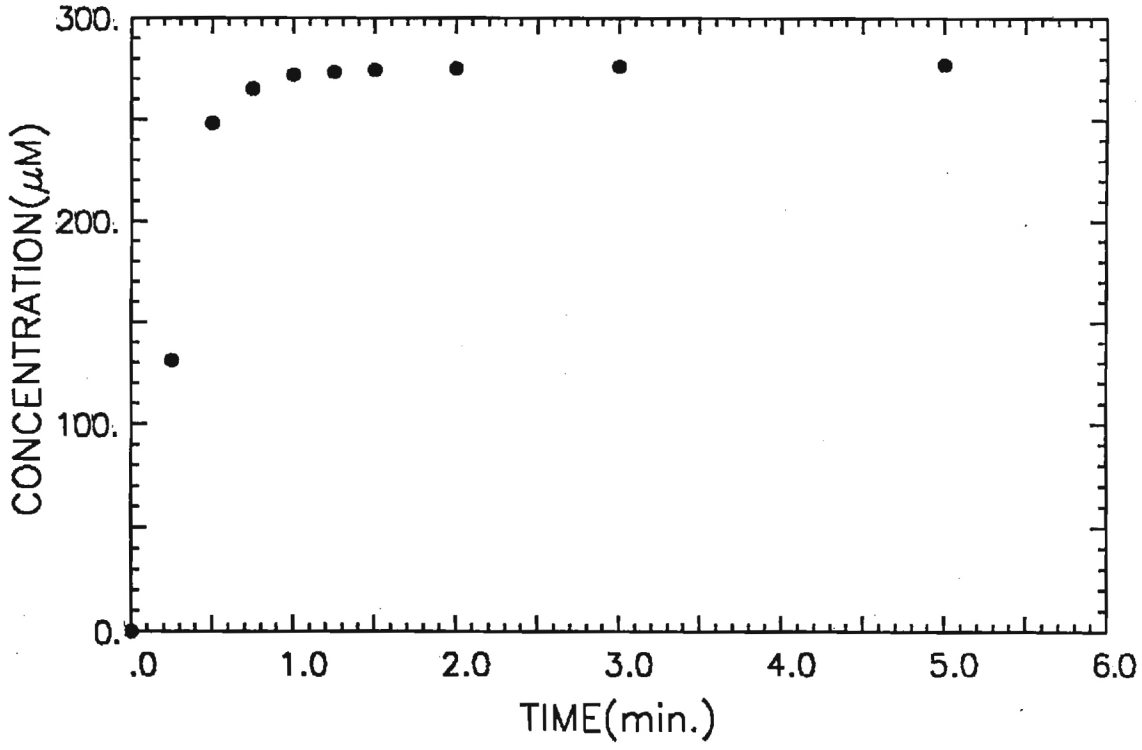

Figure A2-30. BATCH DESORPTION OF M.O. FROM XAD-16(4)

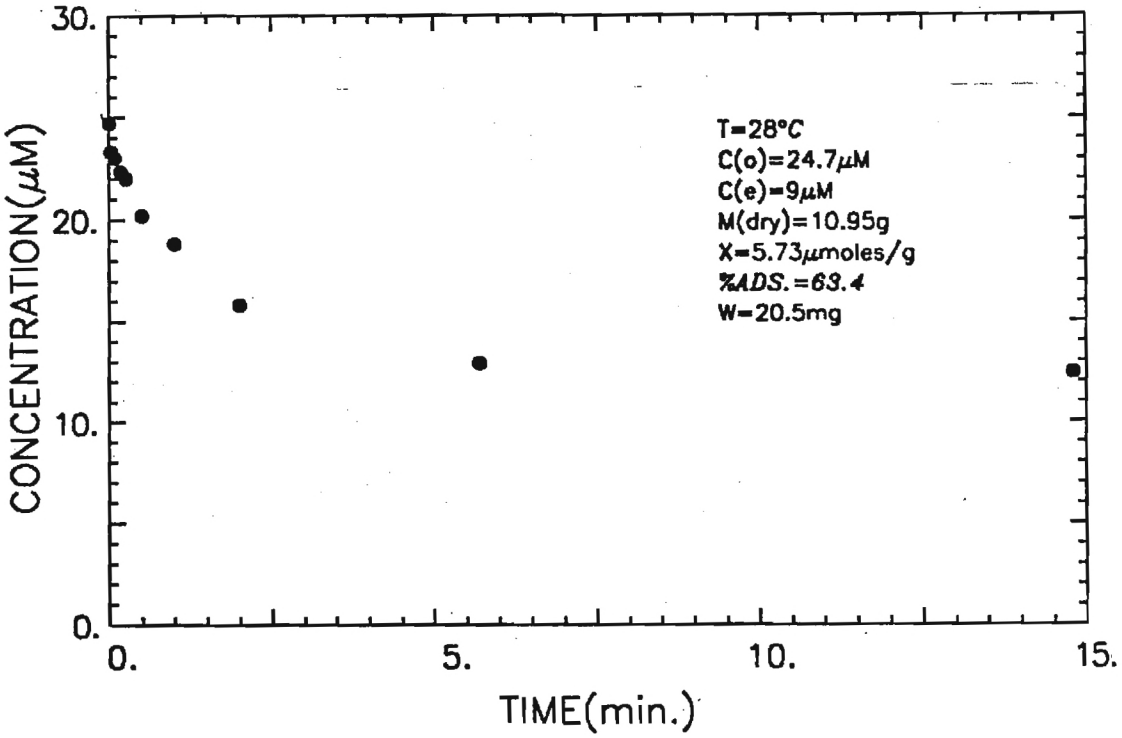

Figure A2-31. BATCH ADSORPTION OF M.O. ON S-761

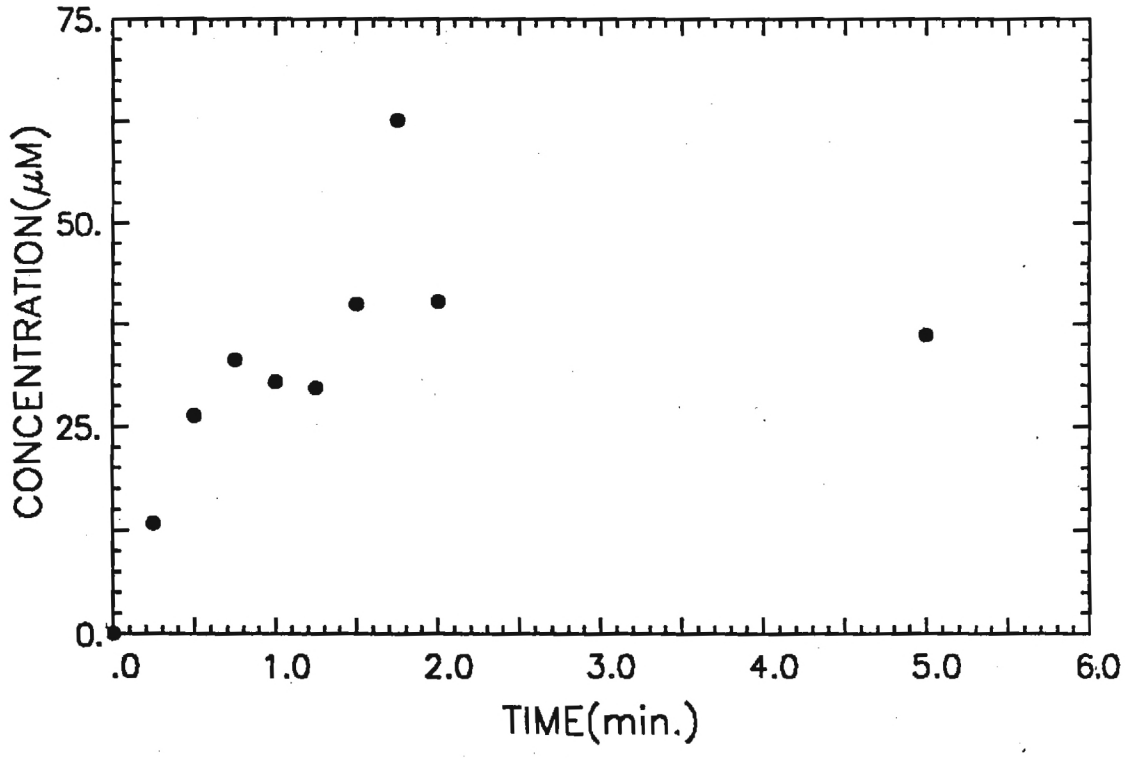

Figure A2-32. BATCH DESORPTION OF M.O. FROM S-761

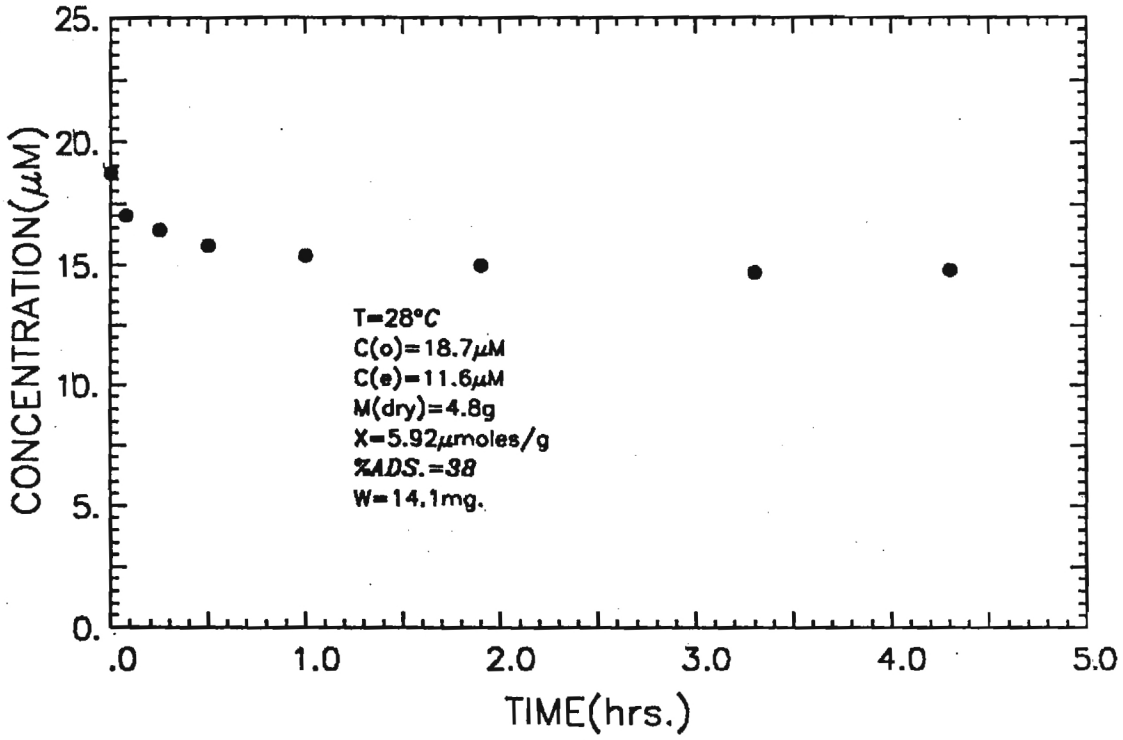

Figure A2-33. BATCH ADSORPTION OF R40 ON XAD-16(1)

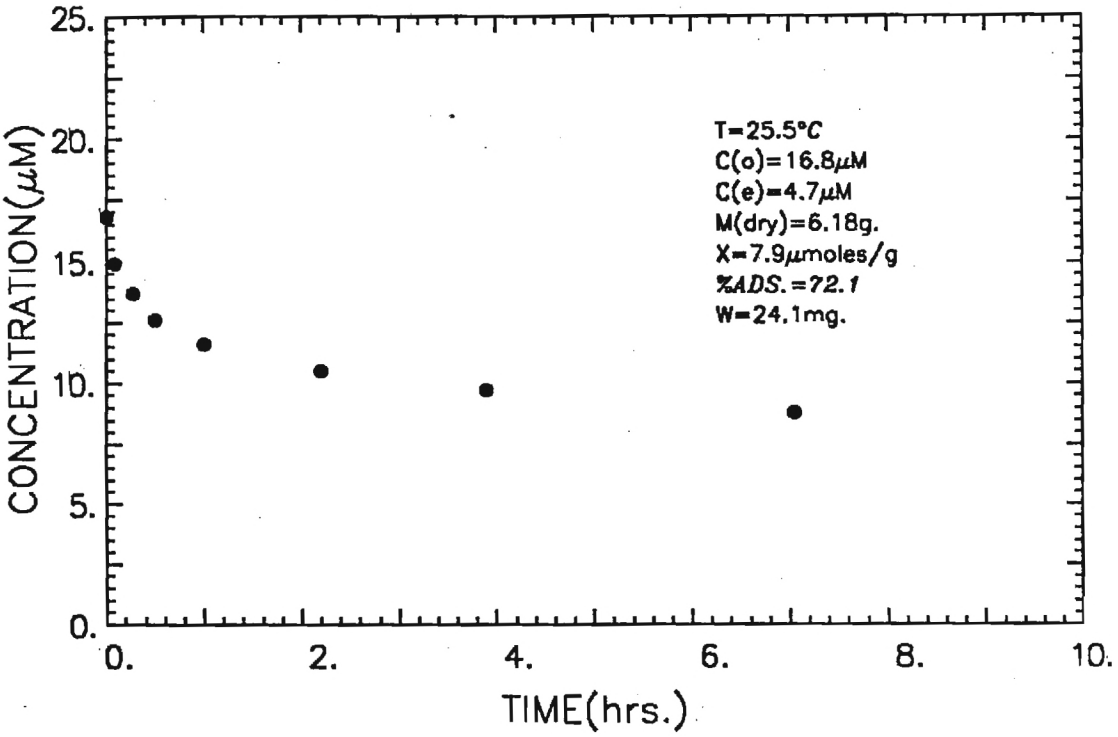

Figure A2-34. BATCH ADSORPTION OF R40 ON XAD-16(2)

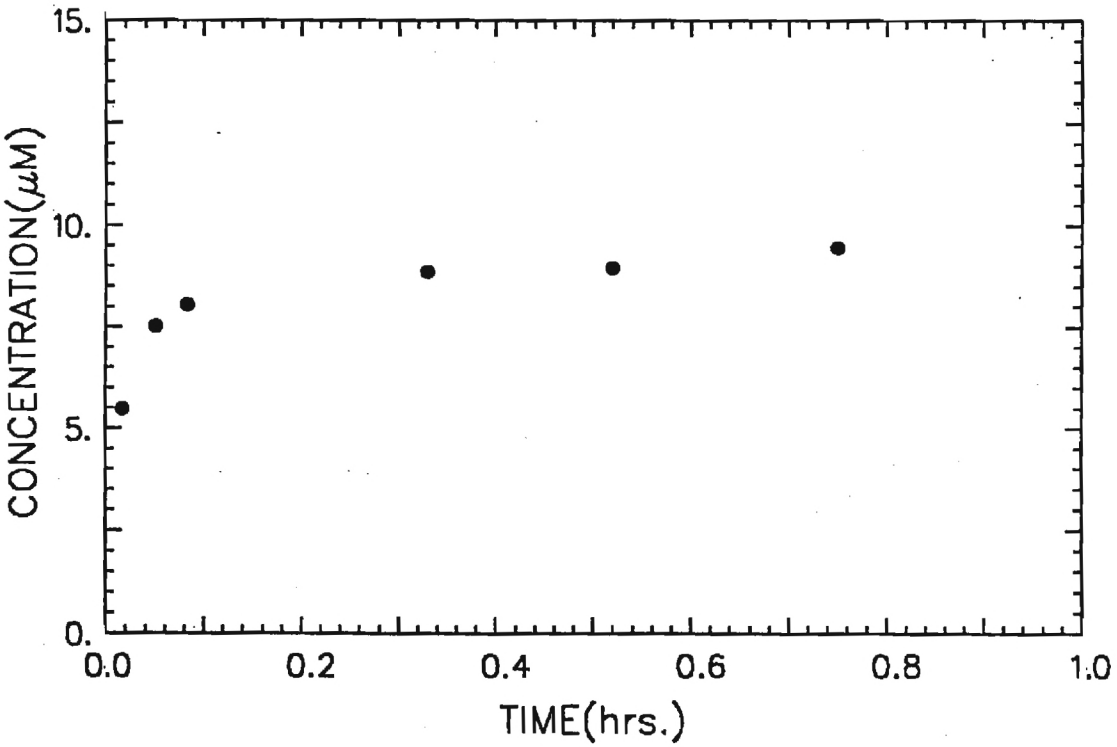

Figure A2-35 BATCH DESORPTION OF R40 FROM XAD-16(2)

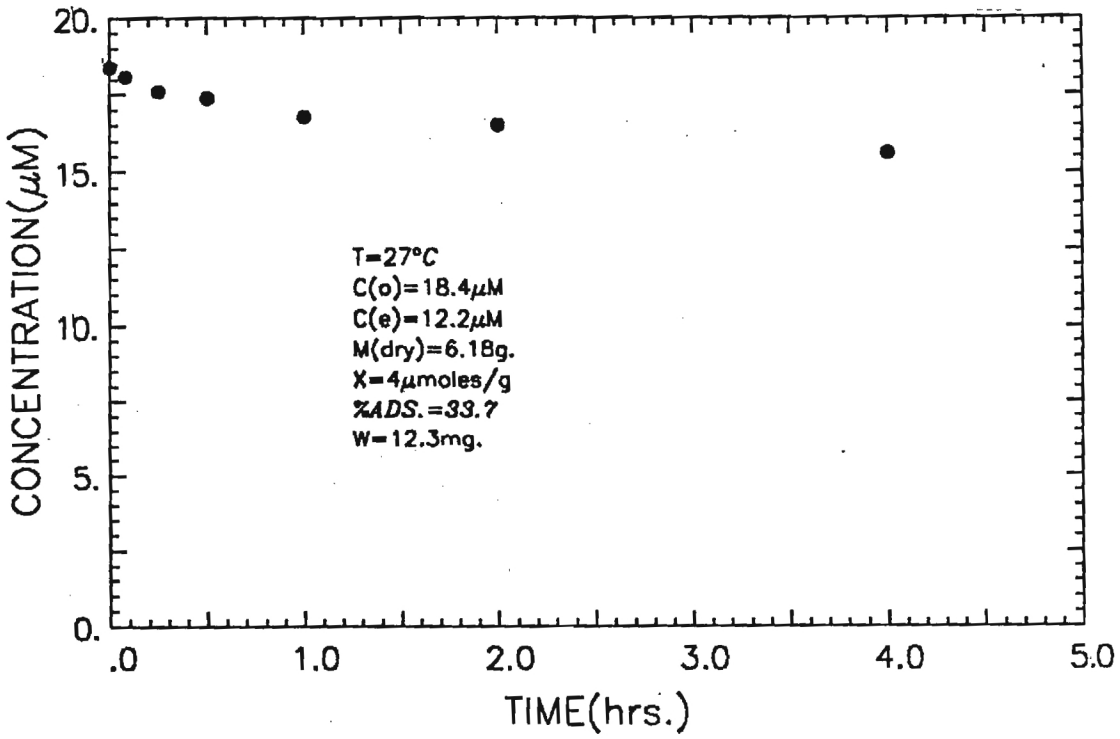

Figure A2-36. BATCH ADSORPTION OF R40 ON XAD-16(3)

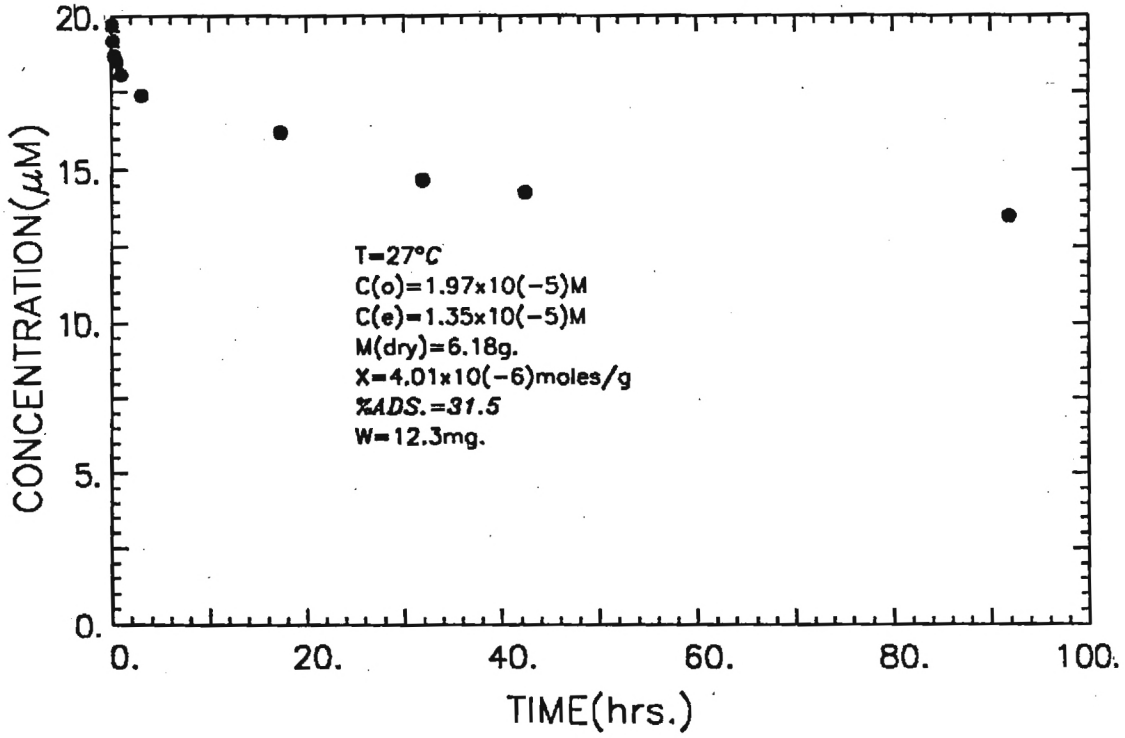

Figure A2-37. BATCH ADSORPTION OF R40 ON XAD-16(4)

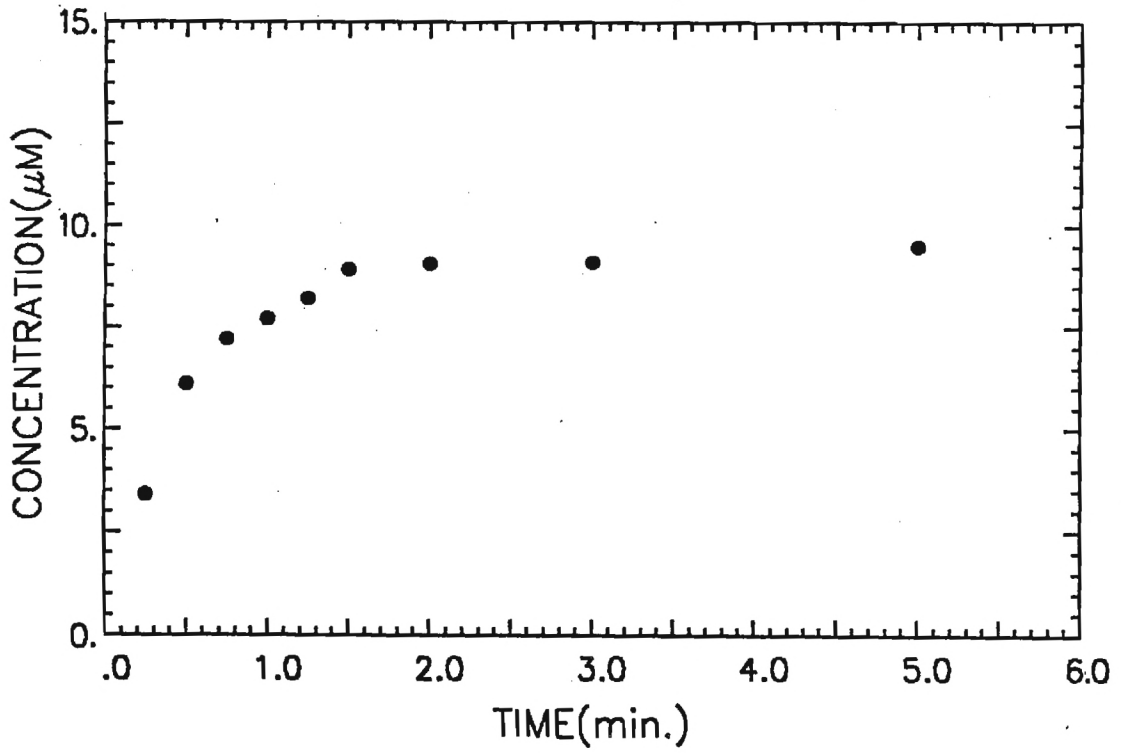

Figure A2-38. BATCH DESORPTION OF R40 FROM XAD-16(4)

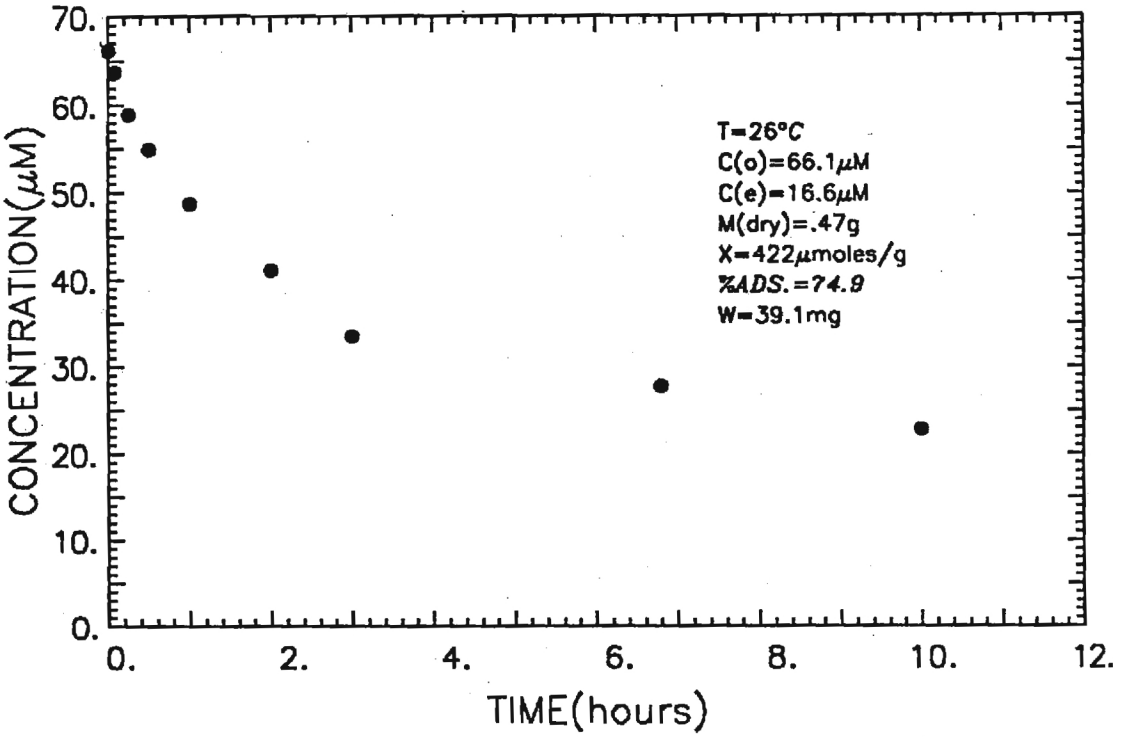

Figure A2-39. BATCH ADSORPTION OF 4-AAB ON XAD-7(1)

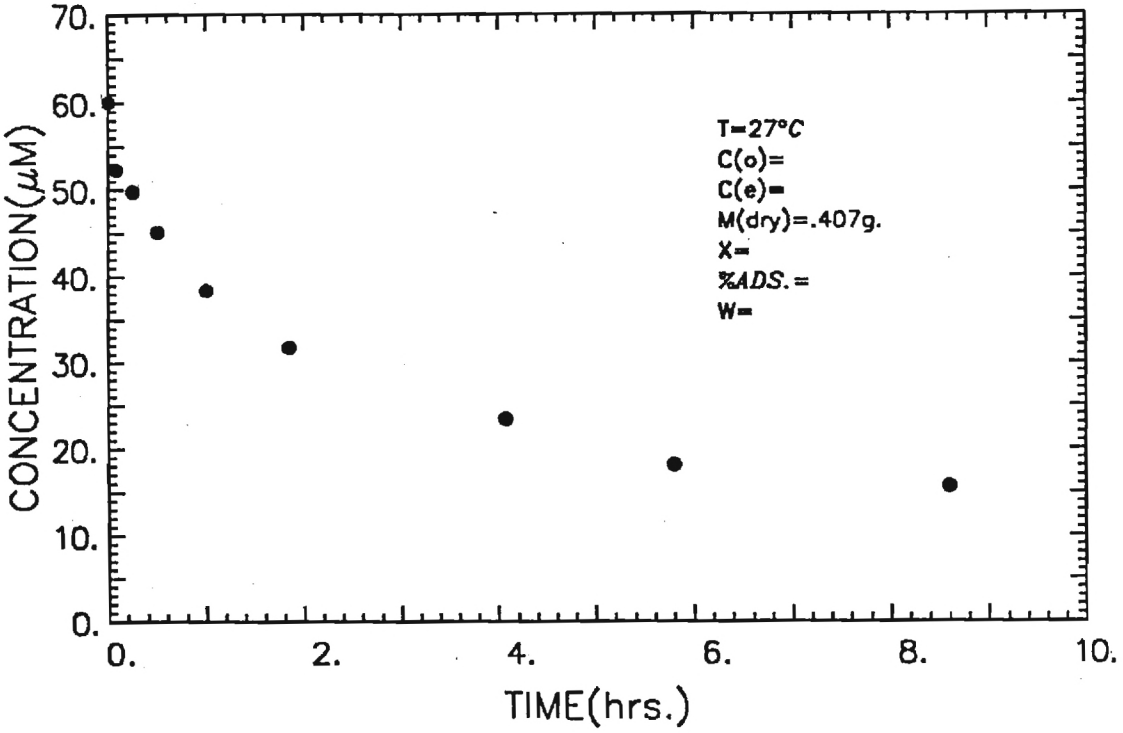

Figure A2-40. BATCH ADSORPTION OF 4AAB ON XAD-7(2)

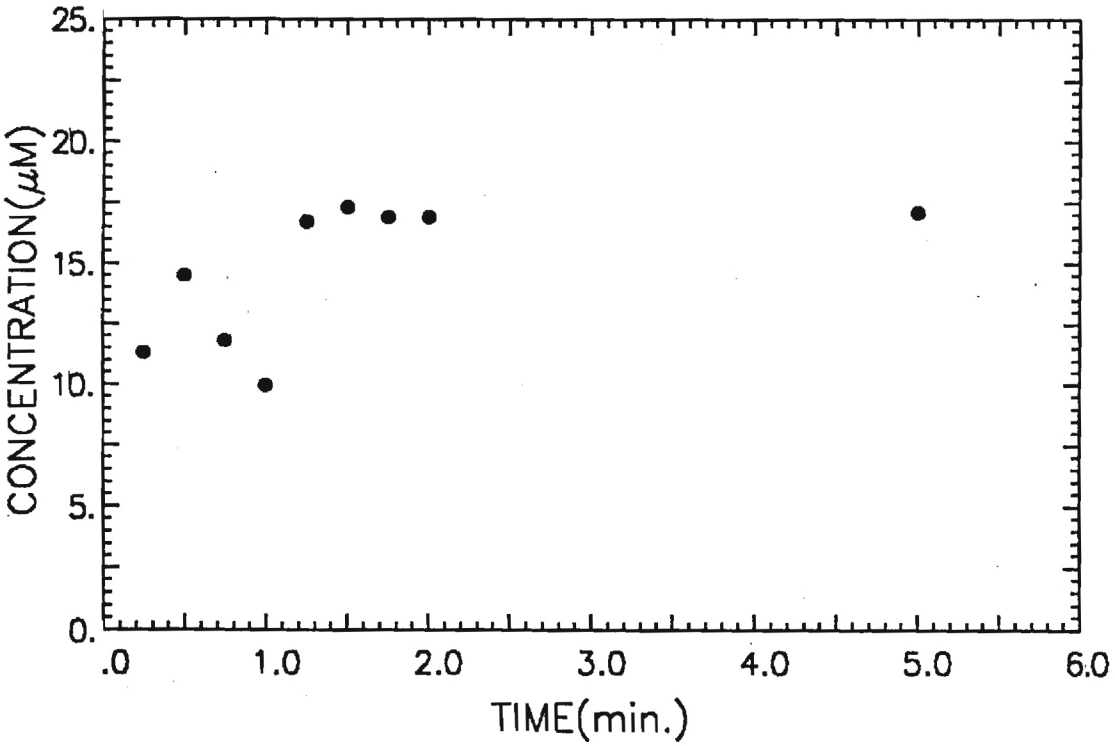

Figure A2-41.BATCH DESORPTION OF 4AAB FROM XAD-7(2)

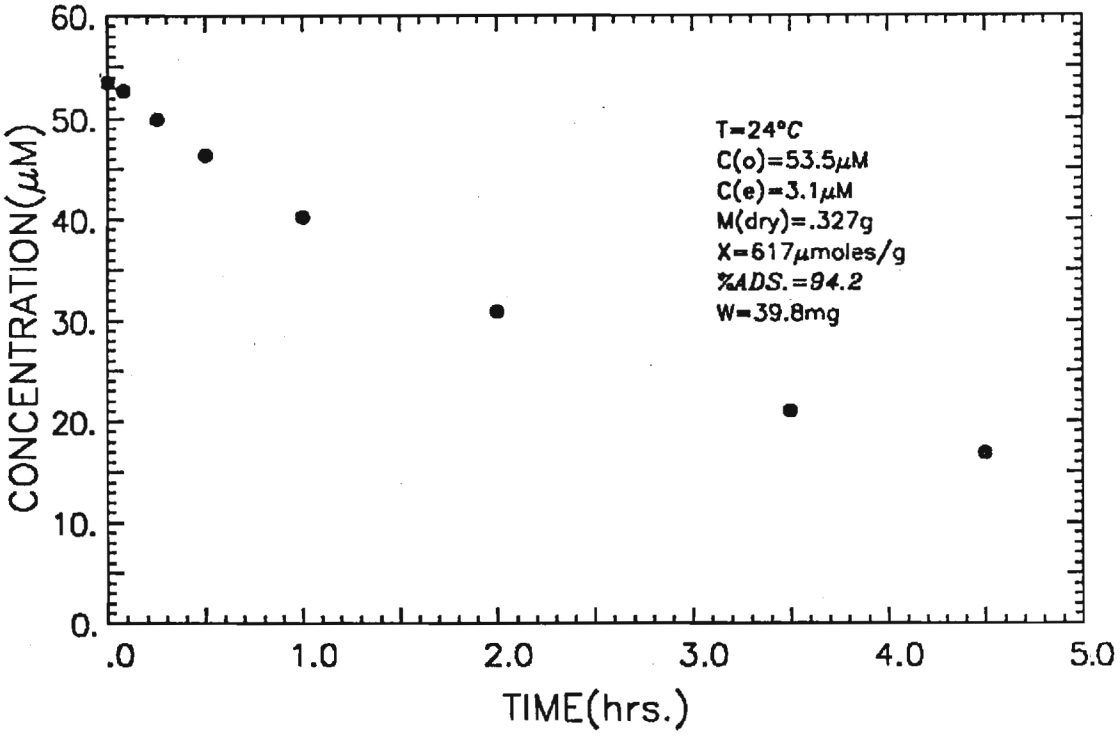

Figure A2-42. BATCH ADSORPTION OF 4-AAB ON XAD-16(1)

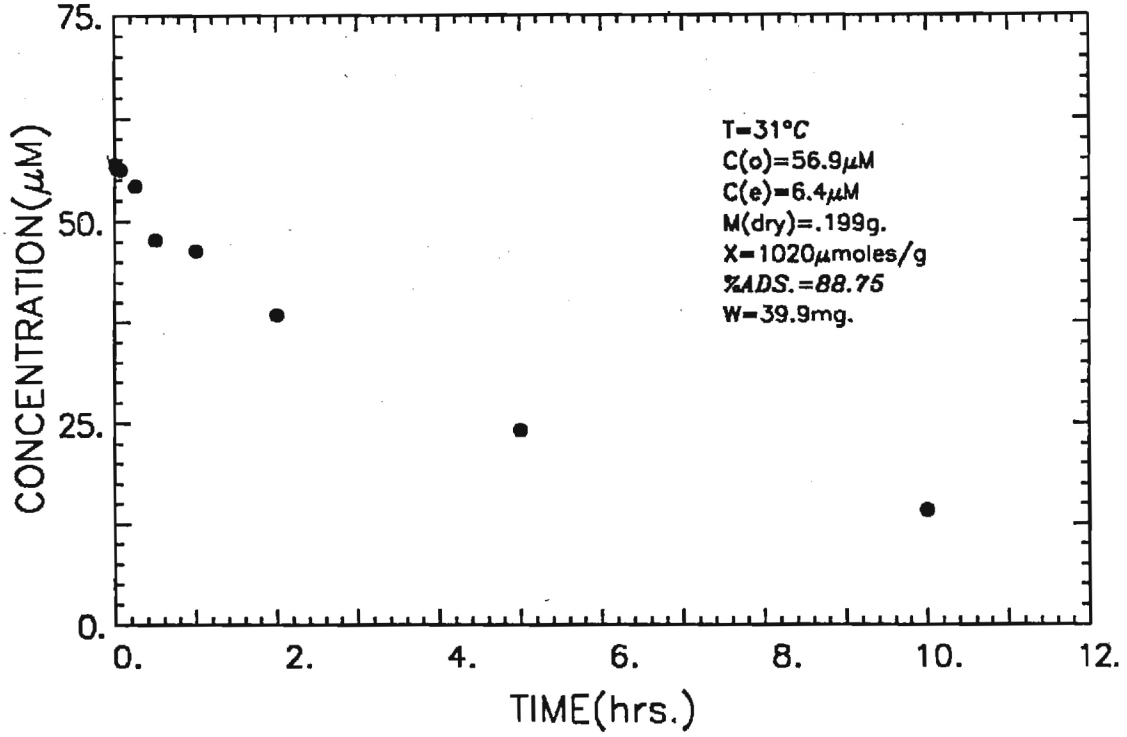

Figure A2-43. BATCH ADSORPTION OF 4AAB ON XAD-16(6)

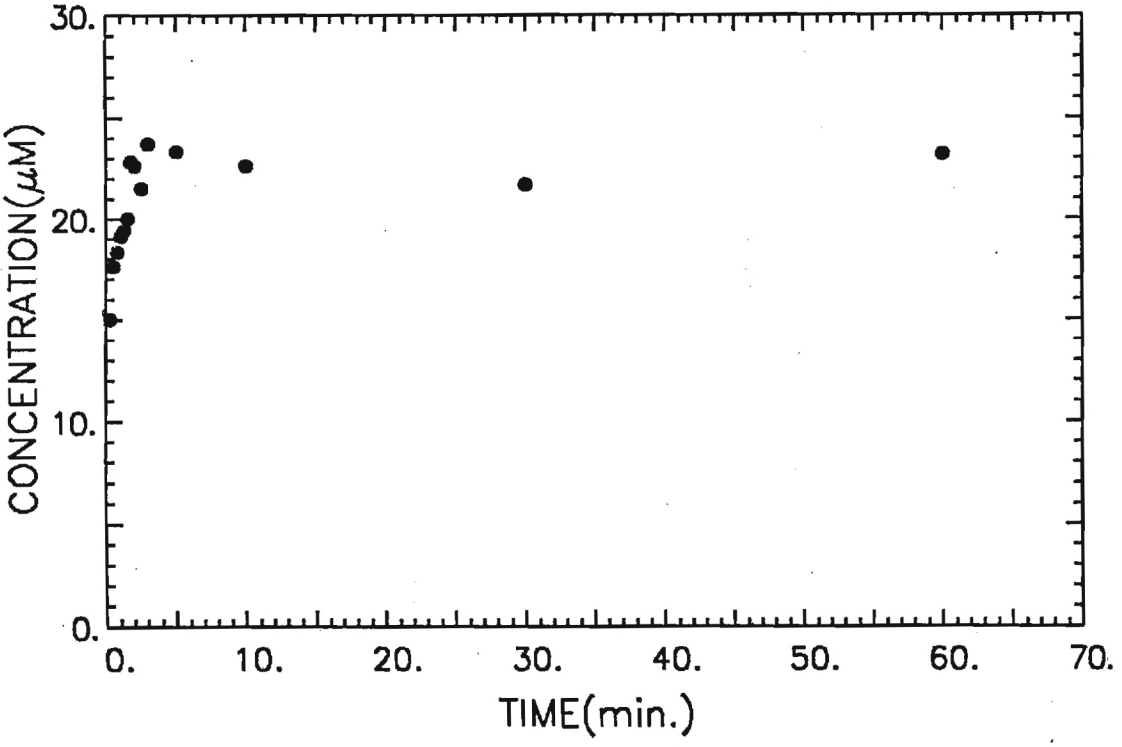

Figure A2-44. BATCH DESORPTION OF 4AAB FROM XAD-16(6)

APPENDIX 3

Column Kinetic Adsorption and Desorption Curves

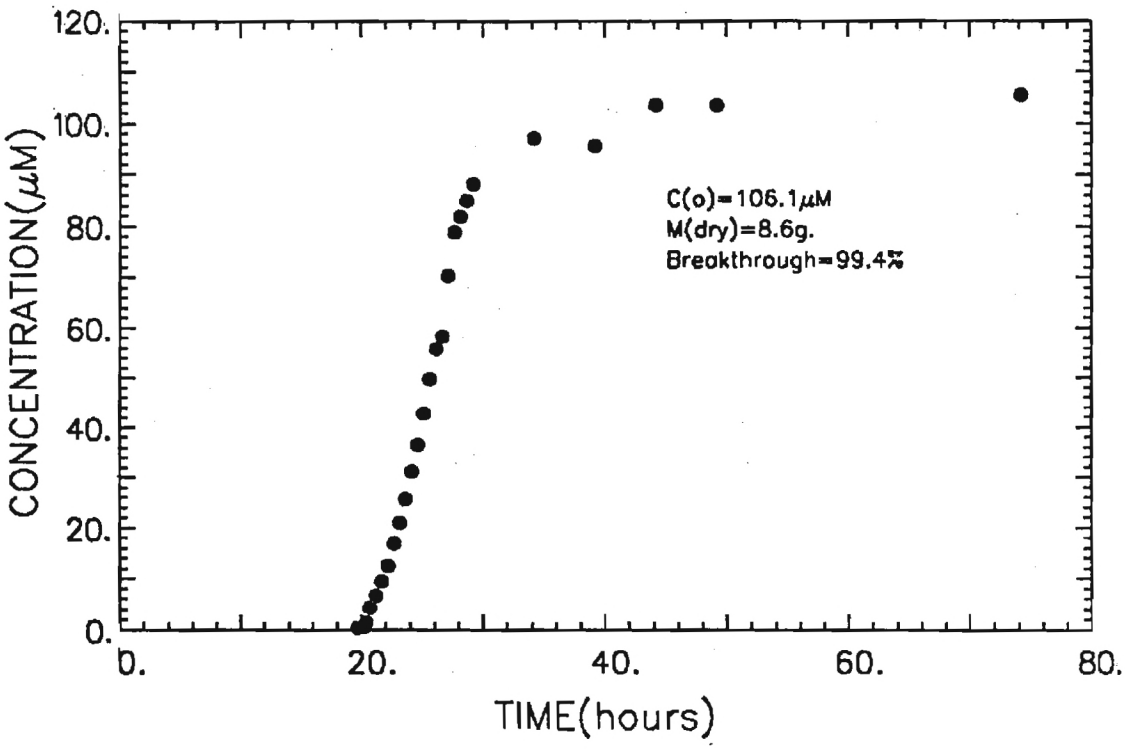

Figure A3-1. COLUMN ADSORPTION OF PNP ON XAD-16 (1)

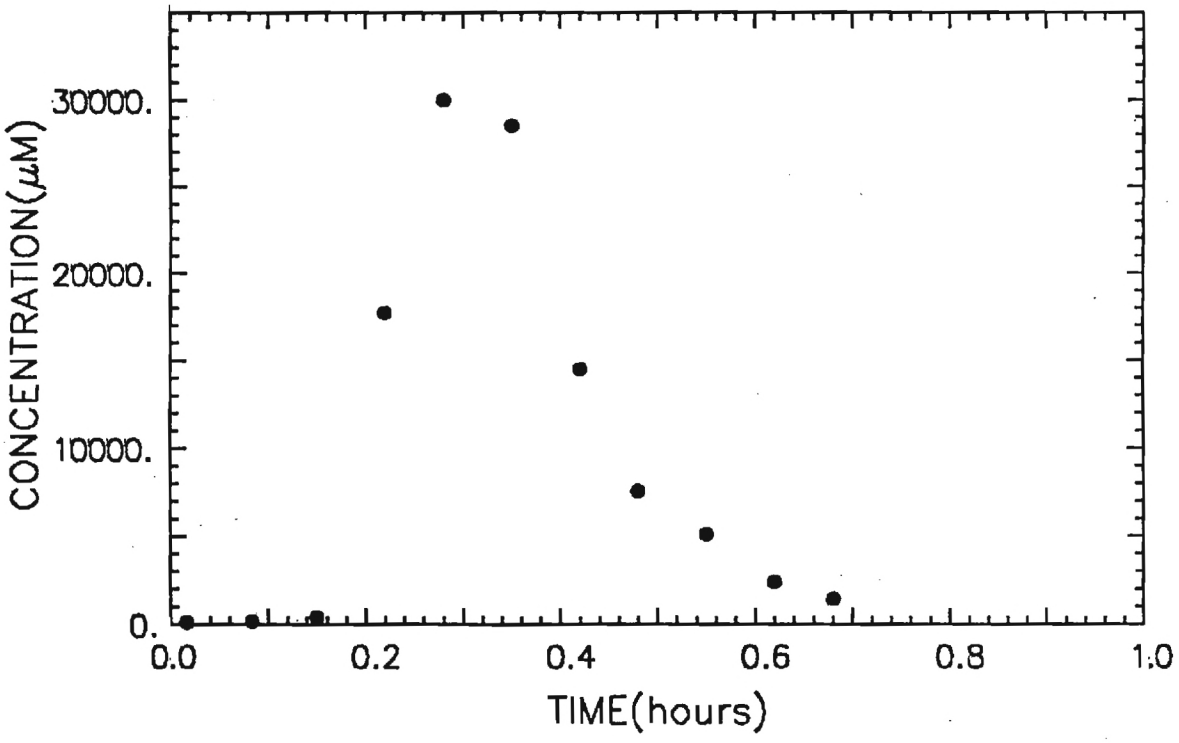

Figure A3-2. COLUMN DESORPTION OF PNP FROM XAD-16(1)

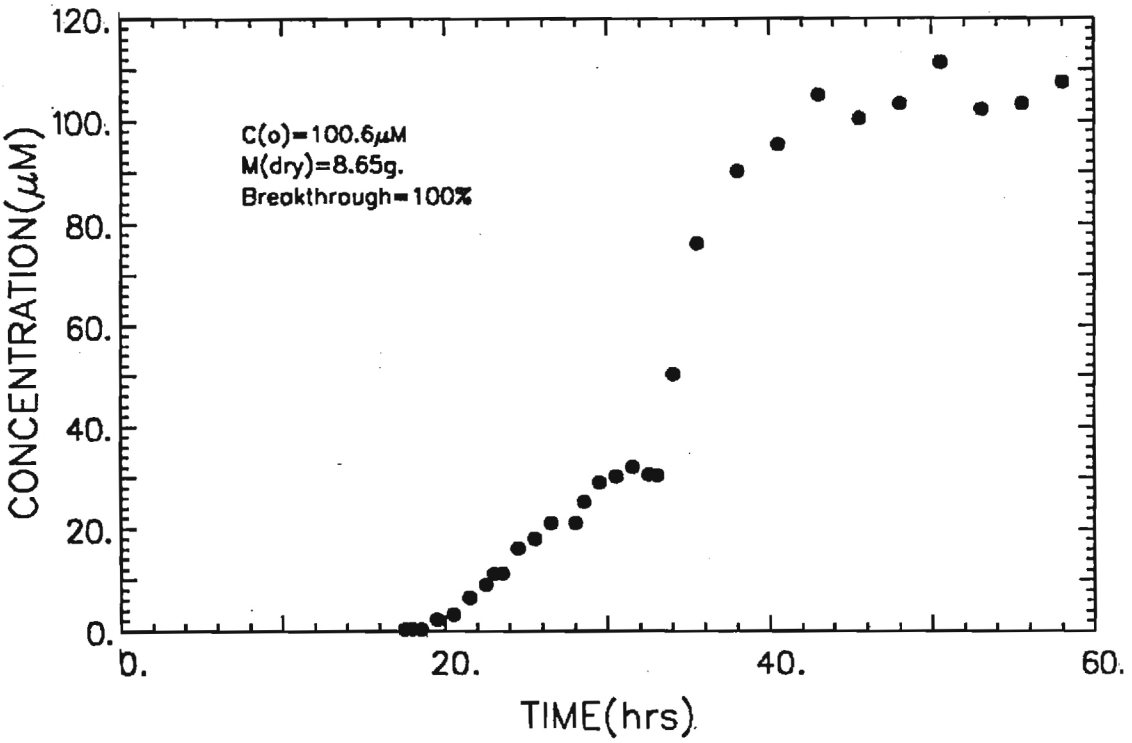

Figure A3-3. COLUMN ADSORPTION OF PNP ON XAD-16(2)

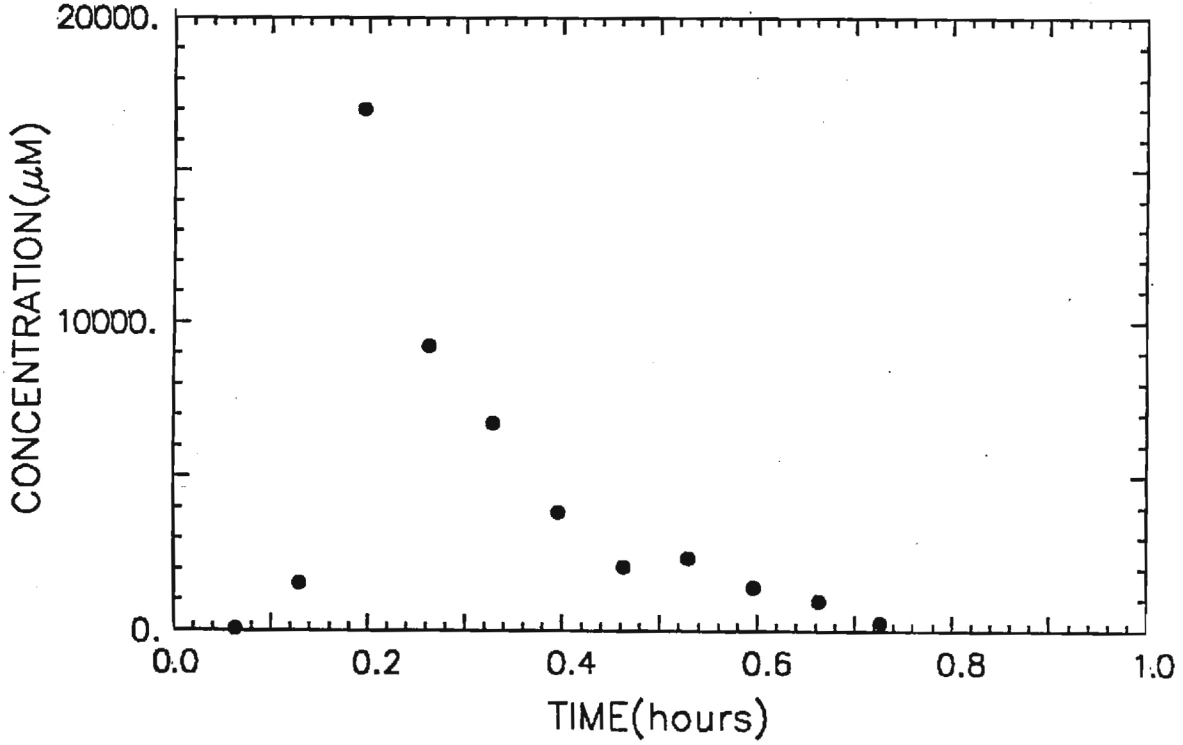

Figure A3-4. COLUMN DESORPTION OF PNP FROM XAD-16(2)

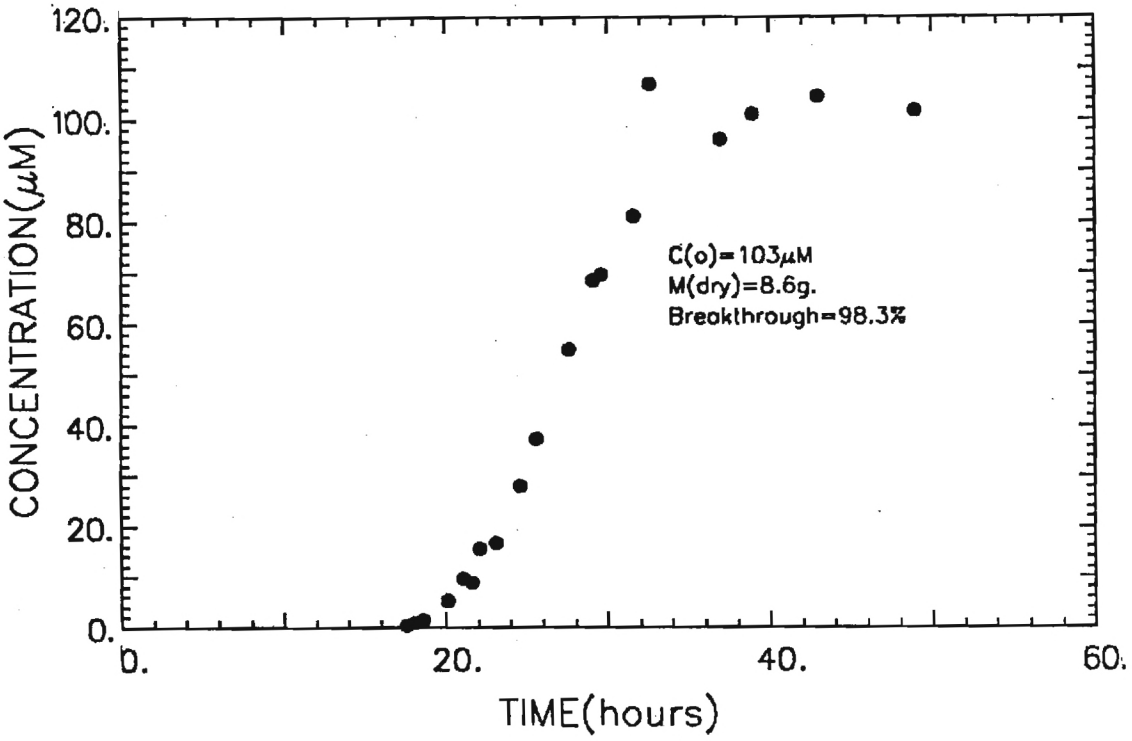

Figure A3-5. COLUMN ADSORPTION OF PNP ON XAD-16 (3)

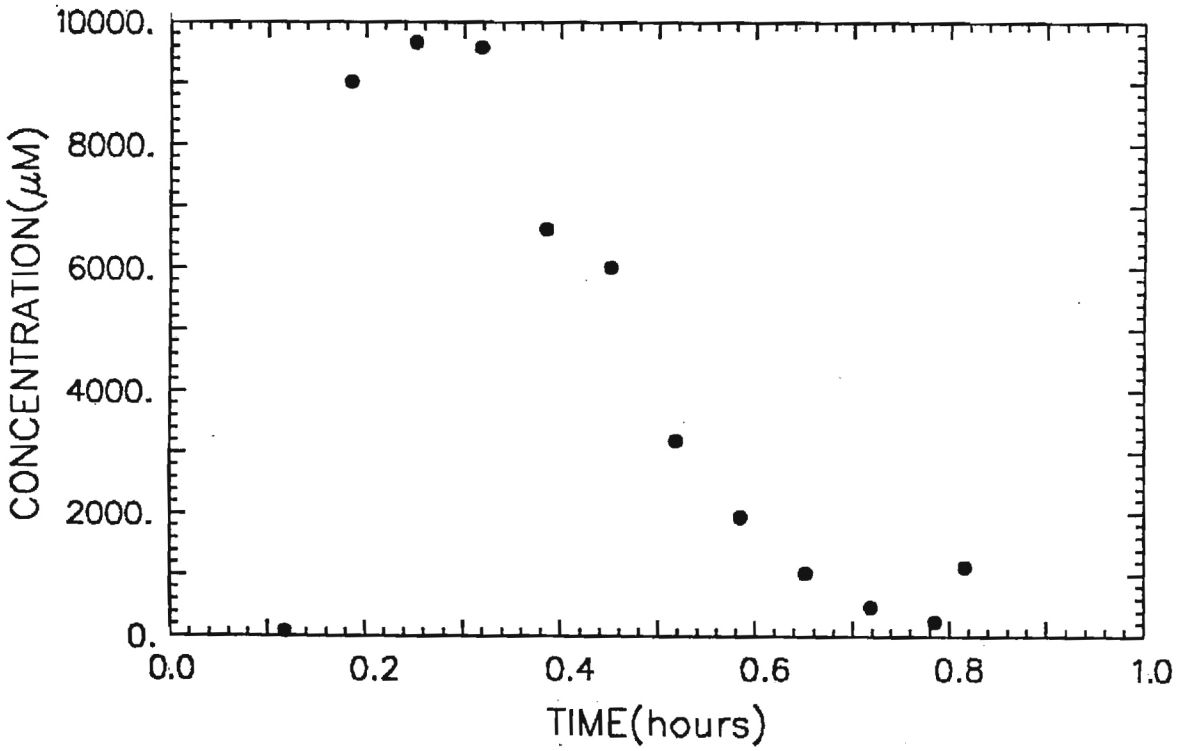

Figure A3-6. COLUMN DESORPTION OF PNP FROM XAD16(3)

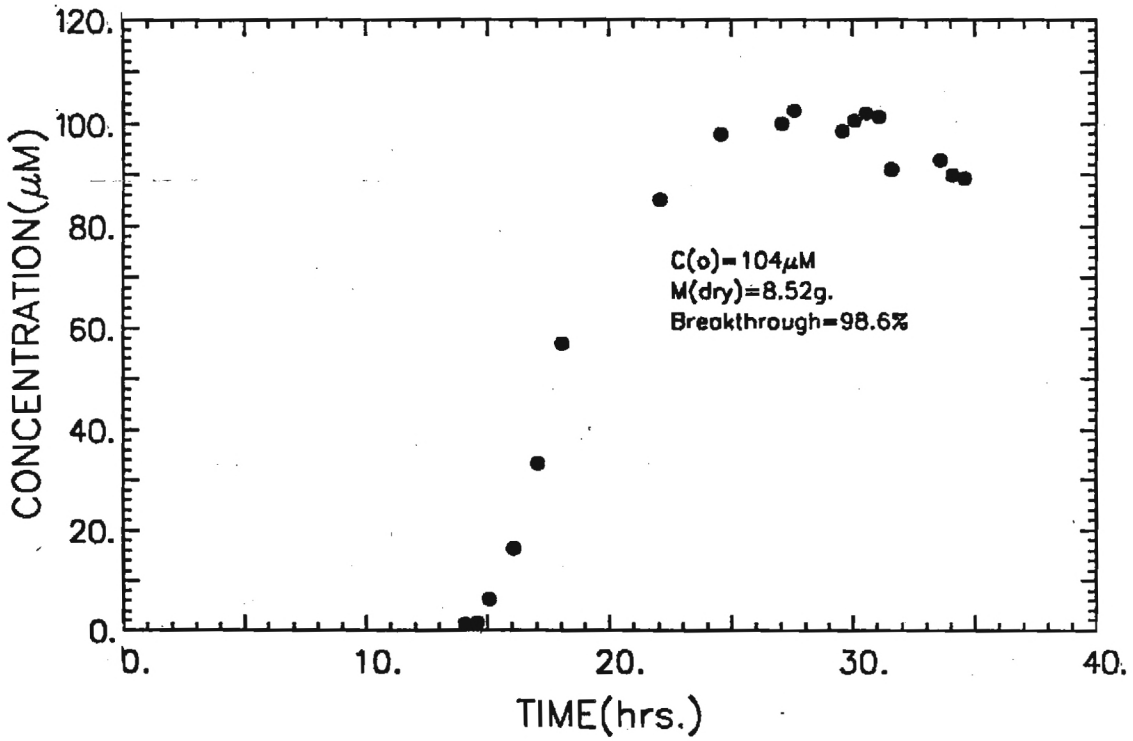

Figure A3-7. COLUMN ADSORPTION OF PNP ON XAD-16(4),pH=5

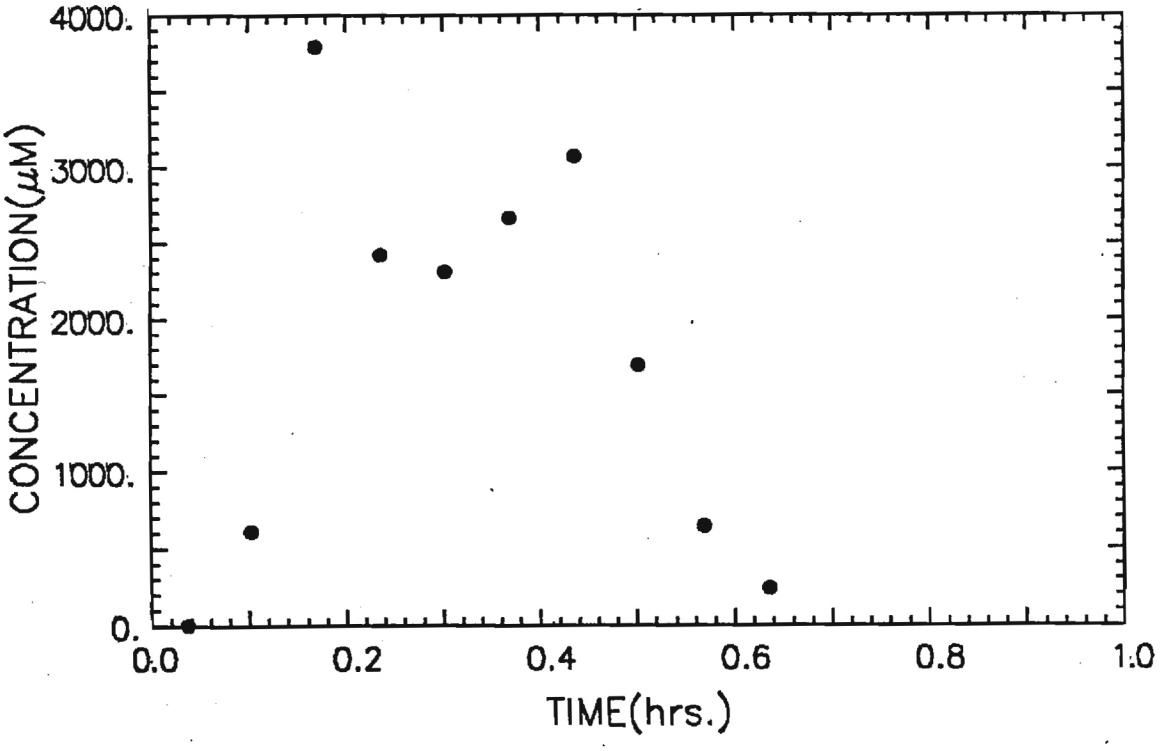

Figure A3-8. COLUMN DESORPTION OF PNP FROM XAD-16(4)

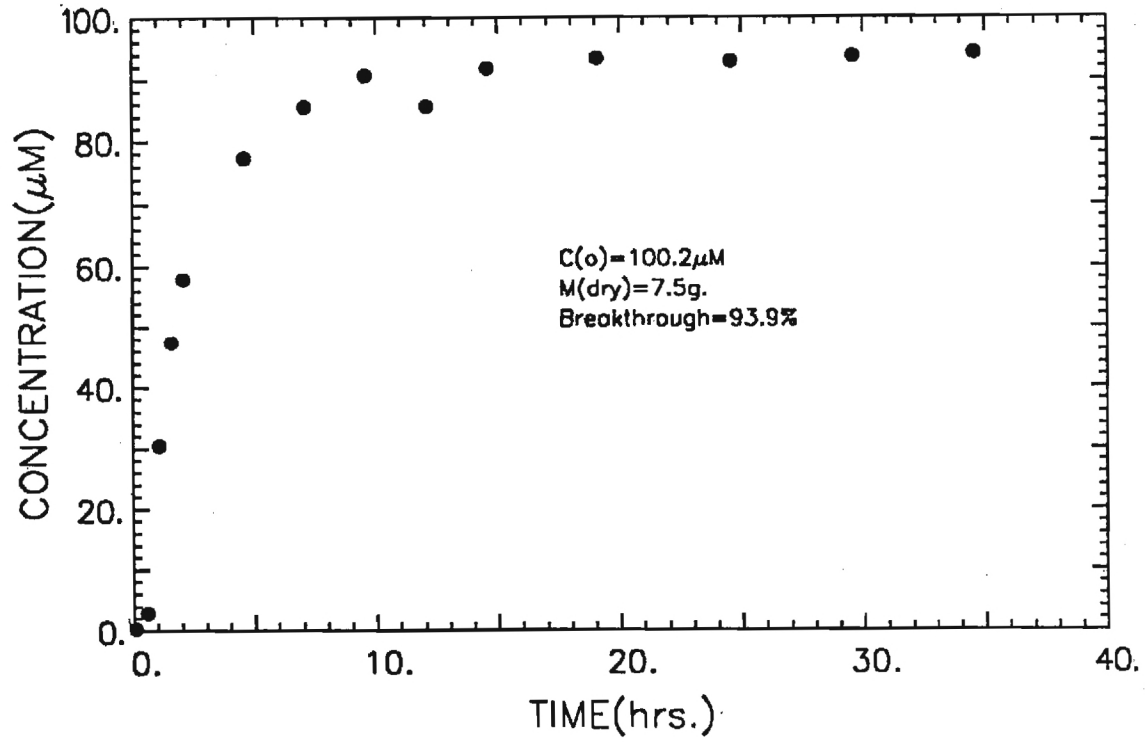

Figure A3-9. COLUMN ADSORPTION OF M.O. ON XAD-7

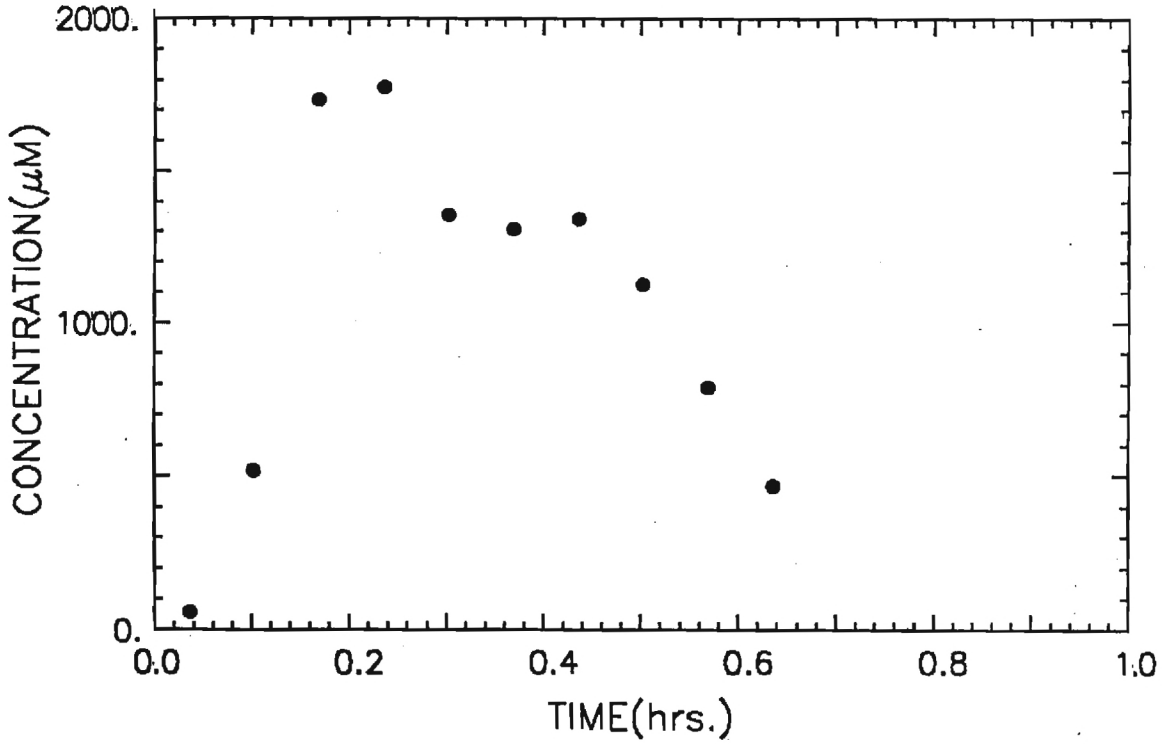

Figure A3-10. COLUMN DESORPTION OF M.O. FROM XAD-7

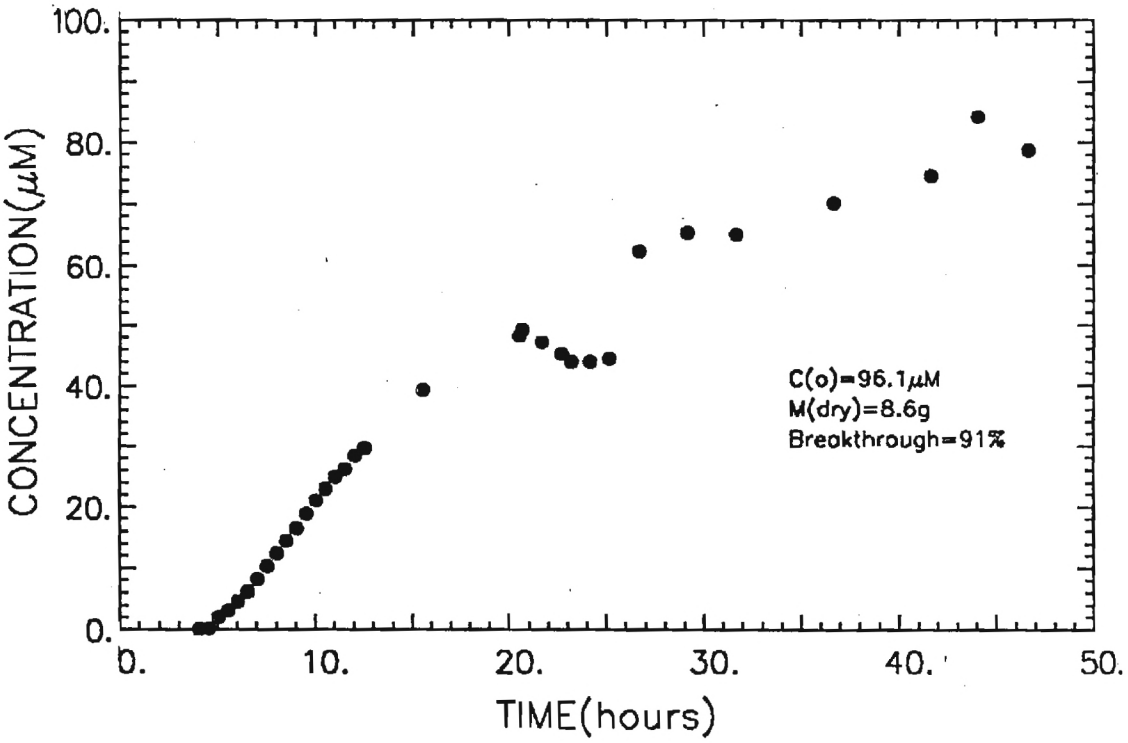

Figure A3-11. COLUMN ADSORPTION OF MO ON XAD-16 (1)

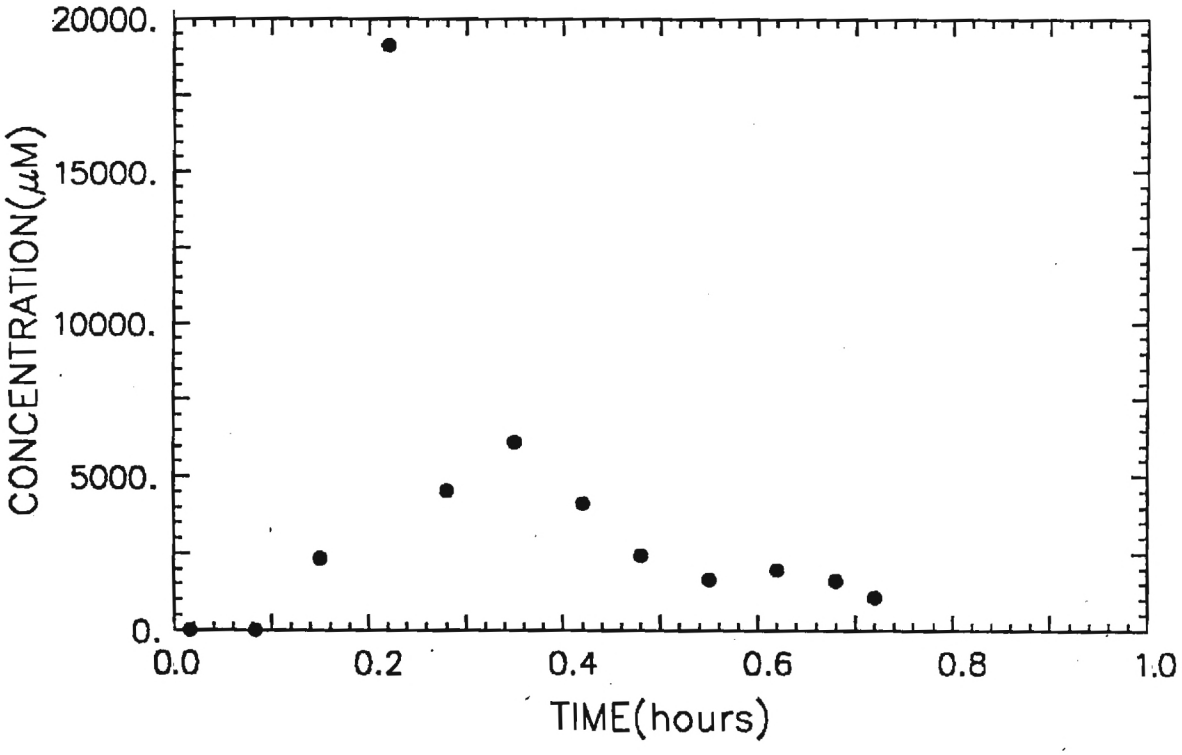

Figure A3-12. COLUMN DESORPTION OF M.O. FORM XAD-16(1)

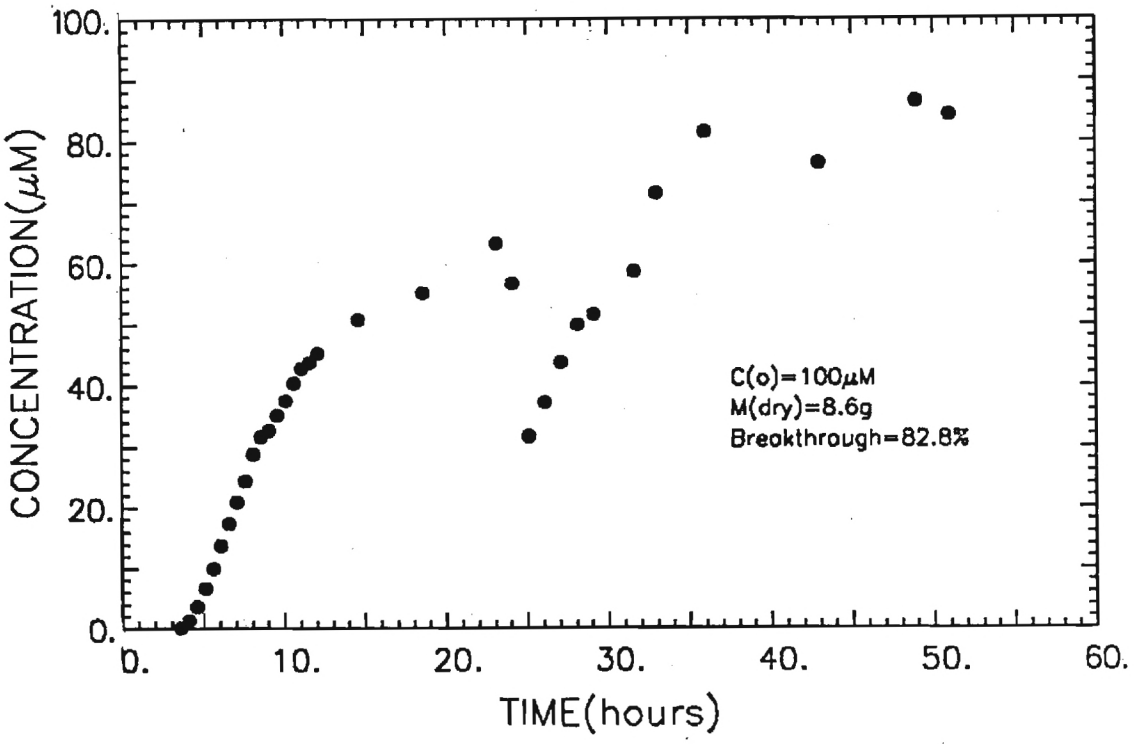

Figure A3-13. COLUMN ADSORPTION OF MO ON XAD-16(2)

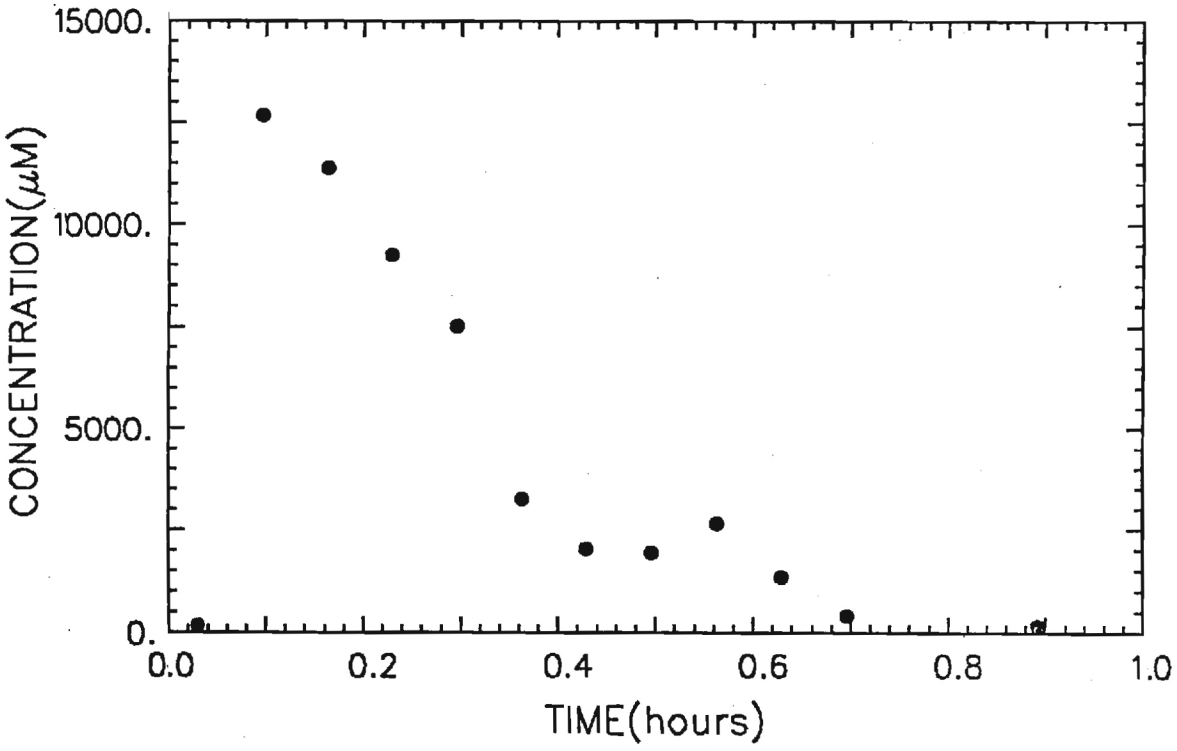

Figure A3-14. COLUMN DESORPTION OF M.O. FROM XAD-16(2)

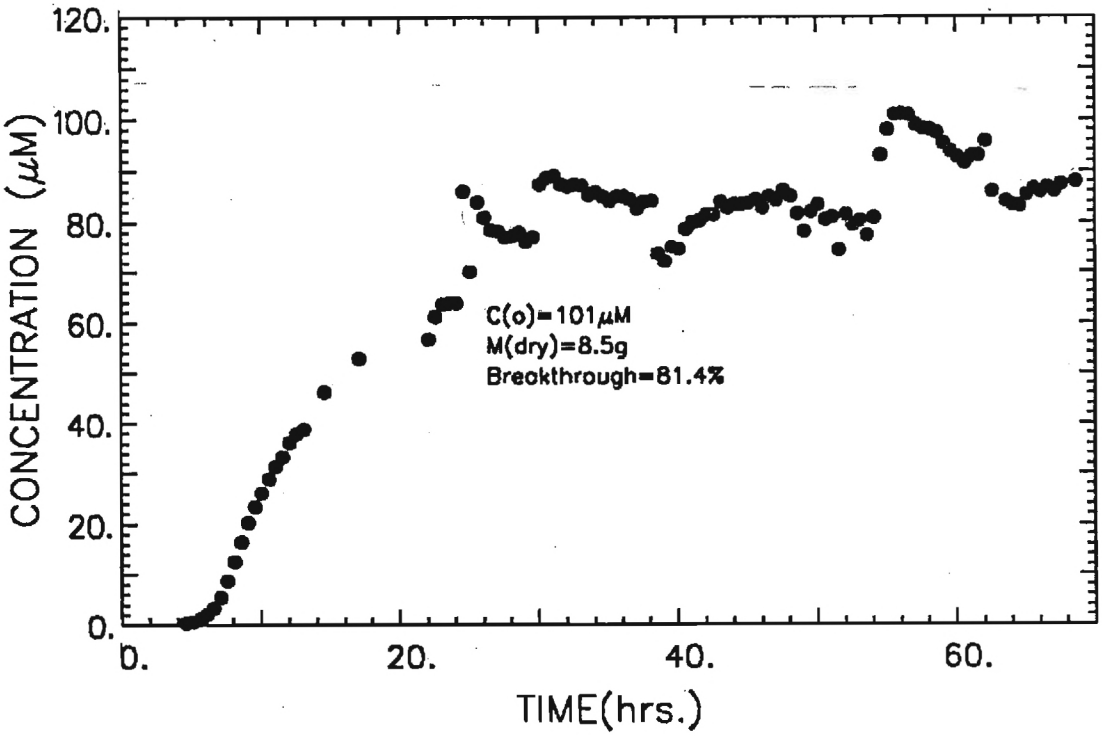

Figure A3-15. COLUMN ADSORPTION OF M.O. ON XAD-16(3)

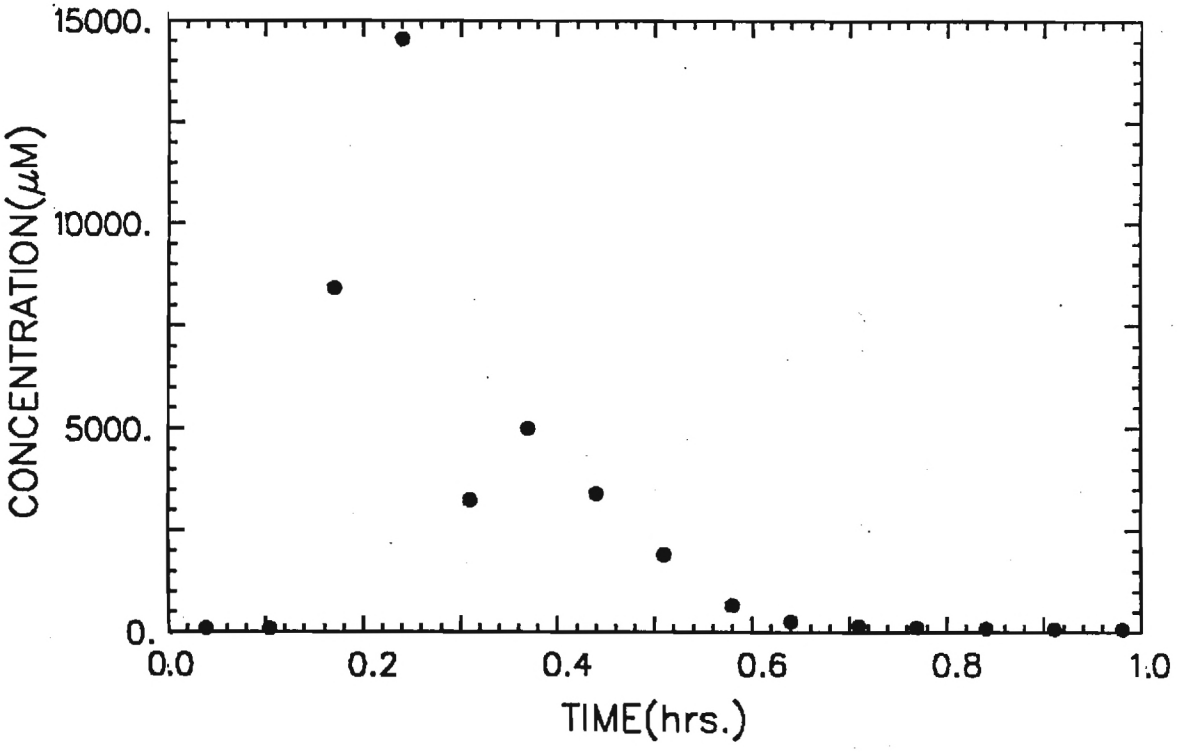

Figure A3-16. COLUMN DESORPTION OF M.O. FROM XAD-16(3)

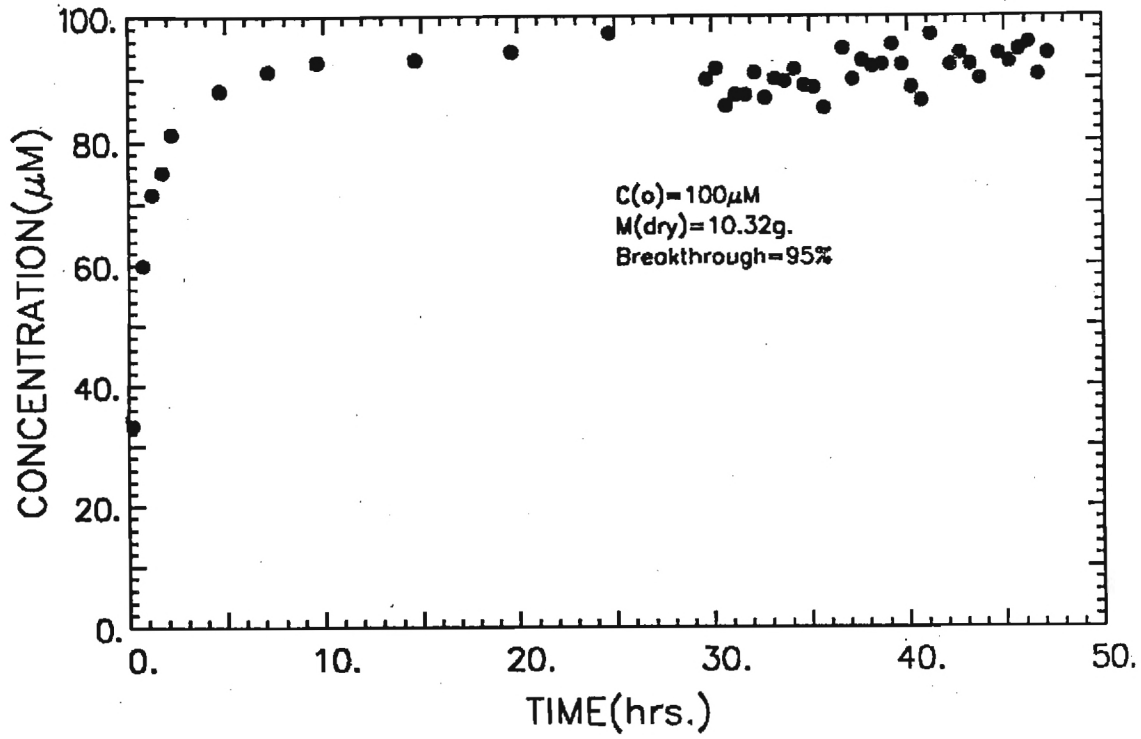

Figure A3-17. COLUMN ADSORPTION OF M.O. ON S-761

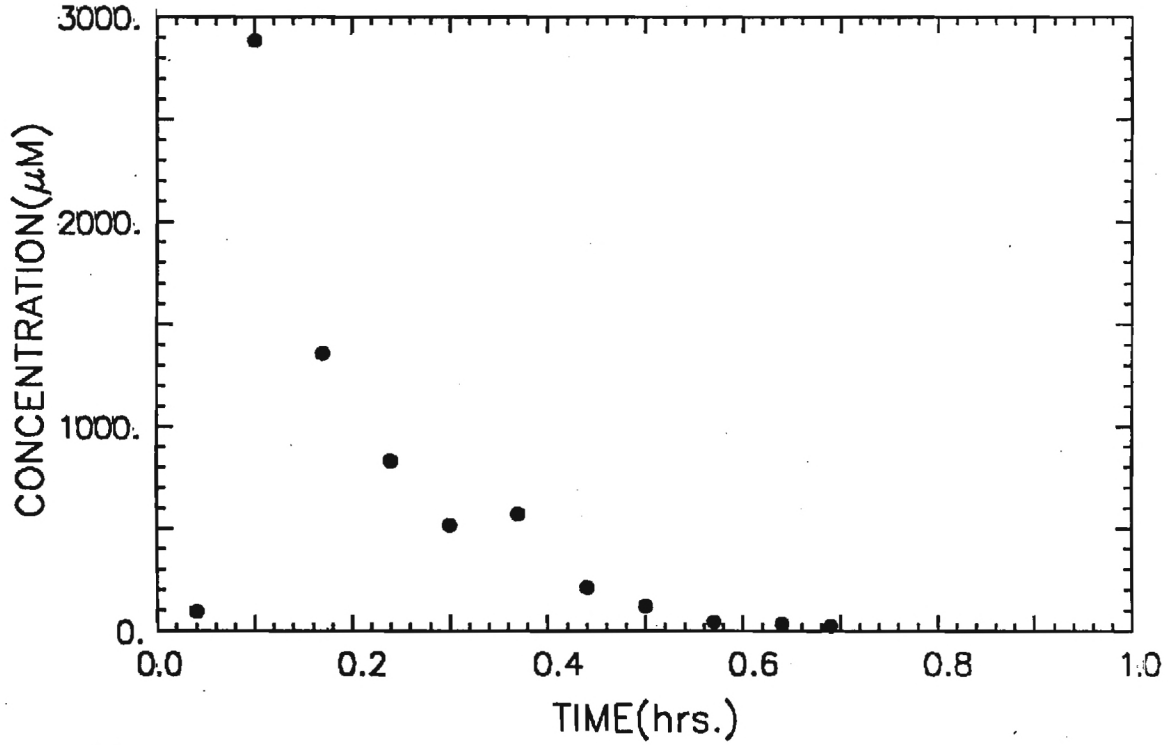

Figure A3-18. COLUMN DESORPTION OF M.O. FROM S-761

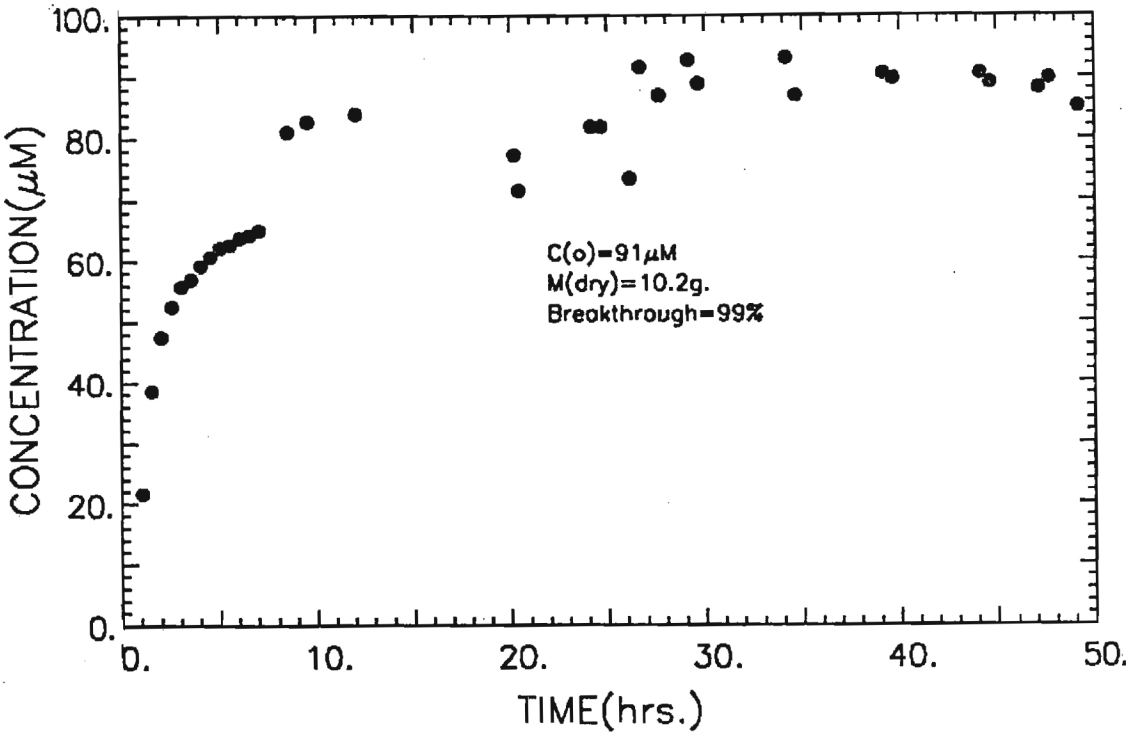

Figure A3-19. COLUMN ADSORPTION OF R40 ON XAD-16(1)

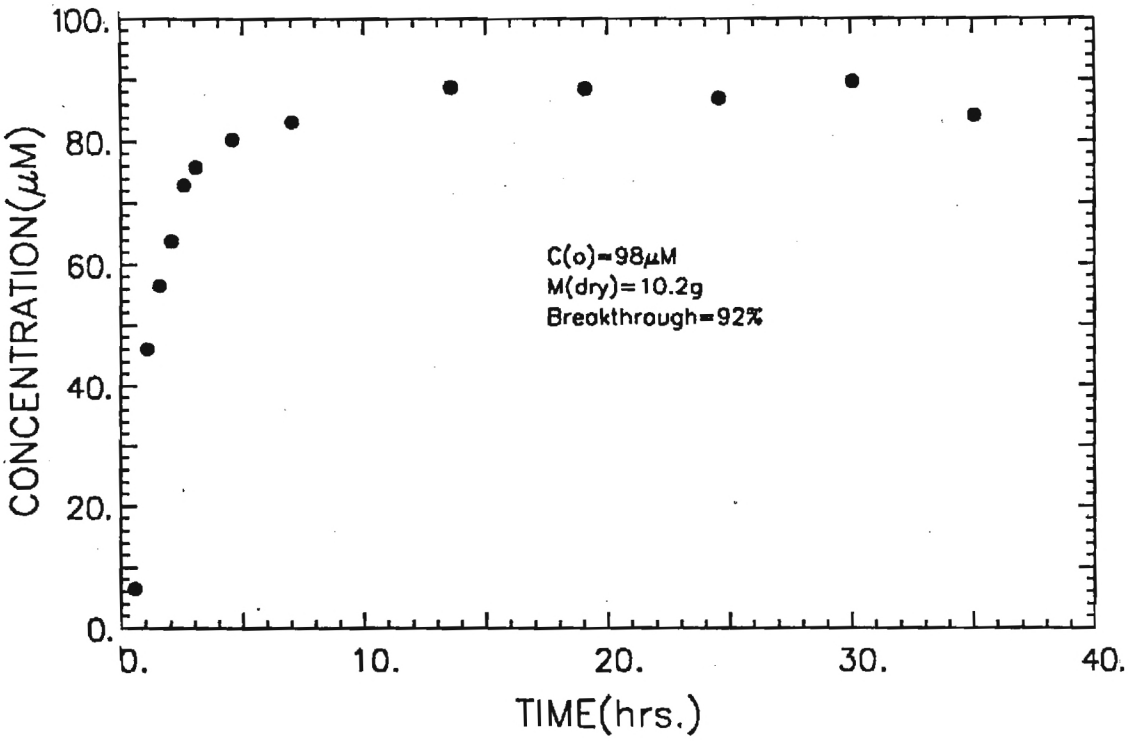

Figure A3-20. COLUMN ADSORPTION OF R40 ON XAD-16(2)

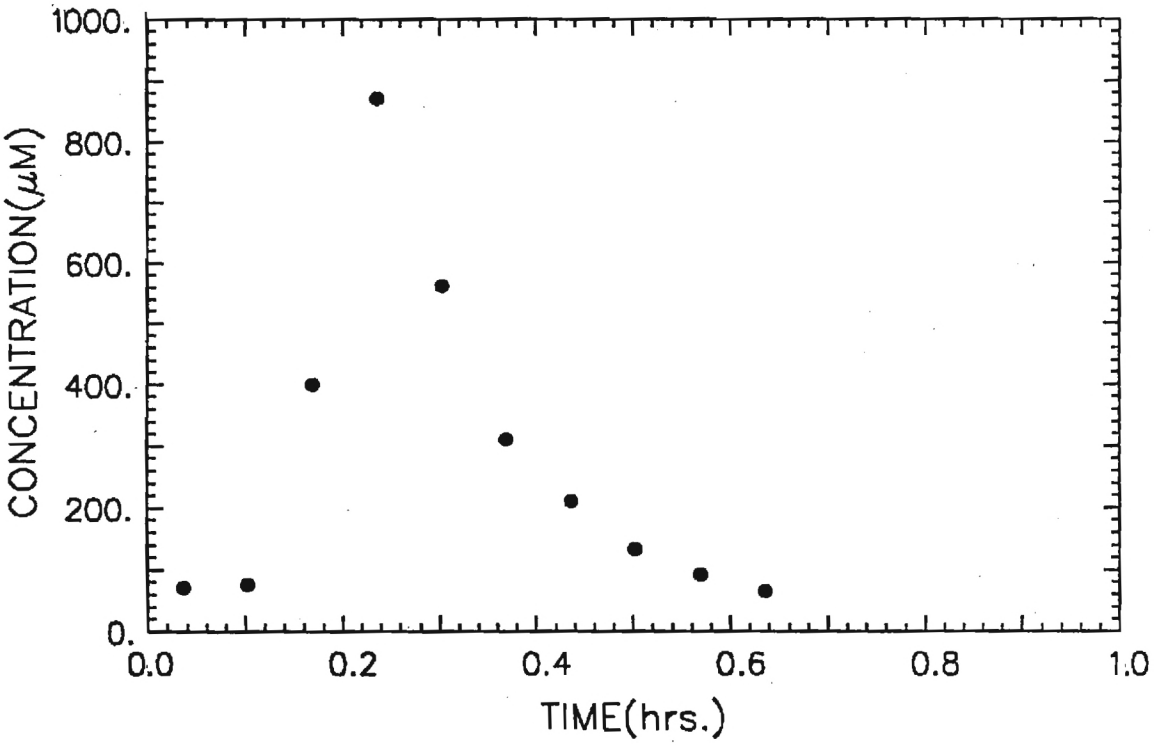

Figure A3-21. COLUMN DESORPTION OF R40 FROM XAD-16(2)

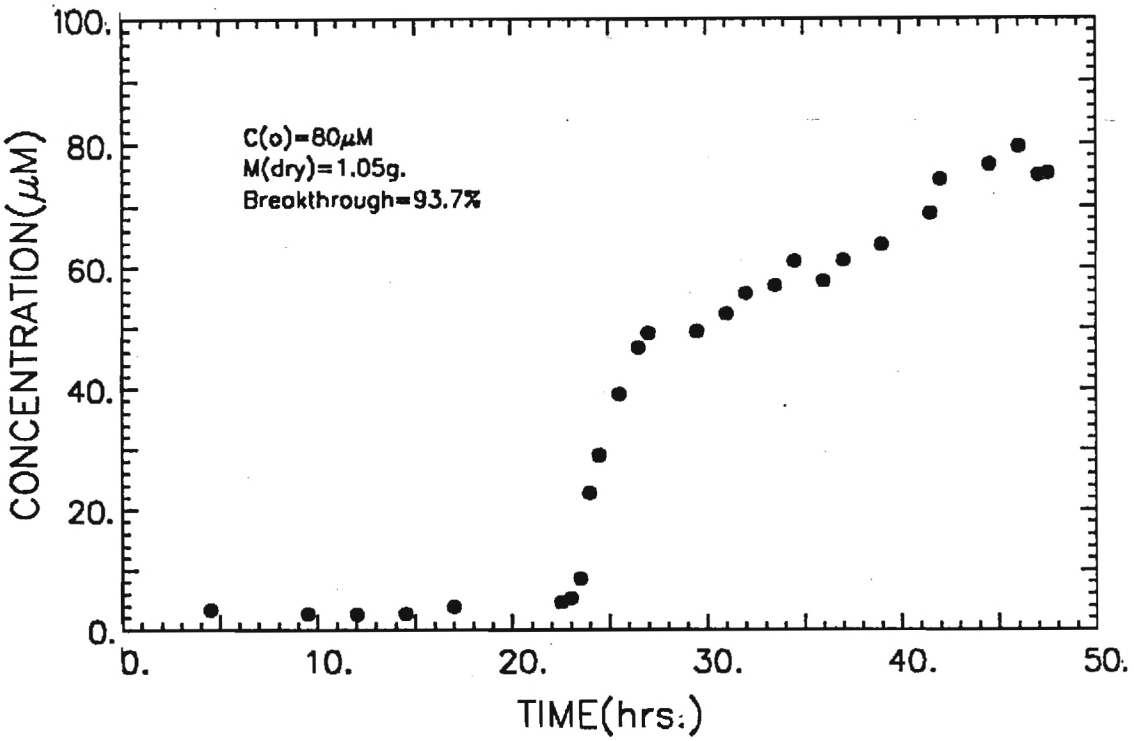

Figure A3-22. COLUMN ADSORPTION OF 4AAB ON XAD-7

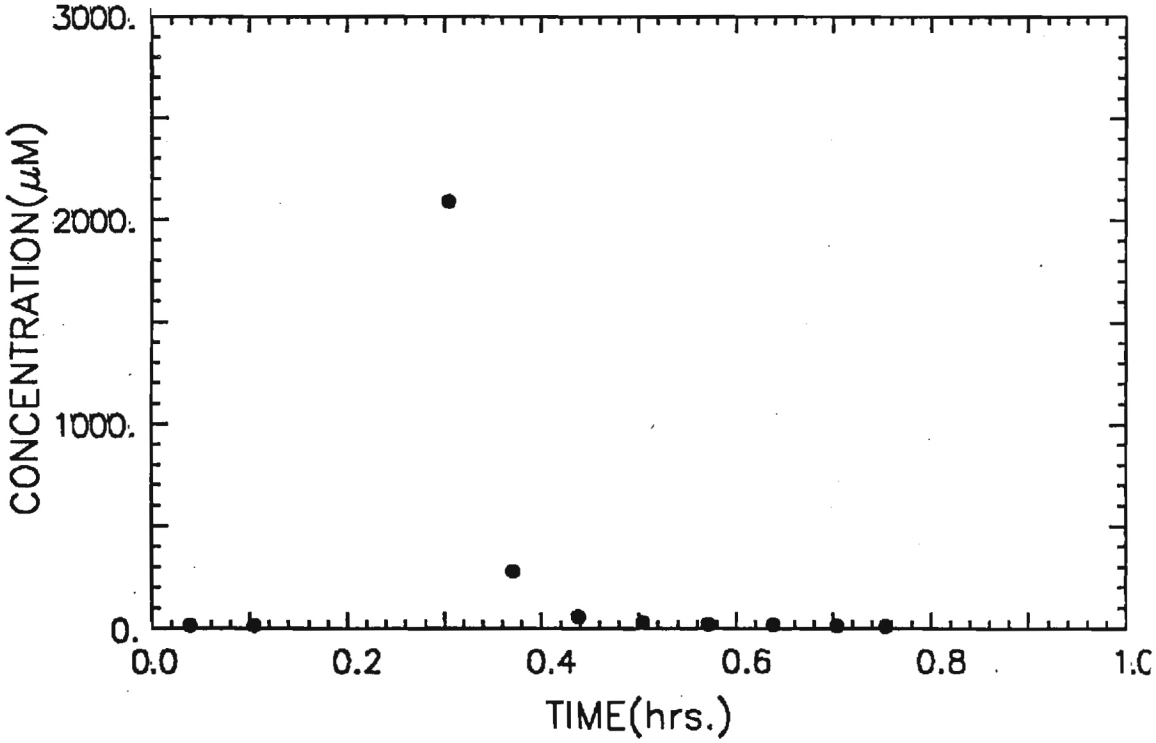

Figure A3-23. COLUMN DESORPTION OF 4AAB FROM XAD-7

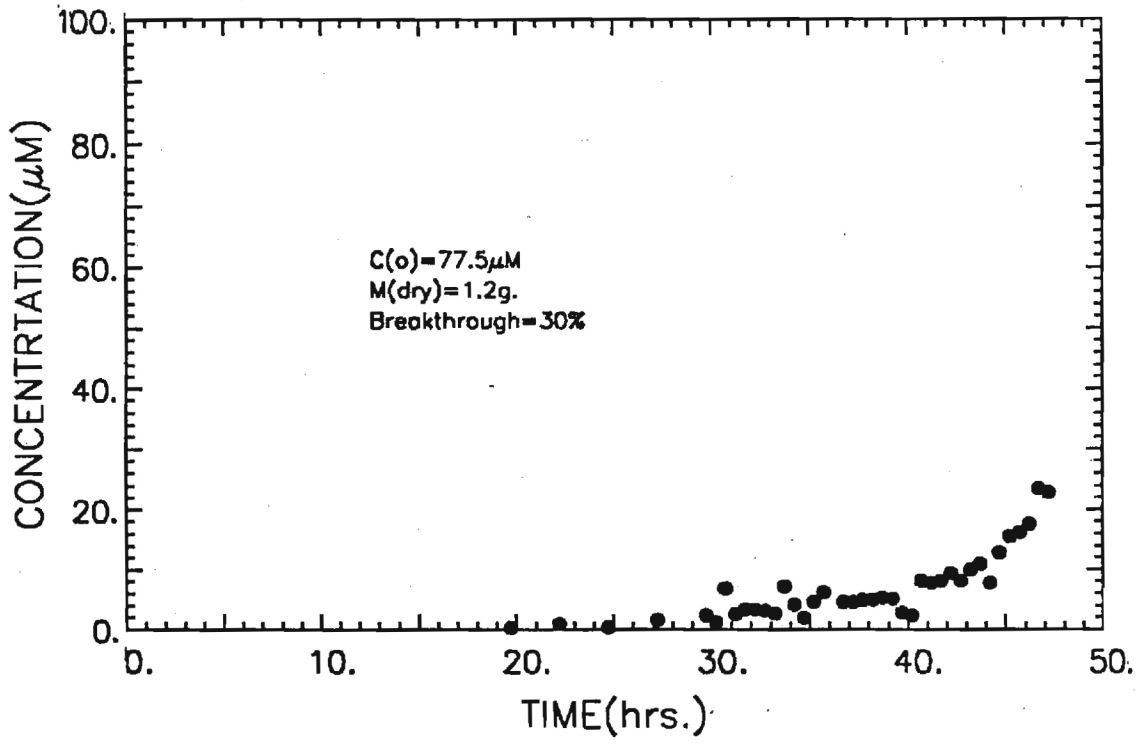

Figure A3-24. COLUMN ADSORPTION OF 4AAB ON XAD-16(1)

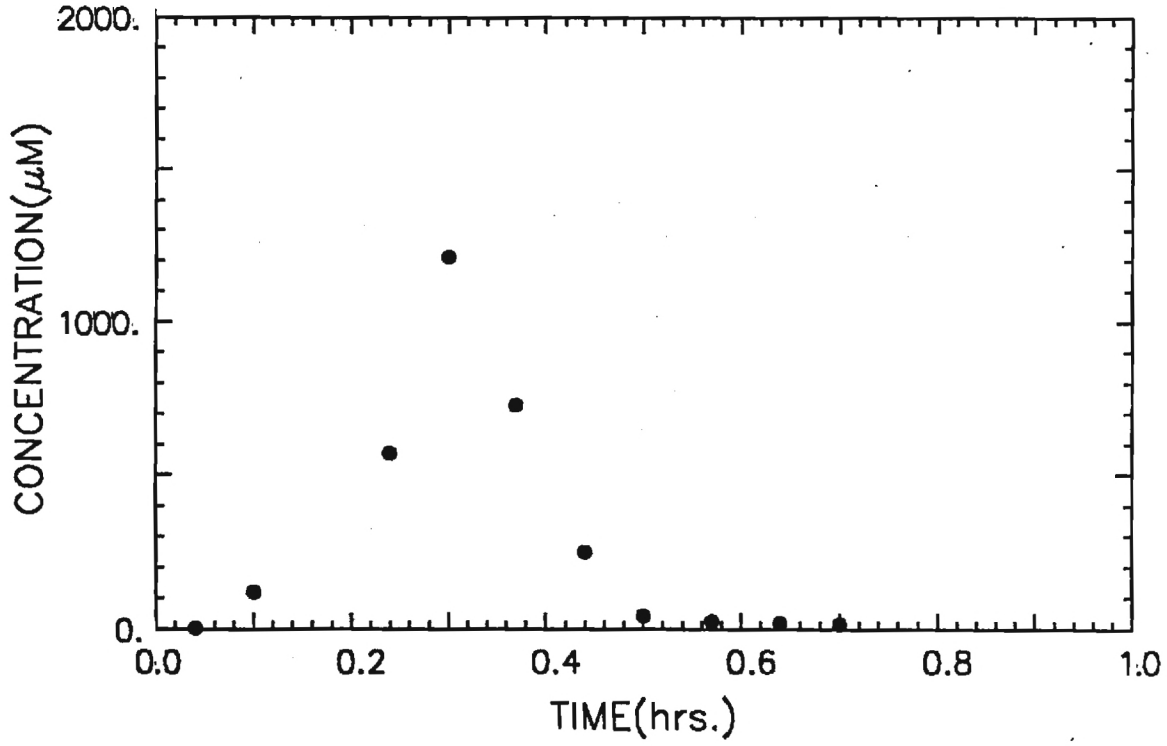

Figure A3-25. COLUMN DESORPTION OF 4AAB FROM XAD-16(1)

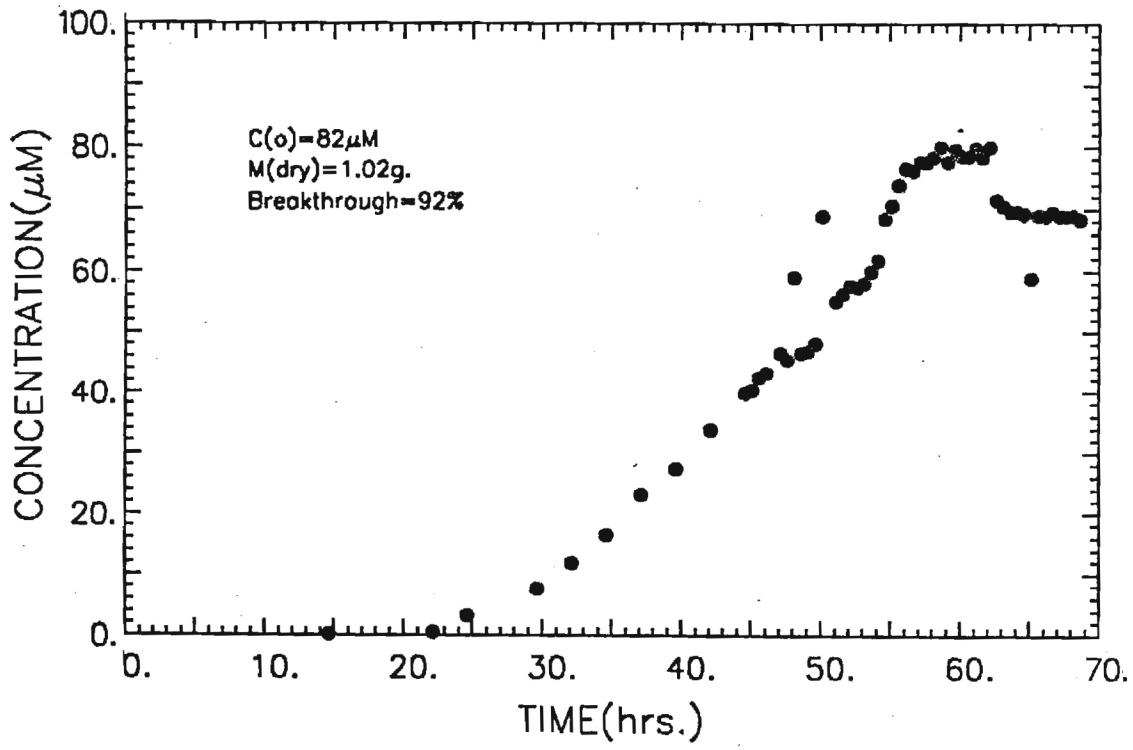

Figure A3-26. COLUMN ADSORPTION OF 4AAB ON XAD-16(2)

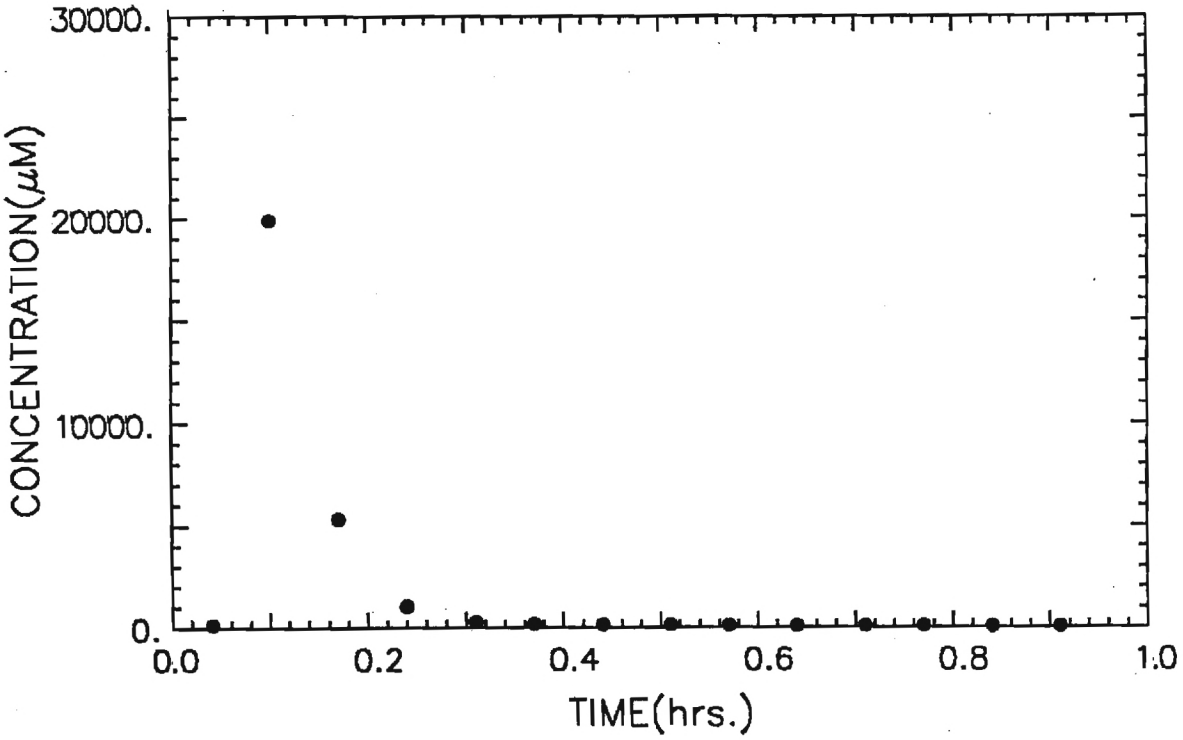

Figure A3-27. COLUMN DESORPTION OF 4AAB FROM XAD-16(2)

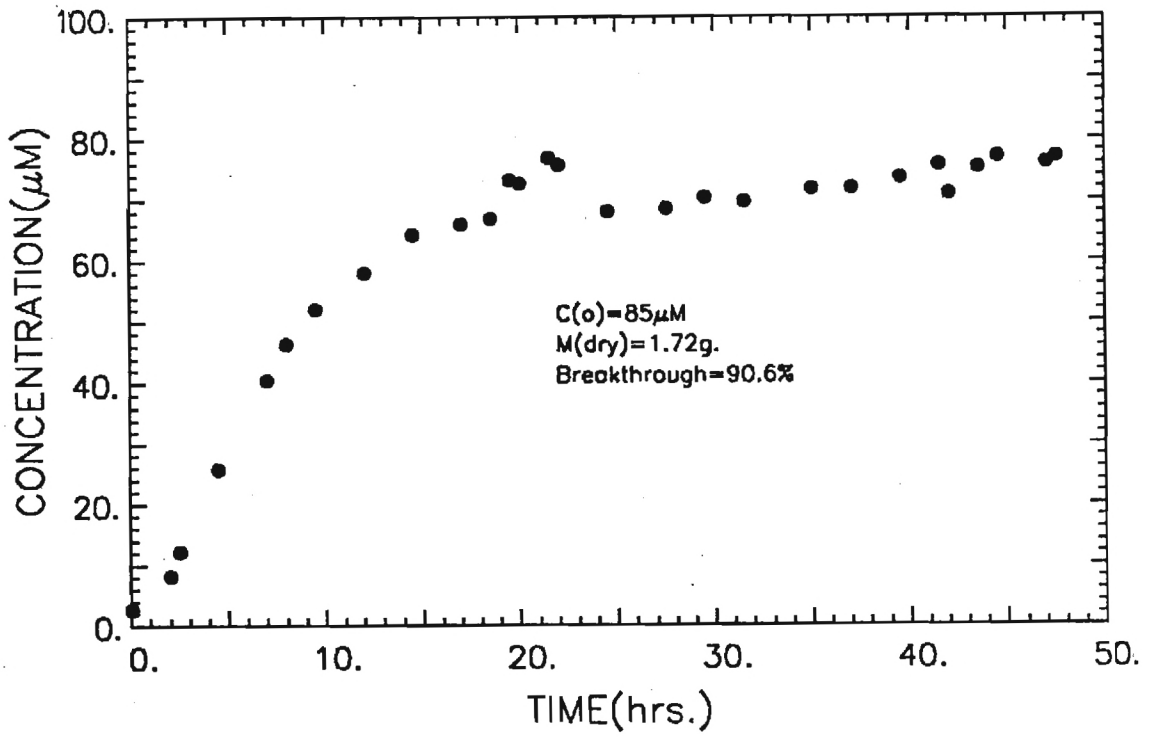

Figure A3-28. COLUMN ADSORPTION OF 4AAB ON S-761

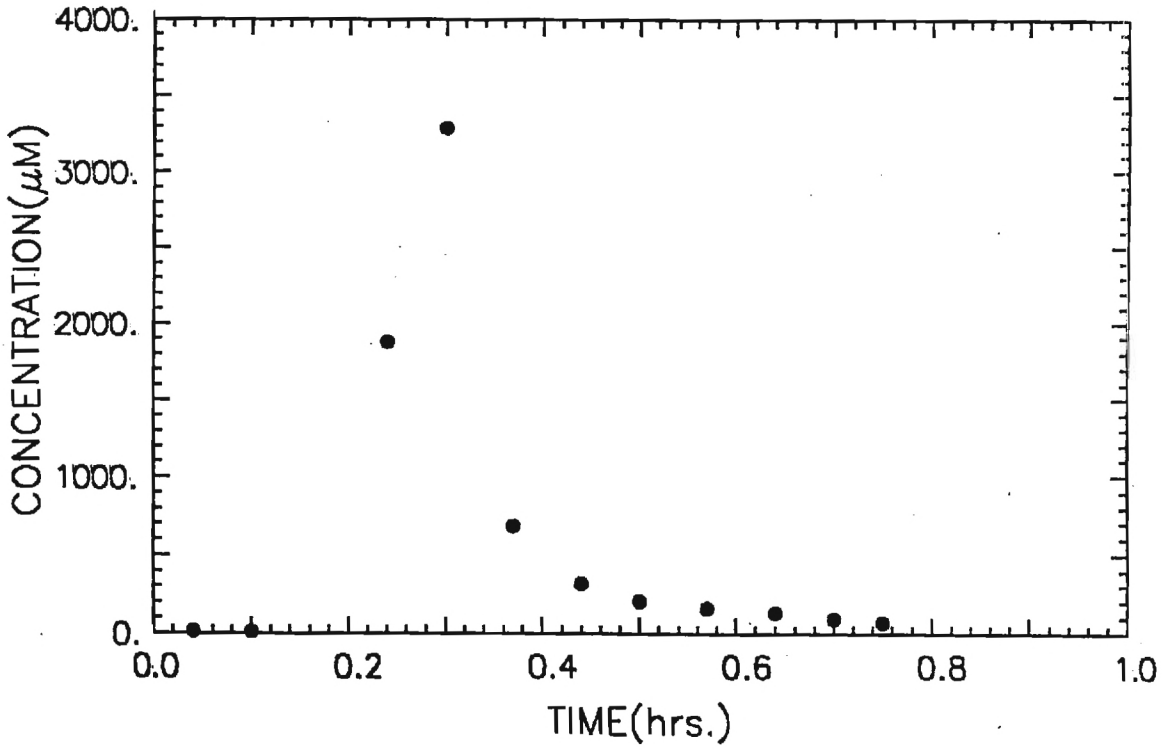

Figure A3-29. COLUMN DESORTION OF 4AAB FROM S-761

APPENDIX 4

Samples of LOTUS 1-2-3 Spreadsheets for the Calculation of Mass Adsorbed and Desorbed

TABLE A4-1. LOTUS 1-2-3- SPREAD SHEET FOR THE THIRD COLUMN ADSORPTION OF P-NITROPHENOL ONTO XAD-16

A TIME hours	B CONCENTRATION micromoles	C FLOW RATE liters/hour	D AVERAGE FLOW liters/hour	E TOTAL FLOW liters	F CUM. FLOW liters	G C(0)-C(E) micromoles	H CONC.ADSORBED micromoles	I MASS ADSORBED milligrams	J CUM. MASS ADSORBED milligrams
0.00	0	0.576	0.576	0.000	0.000	103.34	103.34	0.000	0.000
17.58	0.35	0.576	0.576	10.126	10.126	102.99	103.17	145.322	145.322
18.08	0.81	0.576	0.576	0.288	10.414	102.53	102.85	4.120	149.443
18.58	1.44	0.576	0.576	0.288	10.702	101.90	102.37	4.101	153.544
20.08	5.22	0.576	0.576	0.864	11.566	98.12	100.25	12.049	165.593
21.08	9.62	0.576	0.576	0.576	12.142	93.72	96.98	7.771	173.364
21.58	8.88	0.576	0.576	0.288	12.430	94.46	95.72	3.835	177.199
22.08	15.56	0.576	0.576	0.288	12.718	87.78	91.75	3.676	180.875
23.08	16.65	0.576	0.576	0.576	13.294	86.69	89.22	7.149	188.024
24.58	28.1	0.576	0.576	0.864	14.158	75.24	82.23	9.883	197.907
25.58	37.54	0.576	0.576	0.576	14.734	65.80	74.02	5.931	203.838
27.58	54.99	0.576	0.576	1.152	15.886	48.35	61.18	9.805	213.643
29.08	68.44	0.576	0.576	0.864	16.750	34.90	48.04	5.774	219.417
31.58	81.03	0.576	0.576	1.440	18.190	22.31	35.18	7.046	226.463
32.08	107.06	0.576	0.576	0.288	18.478	-3.72	15.73	0.630	227.093
32.58	107.06	0.576	0.576	0.288	18.766	-3.72	6.00	0.241	227.334
36.94	96.19	0.576	0.576	2.511	21.277	7.15	6.58	2.298	229.631
38.94	96.19	0.576	0.576	1.152	22.429	7.15	6.86	1.100	230.731
40.94	82.74	0.576	0.576	1.152	23.581	20.60	13.73	2.201	232.932
42.94	104.49	0.576	0.576	1.152	24.733	-1.15			
48.94	102.2	0.576	0.576	3.456	28.189	1.14			
50.94	101.63	0.576	0.576	1.152	29.341	1.71			

TABLE A4-2. LOTUS 1-2-3 SPREADSHEET FOR THE THIRD COLUMN DESORPTION OF P-NITROPHENOL FROM XAD-16

	A	B	C	D	E	F	G	H	I
1	TIME	CONCENTRATION	FLOW RATE	AVG. FLOW RATE	TOTAL FLOW	CUM.FLOW	MEAN CONC.	MASS DESORBED	CUM. MASS DESORBED
2	hours	micromoles	liters/hour	liters/hour	liters	liters	micromoles	milligrams	milligrams
3									
4	0.12	70.58	0.372	0.372	0.044	0.04	70.58	0.43	0.43
5	0.19	9013.00	0.372	0.372	0.025	0.07	4541.79	15.75	16.18
6	0.25	9666.00	0.372	0.372	0.025	0.09	9339.50	31.90	48.07
7	0.32	9590.00	0.372	0.372	0.025	0.12	9628.00	33.38	81.45
8	0.39	6624.00	0.372	0.372	0.025	0.14	8107.00	28.11	109.56
9	0.45	6009.00	0.372	0.372	0.025	0.17	6316.50	21.57	131.13
10	0.52	3189.00	0.372	0.372	0.025	0.19	4599.00	15.94	147.08
11	0.59	1939.00	0.372	0.372	0.025	0.22	2564.00	8.89	155.96
12	0.65	1026.00	0.372	0.372	0.025	0.24	1482.50	5.06	161.03
13	0.72	468.00	0.372	0.372	0.025	0.27	747.00	2.59	163.62
14	0.79	233.00	0.372	0.372	0.025	0.29	350.50	1.22	164.83
15	0.82	126.00	0.372	0.372	0.012	0.30	179.50	0.29	165.12
16	1.32	26.30	0.372	0.372	0.186	0.49	76.15	1.97	167.09
17	1.82	16.30	0.372	0.372	0.186	0.68	21.30	0.55	167.64
18	2.32	10.40	0.372	0.372	0.186	0.86	13.35	0.35	167.99
19	2.82	8.50	0.372	0.372	0.186	1.05	9.45	0.24	168.23
20	3.32	7.50	0.372	0.372	0.186	1.23	8.00	0.21	168.44
21	3.82	6.80	0.372	0.372	0.186	1.42	7.15	0.18	168.62
22	4.32	7.00	0.372	0.372	0.186	1.61	6.90	0.18	168.80

APPENDIX 5

Tentative Model of Adsorption and Desorption Kinetics

I. CLOSED BATCH REACTOR FOR ADSORPTION
(Single-Solute System)

I.1 Development of Governing Equations

The objective is to describe concentration changes in bulk (outside adsorbent particles) in a closed batch reactor with respect to time. This is done basically by connecting a material balance equation, which describes mass transport in adsorbent pore, to another material balance, which describes concentration changes in bulk, through a continuiety condition in external surface film around adsorbent particles and at pore mouth.

For simplicity, a single open end cylindrical pore is assumed to study the intraparticle mass transport as was used by Levenspiel (1972), Suidan (1975), and Kim et al. (1978). The pore is shown schematically in Figure 1 along with a typical concentration profile.

It is assumed that solute compound is transported in the liquid phase through pore (i.e., surface diffusion is ignored) and that there exists local equilibrium in pore between solution and solid phases.

I.1.1 Pore Diffusion. Based on Figure 1 a material balance on solute compound in the solution phase gives

$$D_e \frac{\partial^2 C}{\partial x^2} - \frac{4}{d_p} \frac{\partial q}{\partial t} = \frac{\partial C}{\partial t} \qquad (I.1.1)$$

where C = concentration of solute compound in the solution phase (a function of t and x) (mg/L),

D_e = effective diffusivity of solute compound (cm^2/min),

x = position variable (distance from the pore center) (cm),

d_p = diameter of the pore (cm),

q = mass of solute compound adsorbed per unit surface area (mg/cm^2), and

t = time variable (min),

The variable q, can be replaced with X (mg/g) which is based on unit mass of absorbent instead of unit surface area. Their relationship is

$$X = q\,A \qquad (I.1.2)$$

where A = surface area of adsorbent (cm^2/g).

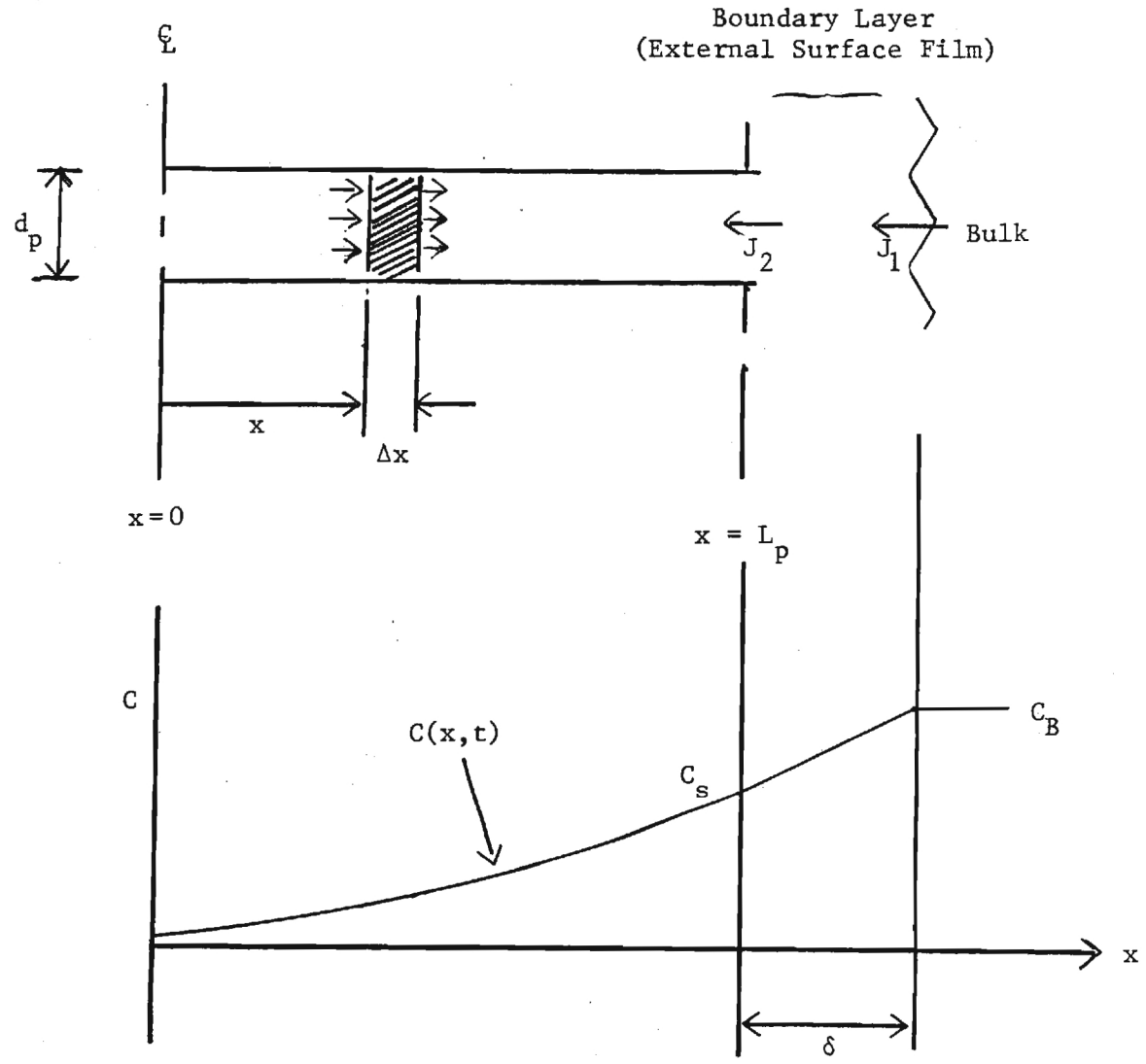

Figure A5-1. Schematic Representation of a Half Pore.

The variable d_p, has the following relationship with pore volume.

$$d_p = \frac{4}{A} V_p \qquad \text{(I.1.3)}$$

where V_p = pore volume (cc/g).

Then, Eq. (I.1.1) becomes

$$D_e \frac{\partial^2 C}{\partial x^2} - \frac{1}{V_p} \frac{\partial X}{\partial t} = \frac{\partial C}{\partial t} \qquad \text{(I.1.4)}$$

In most cases, the accumulation in pore liquid is negligible as compared to that on the solid phase. This was proven to be the base in this study by solving the equation with and without the term for accumulation in the pore liquid. Therefore, Eq. (I.1.4) can be simplified to

$$\frac{\partial X}{\partial t} = D_e V_p \frac{\partial^2 C}{\partial x^2} \qquad \text{(I.1.5)}$$

The relationship between X and C can be described by an adsorption isotherm since the local equilibrium is assumed.

$$X = f(C) \qquad \text{(I.1.6)}$$

If the adsorption isotherm follows the Freundlich equation,

$$f(C) = a\, C^{1/b} \qquad \text{(I.1.7)}$$

where a and b are constants.

A typical initial condition is

$$C = 0 \text{ and } X = 0,\ 0 \leq x \leq L_p \text{ and } t = 0 \qquad \text{(I.1.8)}$$

The boundary conditions are

$$C = C_s, \; x = L_p \text{ and } t \geq 0 \qquad \text{(I.1.9)}$$

$$\frac{\partial C}{\partial x} = 0, \; x = 0 \text{ and } t \geq 0 \qquad \text{(I.1.10)}$$

where C_s = concentration of solute compound at pore mouth (mg/L).

To apply the orthogonal collocation method, which will be discussed later, the position variable x is normalized.

$$\xi = x/L_p \qquad \text{(I.1.11)}$$

Eq. (I.1.5) becomes

$$\frac{\partial X}{\partial t} = \frac{V_p \, D_e}{L_p^{\,2}} \; \frac{\partial^2 C}{\partial \xi^2} \qquad \text{(I.1.12)}$$

Eq. (I.1.8) becomes

$$C = 0 \text{ and } X = 0, \; 0 \leq \xi \leq 1 \text{ and } t = 0 \qquad \text{(I.1.13)}$$

Eq. (I.1.9) and (I.1.10) become

$$C = C_s, \quad \xi = 1 \text{ and } t \leq 0 \qquad \text{(I.1.14)}$$

$$\frac{\partial C}{\partial \xi} = 0, \; \xi = 0 \text{ and } t \geq 0 \qquad \text{(I.1.15)}$$

I.1.2 Transport Through External Surface Film. It is assumed that the mass transport through external surface film (as shown in Figure 1) is quasi-steady-state (i.e., the mass of solute compound does not accumulate in the film).

The mass flux (g/cm^2-min) through the surface of external surface film, J_1, is described as

$$J_1 = - D \frac{\partial C}{\partial x} \cong - \frac{D}{\delta} (C_B - C_s) = - k(C_B - C_s) \qquad (I.1.16)$$

where D = diffusivity of solute compound in solution,

δ = thickness of the external surface film,

C = concentration of solute compound in the film,

C_B = concentration of solute compound in bulk (outside adsorbent particles) (mg/L), and

k = mass transfer coefficient (cm/min).

The mass flux (g/cm^2-min) through pore mouth, J_2, is

$$J_2 = - D_e \left. \frac{\partial C}{\partial x} \right|_{x = L_p} \qquad (I.1.17)$$

Due to the quasi-steady state assumption,

$$J_1 \pi d^2 = J_2 \frac{\pi d_p^2}{4} 2n_p \qquad (I.1.18)$$

where d = diameter of a adsorbent particle (cm), and

n_p = the number of cylindrical pores in an adsorbent particle.

$$n_p = \frac{\pi d^3}{6} \rho V_p / (\frac{\pi}{4} d_p^2 2 L_p) \qquad (I.1.19)$$

where ρ = adsorbent density (g of adsorbent per unit volume of adsorbent - including intraparticle pores).

Eq. (I.1.16) through (I.1.19) result in

$$\frac{6k}{\rho d}(C_B - C_s) = \frac{D_e V_p}{L_p} \left. \frac{\partial C}{\partial x} \right|_{x=L_p} \qquad (I.1.20)$$

After normalization,

$$\frac{6k}{\rho d}(C_B - C_s) = \frac{D_e V_p}{L_p^2}\left.\frac{\partial C}{\partial \xi}\right|_{\xi=1} \qquad \text{(I.1.21)}$$

I.1.3. Bulk Fluid. A material balance on solute compound in bulk fluid in a closed batch reactor yields

$$\frac{dC_B}{dt} = -\frac{6kw}{\rho d}(C_B - C_S) \qquad \text{(I.1.22)}$$

where w = adsorbent concentration (g/cc).

A typical initial condition is

$$C_B = C_o, \; t = 0 \qquad \text{(I.1.23)}$$

where C_o = the initial concentration of solute compound (mg/L).

I.2 Numerical Solution Technique

The governing equations with appropriate initial and boundary conditions [Eq. (I.1.12) through (I.1.15), Eq. (I.1.21), Eq. (I.1.22) and Eq. (I.1.23)] are solved to describe concentration changes in bulk fluid with respect to time. The numerical technique, selected for this study, is the orthogonal collocation method used on finite elements. The orthogonal collocation method was described by Finlayson (1980), Kim et al. (1978), and Thacker et al. (1981). The application of the orthogonal collocation method on finite elements was discussed by Carey and Finlayson (1975), Finlayson (1980), and Kim and Snoeyink (1980).

The procedures for applying the technique are as follows: 1) the pore is divided into several elements; 2) the position variable in the equations is renormalized for each element; and 3) the orthogonal collocation method is applied to each element with consideration of continuiety conditions between elements.

I.2.1 Modification of Governing Equations for Finite Element. Since the detailed procedure was described by Finlayson (1980) and Kim and Snoeyink (1980), only a brief description is given here.

The cylindrical pore is divided into several elements and a new position variable, η_n, is introduced to normalize the distance in each element as shown in Figure 2.

$$\eta_n = \frac{\xi - \xi_n}{\xi_{n+1} - \xi_n} \quad , \quad n=1,2,3,\ldots,e \tag{I.2.1}$$

where e = the number of elements and other variables are shown in Figure 2.

Then Eq. (I.1.12) becomes

$$\frac{\partial X}{\partial t} = \frac{V_p \quad D_e}{L_p^2 \, (\xi_{n+1} - \xi_n)^2} \quad \frac{\partial^2 C}{\partial \eta_n^2} \tag{I.2.2}$$

The initial and boundary conditions [Eq. (I.1.13) through (I.1.15)] are modified to

$$C = 0 \text{ and } X = 0, \; 0 \leq \eta_n \leq 1 \text{ and } t = 0 \tag{I.2.3}$$

$$C = C_s, \; \eta_e = 1 \text{ and } t \geq 0 \tag{I.2.4}$$

$$\frac{\partial C}{\partial \eta_1} = 0, \; \eta_1 = 0 \text{ and } t \geq 0 \tag{I.2.5}$$

The continuity conditions between elements are

$$\frac{1}{\xi_{n+1} - \xi_n} \quad \frac{\partial C}{\partial \eta_n} \bigg|_{\eta_n=1} = \frac{1}{\xi_{n+2} - \xi_{n+1}} \quad \frac{\partial C}{\partial \eta_{n+1}} \bigg|_{\eta_{n+1}=0} \tag{I.2.6}$$

$$C \bigg|_{\eta_n=1} = C \bigg|_{\eta_{n+1}=0} \tag{I.2.7}$$

$$n = 1,2,\ldots,e-1$$

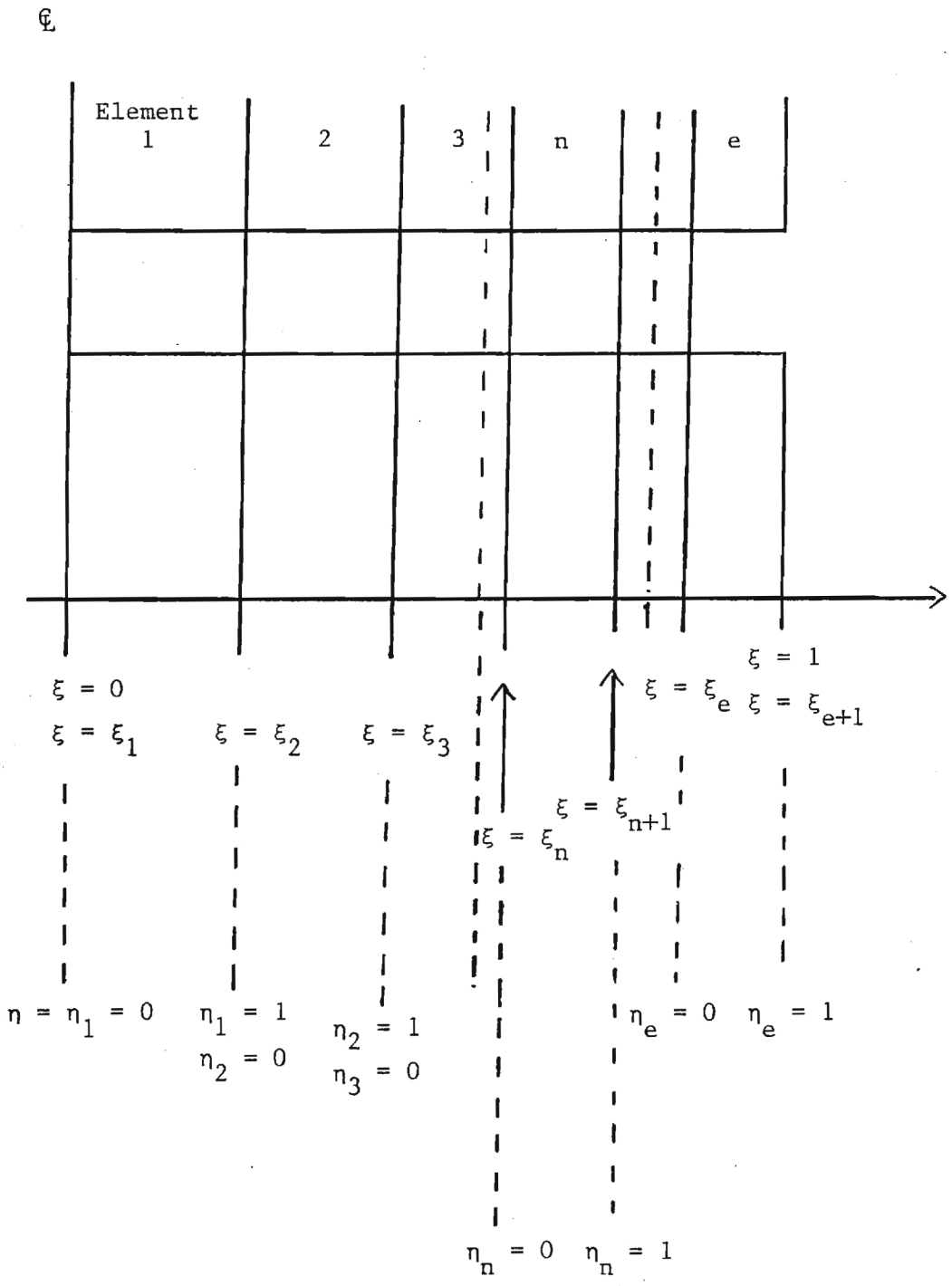

Figure A5-2. Application of Orthogonal Collocation Model in Conjunction with Finite Element Method on Pore.

For the transport through external surface film, Eq. (I.1.21) becomes

$$\frac{6k}{\rho d}(C_B - C_S) = \frac{D_e V_p}{L_p^2 (\xi_{e+1} - \xi_e)} \left.\frac{\partial C}{\partial \eta_e}\right|_{\eta_e = 1} \qquad (I.2.8)$$

where $C_x = C \mid_{\eta_{e=1}}$

There is no change on Eq. (I.1.22) and (I.1.23).

I.2.2 Application of Orthogonal Collocation Method. The application of the orthogonal collocation method to differential equations result in replacement of spatial derivatives with matrices at collocation points as shown below.

$$\frac{dC_i}{d\eta} = \sum_{j=1}^{N_n+2} A_{ij} C_j \qquad (I.2.9)$$

$$\frac{d^2C_i}{d\eta^2} = \sum_{j=1}^{N_n+2} B_{ij} C_j \qquad (I.2.10)$$

where the subscript i denotes a collocation point i, N_n is the number of interior collocation points, and A_{ij} and B_{ij} represent an element of collocation matrices, respectively. The detailed description on the orthogonal collocation method can be found elsewhere (Finlayson, 1980; Kim et al., 1978; Kim and Snoeyink, 1980).

After the application, Eq. (I.2.2) becomes a system of ordinary differential equation.

$$\frac{dX_{ni}}{dt} = \frac{V_p D_e}{L_p^2 (\xi_{n+1} - \xi_n)^2} \sum_{j=1}^{N_n+2} B_{ij}^n G_{nj} \qquad (I.2.11)$$

$$i = 2,3,\ldots, N_n+1$$

$$n = 1,2,\ldots, e$$

where C_{ni} = C at collocation point i in finite element n,

B^{n}_{ij} = an element of collocation matrix B in finite element n, and

X_{ni} = X at collocation point i in finite element n.

The initial condition of Eq. (I.2.3) becomes

$$C_{ni} = 0 \text{ and } X_{ni} = 0$$

$$i = 1,2,\ldots, N_n + 2$$

$$n = 1,2,\ldots, e \text{ and } t = 0 \qquad \text{(I.2.12)}$$

The boundary and continuiety conditions of Eq. (I.2.4) through (I.2.7) are converted to

$$C_{e,N_{n+2}} = C_s, \quad t \geq 0 \qquad \text{(I.2.13)}$$

$$\sum_{j=1}^{N_1+2} A^{1}_{1j} C_{1j} = 0, \quad t \geq 0 \qquad \text{(I.2.14)}$$

$$\frac{1}{\xi_{n+1} - \xi_n} \sum_{j=1}^{N_n+2} A^{n}_{N_n+2} C_{nj} = \frac{1}{\xi_{n+2} - \xi_{n+1}} \sum_{j=1}^{N_{n+1}+2} A^{n+1}_{1j} C_{n+1,j}, \quad t \geq 0 \qquad \text{(I.2.15)}$$

$$n = 1,2,\ldots, e-1$$

$$C_{n,N_n+2} = C_{n+1,1} \quad t \geq 0 \qquad \text{(I.2.16)}$$

$$n = 1,2,\ldots, e-1$$

or the external surface film, Eq. (I.2.8) becomes

$$\frac{6k}{\rho d} (C_B - C_{e,N_e+2}) = \frac{D_e V_p}{L_p^2(\xi_{e+1} - \xi_e)} \sum_{j=1}^{N_e+2} A^{e}_{N_e+2,j} C_{ej} \qquad \text{(I.2.17)}$$

In the bulk fluid, Eq. (I.1.22) and (I.1.23) are rewritten

$$\frac{dC_B}{dt} = -\frac{6kw}{\rho d}\,(C_B - C_{e,N_e+2}) \qquad \text{(I.2.18)}$$

$$C_B = 1,\ t = o \qquad \text{(I.2.19)}$$

The systems of equations, Eq. (I.2.11) through Eq. (I.2.19), contain both differential equations [Eq. (I.2.11) and Eq. (I.2.18)] and linear algebraic equations [Eq. (I.2.14), Eq. (I.2.15) and Eq. (I.2.17)]. The algebraic equations can be solved simultaneously to replace G values at boundaries (e.g., C_{11}, C_{1,N_1+2}, C_{21}, C_{2,N_2+2}, etc.) with C values at interior collocation points. The algebraic equations can be rearranged to result in the following system of equations.

$$a_{11}\,Y_1 + a_{12}\,Y_2 = f_1 \qquad \text{(I.2.20)}$$

$$a_{21}\,Y_1 + a_{22}\,Y_2 + a_{23}\,Y_3 = f_2 \qquad \text{(I.2.21)}$$

$$a_{32}\,Y_2 + a_{33}\,Y_3 + a_{34}\,Y_4 = f_3 \qquad \text{(I.2.22)}$$

$$\cdots\cdots\cdots\cdots$$
$$\cdots\cdots\cdots\cdots$$

$$a_{e+1,e}\,Y_e + a_{e+1,e+1}\,Y_{e+1} = f_{e+1} \qquad \text{(I.2.23)}$$

where $a^1_{11} = A^1_{11}$, $_{11}$

$$a^1_{12} = A_{1,N_1+2},$$

$$f_1 = -\sum_{j=2}^{N_1+1} A_{ij}\,C_{1j},$$

$$a_{n,n-1} = \frac{A^n_{N_n+2,1}}{\xi_{n+1} - \xi_n},$$

$$a_{nn} = \frac{A^n_{N_{n+2},N_{n+2}}}{\xi_{n+1} - \xi_n} - \frac{A^{n+1}_{11}}{\xi_{n+2} - \xi_{n+1}},$$

$$a_{n,n+1} = - \frac{A_1^{n+1}, N_{n+1+2}}{\xi_{n+1} - \xi_{n+1}} ,$$

$$f_n = - \frac{\sum_{j=2}^{N_n+1} A^n_{N_n+2,j} C_{nj}}{\xi_{n+1} - \xi_n} + \frac{\sum_{j=2}^{N_{n+1}+1} A^{n+1}_{1j} C_{n+1,j}}{\xi_{n+2} - \xi_{n+1}}$$

$$a_{e+1,e} = \frac{D_e V_p}{L_p^2 (\xi_{e+1} - \xi_e)} A^e_{N_{e+2},1} ,$$

$$a_{e+1,e+1} = \frac{D_e V_p}{L_p^2 (\xi_{e+1} - \xi_e)} A^e_{N_{e+2},N_{e+2}} + \frac{6k}{\rho d} ,$$

$$f_{e+1} = - \frac{D_e V_p}{L_p^2 (\xi_{e+1} - \xi_e)} \sum_{j=2}^{N_e+1} A^e_{N_e+2,j} G_{ej} + \frac{6k}{\partial d} G_B , \text{ and}$$

Y_n = C value at the boundary between element n-1 and n (e.g., $Y_1 = C_{1,N_1+2} = C_{21}$, etc.).

Basically, Eq. (I.2.20) is equivalent to Eq. (I.2.14), Eq. (I.2.21) and (I.2.22) to (I.2.15), and Eq. (I.2.23) to Eq. (I.2.17). Eq. (I.2.20) through (I.2.23) form a tridiagonal matrix.

The procedure for obtaining numerical solutions (concentration in the bulk fluid versus time) is as follows: 1) using the initial condition [Eq. (I.2.12) and (I.2.19)] and thereafter numerical solutions at each time step, the system of linear algebraic equations [Eq. (I.2.20) through (I.2.23)] are solved first to determine C values at element boundaries; the system of ordinary differential equations [Eq. (I.2.11) and (I.2.18)] are solved using the information obtained from the previous step; 3) C_{ni} values are calculated using Eq. (I.1.6) and X_{ni} values; and, 4) the above steps are repeated as many times as needed. C_B values, the solution of Eq. (I.1.18), describe the concentration changes in the bulk fluid with respect to time. In this study, a package program, DGEAR, is used to solve the system of first-order differential equations. DGEAR is based on a multi step predictor-corrector method (Gear, 1971; Hindmarsh, 1974) in which the time step size is automatically adjusted by the program as the integration proceeds.

II. PACKED BED REACTOR FOR ADSORPTION
(Single-Solute System)

II.1 Development of Governing Equations

The objective is to describe effluent concentration changes with respect to time (i.e., breakthrough curve). The concept is similar to that described in the section of closed batch reactor except the fact that concentration in the bulk fluid is now a function of not only time but also location. Therefore, all equations developed for pore and external surface film previously are still valid for packed bed. Only those equations developed for bulk fluid need to be replaced. These equations are Eq. (I.1.22), (I.1.22), (I.1.23), (I.2.18), and (I.2.19).

II.1.1 Bulk Fluid

A material balance on C_B in packed bed reactor (see Figure 3) gives

$$\frac{\partial C_B}{\partial t} = D_A \frac{\partial^2 C_B}{\partial z^2} - v \frac{\partial C_B}{\partial z} - 6 \frac{kw}{\rho d \varepsilon} (C_B - C_S) \qquad \text{(II.1.1)}$$

where D_A = axial dispersion coefficient (cm^2/min),
v = average interstitial velocity (cm/min),
z = position variable (distance from the inlet), (cm), and
ε = interparticle porosity.

A typical initial condition is

$$C_B = 0, \; t = 0 \text{ and } 0 \leq z \leq L_b \qquad \text{(II.1.2)}$$

where L_B = bed length (cm).

Boundary conditions are

$$C_{BO} = C_B - \frac{D_A}{v} \frac{dC_B}{dz}, \; t \geq 0 \text{ and } z = 0 \qquad \text{(II.1.3)}$$

$$\frac{dC_B}{dz} = 0, \; t \geq 0 \text{ and } z = L_b \qquad \text{(II.1.4)}$$

where C_{BO} in packed bed reactor is influent concentration (mg/L).

After normalization using the notations shown in Figure 3,

$$\frac{\partial C_B}{\partial t} = \frac{D_A}{L_b^2}\frac{\partial^2 C_B}{\partial \alpha^2} + \frac{v}{L_b}\frac{\partial C_B}{\partial \alpha} - \frac{6kw}{\rho \varepsilon d}(C_B - C_S) \qquad \text{(II.1.5)}$$

where $\alpha = (L_b - z)/L_b$

$$C_B = 0,\ t = 0 \text{ and } 0 \leq \alpha \leq 1 \qquad \text{(II.1.6)}$$

$$C_{BO} = C_B + \frac{D_A}{vL_b}\frac{\partial C_B}{\partial \alpha},\ t \geq 0 \text{ and } \alpha = 1 \qquad \text{(II.1.7)}$$

$$\frac{\partial C_B}{\partial \alpha} = 0,\ t \geq 0 \text{ and } \alpha = 0 \qquad \text{(II.1.8)}$$

II.2 Numerical Technique

Again, all discussions presented earlier are still valid here with an exception of the bulk fluid case. Therefore, the treatment of Eq. (II.1.5) through (II.1.8) is discussed only.

II.2.1 Modification of Governing Equations for Finite Element

Packed bed is divided into h elements as shown in Figure 3. Then, Eq. (II.1.5) through (II.1.8) are renormalized in terms of position variable for each element. A new position variable is defined for this purpose.

$$\zeta_m = \frac{\alpha - \alpha_m}{\alpha_{m+1} - \alpha_m},\ m = 1,2,\ldots,h \qquad \text{(II.2.1)}$$

where h = the number of element in packed bed. Then, Eq. (II.1.5) through (II.1.8) are converted to

$$\frac{\partial C_B}{\partial t} = \frac{D_A}{L_b^2(\alpha_{m+1} - \alpha_m)^2} + \frac{v}{L_b(\alpha_{m+1} - \alpha_m)}\frac{\partial C_B}{\partial \alpha} - \frac{6kw}{\rho \varepsilon d}(C_B - C_S) \qquad \text{(II.2.2)}$$

$$C_B = 0,\ t = 0 \text{ and } 0 \leq \zeta_m \leq 1.0 \qquad \text{(II.2.3)}$$

$$C_{BO} = C_B + \frac{D_A}{vL_b(\alpha_{h+1} - \alpha_h)}\frac{\partial C_B}{\partial \zeta_h},\ t \geq 0 \text{ and } \zeta_h = 1 \qquad \text{(II.2.4)}$$

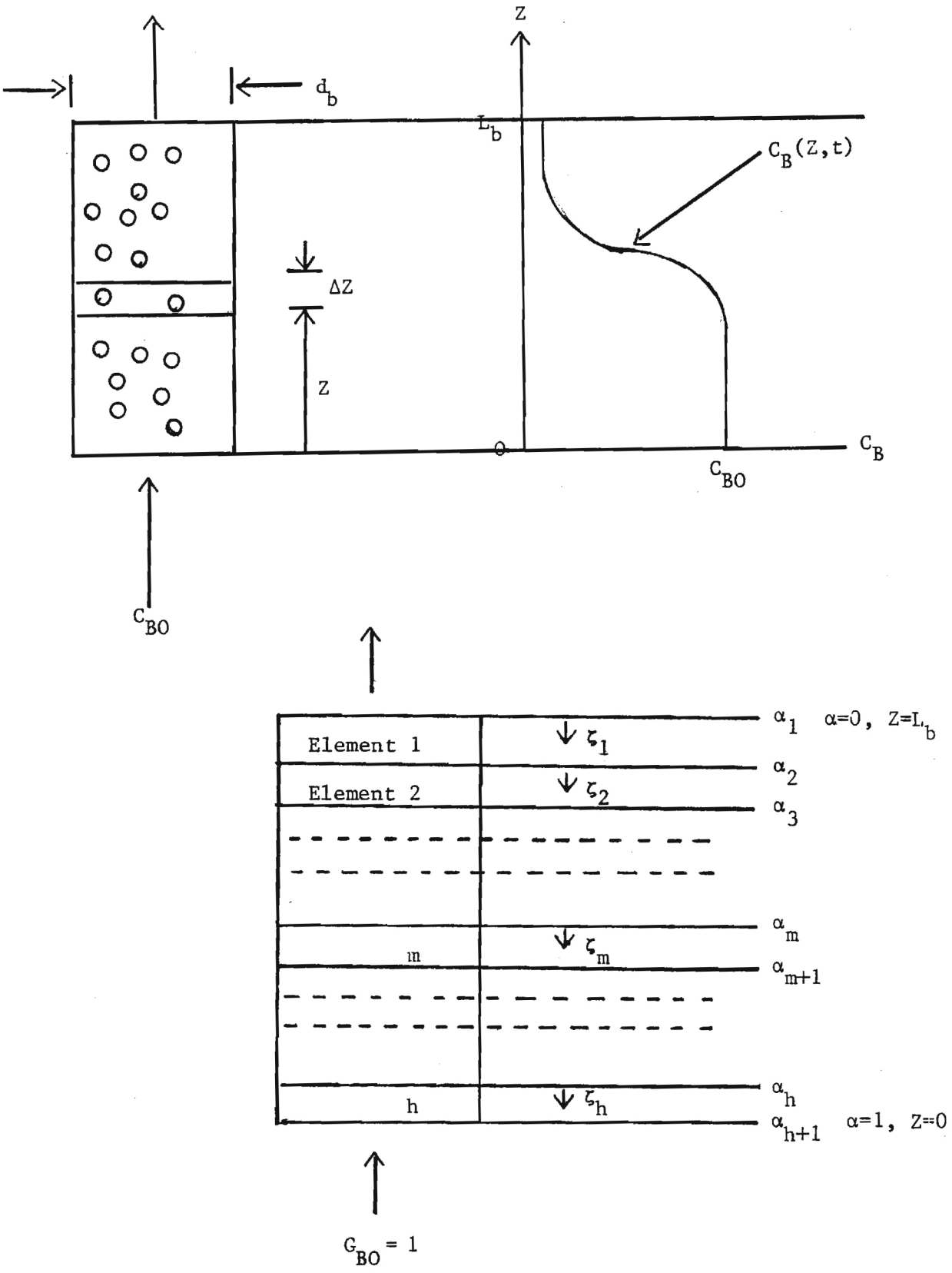

Figure A5-3. Schematic Representation of a Packed Bed.

$$\frac{\partial C_B}{\partial \zeta_1} = 0 \ , \quad t \geq 0 \text{ and } \zeta_1 = 0 \tag{II.2.5}$$

The continuity conditions between elements, which are basically the same as Eq. (I.2.6) and (I.2.7) for pore diffusion, are

$$\frac{1}{\alpha_{m+1} - \alpha_m} \frac{\partial C_B}{\partial \zeta_m} \Bigg|_{\zeta_m = 1} = \frac{1}{\alpha_{m+2} - \alpha_{m+1}} \frac{\partial C_B}{\partial \zeta_{m+1}} \Bigg|_{\zeta_m = 0} \tag{II.2.6}$$

$$C_B \Big|_{\zeta_m = 1} = C_B \Big|_{\zeta_{m+1} = 0} \tag{II.2.7}$$

$$m = 1,2,\ldots,\ h - 1$$

II.2.2 Application of Orthogonal Collocation Method

The application of orthogonal collocation method to Eq. (II.2.2) through (II.2.7) results in

$$\frac{dC_{B,mk}}{dt} = \frac{D_A}{L_b^2 (\alpha_{m+1} - \alpha_m)^2} \sum_{j=1}^{M_m+2} B_{kj}^m C_{B,mj} + \frac{v}{L_b(\alpha_{m+1} - \alpha_m)} \sum_{j=1}^{M_m+2} A_{kj}^m C_{B,mj} - \frac{6kw}{\rho \varepsilon d} (C_{B,mk} - C_{e,N_e+2}) \tag{II.2.8}$$

$$m = 1,2,\ldots,h$$

$$k = 2,3,\ldots,M_m + 1$$

$$C_{B,k} = 0, \ t = 0 \text{ and } k = 1,2,\ldots,M_m+2 \quad m = 1,2,\ldots,h \tag{II.2.9}$$

$$C_{BO} = C_{B,h,M_h+2} + \frac{D_A}{vL_b (\alpha_{h+1} - \alpha)} \sum_{j=1}^{M_h+2} A_{M_h+2,j}^h C_{B,hj} \ , \quad t \geq 0 \tag{II.2.10}$$

$$\sum_{j=1}^{M_1+2} A_{1j}^1 C_{B,1j} = 0 \ , \quad t \geq 0 \tag{II.2.11}$$

$$\frac{1}{\alpha_{m+1} - \alpha_m} \sum_{j=1}^{M_m+2} A_{M_m+2,j}^m C_{B,mj} = \frac{1}{\alpha_{m+2} - \alpha_{m+1}} \sum_{j=1}^{M_m+2} A_{1j}^{m+1} C_{B,m+1,j} \tag{II.2.12}$$

$$m = 1,2,\ldots,h-1$$

$$C_{B,m,M_m+2} = C_{B,m+1,1} \qquad \text{(II.2.13)}$$

$$m = 1,2,\ldots,h-1$$

Eq. (I.2.17), which describes the transport through the external surface film, needs to be further specified because C_B (concentration in the bulk fluid) is a function of location in packed bed whereas it is not in the case of closed batch reactor.

$$\frac{6k}{\rho d}\left(C_{B,mk} - C_{e,N_e+2}\right) = \frac{D_e V_p}{L_p^2 (\xi_{e+1} - \xi_e)} \sum_{j=1}^{N_e+2} A^e_{N_e+2,j} C_{ej} \qquad \text{(II.2.14)}$$

$$m = 1,2,\ldots,h$$

$$k = 2,3,\ldots,M_m+1$$

where $C_{B,mk} = C_B$ at collocation point k in element m of packed bed.

Now, to describe a breakthrough curve, the following system of equations need to be solved:

1) Eq. (I.2.11) through (I.2.16) for pore diffusion;

2) Eq. (II.2.14) for transport through external surface film; and

3) Eq. (II.2.8) through (II.2.13) for transport in the bulk fluid of packed bed.

As was in the case of closed batch reactor, the aforementioned equations contain both differential equations [Eq. (I.2.11) and (II.2.8)], and linear algebraic equations [Eq. (I.2.14), (I.2.15), (II.2.10), (II.2.11), (II.2.12), and (II.2.14)].

The procedure for replacing boundary C values in pore was already discussed, which involves solving a system of linear algebraic equations resulted from Eq. (I.2.14), (I.2.15), and (I.2.17). The only difference in the case of packed bed is the use of Eq. (II.2.14) instead of Eq. (I.2.17), which results in a slight modification in Eq. (I.2.23), i.e.,

$$f_{e+1} = -\frac{D_e V_p}{L_p^2 (\xi_{e+1} - \xi_e)} \sum_{j=2}^{N_e+1} A^e_{N_e+2,j} C_{ej} + \frac{6k}{\rho d} C_{B,mk} \qquad \text{(II.2.15)}$$

where C_B is further specified by the location in packed bed and thus $C_{B,mk}$ represents G_B at collocation point k in element m.

The procedure for determining boundary C_B values between elements in packed bed is the same as that used in the case of boundary C values in pore except that Eq. (II.2.10), (II.2.11), and (II.2.12) are used. Rearranging these equations,

$$b_{11} Z_1 + b_{12} Z_2 = d_1 \qquad \text{(II.2.16)}$$

$$b_{21} Z_1 + b_{22} Z_2 + b_{23} Z_3 = d_2 \qquad \text{(II.2.17)}$$

$$b_{32} Z_2 + b_{33} Z_3 + b_{34} Z_4 = d_3 \qquad \text{(II.2.18)}$$

$$b_{h+1,h} Z_h + b_{h+1,h+1} Z_{h+1} = d_{h+1} \qquad \text{(II.2.19)}$$

where

$$b_{11} = A^1_{11},$$

$$b_{12} = A^1_{1,M_1+2},$$

$$d_1 = - \sum_{j=2}^{M_1+1} A^1_{1j} C_{B,1j},$$

$$b_{m,m-1} = \frac{1}{\alpha_{m+1} - \alpha_m} A^m_{M_m+2,1},$$

$$b_{mm} = \frac{A^m_{M_m+2,M_m+2}}{\alpha_{m+1} - \alpha_m} - \frac{A^{m+1}_{11}}{\alpha_{m+2} - \alpha_{m+1}},$$

$$b_{m,m+1} = - \frac{A^{m+1}_{1,M_{m+1}+2}}{\alpha_{m+2} - \alpha_{m+1}},$$

$$d_m = - \frac{\sum_{j=2}^{M_m+1} A^m_{M_m+2,j} C_{B,mj}}{\alpha_{m+1} - \alpha_m} + \frac{\sum_{j=2}^{M_{m+1}+1} A^{m+1}_{1j} C_{B,m+1,j}}{\alpha_{m+2} - \alpha_{m+1}},$$

$$b_{h+1,h} = \frac{D_A}{v_{L_b}\,(\alpha_{h+1} - \alpha_h)}\, A^h_{M_h+2,1},$$

$$b_{h+1,h+1} = 1 + \frac{D_A}{v_{L_b}\,(\alpha_{h+1} - \alpha_h)}\, A^h_{M_h+2,M_h+2},$$

$$d_{h+1} = C_{BO} - \frac{D_A}{v_{L_b}\,(\alpha_{h+1} - \alpha_h)} \sum_{j=2}^{M_h+1} A^h_{M_h+2,j}\, C_{B,hj}, \text{ and}$$

Z_m = C_B value at the boundary between element m-1 and m e.g., $Z_1 = C_{B,11}$, $Z_2 = C_{B,1,N_1+2} = C_{B,21}$, etc.).

The superscript in the above equations represents a specific finite element in packed bed. Eq.(II.2.16) is equivalent to Eq.(II.2.11), Eq.(II.2.17) and (II.2.18) to Eq.(II.2.12), and Eq.(II.2.19) to Eq.(II.2.10). Again, these equations form a tridiagonal matrix.

The procedure for determining a breakthrough curve is as follows: 1) using initial conditions [Eq. (I.2.12) and (II.2.9)] and thereafter numerical solutions at current time step, the system of linear algebraic equations [Eq.(I.2.20) through (I.2.23) with the modication shown in Eq.(II.2.15)] are solved to determine C values at pore-element boundaries; 2) using initial conditions [Eq.(II.2.9)] and thereafter numerical solutions at current time step, the system of linear algebraic equations [Eq. (II.2.16) through (II.2.19)] are solved to determine C_B values at bed-element boundaries; 3) the system of ordinary differential equations [Eq. (I.2.11) and (II.2.8)] are solved using the information obtained from the previous steps; 4) C_{ni} values are calculated using Eq. (I.1.6) and X_{ni} values; and 5) the above steps are repeated as many times as necessary to obtain a desired breakthrough curve.

III. APPLICATION OF QUASILINEARIZATION TO A CLOSED BATCH MODEL WHICH IS BASED ON ORTHOGONAL COLLOCATION METHOD IN CONJUNCTION WITH FINITE ELEMENT METHOD

III.1 Application of Quasilinearization

The governing equations, Eq. (I.2.11) and (I.2.18), after the orthogonal collocation and finite element methods are applied are rewritten:

In Pore

$$\frac{dX_{ni}}{dt} = \frac{V_p D_e \sum_{j=1}^{N_n+2} B_{ij}^n C_{nj}}{L_p^2 (\xi_{n+1} - \xi_n)^2} \qquad \text{(III.1.1)}$$

where n = n th element (n = 1,2,...,3)

i = i th collocation point and (i = 2,3,....,N_n+1),

N_n = the number of interior collocation points in the n th element.

In the Bulk Fluid

$$\frac{dC_B}{dt} = - \frac{6kw}{\rho d} (C_B - C_{e,N_e+2}) \qquad \text{(III.1.2)}$$

The role of boundary conditions will be discussed later. A schematic diagram is presented in Figure 4 to show an example which has three finite elements with 2,3, and 4 interior collocation points, respectively.

If the Freundlich isotherm is applicable, then the relationship between X_{ni} and C_{ni} is given by

$$X_{ni} = a\, C_{ni}^{1/b} \qquad \text{(III.1.3)}$$

For convenience, new notations are used for application of quasilinearization.

$$X_{ni} = y_m \qquad \text{(III.1.4)}$$

$$n = 1,2,...e, \quad i = 2,3,...N_n+1, \quad m = 1,2,...N-1, \quad N = \sum_{i=1}^{e} {}_iN + 1$$

$$C_B = y_N \qquad \text{(III.1.5)}$$

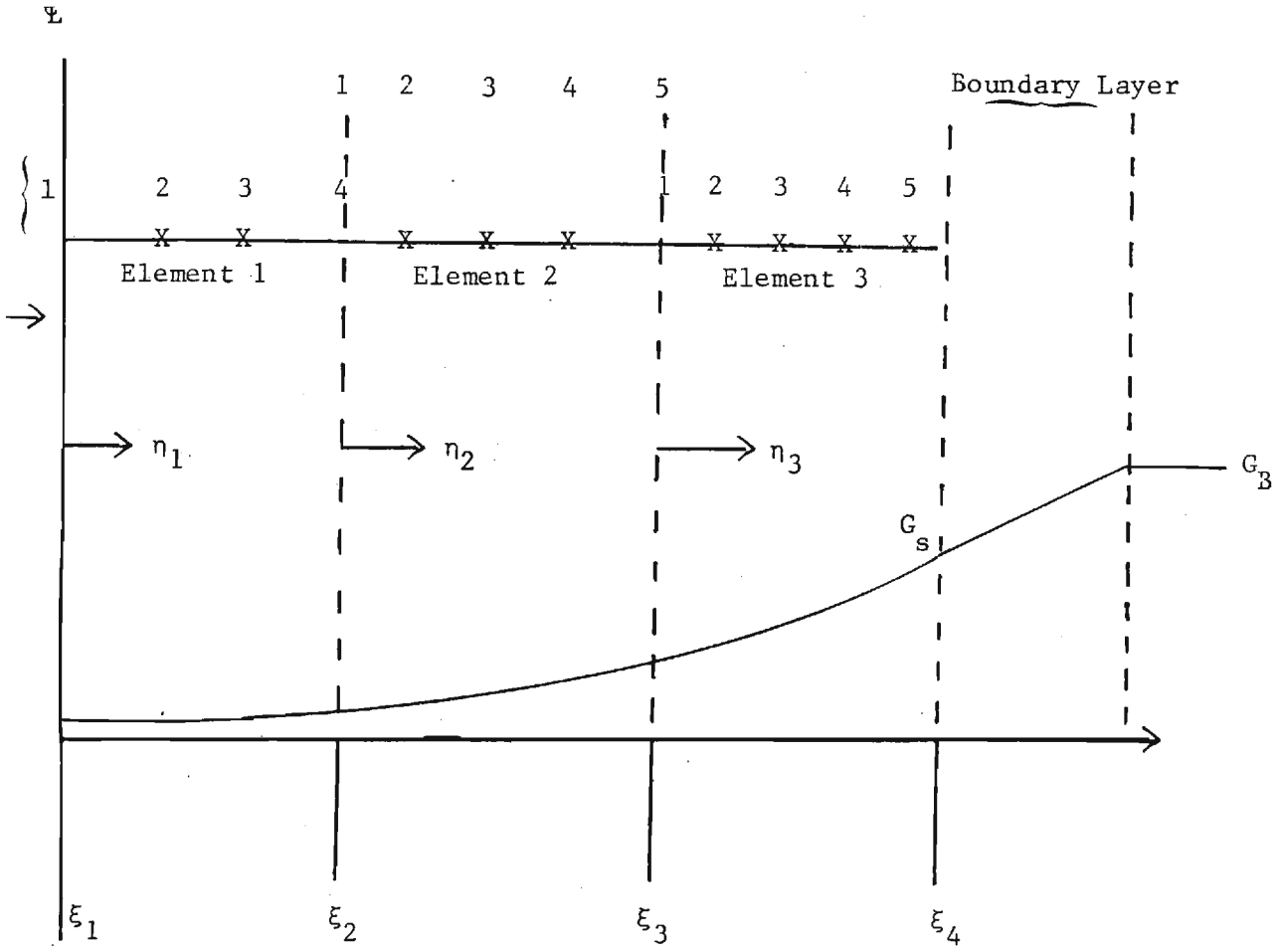

e = 3
N_1 = 2
N_2 = 3
N_4 = 4

$G_s = G_{e,N_e+2}$

Figure A5-4. An Example of 3-Element Pore with 2, 3, and 4 Interior Collection Points, Respectively.

ıe RHS of the governing equations [Eq. (III.1.1) and (III.1.2)] = g_m, = 1,2,...,N [g_1, g_2,..., g_{N-1} from Eq. (III.1.2) and g_N from Eq. (III.1.2)].

/pical initial conditions are

$$y_m = 0, \quad m = 1,2,\ldots,N-1$$

$$y_N = C_o, \quad m = N$$

n other words,

$$\frac{d\bar{y}}{dt} = \bar{g} = g_1 = \frac{dy_1}{dt} = \frac{dX_{12}}{dt} = \frac{V_p D_e \sum_{j=1}^{N_1+2} B_{2j}^1 C_{1j}}{L_p^2 (\xi_2 - \xi_1)^2}$$

$$g_2 = \frac{dy_2}{dt} = \frac{dG_{13}}{dt} = \ldots\ldots\ldots\ldots\ldots\ldots$$
$$\ldots\ldots\ldots\ldots\ldots\ldots\ldots\ldots\ldots\ldots$$

$$g_{N-1} = \frac{dy_{N-1}}{dt} = \frac{dX_{e,N_e+1}}{dt} = \frac{V_p D_e \sum_{j=1}^{N_e+2} B_{N_e+1,j}^e C_{ej}}{L_p^2 (\xi_{e+1} - \xi_e)^2}$$

$$g_N = \frac{dy_N}{dt} = \frac{dC_B}{dt} = -\frac{6kw}{\rho d} = (C_B - C_{e,N_e+2}) \qquad \text{(III.1.6)}$$

The linearization of Eq. (III.1.6) by a Taylor series expansion leads to

$$\frac{dy_m^{r+1}}{dt} = g_m^r + \sum_{\ell=1}^{N} (y_\ell^{r+1} - y_\ell^r) \frac{\partial g_m^r}{\partial y_\ell} + \sum_{j=1}^{K} (a_j^{r+1} - a_j^r) \frac{\partial g_m^r}{\partial a_j} \qquad \text{(III.1.7)}$$

where the subscripts, r and r+1, denote current values and new values, respectively, and a_j is a parameter to be estimated. The term K represents the number of unknown parameters which has a value of 2 for this case. The term $\partial g^r/\partial a_j$ is a derivative of g_m with respective a_j, evaluated with current values and an element of a K x N matrix.

The general solution of Eq. (III.1.7) can be obtained from the method of complementary functions, which is nothing but a linear combination of homogeneous solutions and particular solution with appropriate coefficients.

That is,

$$y_m^{r+1}(t) = p_m(t) + \sum_{j=1}^{K} a_j^{r+1} h_{mj}(t) \quad , \quad m = 1, \ldots, N \qquad \text{(III.1.8)}$$

where p_i is a particular solution and h_{ji} is a homogeneous solution.

Substituting Eq. (III.1.8) into Eq. (III.1.7), derivatizing Eq. (III.1.8) with respect to t, and equating coefficients results in a set of linear differential equations which will provide the particular and homogeneous solutions,

$$\frac{dp_m}{dt} = g_m^r + \sum_{\ell=1}^{N} \left[(p_\ell - y_\ell^r) \frac{\partial g_m^r}{\partial y_\ell}\right] - \sum_{j=1}^{K} a_j^r \frac{\partial g_m^r}{\partial a_j} \qquad \text{(III.1.9)}$$

$$\frac{dh_{mj}}{dt} = \sum_{j=1}^{N} h_{\ell j} \frac{\partial g_m^r}{\partial y_\ell} + \frac{\partial g_m^r}{\partial a_j} \qquad \text{(III.1.10)}$$

with

$$p_m(0) = 0 \qquad m = 1, \ldots, N-1 \qquad \text{(III.1.11)}$$

$$p_N(0) = 1 \qquad \text{(III.1.12)}$$

$$h_{mj}(0) = 0 \qquad m = 1, \ldots, N$$

$$j = 1, \ldots, k \qquad \text{(III.1.13)}$$

Now, the objective of this technique is to find a^{n+1} by minimizing the difference between the corresponding solution of Eq. (III.1.8) and the experimental data. The objective function to be minimized is

$$S = \sum_{i=1}^{L} w_i \left[y_N^{r+1}(t_i) - P_i\right]^2 \qquad \text{(III.1.14)}$$

where w_i is a weighting factor, L is the number of observations, P_i is an observation or a bulk concentration a t_i, and $y^{r+1}(t_i)$ is a solution of Eq. (III.1.8) that corresponds to the bulk concentration $C^{r+1}(t_i)$.

To minimize Eq. (III.1.14), the following derivatives should hold,

$$\frac{\partial S}{\partial a_1^{r+1}} = \ldots = \frac{\partial S}{\partial a_K^{r+1}} = 0 \qquad \text{(III.1.15)}$$

Combining Eq. (III.1.8) and Eq. (III.1.14) with Eq. (III.1.15) produces K linear algebraic equations,

$$\sum_{i=1}^{L} w_i \left(p_N + \sum_{j=1}^{K} a_j^{r+1} h_{N,j} - P_i\right) h_{N,1} = 0$$

$$\cdots\cdots\cdots\cdots\cdots\cdots\cdots\cdots\cdots\cdots$$

$$\sum_{i=1}^{L} w_i \left(p_N + \sum_{j=1}^{K} a_j^{r+1} h_{N,j} - P_i\right) h_{N,K} = 0 \qquad \text{(III.1.16)}$$

After an appropriate rearrangement, this becomes

$$\bar{\bar{D}}\,\bar{a} = \bar{E} \qquad \text{(III.1.17)}$$

where

$$D_{ij} = \sum_{i=1}^{L} w_i h_{N,i} h_{N,j} \qquad \text{(III.1.18)}$$

$$E_j = -\sum_{i=1}^{L} w_i \left(p_N - P_i\right) h_{N,j} \qquad \text{(III.1.19)}$$

and D and E are a K x K symmetric matrix and a K x 1 matrix, respectively.

The cycle of parameter estimation starts from the initial guess of parameters, $a_1,\ldots,a_K$. Then the numerical solutions of Eq. (III.1.9) and Eq. (III.1.10) are obtained and all values of $y^{r+1}(t_i)$ corresponding to experimental data, P_i. This makes it possible to form matrices D and E by Eq. (III.1.18) and Eq. (III.1.19). New values of parameters, now, are calculated by solving the linear algebraic equations, Eq. (III.1.17), which leads to the next cycle if needed. The flow chart for this method is shown in Figure 5.

Quasilinearization is a quadratically convergent technique, which means that the number of correct digits is doubled asymtotically with each iteration, if the initial estimate is reasonably good. It was noted that this method is very sensitive to the initial guess and the type of functions that are worked on. If it converges at all, less than 5 or 6 cycles was needed to get a reasonable value of parameters. More details on quasilinearization can be found elsewhere (Bellman et al., 1967; Lee, 1968; Kim et al., 1978; Higgins and Kim, 1982).

II.2. Evaluation of Derivatives

The derivative terms in Eqs. (III.1.9) and (III.1.10) can be illustrated based on the example shown in Figure 4. The relationships between variables are shown as follows:

The Amount Adsorbed	Liquid-Phase Concentration	Element	Location in Terms of Collocation Point
	$C_{11} - Y_1$	1	1
$X_{12} = y_1$	C_{12}	1	2
$X_{13} = y_2$	C_{13}	1	3
	C_{14} or $C_{21}=Y_2$	1/2	4/1
$X_{22} = y_3$	C_{22}	2	2
$X_{23} = y_4$	C_{23}	2	3
$X_{24} = y_5$	C_{24}	2	4
	C_{25} or $C_{31}=Y_3$	2/3	4/1
$X_{32} = y_6$	C_{32}	3	2
$X_{33} = y_7$	C_{33}	3	3
$X_{34} = y_8$	C_{34}	3	4
$X_{35} = y_9$	C_{35}	3	5
	C_{36} or $C_s=Y_4$	3	6
	$C_B = y_{10}$	-	-

Then, Eq. (III.1.5) can be written with variables, y and Y.

Element 1

$$g_1 = \frac{dy_1}{dt} = \frac{V_p D_e \left(B^1_{21} Y_1 + \sum_{j=2}^{N_1+1} B^1_{2j} C_{1j} + B^1_{2,N_1+2} Y_2\right)}{L_p^2 (\xi_2 - \xi_1)^2}$$

$$g_2 = \frac{dy_2}{dt} = \frac{V_p D_e \left(B^1_{31} Y_1 + \sum_{j=2}^{N_1+2} B^1_{3j} C_{1j} + B^1_{3,N_1+2} Y_2\right)}{L_p^2 (\xi_2 - \xi_1)^2}$$

or

$$g_m = \frac{dy_m}{dt} = \frac{V_p D_e \left(B^1_{m+1,1} Y_1 + \sum_{j=2}^{N_1+2} B^1_{m+1,j} C_{1j} + B^1_{m+1,N_1+2} Y_2\right)}{L_p^2 (\xi_2 - \xi_1)^2}$$

$$m = 1,2,\ldots,N_1 \qquad \text{(III.2.1)}$$

Element 2

$$g_3 = \frac{dy_3}{dt} = \frac{V_p D_e \left(B^1_{21}\, Y_2 + \sum_{j=2}^{N_2+1} B^2_{2j}\, C_{2j} + B^2_{2,N_2+2}\, Y_3\right)}{L_p^2 \left(\xi_3 - \xi_2\right)^2}$$

or

$$g_m = \frac{dy_m}{dt} = \frac{V_p D_e \left(B^2_{m-N_1+1,1}\, Y_2 + \sum_{j=2}^{N_2+1} B^2_{m-N_1+1,j}\, C_{2j} + B^2_{m-N_1+1,N_2+2}\, Y_3\right)}{L_p^2 \left(\xi_3 - \xi_2\right)^2}$$

$$m = N_1+1,\ldots,N_1+N_2 \qquad \text{(III.2.2)}$$

Element 3

$$g_m = \frac{dy_m}{dt} = \frac{V_p D_e \left(B^3_{m-N_1-N_2+1,1}\, y_3 + \sum_{j=2}^{N_2+1} B_{m-N_1-N_2+1,j}\, C_{3j} + B_{m-N_1-N_2+1,N_2+2}\, Y_4\right)}{L_p^2 \left(\xi_4 - \xi_3\right)^2}$$

$$m = N_1+N_2+1,\ldots,N_1+N_2+N_3 \qquad \text{(III.2.3)}$$

In the Bulk

$$g_{10} = \frac{dy_{10}}{dt} = -\frac{6kw}{\rho d}\left(y_{10} - Y_4\right) \qquad \text{(III.2.4)}$$

The derivatives are obtained as follows.

Element 1 ($m = 1,2,\ldots,N_1$)

When $\ell = 1,2,\ldots,N_1$,

$$\frac{\partial g_m}{\partial y_\ell} = \frac{V_p D_e \left(B^1_{m+1,1} \frac{\partial Y_1}{\partial y_\ell} + B^1_{m+1,\ell+1} \frac{\partial C_{1,\ell+1}}{\partial y_\ell} + B_{m+1,N_1+2} \frac{\partial Y_2}{\partial y_\ell}\right)}{L_p^2 \left(\xi_2 - \xi_1\right)^2} \qquad \text{(III.2.5)}$$

$\partial C_{1,\ell+1}/\partial y$ can be evaluated if the adsorption isotherm equation is known. If the Freundlich adsorption isotherm is valid, Eq. (I.1.7) can be rewitten in terms of y for evaluation of the above derivative.

$$X = f(C) = a\, C^{1/b} \qquad \text{(III.2.6)}$$

or

$$C = a^{-b}\, X^{b} \qquad \text{(III.2.7)}$$

or

$$C_{1,\ell+1} = a^{-b}\, y_{\ell}^{b} \qquad \text{(III.2.8)}$$

then

$$\frac{\partial C_{1,\ell+1}}{\partial y_{\ell}} = a^{-b}\, y_{\ell}^{b-1} \qquad \text{(III.2.9)}$$

The terms, $\partial Y_1/\partial y$ and $\partial Y_2/\partial y$, are included because Y_1 and Y_2 are functions of y through boundary conditions (i.e., zero slope at the pore center, continuity at element boundaries, and continuous slope at element boundaries). The evaluation of $\partial X/\partial y$ will be discussed later.

When $\ell = N_1+1, N_1+2, \ldots, N_1+N_2+N_3+1$,

$$\frac{\partial g_m}{\partial y} = \frac{V_p D_e \left(B^1_{m+1,1} \frac{\partial Y_1}{\partial y_{\ell}} + B^1_{m+1,N_1+2} \frac{\partial Y_2}{\partial y_{\ell}}\right)}{L_p^2 (\xi_2 - \xi_1)^2} \qquad \text{(III.2.10)}$$

Element 2 ($m = N_1+1, \ldots, N_1+N_2$)

When $\ell = N_1+1, N_1+2, \ldots, N_1+N_2$,

$$\frac{\partial g_m}{\partial y_{\ell}} = \frac{V_p D_e \left(B^2_{m-N_1+1,1} \frac{\partial Y_2}{\partial y_{\ell}} + B^2_{m-N_1+1,\ell-N_1+1} \frac{\partial C_{2,\ell-N_1+1}}{\partial y_{\ell}} + B^2_{m-N_1+1,N_2+2} \frac{\partial Y_3}{\partial y_{\ell}}\right)}{L_p^2 (\xi_3 - \xi_2)^2} \qquad \text{(III.2.11)}$$

$\partial C_{2,-N_1+1}/\partial y_{\ell}$ can be evaluated similarly as shown in Eq. (III.2.9)

When $\ell = 1, 2, \ldots, N_1$ and $N_1+N_2+1, \ldots, N_1+N_2+N_3+1$,

$$\frac{\partial g_m}{\partial y_{\ell}} = \frac{V_p D_e \left(B^2_{m-N_1+1,1} \frac{\partial Y_2}{\partial y_{\ell}} + B^2_{m-N_1+1,N_2+2} \frac{\partial Y_3}{\partial y_{\ell}}\right)}{L_p^2 (\xi_3 - \xi_2)^2} \qquad \text{(III.2.12)}$$

Element 3 ($m = N_1+N_2+1,\ldots,N_1+N_2+N_3$)

When $\ell = N_1+N_2+1,\ldots,N_1+N_2+N_3$

$$\frac{\partial g_m}{\partial y_\ell} = \frac{V_p D_e \left(B^3_{m-N_1-N_2+1,1}\frac{\partial Y_3}{\partial y_\ell} + B^3_{m-N_1-N_2+1,\ell-N_1-N_2+1}\frac{\partial C_{3,\ell-N_1-N_2+1}}{\partial y_\ell} + B^3_{m-N_1-N_2+1,N_3+2}\frac{\partial Y_4}{\partial y_\ell}\right)}{L_p^2\,(\varepsilon_4 - \varepsilon_3)^2} \qquad \text{(III.2.13)}$$

$\partial C_{3,\ell-N_1-N_2+1}/\partial y_\ell$ can be evaluated similarly as shown in Eq. (III.2.9).

When $\ell = 1,2,\ldots,N_1+N_2$ and $N_1+N_2+N_3+1$,

$$\frac{\partial g_m}{\partial y_\ell} = \frac{V_p D_e \left(B^3_{m-N_1-N_2+1,1}\,\frac{\partial Y_3}{\partial y_\ell} + B^3_{m-N_1-N_2+1,N_3+2}\,\frac{\partial Y_4}{\partial y_\ell}\right)}{L_p^2\,(\xi_4 - \xi_3)^2} \qquad \text{(III.2.14)}$$

In the Bulk ($m = 10$)

When $\ell = 1,2,\ldots,N_1+N_2+N_3$,

$$\frac{\partial g_{10}}{\partial y_\ell} = -\frac{6kw}{\rho d}\,\frac{\partial Y_4}{\partial y_\ell} \qquad \text{(III.2.15)}$$

When $\ell = m = 10$,

$$\frac{\partial g_{10}}{\partial y_{10}} = -\frac{6kw}{\rho d}\left(1 - \frac{\partial Y_4}{\partial y_{10}}\right) \qquad \text{(III.2.16)}$$

The derivatives of g_m with respect to a_j are

$$\frac{\partial g_m}{\partial a_1} = g_m/a_1 \qquad \text{(III.2.17)}$$

where $a_1 = D$ and $m = 1,2,\ldots,N_1+N_2+N_3$.

$$\frac{\partial g_{10}}{\partial a_1} = 0 \qquad \text{(III.2.18)}$$

$$\frac{\partial g_m}{\partial a_2} = 0 \qquad \text{(III.2.19)}$$

where $a_2 = k$ and $m = 1,2,\ldots,N_1+N_2+N_3$.

$$\frac{\partial g_{10}}{\partial a_2} = -\frac{6kw}{\rho d}(y_{10} - Y_4) = g_{10}/a_2 \qquad \text{(III.2.20)}$$

Then, the structures of $\partial g/\partial y$ and $\partial g/\partial a$ matrices can be illustrated in terms of Eq. number in this section as follows:

1) $\dfrac{\partial g_\ell}{\partial y_m}$

		y										
	m / ℓ	1	2	3	4	5	6	7	8	9	10(=N)	
	1	(5)	(5)	(10)	(10)	(10)	(10)	(10)	(10)	(10)	(10)	
	2	(5)	(5)	(10)	(10)	(10)	(10)	(10)	(10)	(10)	(10)	1
	3	(12)	(12)	(11)	(11)	(11)	(12)	(12)	(12)	(12)	(12)	
g	4	(12)	(12)	(11)	(11)	(11)	(12)	(12)	(12)	(12)	(12)	2
	5	(12)	(12)	(11)	(11)	(11)	(12)	(12)	(12)	(12)	(12)	
	6	(14)	(14)	(14)	(14)	(14)	(13)	(13)	(13)	(13)	(14)	
	7	(14)	(14)	(14)	(14)	(14)	(13)	(13)	(13)	(13)	(14)	3
	8	(14)	(14)	(14)	(14)	(14)	(13)	(13)	(13)	(13)	(14)	(=e)
	9	(14)	(14)	(14)	(14)	(14)	(13)	(13)	(13)	(13)	(14)	
(N=)	10	(15)	(15)	(15)	(15)	(15)	(15)	(15)	(15)	(15)	(16)	
		1		2			3 (=e)					

2) $\frac{\partial g_\ell}{\partial a_j}$

$a_1 = D$
$a_2 = k$

	ℓ \ j	1	2 (=K)	
g	1	(17)	0	
	2	(17)	0	1
	3	(17)	0	
	4	(17)	0	2
	5	(17)	0	
	6	(17)	0	
	7	(17)	0	
	8	(17)	0	3 (=e)
	9	(17)	0	
(N=)	10	0	(20)	Finite Element

To determine $\partial Y/\partial y$, the following boundary conditions need to be differentiated.

At the pore center,

$$\sum_{j=1}^{N_1+2} A_{1j}^1 \, C_{1j} = 0$$

or

$$A_{11}^1 \, Y_1 + \sum_{j=2}^{N_1+1} A_{1j} \, C_{1j} + A_{1,N_1+2}^1 \, Y_2 = 0 \qquad \text{(III.2.21)}$$

At the boundary between elements,

$$\frac{1}{\xi_{n+1} - \xi_n} \sum_{j=1}^{N_n+2} A_{N_n+2,j}^n \, C_{nj} - \frac{1}{\xi_{n+2} - \xi_{n+1}} \sum_{j=1}^{N_{n+1}+2} A_{1j}^{n+1} \, C_{n+1,j} = 0$$

where $n = 1, \ldots, e-1$ (here, $e = 3$)

or

$$\frac{1}{\xi_{n+1} - \xi_n} \left(A^n_{N_n+2,1} \, Y_n + \sum_{j=2}^{N_n+2} A^n_{N_n+2,j} \, C_{nj} + A^n_{N_n+2,N_n+2} \, Y_{n+1} \right)$$

$$- \frac{1}{\xi_{n+2} - \xi_n} \left(A^{n+1}_{11} \, X_{n+1} + \sum_{j=2}^{N_{n+1}+2} A^{n+1}_{1j} \, C_{n+1,j} + A^{n+1}_{1,N_{n+1}+2} \, Y_{n+2} \right) = 0 \qquad \text{(III.2.22)}$$

At the pore mouth,

$$\frac{D_e V_p}{L_p^2 (\xi_4 - \xi_3)} \sum_{j=1}^{N_3+2} A^3_{N_3+2,j} \, C_{3j} - \frac{6k}{\rho_s d} (C_B - Y_4) = 0$$

or

$$\frac{D_e V_p}{L_p^2 (\xi_4 - \xi_3)} \left(A^3_{N_3+2,1} \, Y_3 + \sum_{j=2}^{N_3+2} A^3_{N_3+2,j} \, C_{3j} + A^3_{N_3+2,N_3+2} \, Y_4 \right)$$

$$- \frac{6k}{\rho d} (y_{10} - Y_4) = 0 \qquad \text{(III.2.23)}$$

The following equations are obtained after differentiating Eq. (III.2.21) through (III.2.23) with respect to y.

At the pore center

$$A^1_{11} \frac{\partial Y_1}{\partial y_\ell} + A^1_{1,N_1+2} \frac{\partial Y_2}{\partial y_\ell} = - A^1_{1,\ell+1} \frac{\partial C_{1,\ell+1}}{\partial y_1}, \quad \ell = 1,2,\ldots N_1 \qquad \text{(III.2.24)}$$

$$= 0, \quad \ell = N_1+1,\ldots,N_1+N_2+N_3+1 \qquad \text{(III.2.25)}$$

At the boundary between Element 1 and 2

$$\frac{1}{\xi_2-\xi_2} A^1_{N_1+2,1} \frac{\partial Y_1}{\partial y_\ell} + \left(\frac{1}{\xi_2-\xi_1} A^1_{N_1+2,N_1+2} - \frac{1}{\xi_3-\xi_2} A^2_{11}\right) \frac{\partial Y_2}{\partial y_\ell} - \frac{1}{\xi_3-\xi_2} A^2_{1,N_2+2} \frac{\partial Y_3}{\partial y_\ell}$$

$$= - \frac{1}{\xi_2-\xi_1} A_{N_1+2,\ell+1} \frac{\partial C_{1,\ell\ 1}}{\partial y_\ell} , \ \ell = 1,2,\ldots N_1 \qquad \text{(III.2.26)}$$

$$= \frac{1}{\xi_3-\xi_2} A^2_{1,\ell-N_1+1} \frac{\partial C_{2,\ell-N_1+1}}{\partial y_\ell} , \ \ell = N_1+1,\ldots N_2 \qquad \text{(III.2.27)}$$

$$= 0, \ \ell = N_1+N_2+1,\ldots,N_1+N_2+N_3+1 \qquad \text{(III.2.28)}$$

At the boundary between Element 2 and 3

$$\frac{1}{\xi_3-\xi_2} A^2_{N_2+2,1} \frac{\partial Y_2}{\partial y_\ell} + \left(\frac{1}{\xi_3-\xi_2} A^2_{N_2+2,N_2+2} - \frac{1}{\xi_4-\xi_3} A^3_{11}\right) \frac{\partial Y_3}{\partial y_\ell} - \frac{1}{\xi_4-\xi_3} A^3_{1,N_3+2} \frac{\partial Y_4}{\partial y_\ell}$$

$$= 0 \ , \ \ell = 1,2,\ldots,N_1 \qquad \text{(III.2.29)}$$

$$= - \frac{1}{\xi_3-\xi_2} A^2_{N_2+2,\ell-N_1+1} \frac{\partial C_{2,\ell-N_1+1}}{\partial y_\ell} , \ \ell = N_1+1,\ldots,N_1+N_2 \qquad \text{(III.2.30)}$$

$$= \frac{1}{\xi_4-\xi_3} A^3_{1,\ell-N_1-N_2+1,} \frac{\partial C_{3,\ell-N_1-N_2+1}}{\partial y_\ell} , \ \ell = N_1+N_2+1,\ldots,N_1+N_2+N_3 \qquad \text{(III.2.31)}$$

$$= 0 \ , \ \ell = 10 = N_1+N_2+N_3+1 = N \qquad \text{(III.2.32)}$$

At the pore mouth

$$\frac{D_e V_p}{L_p^2 (\xi_4 - \xi_3)} A^3_{N_3+2,1} \frac{\partial Y_3}{\partial y_\ell} + \left(\frac{D_e V_p}{L_p^2 (\xi_4 - \xi_3)} A^3_{N_3+2,N_3+2} + \frac{6k}{\rho d}\right) \frac{\partial Y_4}{\partial y_\ell}$$

$$= 0 \quad , \quad \ell = 1,2,\ldots,N_1 \qquad \text{(III.2.33)}$$

$$= 0 \quad , \quad \ell = N_1+1,\ldots,N_1+N_2 \qquad \text{(III.2.34)}$$

$$= -\frac{D_e V_p}{L_p^2 (\xi_4 - \xi_3)} A^3_{N_3+2,\ell-N_1-N_2+1} \frac{\partial C_{3,\ell-N_1-N_2+1}}{\partial y_\ell} \quad , \quad \ell = N_1+N_2+1,\ldots,N_1+N_2+N_3 \qquad \text{(III.2.35)}$$

$$= \frac{6k}{\rho d} \quad , \quad \ell = 10 \qquad \text{(III.2.36)}$$

Eq. (III.2.24) through (III.2.36) form the following matrices.

$$\frac{\partial Y_i}{\partial y_1} \quad , \quad i = 1,2,3,4$$

$$\begin{bmatrix} A^1_{11} & A^1_{14} & 0 & 0 \\ \frac{A^1_{41}}{\xi_2-\xi_1} & \frac{A^1_{44}}{\xi_2-\xi_1} - \frac{A^2_{11}}{\xi_3-\xi_2} & -\frac{A^2_{15}}{\xi_3-\xi_2} & 0 \\ 0 & \frac{A^2_{51}}{\xi_3-\xi_2} & \frac{A^2_{55}}{\xi_3-\xi_2} - \frac{A^3_{11}}{\xi_4-\xi_3} & -\frac{A^3_{16}}{\xi_4-\xi_3} \\ 0 & 0 & \frac{D_e V_p}{L_p^2(\xi_4-\xi_3)} A^3_{61} & \frac{D_e V_p}{L_p^2(\xi_4-\xi_3)} A^3_{66} + \frac{6k}{\rho d} \end{bmatrix} \begin{bmatrix} \frac{\partial Y_1}{\partial y_1} \\ \frac{\partial Y_2}{\partial y_1} \\ \frac{\partial Y_3}{\partial y_1} \\ \frac{\partial Y_4}{\partial y_1} \end{bmatrix} = \begin{bmatrix} -A^1_{12} \frac{\partial C_{12}}{\partial y_1} \\ -\frac{A^1_{42}}{\xi_2-\xi_1} \frac{\partial C_{12}}{\partial y_1} \\ 0 \\ 0 \end{bmatrix}$$

$$\frac{\partial y_i}{\partial y_2} \quad , \quad i = 1,2,3,4$$

$$\begin{bmatrix} A^1_{11} & A^1_{14} & 0 & 0 \\ \frac{A^1_{41}}{\xi_2-\xi_1} & \frac{A^1_{44}}{\xi_2-\xi_1} - \frac{A^2_{11}}{\xi_3-\xi_2} & -\frac{A^2_{15}}{\xi_3-\xi_2} & 0 \\ 0 & \frac{A^2_{51}}{\xi_3-\xi_2} & \frac{A^2_{55}}{\xi_3-\xi_2} - \frac{A^3_{11}}{\xi_4-\xi_3} & -\frac{A^3_{16}}{\xi_4-\xi_3} \\ 0 & 0 & \frac{D_e V_p}{L_p^2(\xi_4-\xi_3)} A^3_{61} & \frac{D_e V_p}{L_p^2(\xi_4-\xi_3)} A^3_{66} + \frac{6k}{\rho d} \end{bmatrix} \begin{bmatrix} \frac{\partial y_1}{\partial y_2} \\ \frac{\partial y_2}{\partial y_2} \\ \frac{\partial y_3}{\partial y_2} \\ \frac{\partial y_4}{\partial y_2} \end{bmatrix} = \begin{bmatrix} -A^1_{13} \frac{\partial C_{13}}{\partial y_2} \\ -\frac{A^1_{43}}{\xi_2-\xi_1} \frac{\partial C_{13}}{\partial y_2} \\ 0 \\ 0 \end{bmatrix}$$

$$\frac{\partial y_i}{\partial y_3} \quad , \quad i = 1,2,3,4$$

$$\begin{bmatrix} A^1_{11} & A^1_{14} & 0 & 0 \\ \frac{A^1_{41}}{\xi_2-\xi_1} & \frac{A^1_{44}}{\xi_2-\xi_1} - \frac{A^2_{11}}{\xi_3-\xi_2} & -\frac{A^2_{15}}{\xi_3-\xi_2} & 0 \\ 0 & \frac{A^2_{51}}{\xi_3-\xi_2} & \frac{A^2_{55}}{\xi_3-\xi_2} - \frac{A^3_{11}}{\xi_4-\xi_3} & -\frac{A^3_{16}}{\xi_4-\xi_3} \\ 0 & 0 & \frac{D_e V_p}{L_p^2(\xi_4-\xi_3)} A^3_{61} & \frac{D_e V_p}{L_p^2(\xi_4-\xi_3)} A^3_{66} + \frac{6k}{\rho d_s} \end{bmatrix} \begin{bmatrix} \frac{\partial y_1}{\partial y_3} \\ \frac{\partial y_2}{\partial y_3} \\ \frac{\partial y_3}{\partial y_3} \\ \frac{\partial y_4}{\partial y_3} \end{bmatrix} = \begin{bmatrix} 0 \\ \frac{A^2_{12}}{\xi_3-\xi_2} \frac{\partial C_{22}}{\partial y_3} \\ -\frac{A^2_{52}}{\xi_3-\xi_2} \frac{\partial C_{22}}{\partial y_3} \\ 0 \end{bmatrix}$$

$$\frac{\partial y_i}{\partial y_4} \quad , \quad i = 1,2,3,4$$

$$\begin{matrix}
A^1_{11} & A^1_{14} & 0 & 0 & \frac{\partial y_1}{\partial y_4} = 0 \\
\frac{A^1_{41}}{\xi_2-\xi_1} & \frac{A^1_{44}}{\xi_2-\xi_1} - \frac{A^2_{11}}{\xi_3-\xi_2} & -\frac{A^2_{15}}{\xi_3-\xi_2} & 0 & \frac{\partial y_2}{\partial y_4} - \frac{A^2_{13}}{\xi_3-\xi_2}\frac{\partial C_{23}}{\partial y_4} \\
0 & \frac{A^2_{51}}{\xi_3-\xi_2} & \frac{A^2_{55}}{\xi_3-\xi_2} - \frac{A^3_{11}}{\xi_4-\xi_3} & -\frac{A^3_{16}}{\xi_4-\xi_3} & \frac{\partial y_3}{\partial y_4} - \frac{A^2_{53}}{\xi_3-\xi_2}\frac{\partial C_{23}}{\partial y_4} \\
0 & 0 & \frac{D_e V_p}{L_p^2(\xi_4-\xi_3)} A^3_{61} & \frac{D_e V_p}{L_p^2(\xi_4-\xi_3)} A^3_{66} + \frac{6k}{\rho d} & \frac{\partial y_4}{\partial y_4} \quad 0
\end{matrix}$$

$$\frac{\partial y_i}{\partial y_5} \quad , \quad i = 1,2,3,4$$

$$\begin{matrix}
A^1_{11} & A^1_{14} & 0 & 0 & \frac{\partial y_1}{\partial y_5} = 0 \\
\frac{A^1_{41}}{\xi_2-\xi_1} & \frac{A^1_{44}}{\xi_2-\xi_1} - \frac{A^2_{11}}{\xi_3-\xi_2} & -\frac{A^2_{15}}{\xi_3-\xi_2} & 0 & \frac{\partial y_2}{\partial y_5} \quad \frac{A^2_{14}}{\xi_3-\xi_2}\frac{\partial C_{24}}{\partial y_5} \\
0 & \frac{A^2_{51}}{\xi_3-\xi_2} & \frac{A^2_{55}}{\xi_3-\xi_2} - \frac{A^3_{11}}{\xi_4-\xi_3} & -\frac{A^3_{16}}{\xi_4-\xi_3} & \frac{\partial y_3}{\partial y_5} - \frac{A^2_{54}}{\xi_3-\xi_2}\frac{\partial C_{24}}{\partial y_5} \\
0 & 0 & \frac{D_e V_p}{L_p^2(\xi_4-\xi_3)} A^3_{61} & \frac{D_e V_p}{L_p^2(\xi_4-\xi_3)} A^3_{66} + \frac{6k}{\rho d} & \frac{\partial y_4}{\partial y_5} \quad 0
\end{matrix}$$

$$\frac{\partial y_i}{\partial y_6} \quad , \quad i = 1,2,3,4$$

$$\begin{matrix} A_{11}^1 & A_{14}^1 & 0 & 0 \\ \frac{A_{41}^1}{\xi_2-\xi_1} & \frac{A_{44}^1}{\xi_2-\xi_1} - \frac{A_{11}^2}{\xi_3-\xi_2} & -\frac{A_{14}^2}{\xi_3-\xi_2} & 0 \\ 0 & \frac{A_{51}^2}{\xi_3-\xi_2} & \frac{A_{55}^2}{\xi_3-\xi_2} - \frac{A_{11}^3}{\xi_4-\xi_3} & -\frac{A_{16}^3}{\xi_4-\xi_3} \\ 0 & 0 & \frac{D_d V_p}{L_p^2(\xi_4-\xi_3)} A_{61}^3 & \frac{D_e V_p}{L_p^2(\xi_4-\xi_3)} A_{66}^3 + \frac{6k}{\rho d} \end{matrix} \begin{matrix} \frac{\partial y_1}{\partial y_6} \\ \frac{\partial y_2}{\partial y_6} \\ \frac{\partial y_3}{\partial y_6} \\ \frac{\partial y_4}{\partial y_6} \end{matrix} = \begin{matrix} 0 \\ 0 \\ \frac{A_{12}^3}{\xi_4-\xi_3} \frac{\partial C_{32}}{\partial y_6} \\ -\frac{D_e V_p}{L_p^2(\xi_4-\xi_3)} A_{62}^3 \frac{\partial C_{32}}{\partial y_6} \end{matrix}$$

$$\frac{\partial y_i}{\partial y_7} \quad , \quad i = 1,2,3,4$$

$$\begin{matrix} A_{11}^1 & A_{14}^1 & 0 & 0 \\ \frac{A_{41}^1}{\xi_2-\xi_1} & \frac{A_{44}^1}{\xi_2-\xi_1} - \frac{A_{11}^2}{\xi_3-\xi_2} & -\frac{A_{15}^2}{\xi_3-\xi_2} & 0 \\ 0 & \frac{A_{51}^2}{\xi_3-\xi_2} & \frac{A_{55}^2}{\xi_3-\xi_2} - \frac{A_{11}^3}{\xi_4-\xi_3} & -\frac{A_{16}^3}{\xi_4-\xi_3} \\ 0 & 0 & \frac{D_e V_p}{L_p^2(\xi_4-\xi_3)} A_{61}^3 & \frac{D_e V_p}{L_p^2(\xi_4-\xi_3)} A_{66}^3 + \frac{6k}{\rho d} \end{matrix} \begin{matrix} \frac{\partial y_1}{\partial y_7} \\ \frac{\partial y_2}{\partial y_7} \\ \frac{\partial y_3}{\partial y_7} \\ \frac{\partial y_4}{\partial y_7} \end{matrix} = \begin{matrix} 0 \\ 0 \\ \frac{A_{13}^3}{\xi_4-\xi_3} \frac{\partial C_{33}}{\partial y_7} \\ -\frac{D_e V_p}{L_p^2(\xi_4-\xi_3)} A_{63}^3 \frac{\partial C_{33}}{\partial y_7} \end{matrix}$$

$$\frac{\partial y_i}{\partial y_8} \quad , \quad i = 1,2,3,4$$

$$\begin{matrix} A^1_{11} & A^1_{14} & 0 & 0 \\ \frac{A^1_{41}}{\xi_2-\xi_1} & \frac{A^1_{44}}{\xi_2-\xi_1} - \frac{A^2_{11}}{\xi_3-\xi_2} & -\frac{A^2_{15}}{\xi_3-\xi_2} & 0 \\ 0 & \frac{A^2_{51}}{\xi_3-\xi_2} & \frac{A^2_{55}}{\xi_3-\xi_2} - \frac{A^3_{11}}{\xi_4-\xi_3} & -\frac{A^3_{16}}{\xi_4-\xi_3} \\ 0 & 0 & \frac{D_e V_p}{L_p^2(\xi_4-\xi_3)} A^3_{61} & \frac{D_e V_p}{L_p^2(\xi_4-\xi_3)} A^3_{66} + \frac{6k}{\rho d} \end{matrix} \begin{matrix} \frac{\partial y_1}{\partial y_8} \\ \frac{\partial y_2}{\partial y_8} \\ \frac{\partial x_3}{\partial y_8} \\ \frac{\partial y_4}{\partial y_8} \end{matrix} = \begin{matrix} 0 \\ 0 \\ \frac{A^3_{14}}{\xi_4-\xi_3} \frac{\partial C_{34}}{\partial y_8} \\ -\frac{D_e V_p}{L_p^2(\xi_4-\xi_3)} A^3_{64} \frac{\partial C_{34}}{\partial y_8} \end{matrix}$$

$$\frac{\partial y_i}{\partial y_9} \quad , \quad i = 1,2,3,4$$

$$\begin{matrix} A^1_{11} & A^1_{14} & 0 & 0 \\ \frac{A^1_{41}}{\xi_2-\xi_1} & \frac{A^1_{44}}{\xi_2-\xi_1} - \frac{A^2_{11}}{\xi_3-\xi_2} & -\frac{A^2_{15}}{\xi_3-\xi_2} & 0 \\ 0 & \frac{A^2_{51}}{\xi_3-\xi_2} & \frac{A^2_{55}}{\xi_3-\xi_2} - \frac{A^3_{11}}{\xi_4-\xi_3} & -\frac{A^3_{16}}{\xi_4-\xi_3} \\ 0 & 0 & \frac{D_e V_p}{L_p^2(\xi_4-\xi_3)} A^3_{61} & \frac{D_e V_p}{L_p^2(\xi_4-\xi_3)} A^3_{66} + \frac{6k}{\rho d} \end{matrix} \begin{matrix} \frac{\partial y_1}{\partial y_9} \\ \frac{\partial x_2}{\partial y_9} \\ \frac{\partial y_3}{\partial y_9} \\ \frac{\partial y_4}{\partial y_9} \end{matrix} = \begin{matrix} 0 \\ 0 \\ \frac{A^3_{15}}{\xi_4-\xi_3} \frac{\partial C_{35}}{\partial y_9} \\ -\frac{D_e V_p}{L_p^2(\xi_4-\xi_3)} A^3_{65} \frac{\partial C_{35}}{\partial y_9} \end{matrix}$$

$$\frac{\partial y_i}{\partial y_{10}} \quad , \quad i = 1,2,3,4$$

$$\begin{bmatrix} A_{11}^1 & A_{14}^1 & 0 & 0 \\ \frac{A_{41}^1}{\xi_2-\xi_1} & \frac{A_{44}^1}{\xi_2-\xi_1} - \frac{A_{11}^2}{\xi_3-\xi_2} & -\frac{A_{15}^2}{\xi_3-\xi_2} & 0 \\ 0 & \frac{A_{51}^2}{\xi_3-\xi_2} & \frac{A_{55}^2}{\xi_3-\xi_2} - \frac{A_{11}^3}{\xi_4-\xi_3} & -\frac{A_{16}^3}{\xi_4-\xi_3} \\ 0 & 0 & \frac{D_e V_p}{L_p^2(\xi_4-\xi_3)} A_{61}^3 & \frac{D_e V_p}{L_p^2(\xi_4-\xi_3)} A_{66}^3 + \frac{6k}{\rho d} \end{bmatrix} \begin{bmatrix} \frac{\partial y_1}{\partial y_{10}} \\ \frac{\partial y_2}{\partial y_{10}} \\ \frac{\partial y_3}{\partial y_{10}} \\ \frac{\partial y_4}{\partial y_{10}} \end{bmatrix} = \begin{bmatrix} 0 \\ 0 \\ 0 \\ \frac{6k}{\rho d} \end{bmatrix}$$

IV. CLOSED BATCH REACTOR FOR DESORPTION
(Single-Solute System)

IV.1 Development of Governing Equations

The system of equations developed in Section I is still valid in describing desorption phenomenon which is caused due to decreased bulk concentration, as long as the adsorption isotherm equation does not change (i.e., complete reversibility and no hysteresis). Therefore, washing spent adsorbent with clean water can be described using the same system of equations if the adsorption is reversible.

However, when adsorption isotherm changes during desorption, these equations cannot be used to describe the desorption phenomenon unless some modifications are made. For example, the change of adsorption isotherms takes place when a solvent such as methanol is used as a desorbing agent (regenerant), because the adsorbability of a solute is typically much lower in regenerant. In order to address the change of isotherm, Eq. (I.1.6) needs to be modified. The adsorption capacity (defined by an isotherm equation) will change as regenerant molecules diffuse into adsorbent pores altering the composition of the liquid phase. Therefore, the isotherm equation should reflect the effect of the liquid-phase composition (i.e., concentration of the regenerant). Again, let's take the Freundlich equation as an example. Eq. (I.1.7) can be rewritten to incorporate this effect.

$$X = f(C) = a(u)\, C^{1/b} \qquad \text{(IV.1.1)}$$

where u = the fraction of regenerant in the liquid phase.

The above equation is based on the assumption that the constant b is not affected by the presence of regenerant. This assumption may have to be justified experimentally, however. Similarly, if the Langmuir equation is used:

$$X = f(C) = \frac{a(u)\, C}{1 + b\, C} \qquad \text{(IV.1.2)}$$

Nkedi-Kizza *et al.* (1985) studied the effect of organic solvent on adsorption of hydrophobic compounds on soils. They showed that the adsorption coefficient (the slope of linear adsorption isotherm) decreased exponentially as the solvent concentration increased. Assuming that this is applicable here, a(u) can be expressed as follows:

$$a(u) = a_o \exp(-k_d\, u) \qquad \text{(IV.1.3)}$$

where a_o = a constant value when there is no regenerant present, and
k_d = adsorption capacity reduction coefficient.

In order to evaluate u, an expression of u as a function of t and x or ξ (i.e., the concentration profile of u in pore), which is the solution of the mass transport equation for regenerant in pore, needs to be developed. The transport equation can be developed as follows by considering a material balance of regenerant in pore.

$$D_r \frac{\partial^2 u}{\partial x^2} = \frac{\partial u}{\partial t} \qquad \text{(IV.1.4)}$$

or

$$\frac{D_r}{L_p^2} \frac{\partial^2 u}{\partial \xi^2} = \frac{\partial u}{\partial t} \qquad \text{(IV.1.5)}$$

where D_r = effective diffusivity of regenerant (cm^2/min).

The initial and boundary conditions are:

$$u = 0, \quad 0 \leq x < L_p, \quad 0 < \xi < 1, \quad t = 0, \qquad \text{(IV.1.6)}$$

$$u = 1, \quad x = L_p, \ \xi = 1, \quad t \geq 0 \qquad \text{(IV.1.7)}$$

$$\frac{\partial u}{\partial x} = \frac{\partial u}{\partial \xi} = 0, \quad x = 0, \ \xi = 0, \quad t \geq 0 \qquad \text{(IV.1.8)}$$

The above equations represent the diffusional phenomenon of regenerant molecules in pore when the bulk solution is replaced instantaneously with the regenerant. These equations can be solved to result in the following solution as a function of t and ξ (Carslaw and Jaeger, 1959).

$$u = \sum_{n=0}^{\infty} (-1)^n \operatorname{erfc} \frac{(2n+1) - \xi}{2\sqrt{st}} + \sum_{n=0}^{\infty} (-1)^n \operatorname{erfc} \frac{(2n+1) + \xi}{2\sqrt{st}} \qquad \text{(IV.1.9)}$$

where $s = \dfrac{D_r}{L_p^2}$. (IV.1.10)

IV.2 Numerical Solution Technique

The same procedure described in Section I is used except the use of the modified isotherm equation containing u.

V. PACKED BED REACTOR FOR DESORPTION
(Single-Solute System)

The procedure described in Section II is still valid here with those modifications described in Section IV for pore. However, in order to use those modifications, it is assumed that the regenerant moves as a plug flow initially (i.e., there is no mixing in the bulk fluid between water and regenerant).

REFERENCES

Bellman, R., Jacquez, J., Kalaba, R., and Schwimmer, S., "Quasilinearization and the Estimation of Chemical Rate Constants from Raw Kinetic Data," Mathematical Bioscience, 1, 71 (1967).

Carey, G. F., and Finlayson, B. A., "Orthogonol Collocation on Finite Elements," Chem. Eng. Sci., 18, 587 (1975).

Carslaw, H. S., and Jaeger, J. C., Conduction of Heat in Solids, 3rd Ed., Oxford (1959).

Finlayson, B. A., Nonlinear Analysis in Chemical Engineering, McGraw-Hill, New York, NY (1980).

Gear, C. W., Numerical Initial Value Problems in Ordinary Differential Equations, Prentice-Hall, Englewood Cliffs, NY (1971).

Hindmarsh, A. C., "GEAR: Ordinary Differential Equation System Solver," Lawrence Livermore Laboratory, Report UCID-30001, Revision 3 (1974).

Kim, B. R., Schmitz, R. A., Snoeyink, V. L., and Tauxe, G. W., "Analysis of Models for Dichloramine Removal by Activated Carbon in Batch and Packed-Bed Reactors Using Quasilinearization and Orthogonal Collocation Methods," Water Research, 12, 319 (1978).

Kim, B. R., and Snoeyink, V. L., "The Monochloramaine-Activated Carbon Reaction: A Mathematical Model Solved Using the Orthogonal Collocation Method on Finite Element," Chapter in Activated Carbon Adsorption of Organics from the Aqueous Phase, Vol. I, I. Suffet and M. McGuire (eds.), Ann Arbor Science Publishers (1980).

Lee, E. S., Quasilinearization and Invariant Imbedding, Academic Press, New York and London (1968).

Levenspiel, O., Chemical Reaction Engineering, John Wiley & Sons, Inc., New York, NY (1972).

Nkedi-Kizza, P., Rao, P. S. C., and Hornsby, A. G., "Influence of Organic Cosolvents on Sorption of Hydrophobic Organic Chemicals by Soils," Env. Sci. and Tech., 19, 975 (1985).

Suidan, M. T., "Reduction of Aqueous Free Chlorine with Granular Activated Carbon," Ph.D. Thesis, Department of Civil Engineering, University of Illinois, Urbana, IL (1975).

Thacker, W. E., Snoeyink, V. L., and Crittenden, J. C., "Modeling of Activated Carbon and Coal Gasification Char Adsorbents in Single-Solute and Biosolute Systems," UILU-WRC-81-0161, Water Resources Center, University of Illinois, Urbana, IL (1981).